Defining the contribution of dorsal vagal complex astrocytes to the regulation of food intake

Submitted by

Alastair James MacDonald

to the University of Exeter as a thesis for the degree of

Doctor of Philosophy in Medical Studies

in March 2020.

Signature: 

Abstract

Food intake is controlled by the coordinated action of numerous brain regions but a complete understanding of the process remains elusive. The nucleus of the solitary tract (NTS), located in the brainstem dorsal vagal complex (DVC) is the first site for integration of visceral synaptic and hormonal cues that act to inhibit food intake. NTS neurons receive synaptic input from sensory neurons of the vagus nerve that relay signals of gastrointestinal stretch and nutrient content. In response to these signals of ingestion, NTS neurons signal to higher brain centres in the hypothalamus and midbrain to inhibit hunger and promote meal termination.

A role for astrocytes in brain circuits controlling food intake has begun to be identified. Hypothalamic astrocyte signalling has been implicated in regulating energy homeostasis. Despite a wealth of evidence showing astrocytes in the NTS/DVC are involved in synaptic integration of vagal signals and control of autonomic physiology, the potential role of these cells in feeding control has not been investigated.

We hypothesised that NTS astrocytes, and those in the wider DVC, would be responsive to increases in food intake and, in turn, their activation would act in concert with NTS neurons to drive a corresponding suppression of food intake. To investigate this prospect we used dietary manipulation, immunohistochemistry, selective chemogenetic manipulation of DVC astrocytes, behavioural assays and electrophysiology in mice.

The key findings of these studies show that in response to acute nutrient excess and gastric distention NTS astrocytes increase their expression of the cytoskeletal glial fibrillary acidic protein and adopt a more ramified morphology, indicative of activation. We also show that selective activation of Gq-protein-coupled receptor signalling in DVC astrocytes suppresses nocturnal food intake and refeeding after a fast. These studies provide evidence that astrocytes may be integrators and effectors of satiety signals and appropriate feeding responses in the DVC.

Acknowledgements

I have been very fortunate to be surrounded by supportive people throughout this PhD including my supervisory team. I would like to thank my primary supervisor Dr Kate Ellacott for her insight, for encouraging me to take all the amazing opportunities I have had and for giving me the freedom to shape the project to what interests me most. I would also like to thank my second supervisor Professor Tony Pickering for hosting me in his lab and providing his expertise and guidance. Finally I would like to thank my third supervisor Dr Craig Beall for giving great advice in a familiar accent.

I have also been lucky to be surrounded by a great team of lab mates. In particular I would like to thank Dr Fiona Holmes for facilitating my experiments in Bristol and for her hospitality during that time. In addition I would like to thank Dr Lydia Hanna facilitating my electrophysiology experiments in Exeter. I would also like to thank members of the Ellacott, Beall and Pickering labs past and present, especially; Nicole, Josie, Ben, Paul, Ana, Katherine, Nadia, Hannah and Julia for making the lab such a nice environment to work in.

I would very much like to thank everyone who made my time at Washington State University so special. It was truly a highlight of the PhD. In particular Professor Suzanne Appleyard who accommodated me in her lab and her family who accommodated me in their home. I must also thank Drew Neyens, who took a month out of his own busy schedule to show me the ropes in the lab and the sights of Washington State outside of it.

I of course would like to thank my family; my parents Jennifer and Hector, and my brothers Andrew and William. Their support and encouragement from applying for the PhD all the way to its completion has been brilliant and I hope I have made them proud. My trips home to visit them and our holidays in Spain have been the perfect PhD breaks.

Finally I must thank my partner, Erica Brady, for moving to the farthest end of the country with me to start our PhD journeys. I would not have been able to do this without her help. Her support and patience are endless and I thank her for always having time to help me or just listen. Knowing that she believes in me and that we are doing this together is my main source of motivation.

Table of Contents

Title page 1

Abstract 2

Acknowledgements 3

Publications arising from this thesis 11

List of abbreviations 12

List of figures 17

List of tables 21

Author's declaration 22

Chapter 1 23

1.1 | Food intake is controlled by the brain to maintain energy balance 24

1.2 | An overview of key neural circuits controlling food intake 27

1.2.1 | Hypothalamic circuits 28

1.2.2 | Midbrain and Hindbrain circuits controlling food intake 37

1.2.3 | Peripheral circuits 51

1.2.4 | An ARC^{AgRP} hunger-based framework of central appetite control 54

1.3 | Astrocytes 58

1.3.1 | Homeostatic functions of astrocytes 59

1.3.2 | Ca^{2+} ionic signalling 60

1.3.3 | Gliotransmission and synaptic modulation 63

1.3.4 | Astrocyte structural plasticity 64

1.4 | Hypothalamic astrocytes and feeding behaviour 64

1.5 | NTS astrocytes 72

1.5.1 | Astrocytes modulate synaptic transmission in the NTS 72

1.5.2 | Physiological and environmental stimuli modulate the morphology of NTS astrocytes 78

1.5.3 | Regulation of cardiorespiratory physiology by NTS astrocytes 83

1.5.4 | Regulation of blood glucose and the counter-regulatory response by NTS astrocytes 85

1.5.5 | Regulation of food intake by NTS astrocytes 87
1.6 | Summary and Statement of Aims 89
Chapter 2 91
2.1 | Key Materials 92
2.2 | Mice 97
2.3 | Methods used in Chapter 3 99
2.3.1 | Dark-phase high-fat feeding studies 99
2.3.2 | Dark-phase fasting studies 99
2.3.3 | Diet induced obese studies 99
2.3.4 | GFAP immunohistochemistry 100
2.3.5 | Image acquisition and analysis 100
2.4 | Methods used in Chapter 4 103
2.4.1 | AAV vector injection 103
2.4.2 | Immunohistochemistry of AAV injected mice 104
2.4.3 | AAV injection mapping 107
2.4.4 | Validating AAV transduction of astrocytes 107
2.4.5 | Validating DREADD activation of astrocytes 107
2.4.6 | c-FOS quantification 107
2.4.7 | Dark phase food intake measurements 108
2.4.8 | Fast induced re-feeding experiments 108
2.4.9 | Conditioned place aversion 108
2.4.10 | Home cage food seeking 109
2.4.11 | Tail flick test 110
2.5 | Methods used in Chapter 5: Mutli-electrode array (MEA) recordings .. 110
2.5.1 | Solutions 110
2.5.2 | Coronal NTS slice preparation 111
2.5.3 | Data processing and analysis 112
2.6 | Methods used in Chapter 5: Whole cell patch clamp recordings 113

2.6.1 | Solutions 113
2.6.2 | Horizontal NTS slice preparation 114
2.6.3 | Whole cell patch clamp electrophysiology 115
2.6.4 | Data analysis 115
2.7 | Statistical analysis 116
Chapter 3 117
3.1 | Introduction 118
3.2 | Aims and hypotheses 119
3.3 | Results 120
3.3.1 | High fat chow induced acute hyperphagia in mice 120
3.3.2 | High fat chow hyperphagia increased the number of GFAP immunoreactive astrocytes in the postremal NTS 123
3.3.3 | High fat chow induced hyperphagia increased the morphological complexity of GFAP immunoreactive astrocytes in the postremal NTS ... 125
3.3.4 | Overnight fasting did not increase the number of GFAP immunoreactive astrocytes in the NTS 128
3.3.5 | Overnight fasting increased the morphological complexity of pNTS GFAP immunoreactive astrocytes 130
3.3.6 | Prolonged consumption of a high fat diet results in greater body weight 132
3.3.7 | GFAP immunoreactivity in the NTS was not increased in mice after 13-weeks of consumption of a high fat diet 134
3.3.8 | 13 week consumption of a high fat diet increased the process number and maximum process length of pNTS astrocytes 136
3.3.9 | Using nested analysis to evaluate the effect of mouse on cellular morphology 138
3.4 | Discussion 141
3.4.1 | Comparisons between NTS and hypothalamic astrocyte responses to energy balance manipulation 141

3.4.2 | Comparisons to other stimuli shown to modify NTS astrocyte GFAP expression or morphology 142
3.4.3 | Evidence for physiological consequences of astrocyte reorganisation 143
3.4.4 | Opposing stimuli generate similar responses 145
3.4.5 | Potential signals that activate NTS astrocytes 145
3.5 | Conclusion 147
Chapter 4 149
4.1 | Introduction 150
4.2 | Aims and hypothesis 152
4.3 | Results 153
4.3.1 | A viral-genetic strategy for chemogenetic activation of DVC astrocytes 153
4.3.2 | Quantification of viral infection 155
4.3.3 | Cell type specificity of viral infection 157
4.3.4 | Chemogenetic activation of DVC astrocytes induced morphological plasticity 159
4.3.5 | Chemogenetic activation of DVC astrocytes suppressed food intake 162
4.3.6 | Expression of hM3Dq outside the DVC did not account for the effect of CNO on food intake 165
4.3.7 | Chemogenetic activation of DVC astrocytes reproducibly suppressed food intake 167
4.3.8 | Chemogenetic activation of DVC astrocytes suppressed food intake at a lower dose of CNO 170
4.3.9 | Chemogenetic activation of DVC astrocytes suppressed food intake following an overnight fast 173
4.3.10 | Chemogenetic activation of DVC astrocytes did not induce conditioned place aversion 175

4.3.11 | Chemogenetic activation of DVC astrocytes did not acutely effect locomotion 178

4.3.12 | Chemogenetic activation of DVC astrocytes reduced food seeking independent of locomotion and drinking 180

4.3.13 | Chemogenetic activation of DVC astrocytes is not analgesic 184

4.3.14 | Chemogenetic activation of DVC astrocytes reduced nocturnal feeding and refeeding after a fast in mice with restricted viral transduction 186

4.3.15 | Chemogenetic activation of DVC astrocytes induced c-FOS immunoreactivity in the NTS and AP 189

4.3.16 | Chemogenetic activation of DVC astrocytes induced c-FOS immunoreactivity in the lPBN 191

4.3.17 | Chemogenetic activation of DVC astrocytes did not induce c-FOS immunoreactivity in the PVH 193

4.3.18 | Stimulation of Gi-GPCR signalling in DVC astrocytes did not alter nocturnal food intake in DVC::GFAP^{hM4Di} mice 195

4.3.19 | A greater dose of CNO did not alter feeding behaviour in DVC::GFAP^{hM4Di} mice 199

4.3.20 | Stimulation of Gi-GPCR signalling in DVC astrocytes did not affect refeeding after a 12 hour fast in DVC::GFAP^{hM4Di} mice 202

4.3.21 | Stimulation of Gi-GPCR signalling in DVC astrocytes attenuated cholecystokinin-induced satiety 204

4.3.22 | Stimulation of Gi-GPCR signalling in DVC astrocytes did not induce c-FOS immunoreactivity in the NTS 207

4.4 | Discussion 209

4.4.1 | Comparisons to ARC astrocytes 209

4.4.2 | Potential mechanisms of astrocyte-neuron communication underlying the effects induced by chemogenetic activation of DVC astrocytes 210

4.4.3 | Absence of conditioned place aversion following chemogenetic DVC astrocyte activation or LPS conditioning 211

4.4.4 | Does chemogenetic activation recapitulate physiological activity of NTS astrocytes 213

4.4.5 | Technical limitations of viral spread 214

4.4.6 | Specificity of CNO for hM-DREADDs 215

4.4.7 | Factors underlying the differential effects of DVC::GFAP^{hM3Dq} and DVC::GFAP^{hM4Di} activation on feeding 215

4.5 | Conclusion 216

Chapter 5 217

5.1 | Introduction 218

5.2 | Aims and hypotheses 220

5.3 | Results 220

5.3.1 | Perforated Multi-Electrode Array allows population recording in the NTS 220

5.3.2 | High fat chow hyperphagia increased the firing rate of NTS channels at baseline 224

5.3.3 | High fat chow hyperphagia increased the firing rate of pNTS channels at baseline 229

5.3.4 | Firing rate of channels in cNTS and rNTS at baseline 233

5.3.5 | NMDA increased MU firing rate in pNTS channels and this effect was potentiated by co-application of D-serine 235

5.3.6 | In the pNTS channels from high fat chow fed mice showed greater responses to NMDA-R agonists 242

5.3.7 | Whole-cell patch clamp in the horizontal slice to investigate glial glutamate reuptake 247

5.3.8 | DHK reduced the size of evoked EPSCs into NTSTH neurons 249

5.3.9 | DHK did not affect the frequency of spontaneous or asynchronous EPSCs into NTSTH neurons 252

5.4 | Discussion 255

5.4.1 | Perforated Multi-Electrode Array allows population recording in the NTS 255

5.4.2 | Assessment of the differential contribution of NMDA-R agonist binding sites to MU firing rate 256

5.4.3 | Mechanisms underlying EAAT2 blockade reducing evoked EPSC in NTS^{TH} neurons 257

5.5 | Conclusion 258

Chapter 6 260

6.1 | Key findings and contributions to scientific knowledge 261

6.2 | Core limitations of work 265

6.2.1 | Reliance on inducible manipulations to infer function 265

6.2.2 | Reliance on *ex vivo* and *post-mortem* measurements to infer real time activity 266

6.2.3 | Use of male mice 267

6.3 | Outstanding questions and future directions 267

6.3.1 | Signal detection: What are the cues that activate NTS astrocytes? 267

6.3.2 | Signal processing: What is the real time Ca^{2+} 'code' of NTS/DVC astrocytes and how does it relate to food intake? 271

6.3.3 | Signal propagation: How do astrocytes modulate vagal and NTS signalling to reduce food intake? 271

6.3.4 | Outstanding conceptual questions 276

6.4 | Conclusion 277

References 278

Publications arising from this thesis

MacDonald AJ, Holmes FE, Beall C, Pickering AE, Ellacott KLJ. Regulation of food intake by astrocytes in the brainstem dorsal vagal complex. Glia. 2019; epub ahead of print. https://doi.org/10.1002/glia.23774

MacDonald AJ, Robb JL, Morrissey NA, Beall C, Ellacott KLJ. Astrocytes in neuroendocrine systems: An overview. Journal of Neuroendocrinology. 2019; 31(5), e12726. https://doi.org/10.1111/jne.12726

List of abbreviations

For the convenience of the reader abbreviations are defined in the following list:

2-DG	2-deoxyglucose
3V	third ventricle
4V	fourth ventricle
5-HT	5-hydroxytryptamine/serotonin
5-HT_{2C}R	serotonin receptor 2C
6-OHDA	6-hydroxydopamine
α-MSH	alpha-melanocyte stimulating hormone
β-MSH	beta-melanocyte stimulating hormone
AAV	adeno associated viral vector
ACBP	acyl-CoA binding protein
Ach	acetylcholine
aCSF	artificial cerebrospinal fluid
Ado	adenosine
AgRP	agouti-related protein
AMPA	α-amino-3-hydroxy-5-methyl-4-isoxazolepropionic acid
AMPA-R	α-amino-3-hydroxy-5-methyl-4-isoxazolepropionic acid receptor
ANLS	astrocyte-neuron lactate shuttle
ANOVA	analysis of variance
AP	area postrema
ARC	arcuate nucleus of the hypothalamus
ATP	adenosine triphosphate
BNST	bed nucleus of the stria terminalis
CA1	cornu ammonis 1
Calc-R	calcitonin receptor
CCK	cholecystokinin
CCK-R	cholecystokinin receptor
CeA	central extended amygdala
CGRP	calcitonin gene related peptide
ChAT	choline actetyltransferase

CNO	clozapine-N-oxide
CNS	central nervous system
cNTS	caudal nucleus of the solitary tract
CPA	conditioned place aversion
CRR	counterregulatory response to hypoglyceamia
CSF	cerebrospinal fluid
DAPI	4',6-diamidino-2-phenylindole
DBH	dopamine beta hydroxylase
DHK	dihydrokainate
DIO	diet induced obesity
diORF	double-inverted open reading frame
DMX/X	dorsal motor nucleus of the vagus
DREADDs	designer receptors exclusively activated by designer drugs
DVC	dorsal vagal complex
E	embryonic day
EAAT1	excitatory amino acid transporter 1
EAAT2	excitatory amino acid transporter 2
EGFP	enhanced green fluorescent protein
EGTA	ethylene glycol-bis(β-aminoethyl ether)-N,N,N',N'-tetraacetic acid
EPSC	excitatory postsynaptic current
EPSP	excitatory postsynaptic potential
FAC	fluoroacetate
FC	fluorocitrate
Flp	flippase
FRT	flippase recognition target
GABA	γ-amino butyric acid
GDF15	growth differentiation factor 15
GFAP	glial fibrillary acidic protein
GFRAL	glial cell-derived neurotrophic factor receptor alpha-like
GHSR1A	growth hormone secretagogue receptor 1A
GI	gastrointestinal
GLAST	glutamate aspartate transporter
GLP1	glucagon-like peptide 1

GLP1-R	glucagon-like peptide 1 receptor
GLT1	glutamate transporter 1
GLUT	glucose transporter
GPCR	G-protein coupled receptor
GS	glutamine synthetase
GTP	guanosine triphosphate
HEPES	4-(2-hydroxyethyl)-1-piperazineethanesulphonic acid
hGFAP	human glial fibrillary acidic protein promoter
HGN	hypoglossal nucleus
i.c.v	intracerebroventricular
i.p.	intraperitoneal
IHC	immunohistochemistry
I_{KA}	A-type potassium current
IP3	inositol trisphosphate
IP3R2	inositol trisphosphate receptor type 2
IPSC	inhibitory postsynaptic current
IR	immunoreactivity
LC^{PFC}	prefrontal cortex projecting locus coeruleus neurons
LepRb	longform leptin receptor
LH	lateral hypothalamus
LiCl	lithium chloride
loxP	locus of crossing over P
lPBN	lateral parabrachial nucleus
LPS	lipopolysaccharide
mACh-R	muscarinic acetylcholine receptor
MC4R	melanocortin 4 receptor
MCT	monocarboxylate transporter
MEA	multi-electrode array
mGlu-R	metabotropic glutamate receptor
mRNA	messenger RNA
MU	multi unit
MUA	multi unit activity
NAc	nucleus accumbens
nACh-R	nicotinic acetylcholine receptor

NDS	normal donkey serum
NeuN	neuronal nuclear protein
NF-κB	nuclear factor kappa B
NG	nodose ganglion/nodose ganglia
NMDA	N-methyl-D-aspartate
NMDA-R	N-methyl-D-aspartate receptor
NPY	neuropeptide Y
NTS	nucleus of the solitary tract
ODN	octadecaneuropeptide
OXT	oxytocin
OXTR	oxytocin receptor
P	postnatal day
PAR	protease activated receptor
PBS	phosphate buffered saline
PDYN	prodynorphin
PFA	paraformaldehyde
Pfkfb3	6-phosphofructo-2-kinase
pMEA	perforated multi-electrode array
pNTS	postremal nucleus of the solitary tract
POMC	proopiomelanocortin
PPG	preproglucagon
pSTAT3	phospho-signal transducer and activator of transcription 3
PVH	paraventricular nucleus of the hypothalamus
PVH_M	paraventricular nucleus of the hypothalamus, magnocellular region
PYY	peptide tyrosine tyrosine
RM ANOVA	repeated measures analysis of variance
rNTS	rostral nucleus of the solitary tract
scRNA-seq	single cell RNA sequencing
SIDS	sudden infant death syndrome
SIM1	single minded 1
SON	supraoptic nucleus of the hypothalamus
SST	somatostatin
ST	solitary tract

STZ	streptozotocin
TAA	thioacetamide
TBOA	threo-β-benzyloxyaspartic acid
TeLC	tetanus toxin light chain
TH	tyrosine hydroxylase
VEGF	vascular endothelial growth factor
VGAT	vescular γ-amino buytric acid transporter
VGKC	voltage gated potassium channel
VIP	vasoactive intensinal polypeptide
VLM	ventrolateral medulla
VTA	ventral tegmental area

List of figures

Figure 1.1 The brain integrates cues from the periphery to regulate food intake.

Figure 1.2.1 ARC^{AgRP} neurons send distinct projections to subcortical nuclei to drive food intake.

Figure 1.2.2 A simplified schematic diagram of the neurochemical organisation of appetite controlling populations in the NTS.

Figure 1.2.3 Brain circuits engaged by hunger and satiety.

Figure 1.4.1 Schematic summary of potential homeostatic and maladaptive responses of ARC astrocytes to short and long term deviations in energy balance.

Figure 1.5.1 A simplified schematic of astrocyte modulation of synaptic transmission in the NTS.

Figure 2.3.1 Demonstration of specificity of anti-mouse AlexaFluor 568 secondary antibody binding.

Figure 2.4.1 Demonstration of specificity of anti-mouse and anti-rabbit AlexaFluor 488 secondary antibody binding.

Figure 3.3.1 High fat chow feeding induced hyperphagia in mice.

Figure 3.3.2 High fat chow induced hyperphagia increased the number of GFAP immunoreactive astrocytes in the postremal NTS.

Figure 3.3.3 Sholl analysis permits quantitative analysis of GFAP immunoreactive astrocyte morphology.

Figure 3.3.4 High fat chow induced hyperphagia increased the morphological complexity of GFAP immunoreactive astrocytes in the pNTS.

Figure 3.3.5 Overnight fasting did not change the number of GFAP immunoreactive astrocytes in the NTS.

Figure 3.3.6 Overnight fasting increased the morphological complexity of GFAP immunoreactive astrocytes in the pNTS.

Figure 3.3.7 13 weeks of high fat diet intake increased body weight in mice.

Figure 3.3.8 13 weeks of high fat diet intake did not change the number of GFAP immunoreactive astrocytes in the NTS.

Figure 3.3.9 13 weeks of high fat diet intake increased the number of processes and enclosing radius of GFAP immunoreactive astrocytes in the pNTS.

Figure 3.3.10 Morphological analysis with mouse as a nested variable.

Figure 4.3.1 Strategy for chemogenetic control of DVC astrocytes.

Figure 4.3.2 AAV vector spread in individual DVC::GFAP^{hM3Dq} mice.

Figure 4.3.3 Expression of hM3Dq_mCherry in DVC astrocytes.

Figure 4.3.4 Chemogenetic activation increased morphological complexity of DVC astrocytes.

Figure 4.3.5 Chemogenetic activation of DVC astrocytes suppressed food intake.

Figure 4.3.6 Expression of hM3Dq outside the DVC did not account for the effect of CNO on food intake.

Figure 4.3.7 Chemogenetic activation of DVC astrocytes reproducibly suppressed food intake.

Figure 4.3.8 Chemogenetic activation of DVC astrocytes with 0.3 mg/kg CNO suppressed food intake.

Figure 4.3.9 Chemogenetic activation of DVC astrocytes suppressed food intake during re-feeding after a 12 hour fast.

Figure 4.3.10 Chemogenetic activation of DVC astrocytes did not induce conditioned place aversion.

Figure 4.3.11 Chemogenetic activation of DVC astrocytes did not suppress locomotion.

Figure 4.3.12 Chemogenetic activation of DVC astrocytes suppressed food seeking independent of locomotion or drinking.

Figure 4.3.13 Chemogenetic activation of DVC astrocytes did not increase tail-flick latency.

Figure 4.3.14 Lower AAV vector injection volume is still sufficient to supress feeding.

Figure 4.3.15 Chemogenetic activation of DVC astrocytes induced c-FOS immunoreactivity in the NTS and AP.

Figure 4.3.16 Chemogenetic activation of DVC astrocytes induced c-FOS immunoreactivity in the lPBN.

Figure 4.3.17 Chemogenetic activation of DVC astrocytes induced c-FOS immunoreactivity in the PVH.

Figure 4.3.18 Stimulation of Gi-GPCR signalling in DVC astrocytes did not increase food intake.

Figure 4.3.19 Stimulation of Gi-GPCR signalling in DVC astrocytes with 1 mg/kg CNO did not increase food intake.

Figure 4.3.20 Stimulation of Gi-GPCR signalling in DVC astrocytes did not increase food intake after a 12 hour fast.

Figure 4.3.21 Stimulation of Gi-GPCR signalling in DVC astrocytes attenuated CCK-induced satiety after a 12 hour fast.

Figure 4.3.22 Stimulation of Gi-GPCR signalling in DVC astrocytes did not induce c-FOS immunoreactivity in the NTS.

Figure 5.3.1 pMEA recording set up for NTS.

Figure 5.3.2 Recording protocol and drug treatments.

Figure 5.3.3 Food intake and stomach contents of experimental mice.

Figure 5.3.4 Analysis pipeline for pMEA recordings.

Figure 5.3.5 Greater baseline MU firing rate of channels across the NTS from mice fed high fat chow for 12 hours compared to standard chow fed controls.

Figure 5.3.6 Greater baseline MU firing rate of channels in the postremal NTS from mice fed high fat chow for 12 hours compared to standard chow fed controls.

Figure 5.3.7 Firing was greater in slices from high fat chow mice in the cNTS are rNTS.

Figure 5.3.8 Bath application of NMDA increases MU firing rate in the pNTS and this effect is potentiated by co-application of D-serine.

Figure 5.3.9 NMDA-R agonists enhance MU firing in pNTS slices.

Figure 5.3.10 Representative spike waveforms

Figure 5.3.11 Total capacity of NMDA-R mediated firing and co-agonist capacity of NMDA-R mediated firing are greater in pNTS channels from high fat chow fed mice.

Figure 5.3.12 Patch clamp recording in the horizontal brainstem slice.

Figure 5.3.13 Effect of DHK on evoked EPSCs in NTS^{TH} neurons.

Figure 5.3.14 DHK did not affect the frequency of spontaneous and asynchronous EPSCs in NTS^{TH} neurons

Figure 6.1.1 Summary of the main findings of this thesis as they relate to the overarching hypothesis

Figure 6.3.1 Proposed signals leading to NTS astrocyte activation.

Figure 6.3.2 Potential mechanisms of astrocyte-neuron communication in the NTS.

List of tables

Table 1.5.1 Summary of studies which have examined impact of experimental manipulations on NTS astrocyte immunoreactivity and/or morphology.

Table 2.1.1 Summary of antibodies used in the described studies.

Table 2.1.2 Summary of viral vectors used in the described studies.

Table 2.1.3 Summary of chemicals used in the described studies.

Table 2.1.4 Summary of mouse strains and mouse diets used in the described studies.

Table 2.1.5 Summary of software used in the described studies.

Table 2.1.6 Summary of equipment used in the described studies.

Table 2.2.1 Description of mice used for each experiment.

Table 2.5.1 Concentrations of molecules in the 10mM Glucose artificial cerebrospinal fluid (aCSF).

Table 2.5.2 Concentrations of molecules in the 5mM Glucose artificial cerebrospinal fluid (aCSF).

Table 2.5.3 Concentrations of molecules in the slicing solution.

Table 2.6.1 Concentrations of molecules in the external artificial cerebrospinal fluid (aCSF).

Table 2.6.2 Concentrations of molecules in the internal recording pipette solution.

Author's declaration

All work was conducted by the author at the University of Exeter Medical School laboratories, the University of Bristol School of Physiology, Pharmacology and Neuroscience laboratories or the Washington State University Integrative Pharmacology and Neuroscience laboratories with the exception of the following:

Chapter 4

Dr Fiona Holmes performed the tail-flick latency assay described in **section 4.3.13** and **figure 4.3.13**.

Chapter 1

Introduction

1.1 | Food intake is controlled by the brain to maintain energy balance

Energy balance is the process by which energy intake and energy expenditure are matched to ensure the metabolic demands of an organism are met (Hall *et al.*, 2012). In mammals, energy intake is in the form of food intake while energy expenditure comprises of the body's basal metabolic processes required for physiological function in addition to that required for the physical activities necessary for survival (Hall *et al.*, 2012). Energy balance is considered to be under the control of the brain which integrates hormonal and nervous cues to modulate food intake and energy balance to ensure the metabolic needs are met (Kishi and Elmquist, 2005; Rui, 2013). Given the evolutionary pressures that guided development of this system in mammals, energy balance seems to be more protective against starvation than energy surplus (Krashes, Lowell and Garfield, 2016). This is presumably due to starvation being more prohibitive to reproductive success. The appropriate regulation of food intake is essential to defend a mammal against prolonged energy imbalance. Two key brain areas receive information from the periphery in order to regulate food intake: the hypothalamus and the dorsal vagal complex.

The hypothalamus, located on the ventral surface of the brain, is adjacent to the third ventricle (3V) and the circumventricular organ the median eminence. These two features allow hypothalamic cells access to circulating factors in the cerebrospinal fluid (CSF) and blood, respectively (Mullier *et al.*, 2010). Indeed, this brain area is a primary site of action of the two canonical energy balance hormones, leptin and ghrelin which suppress and promote food intake, respectively (Valassi, Scacchi and Cavagnini, 2008). Hypothalamic cells also directly sense nutrients in the form of amino acids (Blouet *et al.*, 2009). Different

nuclei of the hypothalamus are believed to predominantly control food intake and energy expenditure.

The dorsal vagal complex (DVC), located in the brainstem is the second primary sensor of peripheral energy regulatory cues (Grill and Hayes, 2012). In addition to containing a circumventricular organ, the area postrema (AP), the DVC contains a neuronal hub, the nucleus of the solitary tract (NTS) where neurons of the afferent vagus nerves project. These nerves innervate the stomach and intestine and signal nutrient content and physical stretch to the brain following a meal (Berthoud and Neuhuber, 2000; Williams *et al.*, 2016; Bai *et al.*, 2019). Their activity is also modulated by hormones predominantly those released from the gut (Cork, 2018).

The hypothalamus and DVC communicate with each other directly *via* neuronal projections and indirectly *via* downstream integratory nuclei in the midbrain (**Figure 1.1**) (Andermann and Lowell, 2017). This signalling regulates energy balance to ensure appropriate food seeking and ingestion to match energy requirements. In order to ensure food intake the brain generates a feeling of hunger. Once the appropriate amount of food is ingested, the brain integrates neuronal and hormonal cues and generates a signal of satiation. Satiety refers to a state where hunger is suppressed so an animal will stop eating and not begin again until hunger resumes. Hunger and satiety are sensations in opposition that act to promote and suppress food intake, respectively. In a coordinated action with brain circuits regulating energy expenditure this system ensures energy balance. The details of the key brain circuitry underlying this are discussed below.

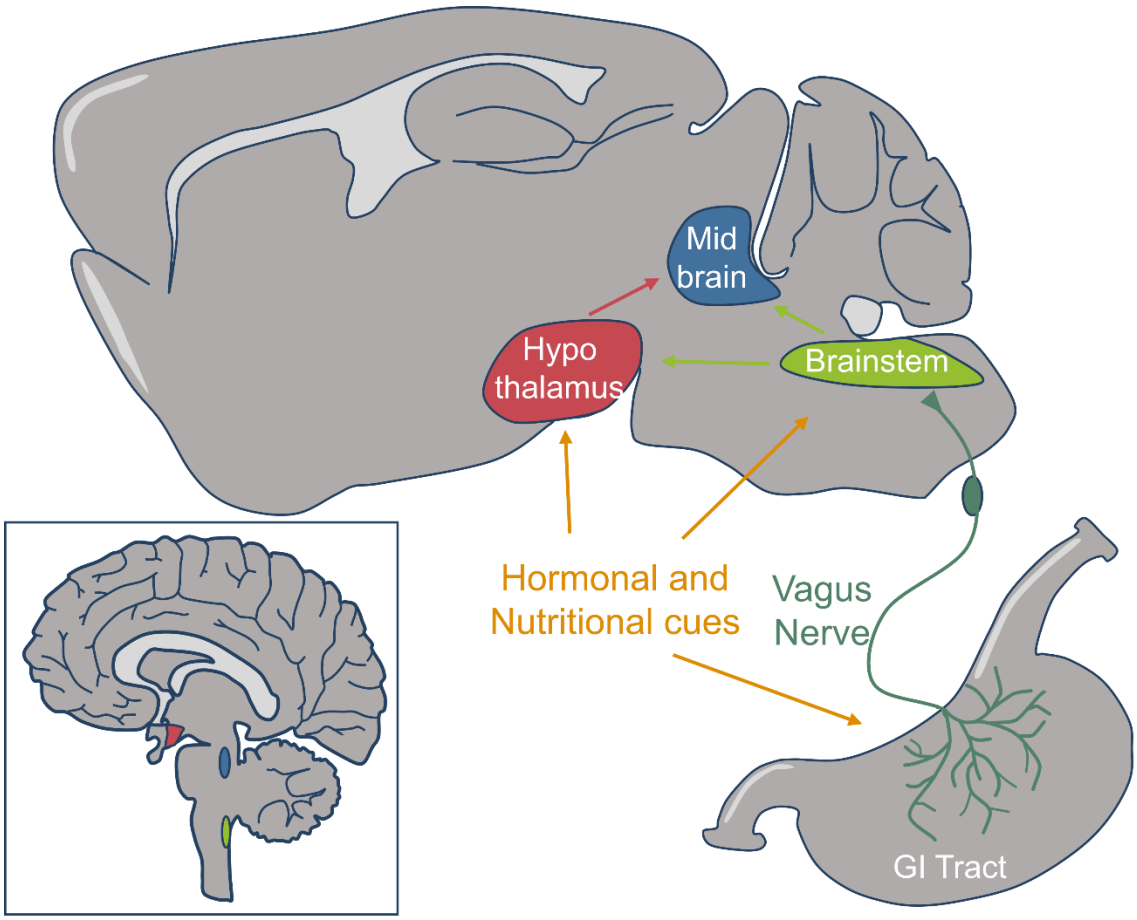

Figure 1.1 | The brain integrates cues from the periphery to regulate food intake. Simplified diagrammatic representation of rodent brain regions controlling food intake. Specific brain nuclei in the hypothalamus (red) and brainstem (light green) are sensitive to hormonal and neuronal input from the rest of the body which reflect internal energy state. Activity of neurons in these brain regions and midbrain integratory centres (blue) drive or suppress food intake in response to these peripheral signals to maintain energy balance. Inset, these same nuclei are found in a corresponding anatomical arrangement in the human brain indicating these systems are evolutionarily conserved.

1.2 | An overview of key neural circuits controlling food intake

Feeding is a highly conserved behaviour critical to the evolutionary success of a species. It is one of the fundamental behaviours and for humans a basic need in Maslow's hierarchy of needs (Maslow, 1943). A key goal of systems neuroscience is to understand how networks of neurons act together to generate behaviour. Feeding has received a lot of attention in the field and as a result the circuitry underlying this behaviour is some of the best understood (Andermann and Lowell, 2017).

Rodents are a common model organism used to study food intake since they have relatively similar digestive anatomy to other mammals, show stereotyped patterns of food intake under laboratory conditions, and (especially in the case of the mouse) they are genetically tractable allowing for the dissection of neuronal circuitry at a very rich level of detail (Luo, Callaway and Svoboda, 2008; Ellacott *et al.*, 2010).

In the last fifteen years there has been a rapid adoption of technologies which allow for the selective manipulation and monitoring of defined neuronal (and non-neuronal) cell populations. Optogenetics employs light sensitive ion channels to allow for selective stimulation or inhibition of neurons with direct pulses of light (Boyden *et al.*, 2005; Boyden, 2011; Deisseroth, 2015). Chemogenetics applies a similar principle but utilises modified G-protein coupled receptors (GPCRs) which recognise a synthetic ligand (e.g. clozapine-N-oxide [CNO]) (Armbruster *et al.*, 2007; Roth, 2016). Cell populations can also be either selectively ablated (killed) or have vesicular release blocked by the expression of the diphtheria toxin receptor or the tetanus toxin light chain (TeLC), respectively (Yamamoto *et al.*, 2003; Luquet *et al.*, 2005). Finally by expressing variants of the genetically encoded Ca^{2+} indicator GCaMP, relative neuronal intracellular Ca^{2+} concentration

($[Ca^{2+}]_i$) and population activity can be monitored in freely moving animals which can be related to behaviour (Tian *et al.*, 2009). Combining these techniques with mice expressing Cre-recombinase in specific cell types of interest has greatly enhanced our understanding of how the brain regulates food intake in mice (Andermann and Lowell, 2017).

1.2.1 | Hypothalamic circuits

Since the discovery that hypothalamic and not pituitary lesions in rats, cats, dogs and humans produces dramatic weight gain (Hetherington and Ranson, 1940; Brobeck, 1946), the hypothalamus has been at the centre of research into the brain's control of food intake. This structure, situated on the ventral surface of the brain beneath the thalamus, consists of anatomically distinct nuclei predominantly associated with driving behaviours that govern survival, homeostasis and reproduction (Sternson, 2013).

1.2.1.1 | The Arcuate Nucleus

Commonly considered to be an 'entry' point into the brain's control of food intake, the arcuate nucleus (ARC) is the primary site of detection for signals driving food intake (Cone, 2005). Its proximity to the third ventricle and median eminence (a circumventricular organ) allow for sensing of circulating factors and signals in the CSF (Yulyaningsih *et al.*, 2017).

Canonically, the ARC is home to two functionally opposed neuronal populations that bi-directionally modulate food intake. These cells are identified by their expression of agouti-related protein (AgRP [ARC^{AgRP} neurons]) or pro-opiomelanocortin (POMC [ARC^{POMC} neurons]). ARC^{AgRP} neurons release AgRP along with neuropeptide Y (NPY) and γ-amino butyric acid (GABA) (Atasoy *et al.*, 2012). There is substantial evidence that ARC^{AgRP} neurons are the main (and

perhaps sole) homeostatic hunger-signalling (orexigenic) population in the brain, although dopaminergic reward pathways outside of the hypothalamus can also drive food intake (Luquet *et al.*, 2005; Denis *et al.*, 2015). In adult mice, selective chemical ablation of ARC^{AgRP} neurons results in starvation showing their importance for survival (Luquet *et al.*, 2005). Furthermore, one of the most robust findings in the field is that the selective activation of ARC^{AgRP} neurons by chemogenetic or optogenetic methods drives voracious eating for the duration of stimulation (Krashes *et al.*, 2011, 2013, 2014; Aponte, Atasoy and Sternson, 2011; Atasoy *et al.*, 2012; Betley *et al.*, 2013; Dietrich *et al.*, 2015; Garfield *et al.*, 2015; Padilla *et al.*, 2016; Y. Chen *et al.*, 2016; Burnett *et al.*, 2016, 2019; Su, Alhadeff and Betley, 2017; Essner *et al.*, 2017; Alhadeff *et al.*, 2018, 2019b; Goldstein *et al.*, 2018; X.-Y. Li *et al.*, 2019).

These neurons are greatly activated by fasting as evidenced by expression of the immediate early gene protein product, c-FOS (a marker of active neurons) in ARC^{AgRP} neurons of fasted mice (Wu *et al.*, 2014). In *ex vivo* slices from fasted mice, ARC^{AgRP} neuronal action potential firing and intrinsic electrical excitability are greater than in slices from *ad libitum* fed control mice (Takahashi and Cone, 2005). Crucially, *in vivo*, $[Ca^{2+}]_i$ is elevated in ARC^{AgRP} neurons by fasting (Betley *et al.*, 2015).

In addition to driving feeding it appears that fasting inhibits competing behaviours to prioritise food seeking, ensuring survival. This is recapitulated by selective optogenetic or chemogenetic activation of ARC^{AgRP} neurons. Behaviours shown to be inhibited include anxiety, fighting, mating, socialising (Burnett *et al.*, 2016; Padilla *et al.*, 2016), sleep (Goldstein *et al.*, 2018), nest building (X.-Y. Li *et al.*, 2019) and even perception of inflammatory pain (Alhadeff *et al.*, 2018). In the absence of food, selective optogenetic and chemogenetic activation of ARC^{AgRP}

neurons stimulates food seeking behaviours like burrowing (Dietrich *et al.*, 2015). Across these studies bulk optogenetic or chemogenetic activation of ARC^{AgRP} neurons mimics the effects of fasting in mice.

These neurons send restricted projections to a number of subcortical nuclei in a one-to-one fashion (i.e. an individual ARC^{AgRP} neuron projects to only one target) (Betley *et al.*, 2013). Of these targets only a subset appear to mediate effects on feeding while others likely act to suppress competing behaviours (Betley *et al.*, 2013; Essner *et al.*, 2017; Alhadeff *et al.*, 2018) (**Figure 1.2.1**). Thus, in states of starvation, ARC^{AgRP} neurons drive feeding and suppress other behaviours to ensure prioritisation of food intake and survival.

In recent work the activity of ARC^{AgRP} neurons has been measured using *in vivo* Ca^{2+} imaging (Betley *et al.*, 2015), fibre photometry (Chen *et al.*, 2015), and electrophysiology (Mandelblat-Cerf *et al.*, 2015).This has revealed that ARC^{AgRP} neuron activity is reduced following the presentation of food and to conditioned cues signalling food intake (Betley *et al.*, 2015; Chen *et al.*, 2015; Mandelblat-Cerf *et al.*, 2015). This 'anticipatory' reduction in activity is transient unless food is then consumed, at which point the reduction in activity is sustained (Betley *et al.*, 2015; Chen *et al.*, 2015; Beutler *et al.*, 2017; Su, Alhadeff and Betley, 2017). Anticipatory reductions in ARC^{AgRP} activity are mediated predominantly by visual detection of food and to a lesser degree olfactory detection (Chen *et al.*, 2015).

Direct intra-gastric infusion of liquid diet or individual macronutrients (carbohydrate, sugar and fat) is sufficient to reduce ARC^{AgRP} activity in fasted mice in a calorie dependent manner as is injection with gut peptides cholecystokinin (CCK), peptide tyrosine tyrosine (PYY) and amylin (Beutler *et al.*, 2017; Su, Alhadeff and Betley, 2017). This gut-brain suppression of ARC^{AgRP}

activity is dependent on vagal signalling since it is abolished by vagotomy and chemogenetic activation of satiety signalling vagal neurons is sufficient to reduce ARC^{AgRP} activity in fasted mice (Alhadeff *et al.*, 2019b; Bai *et al.*, 2019). These data showing the dynamics of ARC^{AgRP} neuron activity *in vivo* has led to the view that ARC^{AgRP} neurons drive food seeking behaviours and once food is both present and consumed this drive is rapidly and sustainably diminished.

As mentioned above, ARC^{POMC} neurons are the functionally opposing population to ARC^{AgRP} neurons within the hypothalamus. ARC^{POMC} neurons release α- and β-melanocyte stimulating hormone (α-MSH and β-MSH respectively; cleavage products of the POMC prohormone) and GABA. Although less robust, their sustained activation with optogenetics or chemogenetics reduces food intake in mice (Aponte, Atasoy and Sternson, 2011; Zhan *et al.*, 2013). Their major projection targets appear to generally match those of ARC^{AgRP} neurons including the central extended amygdala (CeA), paraventricular nucleus of the hypothalamus (PVH), lateral hypothalamus (LH) and lateral parabrachial nucleus (lPBN) (Betley *et al.*, 2013; D. Wang *et al.*, 2015).

The actions of ARC^{AgRP} and ARC^{POMC} derived transmitters bi-directionally regulate the melanocortin 4 receptor (MC4R). At the MC4R, α-MSH and β-MSH are agonists and AgRP is an inverse agonist (Haskell-Luevano and Monck, 2001; Raffan *et al.*, 2016). MC4R is found in many projection targets of ARC^{AgRP} and ARC^{POMC} neurons including the CeA, PVH, LH and lPBN (Mountjoy *et al.*, 1994; Liu *et al.*, 2003). Of these nuclei, it appears that MC4Rs in the PVH are the predominant population in mediating effects on food intake (Shah *et al.*, 2014; Garfield *et al.*, 2015) (See **section 1.2.1.2** below).

Importantly, ARC^{AgRP} neurons directly inhibit ARC^{POMC} neurons *via* GABA release (Atasoy *et al.*, 2012). In fasted mice, ARC^{POMC} neuron $[Ca^{2+}]_i$ rapidly increases upon food presentation and shows sustained elevation following food ingestion (Chen *et al.*, 2015). Their activity is directly inverse to ARC^{AgRP} neurons suggesting these rises in activity are owing to disinhibition (i.e. a reduction in GABAergic tone from ARC^{AgRP} neurons allowing for a net excitation of ARC^{POMC}). These studies show that ARC^{POMC} neurons signal satiety following food intake. In times of caloric need ARC^{POMC} neurons are inhibited directly and their actions are antagonised at projection targets by ARC^{AgRP} neurons to ensure caloric needs are met.

The ARC and its resident AgRP and POMC neurons have been identified as effectors of two major appetite-regulating hormones, ghrelin and leptin. Ghrelin is a hormone released from the stomach: its release is elevated by fasting and inhibited by food intake (Kojima *et al.*, 1999; Ariyasu *et al.*, 2001). Plasma ghrelin also peaks prior to mealtimes in humans (Cummings *et al.*, 2001). Delivery of exogenous ghrelin either into the circulation or directly to the brain ventricles (intracerebroventricular, i.c.v.) increases food intake in rats and induces c-FOS expression in ARC^{AgRP} neurons (Dickson and Luckman, 1997; Nakazato *et al.*, 2001). Ghrelin has been shown to directly activate ARC^{AgRP} neurons *via* the growth hormone secretagogue receptor 1A (GHSR1A) (Cowley *et al.*, 2003). In turn, this inhibits the firing of ARC^{POMC} neurons and is accompanied by an increase in inhibitory postsynaptic currents (IPSCs) in these cells, likely from inhibitory ARC^{AgRP} inputs (Cowley *et al.*, 2003).

Leptin is a hormone released from white adipose tissue and plasma leptin levels reflect body mass leading to the view that leptin is an adipostat (i.e. a hormone that signals the level of energy stored as fat) (Zhang Y *et al.*, 1994; Frederich *et*

al., 1995). In addition to this homeostatic signal, acutely plasma leptin is very low in fasted mice which is likely a mechanism to promote food intake (Ahlma *et al.*, 1996). Leptin activates ARC^{POMC} neurons directly *via* the long form leptin receptor (LepRb) and indirectly by inhibition of ARC^{AgRP} neurons (Cowley *et al.*, 2001). Correspondingly, deletion of LepRb from only POMC neurons results in mild obesity and leptin resistance but not to the same extent as total LepRb deletion (Balthasar *et al.*, 2004). This shows POMC neurons including ARC^{POMC} are a principal, but not the sole, target of leptin for energy homeostasis. Thus, the two populations of ARC neurons are bi-directionally modulated by peripheral signals that stimulate (ghrelin) and inhibit (leptin) food intake.

1.2.1.2 | The Paraventricular Nucleus of the Hypothalamus

One of the best studied projection targets of ARC neurons is the PVH. Sitting adjacent to the third ventricle (3V), neurons in this nucleus receive dense innervation from ARC^{AgRP} and ARC^{POMC} neurons (Bagnol *et al.*, 1999; Haskell-Luevano *et al.*, 1999). In the classic view, ARC^{POMC} neurons release POMC-derived melanocortins (i.e. α-MSH and β-MSH) to stimulate MC4Rs on PVH neurons. Conversely, these same PVH neurons are inhibited by AgRP and NPY released from ARC^{AgRP} neurons *via* inverse agonism of MC4R and potentiation of GABAergic inputs, respectively (Cowley *et al.*, 1999; Cone, 2005).

The majority of neurons in the PVH are marked by expression of the transcription factor single-minded 1 (SIM1) which specifies PVH development (Michaud *et al.*, 1998, 2001). *Mc4r* deficient mice and humans with *MC4R* mutations have increased food intake (hyperphagia) and develop obesity (Huszar *et al.*, 1997; Vaisse *et al.*, 1998; Yeo *et al.*, 1998). Restoration of the MC4R in PVH^{SIM1} neurons of $Mc4r^{-/-}$ mice is sufficient to reduce hyperphagia and obesity associated

with *Mc4r*-deficiency, highlighting the PVH as a key site of MC4R action in the regulation of energy homeostasis (Balthasar *et al.*, 2005).

Indeed, further studies have shown that PVH neurons expressing the MC4R (PVH^{MC4R} neurons) are an important PVH population mediating satiety. Site-specific deletion of the MC4R from the PVH results in hyperphagia and weight gain in mice (Shah *et al.*, 2014). PVH^{MC4R} neurons express c-FOS in the fed state and following refeeding after a fast (Garfield *et al.*, 2015; M. M. Li *et al.*, 2019). PVH^{MC4R} neurons are direct recipients of inhibitory synaptic input from ARC^{AgRP} neurons and disruption of this inhibitory pathway attenuates food intake induced by optogenetic stimulation of ARC^{AgRP} neurons (Garfield *et al.*, 2015). Numerous lines of evidence show that optogenetic and chemogenetic stimulation of PVH^{MC4R} neurons reduces food intake (Garfield *et al.*, 2015; C. Li *et al.*, 2019; M. M. Li *et al.*, 2019). In turn, chemogenetic silencing induces hyperphagia and TeLC-mediated inhibition of transmitter release over long time scales (weeks) leads to weight gain (Garfield *et al.*, 2015; C. Li *et al.*, 2019; M. M. Li *et al.*, 2019).

PVH^{MC4R} neurons exert their satiating effects by providing excitatory glutamatergic drive to neurons of the lPBN in the midbrain which act to suppress appetite (Shah *et al.*, 2014; Garfield *et al.*, 2015; M. M. Li *et al.*, 2019). As mentioned above, under the classical model of ARC to PVH signalling, PVH^{MC4R} neurons are directly activated by melanocortin peptides released from ARC^{POMC} neurons while this activation is antagonised by AgRP release from ARC^{AgRP} neurons. In addition it appears that the rapid effect of ARC^{AgRP} activation on food intake is mediated by GABA and NPY (Aponte, Atasoy and Sternson, 2011; Atasoy *et al.*, 2012). This is consistent with evidence that the AgRP/POMC/MC4R system governs long term energy balance while fast neurotransmitters govern rapid changes in intake (Krashes *et al.*, 2013).

A second population of PVH neurons, identified by expression of prodynorphin (PVH^{PDYN} neurons) additively control satiety with PVH^{MC4R} neurons, collectively accounting for the effects of chemogenetic activation of PVH^{SIM1} neurons (M. M. Li *et al.*, 2019). PVH^{PDYN} neurons show minimal overlap with PVH^{MC4R} neurons and chemogenetic activation of each population separately produces around 50% of the effects of chemogenetic activation of both populations simultaneously or PVH^{SIM1} neurons (M. M. Li *et al.*, 2019). Therefore, PVH satiety neurons consist of two, largely independent populations expressing PDYN or MC4R which additively govern satiety and prevent obesity.

PVH neurons additionally receive input from brainstem nuclei and both cholecystokinin receptor (CCK-R) and glucagon-like peptide1 receptor (GLP1-R) expressing populations suppress appetite (D'Agostino *et al.*, 2016; C. Li *et al.*, 2019) suggesting PVH neurons are regulated by 'bottom-up' signalling from the brainstem in addition to 'top-down' signalling from the ARC (discussed in more detail below see **section 1.2.2.1**).

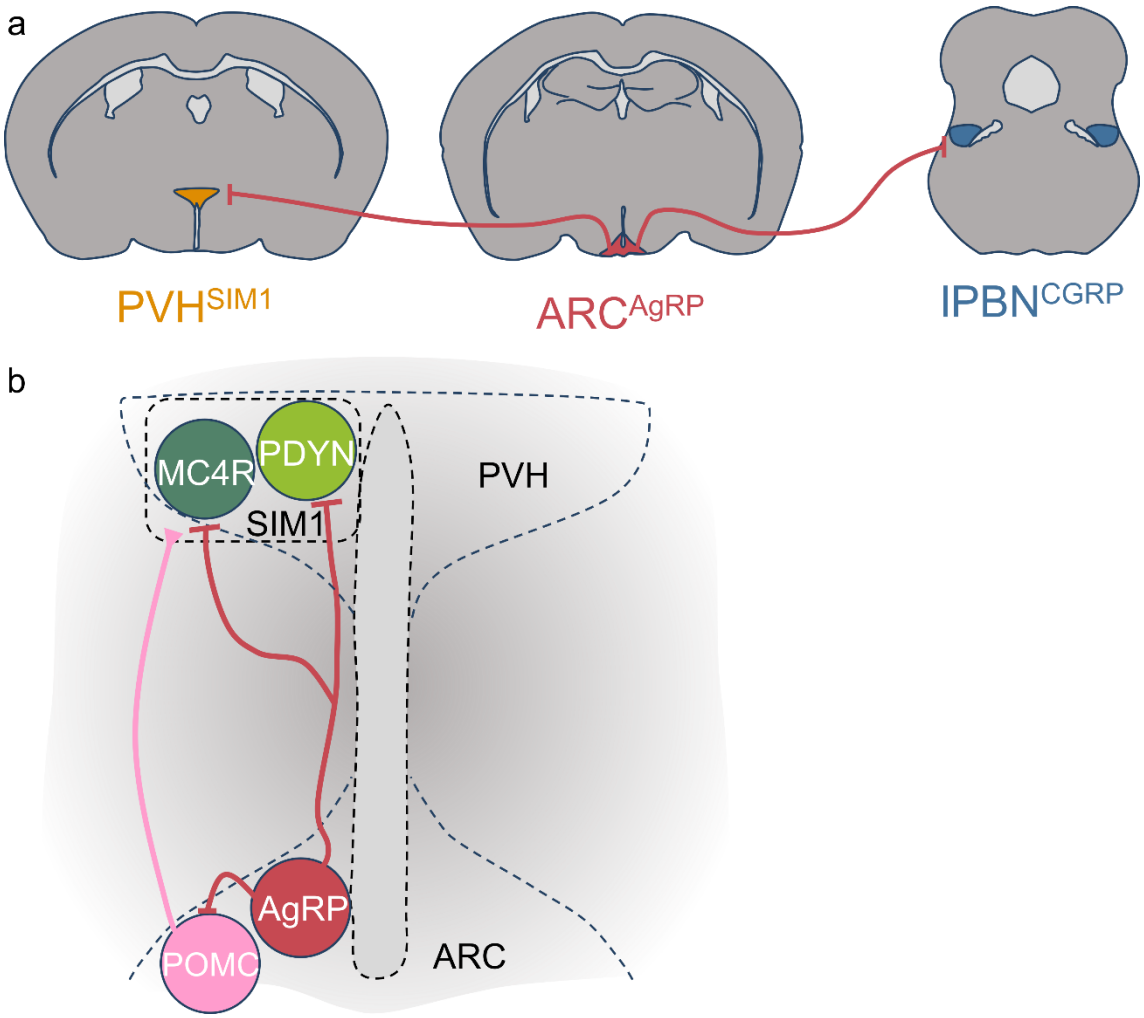

Figure 1.2.1 | ARC^{AgRP} neurons send distinct projections to subcortical nuclei to drive food intake. a, ARC^{AgRP} neurons send projections to the PVH. Selective activation of this projection increases food intake in satiated mice. Selective activation of ARC^{AgRP} projections to the lPBN increases food intake in mice injected with satiating and nauseating agents. **b**, ARC^{AgRP} neurons project within the hypothalamus to inhibit ARC^{POMC} neurons and PVH^{SIM1} neurons. Activation of the subtypes of PVH^{SIM1} neurons (PVH^{MC4R} and PVH^{PDYN}) additively reduce food intake. ARC^{POMC} neurons excite PVH^{MC4R} neurons signalling satiety. AgRP = agouti-related protein, ARC = arcuate nucleus of the hypothalamus, CGRP = calcitonin gene related peptide, lPBN = lateral parabrachial nucleus, MC4R = melanocortin 4 receptor, PDYN = prodynorphin, POMC= proopiomelanocortin, PVH = paraventricular nucleus of the hypothalamus.

1.2.2 | Midbrain and Hindbrain circuits controlling food intake

1.2.2.1 | The Nucleus of the Solitary Tract

If the ARC is to be considered the 'entry point' for signals of hunger then the nucleus of the solitary tract (also known as *Nucleus Tractus Solitarii* [NTS], known as the solitary nucleus in humans) is the entry point for internal satiety signals. The NTS is situated in the dorsal portion of the caudal medulla oblongata. Along with the adjacent AP and the dorsal motor nucleus of the vagus (DMX) it is a component of the dorsal vagal complex (DVC). The AP is a circumventricular organ which allows some circulating factors to enter the NTS e.g. hormones, glucose. The DMX is a preganglionic parasympathetic nucleus whose neurons make up the motor (efferent) branch of the vagus nerve.

Neurons in the NTS are uniquely placed to integrate information from the periphery since they receive synaptic input from the facial and vagal cranial nerves. These inputs are roughly topographically ordered with gustatory information from the facial nerve innervating the tongue (chorda timpani branch) projecting to the rostral NTS (rNTS) (J. Zhang *et al.*, 2019) while viscerosensory neurons of the vagus nerves terminate in the postremal and caudal NTS (pNTS and cNTS, respectively) (Chang *et al.*, 2015; Williams *et al.*, 2016; Han *et al.*, 2018; Min *et al.*, 2019). The vagus nerve innervates almost all of the major organ systems in mammals including the majority of the gastrointestinal (GI) tract from the pharynx to the colon (Berthoud and Neuhuber, 2000). Vagal neurons that innervate the stomach and upper intestine terminate in the pNTS and cNTS (Williams *et al.*, 2016; Han *et al.*, 2018; Bai *et al.*, 2019).

Vagal neurons enter the brain in a bundle called the solitary tract (ST) and form glutamatergic synapses with second order NTS neurons (i.e. NTS neurons directly receiving peripheral input from the vagus nerve) (Andresen and Yang,

1990; Doyle and Andresen, 2001). Stimulation of the ST results in short latency, low failure excitatory postsynaptic currents (EPSCs) in second order NTS neurons which show frequency dependent depression and are sensitive to AMPA-R antagonists (Doyle and Andresen, 2001; Doyle *et al.*, 2004). This shows that NTS-terminating vagal afferents have a high probability of glutamate release from large readily-releasable pools that are rapidly depleted.

Ingestion of food results in neuronal activation in the rodent NTS as indicated by c-FOS expression in response to scheduled feeding or binge eating following a fast (Johnstone, Fong and Leng, 2006; Wu *et al.*, 2014). In addition, injection of the gut peptide cholecystokinin (CCK) induces c-FOS expression in the NTS indirectly by excitation of vagal afferent neurons (Fan *et al.*, 2004; Appleyard *et al.*, 2005). Optogenetic activation of stomach and intestine innervating vagal afferent terminals in the NTS reduces food intake providing causal evidence of the sufficiency of this gut to brain pathway to induce satiety (Han *et al.*, 2018). Vagal afferents with sensory receptors in the stomach and upper intestine sense food intake by detection of stomach stretch and intestinal nutrients (Williams *et al.*, 2016; Bai *et al.*, 2019). These neurons terminate in the cNTS and pNTS (Williams *et al.*, 2016; Han *et al.*, 2018; Bai *et al.*, 2019). Accordingly, optogenetic and chemogenetic activation of specific populations of these gut innervating neurons suppresses food intake (Han *et al.*, 2018; Bai *et al.*, 2019). In addition to innervation from the periphery, the NTS receives afferent inputs from a diverse range of brain nuclei, possibly as a negative feedback mechanism (Holt, Pomeranz, *et al.*, 2019).

Given their anatomical location, connectivity to neurons innervating the stomach and activation by food intake it was hypothesised that NTS neuronal firing signals satiety and results in termination of feeding. Indeed, causal evidence using

chemogenetic modulation of genetically and anatomically defined populations of NTS neurons supports this hypothesis, given that these excitatory manipulations all (with one exception) suppress food intake in some form (Zhan *et al.*, 2013; D'Agostino *et al.*, 2016, 2018; Roman, Derkach and Palmiter, 2016; Alhadeff *et al.*, 2017; Gaykema *et al.*, 2017; Roman, Sloat and Palmiter, 2017; Shi *et al.*, 2017; Boychuk *et al.*, 2019; Holt, Richards, *et al.*, 2019; Aklan *et al.*, 2020).

In contrast to the ARC, the organisational logic of neuronal populations in the NTS is not yet clear. Neurons here express a diverse range of neurotransmitters, neuropeptides and neuromodulators (Garfield *et al.*, 2012). The principal populations identified are discussed below but a proper understanding of the neurochemical organisation of NTS neurons is sorely lacking. In future, the application single-cell RNA sequencing (scRNA-seq) to NTS neurons may reveal markers for functionally distinct subgroups.

1.2.2.1.1 | NTS^{TH} neurons

Neurons in the NTS that express tyrosine hydroxylase (TH; NTS^{TH} neurons) have been identified as one of the key NTS neuronal populations involved in mediating satiety. NTS^{TH} neurons co-express the noradrenaline synthesis enzyme dopamine-beta hydroxylase (DBH) meaning these neurons are noradrenergic (Roman, Derkach and Palmiter, 2016). In addition to noradrenaline, they also release glutamate (Roman, Derkach and Palmiter, 2016; Aklan *et al.*, 2020). These neurons are monosynaptically connected to vagal afferents and show a distinctive response to ST stimulation in *ex vivo* slices (Appleyard *et al.*, 2007). Synaptic integration in these neurons is modulated by ghrelin, extracellular glucose concentration, nicotine, serotonin (5-HT) and opioids (Cui, Li and Appleyard, 2011; Cui, Roberts, Zhao, Andresen, *et al.*, 2012; Cui, Roberts, Zhao, Zhu, *et al.*, 2012; Roberts *et al.*, 2017; Page, Zhu and Appleyard, 2018).

Critically these NTS^{TH} neurons express c-FOS in response to scheduled feeding and refeeding after a fast (Johnstone, Fong and Leng, 2006; Roman, Derkach and Palmiter, 2016). Accordingly, their chemogenetic activation produces hypophagia (reduced food intake) (Roman, Derkach and Palmiter, 2016; Aklan *et al.*, 2020). NTS^{TH} neurons mediate their effect on food intake by activating calcitonin gene related peptide (CGRP) expressing neurons in the lPBN ($lPBN^{CGRP}$ neurons) by glutamate release (Roman, Derkach and Palmiter, 2016). Of note, a small population of NTS^{TH} neurons (~20%) do not project to the lPBN and instead have the opposing function and project to the ARC and stimulate ARC^{AgRP} neurons to increase food intake (Aklan *et al.*, 2020). These neurons are glucose-sensitive and utilise this function to drive food intake when blood glucose is low (Aklan *et al.*, 2020). These ARC projecting NTS^{TH} neurons are the first (and to date only) example of NTS neurons which increase food intake.

Within the NTS, NTS^{TH} neurons are subject to modulation from local neurons. For example, NTS^{TH} neurons are excited by chemogenetic activation of NTS neurons expressing CCK (Roman, Derkach and Palmiter, 2016). NTS^{TH} neurons are also recipients of innervation from NTS neurons expressing pre-proglucagon (PPG) which release glucagon-like peptide1 (GLP1) for which NTS^{TH} neurons express the relevant receptor, GLP1-R (Card *et al.*, 2018).

1.2.2.1.2 | NTS^{CCK} neurons

NTS neurons expressing the peptide CKK (NTS^{CCK} neurons) are a distinct population from NTS^{TH} neurons (Roman, Derkach and Palmiter, 2016; Cheng *et al.*, 2020). NTS^{CCK} neurons also show c-FOS immunoreactivity in response to food intake, gastrointestinal amino acid contents and gastrointestinal sucrose (D'Agostino *et al.*, 2016). The synaptic relationship between NTS^{CCK} neurons and vagal afferents is currently unknown and as such it is not clear if these neurons

are second-order (i.e. direct recipients of vagal input) or higher-order (i.e. indirect sensors of satiety signals) viscerosensory neurons. Chemogenetic activation of all NTS^{CCK} neurons or optogenetic stimulation of NTS^{CCK} terminals in the PVH suppresses food intake in a CCK-R dependent manner (D'Agostino *et al.*, 2016; Roman, Derkach and Palmiter, 2016). These neurons also project to $lPBN^{CGRP}$ neurons to suppress food intake (Roman, Derkach and Palmiter, 2016; Roman, Sloat and Palmiter, 2017; Cheng *et al.*, 2020). Optogenetic stimulation of NTS^{CCK} terminals in the lPBN induces short latency, low-jitter, glutamatergic EPSCs in $lPBN^{CGRP}$ neurons showing these neurons directly release glutamate in the lPBN to exert their feeding suppressive effects (Roman, Derkach and Palmiter, 2016). In contrast, the effect of chemogenetic activation of all NTS^{CCK} neurons and optogenetic stimulation of NTS^{CCK} projections to the PVH are mediated, at least in part, by CCK receptors (D'Agostino *et al.*, 2016).

NTS^{CCK} neurons appear to encode some affective properties of food intake since stimulation of NTS^{CCK} terminals in the PVH is rewarding while stimulation of NTS^{CCK} terminals in the lPBN is aversive (D'Agostino *et al.*, 2016; Roman, Sloat and Palmiter, 2017). Stimulation of NTS^{CCK} neurons in general is sufficient to condition avoidance of a paired flavour (conditioned taste aversion), providing further evidence for aversive salience of NTS^{CCK} signals (Cheng *et al.*, 2020). Given the aversive nature of $lPBN^{CGRP}$ neuronal activation (Campos *et al.*, 2018; Palmiter, 2018) and the direct connection with NTS^{CCK} neurons (Roman, Derkach and Palmiter, 2016) it seems likely that the net effect of these neurons' activation produces aversion.

1.2.2.1.3 | NTS^{POMC} neurons

A population of NTS neurons express POMC (NTS^{POMC}). Similarly to NTS^{TH} neurons, NTS^{POMC} neurons express c-FOS in response to food intake and CCK

administration (Fan *et al.*, 2004; Appleyard *et al.*, 2005). NTS^{POMC} neurons are monosynaptically connected to vagal afferents (Appleyard *et al.*, 2005). Chemogenetic activation of NTS^{POMC} suppresses food intake on a shorter time scale (2 -8 hours) to their hypothalamic (ARC^{POMC}) counterparts (24 hours) (Zhan *et al.*, 2013). Chemogenetic activation of NTS^{POMC} neurons induces c-FOS expression in both NTS^{POMC} and NTS-POMC negative neurons, suggesting these cells send local, excitatory projections (Zhan *et al.*, 2013).

Their function seems to be diverse; in a second study chemogenetic activation of NTS^{POMC} neurons resulted in cardiorespiratory depression (indicative of an increase in parasympathetic tone) and analgesia mediated by endogenous opioids (β-endorphin is another cleavage product of the POMC prohormone) (Cerritelli *et al.*, 2016). This led the authors to propose NTS^{POMC} as autonomic 'output' neurons of the NTS given these observed effects and the finding that NTS^{POMC} neurons send selective projections to a diverse range of brainstem targets including the lPBN (D. Wang *et al.*, 2015; Cerritelli *et al.*, 2016). It appears that POMC (and its cleavage products) are essential for the initial phase of hypophagia induced by injection of a 5-$HT2_C$-R agonist lorcaserin since deletion of the POMC protein from the NTS removes this effect (D'Agostino *et al.*, 2018). This shows that POMC cleavage products are at least one of the transmitters used by this group of cells.

1.2.2.1.4 | NTS^{PPG} neurons

The NTS is also home to a unique population of neurons expressing preproglucagon (PPG; NTS^{PPG} neurons). PPG is a prohormone that can be cleaved by prohormone convertase to yield GLP1. In the periphery GLP1 is released from enteroendocrine cells in the GI tract to excite GLP1-R expressing vagal afferents in response to a meal (reviewed in Cork, 2018). Owing to its short

half-life, peripheral GLP1 likely does not reach the brain making NTS^{PPG} neurons the sole source of GLP1 in the central nervous system (CNS) (Kieffer, Mc Intosh and Pederson, 1995; Holt, Richards, *et al.*, 2019). Given that the GLP1-R is widely expressed in the brain these neurons likely have diverse functions although this remains to be conclusively demonstrated (Cork *et al.*, 2015). Similar to all NTS neuronal populations described previously, chemogenetic activation of NTS^{PPG} neurons suppresses food intake under normal conditions, after a fast, in obese mice and in the presence of palatable food (Gaykema *et al.*, 2017; Shi *et al.*, 2017; Holt, Richards, *et al.*, 2019). Activation of NTS^{PPG} neurons also improves glucose tolerance, likely through modulation of neuronal populations controlling hepatic glucose production (Holt, Richards, *et al.*, 2019).

Similarly to NTS^{CCK} neurons the synaptic relationship of NTS^{PPG} neurons to vagal afferents is unknown; however, Cre-mediated monosynaptic rabies retrograde viral tracing from NTS^{PPG} neurons does yield labelling in vagal sensory neurons indicating at least some of this population are second order interoceptive neurons (Holt, Pomeranz, *et al.*, 2019). NTS^{PPG} project to the PVH and ARC where their activation induces c-FOS expression (Llewellyn-Smith *et al.*, 2011; Gaykema *et al.*, 2017; Shi *et al.*, 2017). In turn, selective chemogenetic activation of $PVH^{GLP1\text{-}R}$ neurons reduces food intake while chronic silencing with TeLC leads to the development of obesity, illustrating the importance of GLP1 signalling in satiety (C. Li *et al.*, 2019).

The presence of projections from NTS^{PPG} neurons to the ventral tegmental area (VTA) and nucleus accumbens (NAc) suggests that NTS^{PPG} neurons may encode the rewarding nature of food intake (Llewellyn-Smith *et al.*, 2011; Alhadeff, Rupprecht and Hayes, 2012). In support of this, delivery of a GLP1-R agonist or

antagonist to the NAc or VTA reduces or increases intake of palatable food, respectively (Alhadeff, Rupprecht and Hayes, 2012).

1.2.2.1.5 | NTS^{GABA} neurons

The NTS also contains inhibitory GABAergic neurons (NTS^{GABA}). These neurons again are monosynaptically connected to viscerosensory vagal afferents (Bailey *et al.*, 2008). NTS^{GABA} neurons are activated by low extracellular glucose and project to preganglionic motor neurons in the DMX, marked by expression of choline acetyltransferase (ChAT; DMX^{ChAT} neurons) (Boychuk *et al.*, 2015). The effects of chemogenetic activation of NTS^{GABA} neurons on food intake has not been described. However, their activation does cause an elevation in blood glucose *via* inhibition of DMX^{ChAT} neurons (Boychuk *et al.*, 2019).

A sub-population of NTS^{GABA} neurons co-express the peptide somatostatin (SST) although not all NTS^{SST} neurons are GABAergic (Thek *et al.*, 2019). These NTS^{SST} neurons are synaptically excited by ST stimulation and provide local inhibition to other NTS neurons to precisely gate synaptic transmission *via* feedforward inhibition (Thek *et al.*, 2019).

1.2.2.1.6 | NTS neurons expressing receptors for peripheral cues

In addition to these populations identified by their neuropeptide expression, a number of NTS neuronal populations identified by expression of specific receptors also contribute to food intake suppression. The glial cell-derived neurotrophic factor receptor alpha-like (GFRAL) is exclusively expressed in the NTS and AP and is the target of growth and differentiation factor 15 (GDF15), a known hypophagia-inducing stimulus produced by damaged tissue (Zimmers *et al.*, 2005; Hsu *et al.*, 2017). GFRAL knockout mice show increased weight gain on a high fat diet compared with wild type controls and are resistant to

hypophagia induced by cisplatin, a chemotherapy agent. When GFRAL neurons are activated by GDF15, c-FOS expression is observed in the DVC and additionally in the lPBN and CeA; centres controlling satiety and aversion, respectively (Carter *et al.*, 2013; Hsu *et al.*, 2017). In addition, administration of GDF15 alongside a novel food is sufficient to cause avoidance of that food on subsequent exposures (Patel *et al.*, 2019). It has therefore been suggested that this GDF15-GFRAL system mediates the nausea and hypophagia induced by peripheral tissue damage (Hsu *et al.*, 2017).

Leptin, the adipose derived hormonal signal reflecting body fat mass, appears to exert part of its satiating effect by direct action on neurons in the NTS. Peripheral leptin administration induces phospho-signal transducer and activator of transcription 3 (pSTAT3) immunoreactivity in NTS^{POMC} neurons, in addition to other unidentified NTS neurons in mice (Ellacott, Halatchev and Cone, 2006). pSTAT3 is a second messenger downstream of LepRb indicating the direct action of peripheral leptin in the NTS. LepRb are expressed on NTS^{POMC}, NTS^{PPG} and NTS^{CCK} neurons and notably are absent from NTS^{TH}, NTS^{GABA} and DMX^{ChAT} neurons, indicating that its expression is not a uniform feature of NTS neurons (Garfield *et al.*, 2012). Functionally, delivery of leptin to either the fourth ventricle (4V) or DVC reduces food intake in rats (Grill *et al.*, 2002). Conversely, genetic deletion of the leptin receptor mRNA or gene from the DVC increases food intake and weight gain on a high fat diet in rats and mice, respectively (Hayes *et al.*, 2010; Scott *et al.*, 2011). Taken together this shows the NTS and wider DVC are a crucial site of action for leptin.

A population of NTS neurons also express the calcitonin receptor (Calc-R [$NTS^{Calc\text{-}R}$]) and deletion of this receptor from the mouse NTS abolishes the satiating but not the aversive effect of peripheral calcitonin injection (Cheng *et al.*,

2020). Around 25% of cells expressing Calc-R in the NTS are NTS^{TH} cells, but CalcR is absent from NTS^{CCK} cells and NTS cells expressing the LepRb. Chemogenetic activation of NTS^{CalcR} neurons reduces food intake and activates non-CGRP expressing lPBN neurons. Conversely, their chronic inhibition by expression of TeLC attenuates c-FOS activation and hypophagia induced by vagally acting agents (CCK and the GLP1-R agonist exendin-4). Their inhibition in this fashion also increases weight gain on a high-fat diet (Cheng *et al.*, 2020).

Finally, it has been shown that NTS neurons directly sense nutrients in the form of amino acids and extracellular glucose (Blouet and Schwartz, 2012; Lamy *et al.*, 2014). This nutrient sensing acts to suppress appetite and sensing is impaired following consumption of a high fat diet (Blouet and Schwartz, 2012; Cavanaugh, Schwartz and Blouet, 2015). In contrast, sensing of local hyperglycaemia drives hepatic glucose production and glucoprivic feeding (Lamy *et al.*, 2014; Boychuk *et al.*, 2019; Aklan *et al.*, 2020).

Taken together these studies indicate that the NTS is populated by neurons that integrate nutritional, hormonal and vagal afferent cues from the periphery and signal these to local DMX^{CHAT} neurons to modulate autonomic outflow and higher brain centres to suppress food intake (**Figure 1.2.2**). One of the most consistent projection targets of NTS satiety signalling neurons is the lPBN where they engage both $lPBN^{CGRP}$ and non-CGRP neurons to suppress food intake.

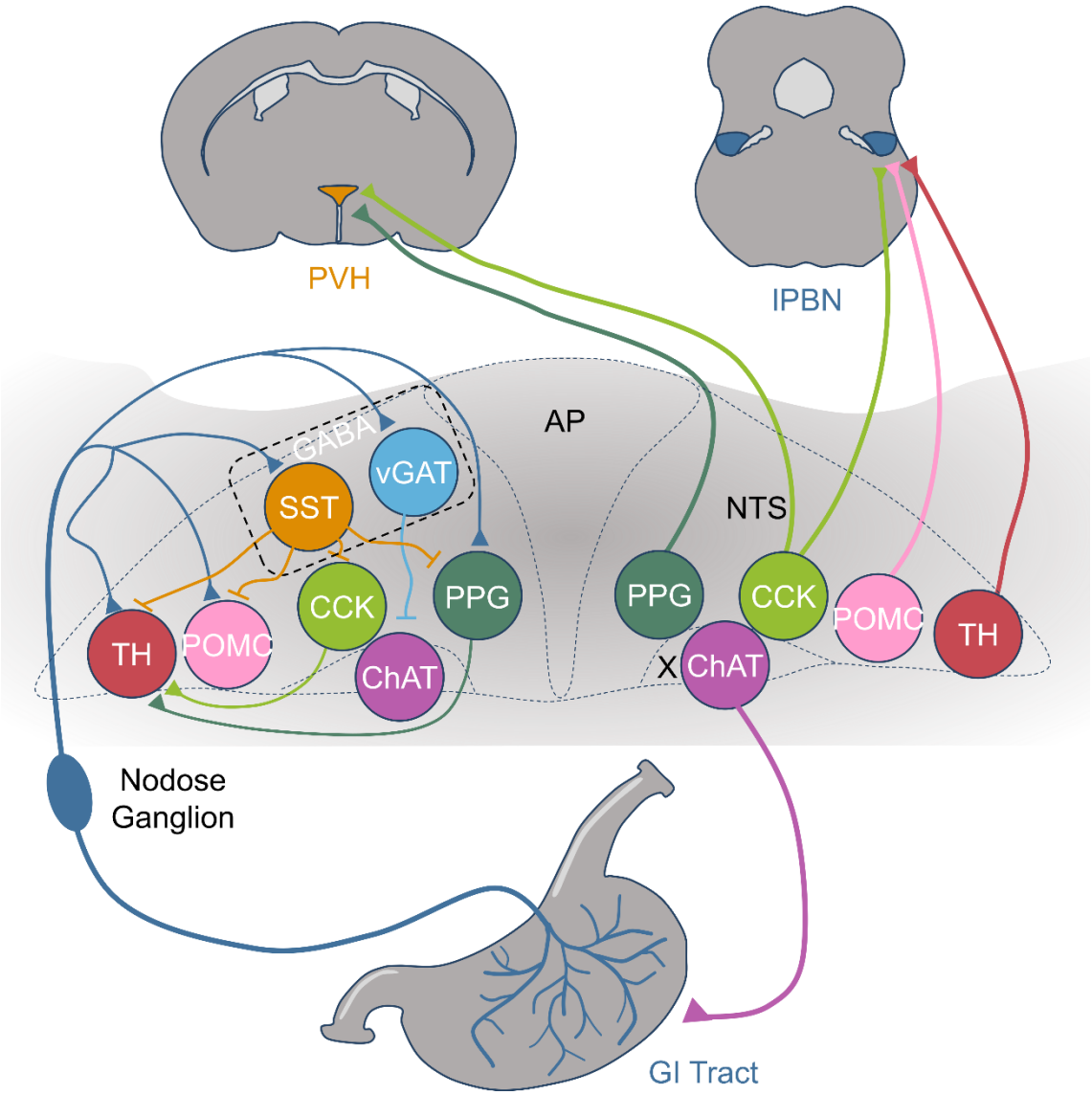

Figure 1.2.2 | A simplified schematic diagram of the neurochemical organisation of appetite controlling populations in the NTS. For simplicity the left portion of the nucleus shows representative vagal inputs and local microcircuitry while the right portion of the nucleus shows representative long range projections shown to suppress food intake and modulate digestion. AP = area postrema, CCK = cholecystokinin, ChAT = choline acetyl transferase, GI = gastrointestinal, lPBN = lateral parabrachial nucleus, NTS = nucleus of the solitary tract, POMC = proopiomelanocortin, PPG = preproglucagon, PVH = paraventricular nucleus of the hypothalamus, TH = tyrosine hydroxylase, SST =

somatostatin, X = dorsal motor nucleus of the vagus, VGAT = vesicular gamma-amino-butric acid transporter.

1.2.2.2 | The Lateral Parabrachial Nucleus

Within the midbrain the lPBN is located lateral to the superior cerebellar peduncle, close to the locus coeruleus. As described above it is the major direct projection target of NTS neurons including NTS^{TH}, NTS^{CCK} and NTS^{POMC} in addition to non-identified NTS neurons that receive input from the gut (D. Wang *et al.*, 2015; Cerritelli *et al.*, 2016; Roman, Derkach and Palmiter, 2016; Han *et al.*, 2018; Bai *et al.*, 2019). The best characterised neurons in the lPBN are identified by the expression of CGRP ($lPBN^{CGRP}$ neurons) (Carter *et al.*, 2013; Palmiter, 2018). Of note, these neurons receive glutamatergic inputs from the NTS in mice and rats (Roman, Derkach and Palmiter, 2016; Alhadeff *et al.*, 2017). $lPBN^{CGRP}$ neurons are bi-directionally connected to forebrain regions including the hypothalamus, CeA and bed nucleus of the stria terminalis (BNST) leading to the view that they relay information from the NTS to the forebrain and in return are modulated by the same forebrain regions (Palmiter, 2018). $lPBN^{CGRP}$ neurons express c-FOS following food intake or intraperitoneal injection of anorexia inducing stimuli lipopolysaccharide (LPS) and lithium chloride (LiCl) (Carter *et al.*, 2013; Campos *et al.*, 2016). In turn, chemogenetic activation of $lPBN^{CGRP}$ neurons reduces food intake while their chemogenetic inhibition preserves food intake in situations where it is normally reduced (e.g. after injection LiCl or LPS, or AgRP neuron ablation) (Carter *et al.*, 2013; Campos *et al.*, 2016).

As mentioned above, optogenetic stimulation of NTS neuronal terminals or chemogenetic activation of lPBN-projecting NTS neurons reduces food intake *via* glutamatergic neurotransmission in mice and rats (Roman, Derkach and Palmiter, 2016; Alhadeff *et al.*, 2017). These NTS populations relay satiety signals from the gut since chemogenetic activation of gut innervating mechanoreceptor neurons induces c-FOS expression in $lPBN^{CGRP}$ neurons (Bai

et al., 2019). The satiety signal generated by CGRP neurons appears to encode negative valence since pairing of optogenetic stimulation of CGRP neurons with a novel food causes avoidance of that food (conditioned taste aversion) and in turn their inhibition with chemogenetics or TeLC attenuates LiCl-mediated conditioned taste aversion (Carter, Han and Palmiter, 2015). They are thought to encode this negative valence by projections to the CeA (Campos *et al.*, 2016).

In addition to this 'bottom-up' signalling from the NTS, the lPBN is also subject to 'top-down' input from forebrain regions to regulate appetite (Campos *et al.*, 2016). ARC^{AgRP} neurons provide direct GABAergic input to $lPBN^{CGRP}$ neurons (Wu, Boyle and Palmiter, 2009). When ARC^{AgRP} neurons are chemically ablated in adult mice these animals cease to eat (Luquet *et al.*, 2005). In mice with ARC^{AgRP} neuronal ablation, $lPBN^{CGRP}$ neurons are hyper-excited, an effect which is rescued by delivery of GABA receptor agonists to the lPBN (Wu, Boyle and Palmiter, 2009). This intervention also restores feeding in these mice (Wu, Boyle and Palmiter, 2009). Secondly, optogenetic stimulation of AgRP terminals in the lPBN prolongs meal length (Campos *et al.*, 2016). Optogenetic stimulation of ARC^{AgRP} terminals in the PBN is sufficient to overcome the hypophagia induced by exogenous administration of CCK, amylin and LiCl (Essner *et al.*, 2017). These studies indicate that this ARC to lPBN projection exists to inhibit $lPBN^{CGRP}$ neuron activity which permits food intake.

It appears that reductions in $lPBN^{CGRP}$ neuron activity are permissive for food intake since the $[Ca^{2+}]_i$ of individual $lPBN^{CGRP}$ neurons is reduced immediately prior to food intake (Campos *et al.*, 2018). Consistent with a role in satiety, $[Ca^{2+}]_i$ of these cells gradually increases with food intake which precedes meal termination (Campos *et al.*, 2018). Finally, the activity of $lPBN^{CGRP}$ is lower following a fast, presumably due to increased inhibitory input from ARC^{AgRP} and

reduced excitatory drive from the NTS (Campos *et al.*, 2018). This shows that lPBN^{CGRP} neurons are modulated by bottom-up (i.e. NTS) and top-down (i.e. hypothalamic) signals to permit or suppress feeding.

The lPBN also contains many CGRP-negative neurons which have also been shown to regulate appetite. As discussed above PVH^{MC4R} neurons project to the lPBN to reduce food intake but these neurons make no connection to lPBN^{CGRP} neurons (Garfield *et al.*, 2015). In keeping with this, PVH^{MC4R} lPBN terminal activation is rewarding to hungry mice which suggests a population of appetite controlling lPBN neurons (independent of lPBN^{CGRP}) that encode positive valance (Garfield *et al.*, 2015). In support of this suggestion, NTS$^{Calc\text{-}R}$ neurons do not mediate aversion and terminate in the lPBN outside areas of CGRP immunoreactivity while NTS^{CCK} neurons whose chemogenetic activation can induce conditioned taste aversion terminate within the CGRP immunoreactive portion of the lPBN (Cheng *et al.*, 2020). Similarly, reward-encoding NTS neurons (recipients of input from reward signalling vagal sensory neurons, see below) terminate outside the CGRP immunoreactive portion of the lPBN, these lPBN neurons project to midbrain dopamine neurons to encode rewarding properties of food intake (Han *et al.*, 2018). The interaction of pathways regulating reward and aversion in food intake is an area of growing interest (Rossi and Stuber, 2018).

1.2.3 | Peripheral circuits

1.2.3.1 | Vagal Sensory Neurons of the Nodose Ganglia

As discussed above, vagal sensory neurons are key to relaying information from the periphery to the brain. In rodents, these neurons account for roughly 80% of vagal fibres, the other 20% being pre-ganglionic parasympathetic neurons in the DMX and nucleus ambiguus (Berthoud and Neuhuber, 2000). These neurons

obey a pseudounipolar morphology and have cell bodies located outside the brain in the nodose ganglia (NG), a bilateral structure located near the jugular vein. In most mammalian species vagal sensory neurons monitor the majority of organ systems including the heart, lungs and digestive tract (Berthoud and Neuhuber, 2000). The activity of chemosensory vagal afferents is regulated by gut-derived hormones, their activity is increased by post prandial signals such as CKK, GLP1 and 5-HT and inhibited by ghrelin (Date *et al.*, 2002; Chambers, Sandoval and Seeley, 2013).

With the advent of genetic technologies, vagal sensory neurons are beginning to be understood in unprecedented detail. Of relevance to this discussion are primarily vagal sensory neurons which innervate the stomach and intestine. In a seminal study, Williams *et al* described two distinct populations of vagal sensory neurons marked by differential expression of two receptors, GLP1-R and GPR65 (Williams *et al.*, 2016). $NG^{GLP1\text{-}R}$ neurons were found to preferentially innervate the stomach and were predominantly mechanosensory, responding to physical distension of the stomach. In contrast NG^{GPR65} neurons innervate the upper intestine and are chemosensory, responding to nutrients. The projection patterns of both populations were mapped and were shown to predominantly terminate in overlapping domains in the pNTS. In functional studies, it was shown that optogenetic stimulation of these populations modulated gastric motility suggesting these neurons drive vago-vagal reflexes controlling digestion (Williams *et al.*, 2016).

A complementary approach using intersectional viral labelling has allowed for stomach innervating vagal sensory neurons to be identified independent of genetic identity (Han *et al.*, 2018). This study revealed a stark lateralisation of the termination fields of these neurons with those in the right NG terminating broadly

in the pNTS while those of the left NG send restricted projections to the AP. Although interesting, in the absence of independent replication it is unclear whether this represents a true lateralisation or a methodological artefact of the position of 'starter' virus injections into the stomach and intestine. This study also demonstrated causal evidence of the sufficiency of these neurons to induce satiety by optogenetic activation of stomach innervating NG neural terminals in the NTS. This stimulation reduced food intake and produced conditioned place preference showing that this connection serves to signal satiety and positive affective properties of ingested food. NTS neurons receiving input from stomach innervating NG neurons were found to project onwards to the lPBN, PVH and the midbrain dopamine system (Han *et al.*, 2018).

ScRNA-seq has revealed 18 distinct clusters of vagal sensory neuron, each with differential expression of genes involved in signal transduction (Kupari *et al.*, 2019). This suggests that vagal neurons are highly specialised and modality-specific in contrast to other, more 'generic' sensory neurons (e.g. jugular ganglion neurons) (Kupari *et al.*, 2019).

ScRNA-seq has also been utilised and combined with functional techniques to better understand the specialisation of NG neurons innervating the GI tract and their role in feeding (Bai *et al.*, 2019). This, study examined the genetic profiles of cells innervating specific targets in the GI tract and selected four populations for further validation. Of these, chemogenetic activation of GLP1-R or oxytocin receptor (OXTR)-expressing vagal neurons or optogenetic activation of their terminals in the NTS was sufficient to suppress food intake in fasted mice. Both receptor-defined subtypes label mechanosensory neurons innervating the stomach and intestine, respectively. Activation of chemosensory Gpr65 or vasoactive intestinal polypeptide (VIP) expressing neurons in the same fashion

did not suppress food intake, suggesting that the main signal for satiety is physical distention of the stomach and intestine. In support of this, chemogenetic activation of GLP1-R and OXTR expressing NG cells induced c-FOS expression in TH and non-TH neurons of the NTS and CGRP and non-CGRP neurons in the lPBN, in addition to rapidly inhibiting ARC^{AgRP} neurons.

This shows that stomach and intestine innervating vagal sensory neurons exert potent bottom-up signalling to both stimulate satiety circuits and inhibit hunger circuits. Since the only projection target of these neurons is the NTS, the NTS must be the principal brain centre mediating these effects.

1.2.4 | An ARC^{AgRP} hunger-based framework of central appetite control

It is helpful here to summarise the wealth of evidence describing neural control of food intake into a conceptual framework of appetite regulation where hunger, and its suppression are the primary drivers and inhibitors of food intake (**Figure 1.2.3**). From the evidence discussed above we arrive at a model in which ARC^{AgRP} neurons drive hunger by direct inhibition of PVH^{SIM1} and $lPBN^{CGRP}$ neurons (Atasoy *et al.*, 2012; Essner *et al.*, 2017; M. M. Li *et al.*, 2019). In addition, excitatory inputs from the NTS to $lPBN^{CGRP}$ neurons are presumably reduced in times of hunger owing to reduced GI-derived vagal input and active suppression by ghrelin (Date *et al.*, 2002; Cui, Li and Appleyard, 2011). Thus, ARC^{AgRP} neurons exert a potent 'brake' on $lPBN^{CGRP}$ excitability in times of hunger, which in the absence of excitatory drive from the NTS is unopposed (Campos *et al.*, 2016). Furthermore, ARC^{AgRP} neurons project to other brain nuclei to suppress other behaviours and competing needs to ensure food seeking is prioritised (Burnett *et al.*, 2016; Padilla *et al.*, 2016; Alhadeff *et al.*, 2018; Goldstein *et al.*, 2018; X.-Y. Li *et al.*, 2019).

Once food is found/presented, ARC^{AgRP} activity is rapidly reduced by top-down sensory processing (Betley *et al.*, 2015; Chen *et al.*, 2015). For this to persist, food must be ingested (Beutler *et al.*, 2017; Su, Alhadeff and Betley, 2017). $lPBN^{CGRP}$ neurons reduce their activity immediately prior to feeding indicating this is permissive to food intake (Campos *et al.*, 2018). Presumably this pre-ingestive inhibition is mediated by the second phase of ARC^{AgRP} activation following detection but before ingestion (Beutler *et al.*, 2017; Su, Alhadeff and Betley, 2017).

Once food is eaten, mechanosensory neurons innervating the stomach and intestine excite neurons of the NTS which in turn excite lPBN neurons (including $lPBN^{CGRP}$) and, by an unknown circuit, inhibit ARC^{AgRP} (Beutler *et al.*, 2017; Su, Alhadeff and Betley, 2017; Han *et al.*, 2018; Alhadeff *et al.*, 2019a; Bai *et al.*, 2019). $lPBN^{CGRP}$ neuron activity accumulates throughout a meal, presumably driven by increased NTS input, and once a certain threshold is reached feeding is terminated (Campos *et al.*, 2018).

In this model the main driver of food intake is ARC^{AgRP} neuron activity which is unopposed during hunger. During the switch to satiety, signals from the NTS dominate, inhibiting ARC^{AgRP} and providing excitation to the PVH and lPBN to suppress hunger and reduce further food intake. This illustrates the importance of NTS satiety signalling since in the absence of this pathway, the sole focus of an animal would be food intake and seeking regardless of how much energy was already ingested.

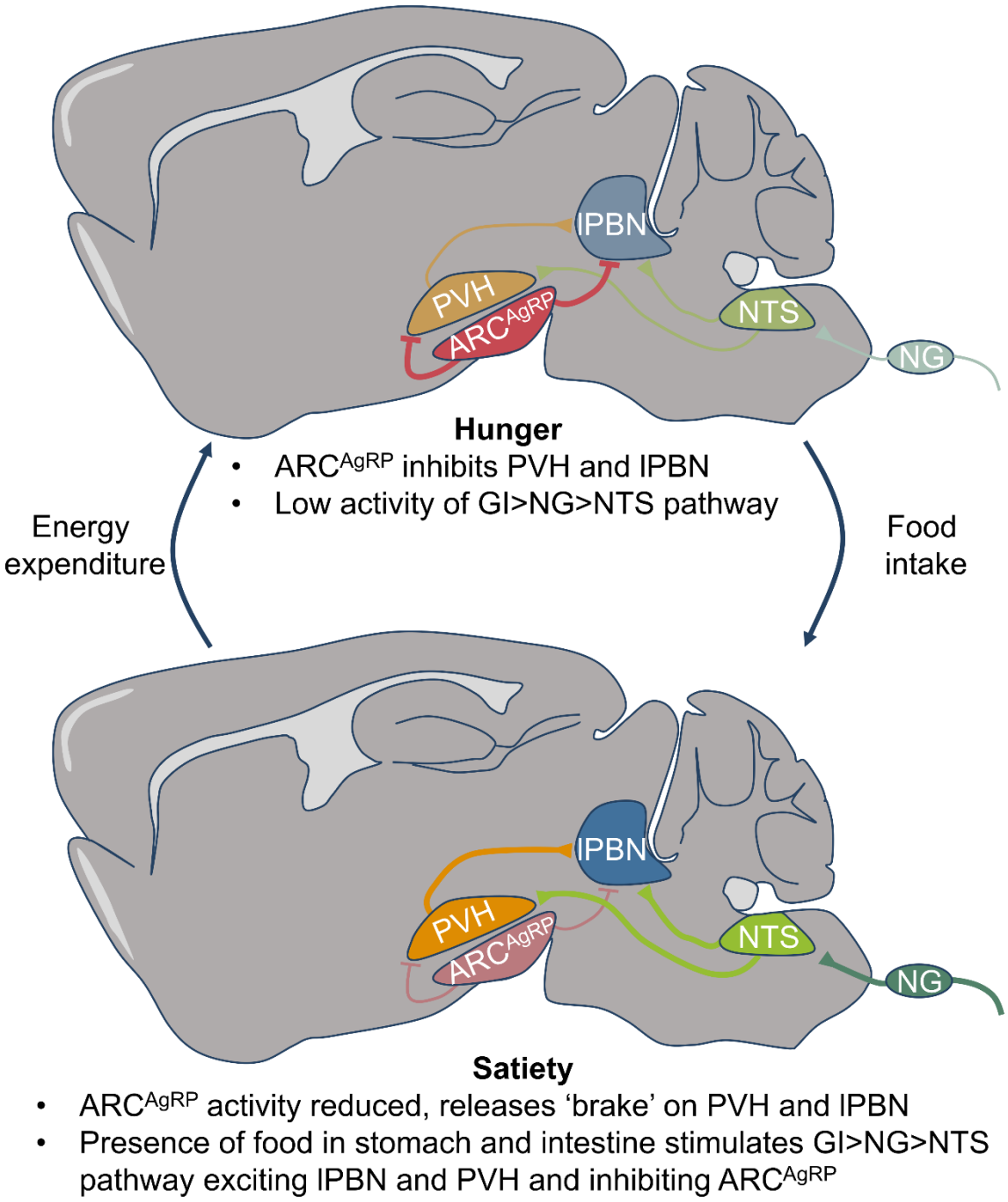

Figure 1.2.3 | Brain circuits engaged by hunger and satiety. In a state of hunger ARC^{AgRP} neurons are active and inhibiting anorexigenic neurons in the PVH and lPBN. There is a low level of input from GI-tract innervating NG neurons to the NTS and thus the ARC^{AgRP} signal dominates, inhibiting the other circuit nodes. Upon food intake NG neurons sense gastric and intestinal stretch and, in turn, excite neurons of the NTS. NTS neurons reduce further food intake *via* projections to the PVH and lPBN. In addition, ARC^{AgRP} are rapidly inhibited

following ingestion in a vagal (and therefore NTS) dependent fashion *via* an unknown circuit reducing inhibition into PVH and lPBN. Therefore, with increased NTS tone and decreased ARC^{AgRP} activity the satiety signal prevails. AgRP = agouti related protein, ARC = arcuate nucleus of the hypothalamus, lPBN = lateral parabrachial nucleus, NG = nodose ganglion, NTS = nucleus of the solitary tract, PVH = paraventricular nucleus of the hypothalamus.

1.3 | Astrocytes

In addition to neurons, the CNS consists of neuroepithelium-derived macroglia and mesoderm-derived microglia. Of the macroglia, astrocytes and oligodendrocytes are the predominant cell types. Oligodendrocytes principally myelinate axons but can also actively communicate with neurons to ensure energy demands of axons are met (Saab *et al.*, 2016). Astrocytes differentiate from neural progenitor cells late in prenatal development (i.e. after neurogenesis, E10-E16 in mice) and continue to populate the CNS in early postnatal development (Molofsky and Deneen, 2015). They likely evolved to meet the increased homeostatic and information processing demand of an expanding nervous system since their number and functions become greater as the complexity of the brain increases (Nedergaard, Ransom and Goldman, 2003; Oberheim *et al.*, 2006). Under normal conditions astrocytes tightly control the CNS microenvironment by transport and buffering of ions and neurotransmitters (Verkhratsky and Nedergaard, 2016). In cases of brain injury or disease astrocytes adopt an inflammatory phenotype induced by factors secreted from microglia, the brain's resident macrophages (Liddelow *et al.*, 2017). This appears to be a maladaptive response since inflamed astrocytes lose their homeostatic functions and promote cell death (Liddelow *et al.*, 2017; Yun *et al.*, 2018).

Astrocytes are highly ramified glial cells that tile the entire CNS and provide structural and metabolic support to neurons. They have small cell bodies relative to neurons and typically have ~5 primary processes which highly ramify into numerous small processes that contact individual synapses (Ogata and Kosaka, 2002; Reeves, Shigetomi and Khakh, 2011; Shigetomi *et al.*, 2013). As a result, astrocytes occupy a very large volume (or territory) and have minimal overlap with other astrocytes, although this varies between brain regions (Ogata and

Kosaka, 2002; SheikhBahaei *et al.*, 2018). In addition to contacting neuronal synapses, astrocyte processes can contact cerebral blood vessels. These processes are referred to as 'endfeet'. Because of this feature, astrocytes are uniquely positioned to contact both synapses and the circulation and have been proposed to mediate neurovascular coupling (Zonta *et al.*, 2003). However, *in vivo* evidence does not fully support this since observed and evoked $[Ca^{2+}]_i$ events in astrocytes do not alter blood vessel diameter in the mouse visual cortex (Bonder and McCarthy, 2014)

1.3.1 | Homeostatic functions of astrocytes

The best described and understood functions of astrocytes are to maintain ionic and chemical homeostasis in the brain.

For example, one of the main functions of astrocytes is the transport of glutamate from the synaptic cleft (Bak, Schousboe and Waagepetersen, 2006). This maintains glutamate levels within a narrow range to prevent excitotoxicity and preserve the tight temporal fidelity of synaptic transmission. Astrocytes express two excitatory amino acid transporters (EAATs). EAAT1 (also known as glutamate-aspartate transporter [GLAST]) is predominantly expressed in the cerebellum and circumventricular regions. EAAT2 (also known as glutamate transporter 1 [GLT-1]) is the major glutamate transporter in the majority of the brain parenchyma (Lehre *et al.*, 1995). Once transported into the astrocyte, glutamate is rapidly metabolised to glutamine by glutamine synthetase (GS) which can then be returned to the presynaptic neuron by low affinity transporters (van den Berg and Garfinkel, 1971; Martinez-Hernandez, Bell and Norenberg, 1977). In the presynaptic neuron glutamine is metabolised back to glutamate and can be repackaged into synaptic vesicles and released again. This is known as the glutamate-glutamine shuttle (Erecinska and Silver, 1990).

Astrocytes are also believed to be the predominant source of lactate in the brain. Astrocytes and neurons have distinct cellular metabolism. Astrocytes express an enzyme 6-phosphofructo-2-kinase (Pfkfb3), which regulates metabolism of glucose by glycolysis (Herrero-Mendez *et al.*, 2009). This provides lactate as a fuel for the tricarboxylic acid cycle. Pfkfb3 is absent from neurons explaining their low glycolytic rate; neurons cannot utilise glycolysis even under cellular stress (Herrero-Mendez *et al.*, 2009). Under normal conditions neurons utilise oxidative phosphorylation to generate ATP (Bélanger, Allaman and Magistretti, 2011).

Due to this apparent cellular compartmentalisation of glucose metabolism within the brain, a model has emerged of energetic support of neurons by astrocytes termed the astrocyte-neuron lactate shuttle (ANLS) (Pellerin *et al.*, 1998; Pellerin and Magistretti, 2012). According to the ANLS model, astrocytes are able to take up circulating glucose *via* glucose transporters (GLUT) expressed on vessel-contacting endfeet. This glucose is then metabolised to lactate in the astrocyte before being released *via* monocarboxylate transporters (MCT) and absorbed by neurons and used for cellular fuel. This model was (Chih, Lipton and Roberts, 2001) and remains a subject of controversy (Bak and Walls, 2018; Barros and Weber, 2018).

1.3.2 | Ca^{2+} ionic signalling

Astrocytes are not generally considered electrically excitable cells since they have a hyperpolarised resting membrane potential and show a roughly linear membrane potential changes in response to current steps (Lalo *et al.*, 2006; Panatier *et al.*, 2011). This meant for some time that they were ignored as signalling cells within the brain. However, with concurrent advances in fluorescent Ca^{2+} imaging and astrocyte cell culture in the 1990s it was discovered that in fact astrocytes increase their $[Ca^{2+}]_i$ in response to exogenously applied glutamate

(Cornell-Bell *et al.*, 1990). This finding, initially shown *in vitro,* has since been demonstrated in *ex vivo* brain slices and crucially *in vivo* in response to sensory stimulation in mice (Porter and McCarthy, 1996; Wang *et al.*, 2006). Thus, this provides an ionic mechanism by which astrocytes can sense local synaptic activity and raises the possibility that these Ca^{2+} signals drive a response.

Since this initial discovery astrocytes in various brain regions have been shown to express receptors for, and increase $[Ca^{2+}]_i$ in response to, almost all known neurotransmitters including the 'fast' transmitters glutamate (Wang *et al.*, 2006) and GABA (MacVicar *et al.*, 1989). In addition astrocytes have also been shown to respond to neuromodulators such as dopamine (Vaarmann, Gandhi and Abramov, 2010; Jennings *et al.*, 2017), 5-HT (Schipke, Heuser and Peters, 2011), acetylcholine (Araque *et al.*, 2002) and noradrenaline (Duffy and MacVicar, 1995; Ding *et al.*, 2013) and non-canonical transmitters like endocannabinoids (Martín *et al.*, 2015).

Astrocyte Ca^{2+} signalling appears to operate over a diverse range of activity (Volterra, Liaudet and Savtchouk, 2014; Bazargani and Attwell, 2016). Large Ca^{2+} transients in the soma and major processes of astrocytes are thought to be downstream of Gq-GPCR activation and inositol trisphosphate (IP_3) production. Activation of Gq-GPCRs on astrocytes with a cocktail of agonists for metabotropic glutamate receptors (mGlu-R), histamine receptors and muscarinic acetylcholine receptors (mACh-R) induces IP_3 production (Petravicz, Fiacco and McCarthy, 2008). This activates release of Ca^{2+} from intracellular stores via IP_3 receptors type 2 (IP_3R2) (Petravicz, Fiacco and McCarthy, 2008). Spontaneous and ATP-evoked somatic Ca^{2+} elevations are greatly reduced in IP_3R2 knock out mice while there are no clear alterations in synaptic transmission, neurovascular coupling or performance in laboratory behavioural tasks (Petravicz, Fiacco and

McCarthy, 2008; Nizar *et al.*, 2013; Bonder and McCarthy, 2014; Petravicz, Boyt and McCarthy, 2014). However, this model is a germline knockout model which may have some developmental compensatory effects versus an inducible knockout model (El-Brolosy and Stainier, 2017).

In addition to this large-scale slow activity, rapid Ca^{2+} transients have been observed in microdomains of fine astrocyte process and can occur independently of somatic activity and other microdomains (Kanemaru *et al.*, 2014). This desynchronised, focal activity persists in IP_3R2 knockout mice (although with a lower amplitude than wild type) and is therefore mechanistically distinct from larger, global transients to some degree (Kanemaru *et al.*, 2014; Srinivasan *et al.*, 2015). These focal events are observed in response to sensory and synaptic stimulation implicating them in neural information processing (Srinivasan *et al.*, 2015; Bindocci *et al.*, 2017). It has been proposed that focal Ca^{2+} events in astrocytes summate to drive larger global events in a manner analogous to the summation of excitatory postsynaptic potentials (EPSPs) to action potentials in neurons (Kanemaru *et al.*, 2014; Bazargani and Attwell, 2016). A second interesting suggestion is the possibility that astrocytes integrate local synaptic activity (represented by focal events) and neuromodulatory tone (driven by activation of GPCRs and global events) and act as coincidence detectors or relay neuromodulatory signals to active synapses (Bazargani and Attwell, 2017; Papouin, Dunphy, *et al.*, 2017). Therefore it appears that $[Ca^{2+}]_i$ signalling in astrocytes consists of a diverse range of signalling in individual micro domains and slower signalling in the soma and across the whole cell (Volterra, Liaudet and Savtchouk, 2014; Bazargani and Attwell, 2016).

1.3.3 | Gliotransmission and synaptic modulation

Along with an appreciation for astrocyte Ca^{2+} dynamics came the concept of 'gliotransmission'. Gliotransmission refers to the process whereby astrocytes respond to synaptic transmission (e.g. glutamate) by elevating $[Ca^{2+}]_i$ which causes the release (*via* vesicular transmission) of neuroactive molecules (termed gliotransmitters) that modulate transmission at the synapse (Nedergaard, 1994; Parpura *et al.*, 1994; Araque *et al.*, 1999, 2014; Mothet *et al.*, 2005). Further studies showed mixed evidence for the existence of gliotransmission under physiological conditions (Hamilton and Attwell, 2010; Fiacco and McCarthy, 2018). For this reason, gliotransmission remains controversial and is publicly debated in the pages of Trends in Neurosciences (Wolosker, Balu and Coyle, 2016, 2017; Papouin, Henneberger, *et al.*, 2017) and The Journal of Neuroscience (Fiacco and McCarthy, 2018; Savtchouk and Volterra, 2018).

Despite this controversy there is good evidence that astrocytes release or control extracellular levels of glutamate, D-serine and ATP (Papouin, Dunphy, *et al.*, 2017; Schwarz *et al.*, 2017; Durkee *et al.*, 2019). The area most studied in this context is the *cornu Ammonis* 1 (CA1) region of the hippocampus, where gliotransmitters have been observed to modulate neuronal excitability and mediate forms of synaptic plasticity. Stimulation of GPCRs selectively expressed on CA1 astrocytes leads to elevated extracellular glutamate which increases the frequency of NMDAR-dependent slow inward currents in CA1 neurons that increase neuronal excitability (Durkee *et al.*, 2019). Secondly, D-serine (a co-agonist of the NMDAR) is released from CA1 astrocytes which enhances long term potentiation (Papouin, Dunphy, *et al.*, 2017; Adamsky *et al.*, 2018; Robin *et al.*, 2018). The third major gliotransmitter is ATP, which is rapidly converted in the synapse to adenosine. In CA1, stimulation of astrocytes by Ca^{2+} uncaging

depresses synaptic transmission at some synapses by activation of neuronal adenosine receptors (Covelo and Araque, 2018). This mechanism potentially improves the specificity of long term potentiation (Covelo and Araque, 2018). This shows that selective manipulation of astrocytes alters the availability of gliotransmitters at synapses to modulate neuronal activity and information processing.

1.3.4 | Astrocyte structural plasticity

Astrocytes throughout the brain show dynamic expression of the cytoskeletal glial fibrillary acidic protein (GFAP), which is regulated in response to local variations in the brain microenvironment (Hajós and Kálmán, 1989; Kálmán and Hajós, 1989; Li *et al.*, 2020). For example, cortical astrocytes show low basal GFAP expression but dramatically upregulate this protein in response to tissue injury suggesting that this change serves as a reactive and possibly neuroprotective role (Hirrlinger *et al.*, 2006). Since GFAP forms intermediate filaments that make up the astrocyte cytoskeleton, changes in its expression result in altered morphology and increased branching of the cells. Precisely how this morphological change relates to cell function is still unclear, but it may allow dynamic ensheathment of synapses. Broadly speaking, high GFAP expression and branched morphology is considered to be indicative of astrocyte activation (also known in some pathophysiological cases as astrogliosis) (Sofroniew, 2015).

1.4 | Hypothalamic astrocytes and feeding behaviour

Given that astrocytes regulate neuronal activity by sensing neurotransmitters and altering both homeostatic and active processes accordingly, it is unsurprising that astrocytes in the ARC and wider hypothalamus are regulated by changes in food intake. In turn, it appears their response to changes in food intake alters the activity of ARC^{AgRP} and ARC^{POMC} neurons to restore energy balance.

Astrocyte activation (commonly measured by GFAP immunoreactivity) reflects energy states in genetically obese and diet induced obese (DIO; chronic feeding of only a high fat diet typically over a number of weeks) mice and rats (Horvath *et al.*, 2010; Thaler *et al.*, 2012; Buckman *et al.*, 2013; Douglass *et al.*, 2017). ARC GFAP gene expression and astrocytic ensheathment of ARC^{POMC} neurons is increased in DIO rats (Horvath *et al.*, 2010). In these rats this large number of astrocyte contacts on ARC^{POMC} cell bodies is accompanied by a decrease in the number of synaptic inputs to these cells (Horvath *et al.*, 2010). This may impair synaptic integration in ARC^{POMC} and thus reduced neural activity critical for the inhibition of food intake, biasing the rats towards eating.

Following this seminal study, other groups demonstrated that DIO mice and rats show an increase in GFAP expression (both at the gene and protein level) and altered morphology of astrocytes in the ARC and other hypothalamic nuclei (Thaler *et al.*, 2012; Buckman *et al.*, 2013). Hypothalamic astrogliosis is also seen in *Mc4r*$^{-/-}$ mice which become obese on standard chow diet due to excess food intake, suggesting that the gliosis can occur because of obesity in the absence of high-fat diet consumption (Buckman *et al.*, 2013). Returning DIO mice to a standard chow diet results in weight loss and reversal of the astrogliosis, highlighting the plastic nature of this response (Berkseth *et al.*, 2014).

The physiological significance of these changes is reinforced by studies indicating that inducing inflammatory signalling by stimulating the nuclear factor kappa B (NF-κB) pathway selectively in astrocytes results in obesity, while preventing inflammation by suppressing the same pathway preserves astrocytic function, protecting against weight gain on a high fat diet (Zhang *et al.*, 2017). Supporting this supposition, brain-wide inhibition of astrocyte NF-κB signalling during the induction of DIO is protective against hypothalamic inflammation and

prevents subsequent weight gain (Douglass *et al.*, 2017). Together, these studies implicate astrocyte inflammatory processes, under the control of the NF-κB pathway, in the development and maintenance of DIO. This could potentially be mediated by a loss of homeostatic functions and structural plasticity in chronically activated astrocytes (Liddelow *et al.*, 2017; Zhang *et al.*, 2017).

While supportive evidence for obesity-associated glial changes from human studies is limited, there is a positive correlation between body mass index and signatures of hypothalamic gliosis, measured by image hyper-intensity in magnetic resonance imaging scans (Thaler *et al.*, 2012), suggesting that the obesity-associated changes seen in rodents are present in humans.

The response of hypothalamic astrocytes in rodents to a high-fat diet appears to be biphasic: there is an initial increase in expression of GFAP and pro-inflammatory markers during the first 24-72h on a high-fat diet, which then transiently subsides before returning after 14 days on the diet (Thaler *et al.*, 2012; Buckman *et al.*, 2015; Balland and Cowley, 2017). Inhibition of astrocyte NF-κB mediated inflammatory signalling in mice during the initial phase of high-fat feeding (24 hours) abolishes diet-associated changes in hypothalamic GFAP expression and augments high-fat diet-induced binge eating (Buckman *et al.*, 2015). This has led to the suggestion that the initial phase of astrogliosis is partly a homeostatic physiological response to maintain energy balance while the second inflammatory phase is a pathophysiological response to prolonged energy imbalance.

Further evidence for a role of astrocytes in the physiological response to energy variation comes from experiments where mice are pushed out of homeostasis into negative energy balance by fasting. In fasted rats there is a greater

expression of GFAP in the hypothalamus when compared with ad libitum fed controls (Fuente-Martín *et al.*, 2012). In mice fasting results in changes to the primary (GFAP immunoreactive) and fine (GFAP negative) astrocytic cytoskeletal processes in the ARC (N. Chen *et al.*, 2016; Zhang *et al.*, 2017). Taken together these studies indicate that hypothalamic astrocytes are sensitive to acute deviations in energy homeostasis.

In common with ARC neurons, ARC astrocytes can directly sense and respond to appetite-modulating hormones via receptors expressed on their surface. Astrocytes neighbouring the 3V express LepRb and this expression is increased in obese mice (Cheunsuang and Morris, 2005; Pan *et al.*, 2008; Hsuchou *et al.*, 2009). Functional studies indicate that chronic (14 day) i.c.v delivery of exogenous leptin increases hypothalamic expression of GFAP and increases astrocyte process length in rats (García-Cáceres *et al.*, 2011). The same treatment also reduces expression of synaptic proteins, suggesting increased glial ensheathment of neurons obstructs synapse formation, which may impair integration of feeding cues by these neurons (García-Cáceres *et al.*, 2011). I.c.v delivery of leptin for 14 days in mice decreases the expression of astrocyte glucose and glutamate transporters in the hypothalamus, possibly leading to elevated synaptic glutamate which may further disrupt synaptic transmission in this key brain region (Fuente-Martín *et al.*, 2012).

Selective inducible deletion of LepRb from astrocytes in adult mice revealed reduced ensheathment of ARC neurons by astrocytes (Kim *et al.*, 2014). In accordance with this, these mice showed reduced sensitivity to leptin and increased sensitivity to ghrelin (Kim *et al.*, 2014). These results suggest LepRb on astrocytes are crucial for anatomical wiring of ARC^{AgRP} and ARC^{POMC} circuits and that this wiring ensures appropriate responses to endocrine signals that

modulate food intake. These data are supported by evidence from a second mouse model with germline astrocyte-specific deletion of leptin receptors which shows an increased body-weight and fat-mass gain on a high fat diet, accompanied by greater hypothalamic leptin resistance and increased gliosis compared with wild-type controls (Y. Wang *et al.*, 2015). This suggests the action of leptin on astrocytes is protective against obesity in mice.

Like leptin, i.c.v treatment with the orexigenic hormone ghrelin regulates the expression of a number of proteins expressed by hypothalamic astrocytes including structural proteins (GFAP) and transporters (glucose and glutamate transporters) (Fuente-Martín *et al.*, 2016). Immunohistochemical staining identifies GHSR-1A co-localised with GFAP in the rat ARC (Fuente-Martín *et al.*, 2016).

Together these studies on leptin and ghrelin provide evidence that in addition to ARC neurons, ARC astrocytes are direct sensors of endocrine signals regulating energy balance and they may mediate, at least in part, some of the physiological effects of these hormones in the CNS.

The application of chemogenetic technologies for manipulation of ARC astrocyte signalling has provided causal evidence for activation of these cells modulating ARC^{AgRP} and ARC^{POMC} neurons and correspondingly, feeding behaviour. In 2015, Yang and colleagues reported that chemogenetic activation of Ca^{2+} signalling via a Gq-GPCR (hM3Dq) in ARC astrocytes caused a decrease in both nocturnal and ghrelin-induced food intake while enhancing the satiating effects of leptin (Yang, Qi and Yang, 2015). Their work suggests this was mediated by astrocyte-derived adenosine inhibiting ARC^{AgRP} neurons via activation of adenosine A1 receptors (Yang, Qi and Yang, 2015). However, the effect of ARC astrocyte

activation appears to be state-dependent since during the light phase, when mice are typically satiated, chemogenetic activation of ARC astrocytes increased food intake (Yang, Qi and Yang, 2015). A second independent research group, employing a similar hM3Dq chemogenetic methodology, similarly found that activating Ca^{2+} signalling in hypothalamic astrocytes increased food intake during the light phase (N. Chen *et al.*, 2016). This was due to a general activation of neighbouring neurons. Due to the circuit architecture in the ARC (i.e. ARC^{AgRP} neurons inhibit ARC^{POMC} neurons), chemogenetic astrocyte activation led to excitation of ARC^{AgRP} neurons relative to ARC^{POMC} (N. Chen *et al.*, 2016).

This suggests that the effects of ARC astrocyte activation on feeding behaviour may be dependent on the current state of ARC^{AgRP} and ARC^{POMC} circuitry. If ARC^{AgRP} activity drives feeding during the dark phase then artificial (chemogenetic) ARC astrocyte activation inhibits this to suppress feeding (Yang, Qi and Yang, 2015). While in satiated mice, where ARC^{AgRP} neuron activity is lower and ARC^{POMC} dominates (Chen *et al.*, 2015), chemogenetic activation of ARC astrocytes stimulates ARC^{AgRP} resulting in inhibition of ARC^{POMC} and driving food intake (N. Chen *et al.*, 2016). This is consistent with the hypothesis that the endogenous function of ARC astrocyte activation is to restore energy balance (Buckman *et al.*, 2015) since with chemogenetic activation these ARC circuits are 'reset' (i.e. the action of the dominant population at the time of activation is inhibited).

In summary, astrocytes in the ARC are responsive to short-term and prolonged deviations in energy homeostasis. These cells can directly sense appetite-regulating hormones and adjust their morphology, expression of transporters, and potentially release of gliotransmitters accordingly, to alter the firing of neurons that control food intake. Prolonged astrocyte activation in diet-induced

and genetic obesity may be a maladaptive, pathophysiological response that impairs the function of ARC feeding circuits. In contrast, short-term activation induced by fasting or acute intake of a high fat diet may exist to help restore energy balance as evidenced by the state-dependent effects of chemogenetic ARC astrocyte activation (**Figure 1.4.1**).

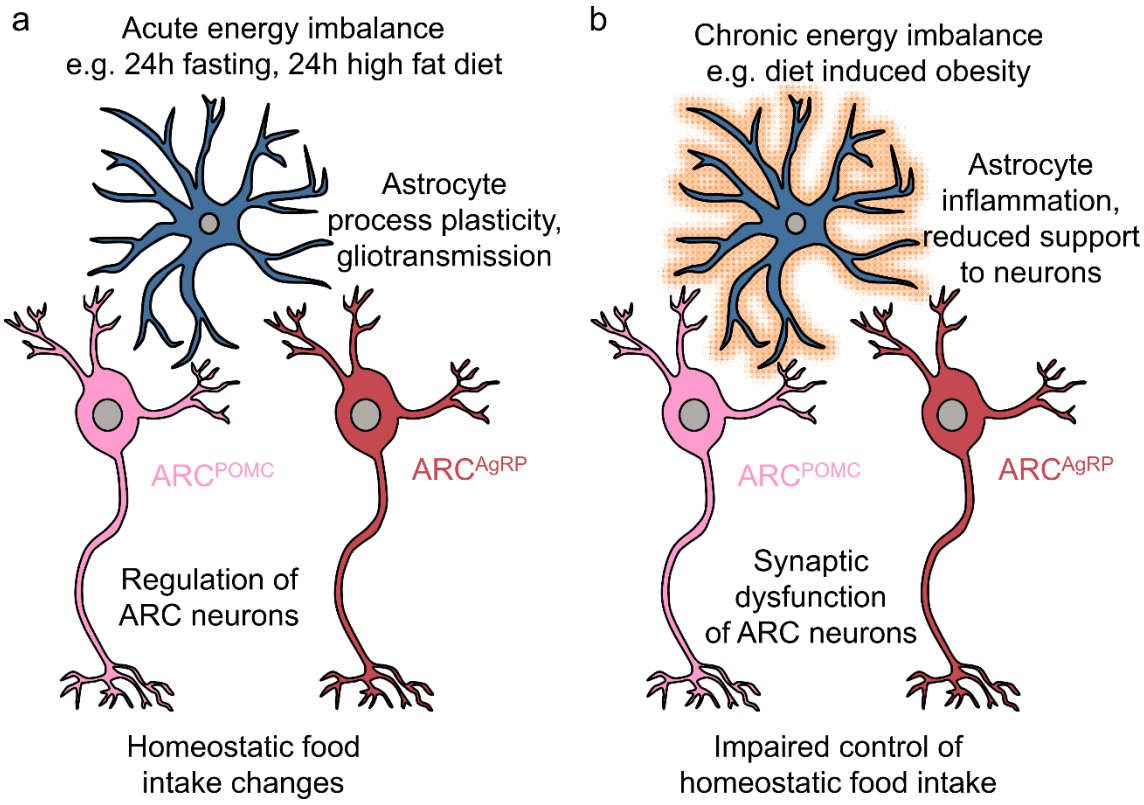

Figure 1.4.1 | Schematic summary of potential homeostatic and maladaptive responses of ARC astrocytes to short and long term deviations in energy balance. a, Astrocytes in the ARC alter their cytoskeletal morphology, expression of transporter proteins and potentially gliotransmitter release in response to acute deviations in food intake. Inhibition of this process exacerbates acute high fat diet intake while mimicking astrocyte activation with chemogenetics drives ARC circuit dynamics towards homeostasis. **b**, In diet induced obesity hypothalamic astrocytes show chronic inflammation. This disrupts their normal function and alters synaptic contacts on ARC neurons. This may lead to impaired signal integration in these neurons and preventing appropriate homeostatic control of food intake. AgRP = agouti related protein, ARC = arcuate nucleus, POMC = proopiomelanocortin.

1.5 | NTS astrocytes

In contrast to the ARC, extrahypothalamic astrocytes have not been extensively studied in the control of food intake. Since astrocytes are of growing interest in understanding neural control of food intake and the NTS is the major brain area outside the hypothalamus that regulates food intake, we now consider the evidence that astrocytes in the NTS and wider DVC might regulate synaptic activity. Much is known about these cells in the context of cardiorespiratory physiology, but their potential role in regulating food intake is relatively understudied.

1.5.1 | Astrocytes modulate synaptic transmission in the NTS

Synaptic transmission between vagal afferent terminals and second-order viscerosensory neurons allows for the appropriate autonomic and behavioural response to physiological challenges. Vagal afferents entering the NTS via the ST release glutamate onto postsynaptic neurons (Andresen and Yang, 1990). This can be modelled experimentally in *ex vivo* brain slices where electrical stimulation of the ST produces short-latency, glutamate-mediated, EPSCs in second-order NTS neurons (Doyle and Andresen, 2001; Doyle *et al.*, 2004). Astrocytes ensheathe glutamatergic synapses in the NTS providing structural evidence for a role in synaptic transmission (Chounlamountry and Kessler, 2011). Indeed, several functional studies (described below) have demonstrated that astrocytes are critically involved in this process.

NTS astrocytes express Ca^{2+} permeable AMPA receptors (AMPA-R). Using Ca^{2+} imaging from astrocytes and neurons in *ex vivo* NTS rat brain slices, McDougal and colleagues demonstrated that astrocytes can detect glutamate released following electrical ST stimulation and respond with increases in $[Ca^{2+}]_i$, both from extra- and intracellular sources (McDougal, Hermann and Rogers, 2011). This

ST stimulation evokes activation of AMPA-R on astrocytes allowing Ca^{2+} influx to the cell, which drives Ca^{2+}-induced Ca^{2+}-release, further increasing $[Ca^{2+}]_i$ via liberation from intracellular stores. These ST-evoked astrocyte $[Ca^{2+}]_i$ elevations are sensitive to the AMPA-R antagonist NBQX but not antagonists for mGlu-R 1 or 5 nor NMDA-R (McDougal, Hermann and Rogers, 2011). Further supporting a role for astrocytic AMPA-R in integrating information encoded by the ST, in a separate study ST stimulation evoked time-locked, inward currents in astrocytes that were abolished by the AMPA-R antagonist DNQX (Accorsi-Mendonça *et al.*, 2013). Although not directly assessed, presumably these currents represent Ca^{2+} entering the cell. These studies show that NTS astrocytes are sensitive to incoming signals from the periphery via vagal afferent glutamate detection.

In addition to sensing ST-derived glutamate, astrocytes also contribute to transmission across the ST-NTS neuron synapse as evaluated using a pharmacological inhibition approach. It is thought that astrocyte function can be selectively inhibited with fluoroacetate (FAC) and its gliotoxic metabolite fluorocitrate (FC). FC inhibits the TCA cycle and both FC and FAC preferentially effect astrocytes (Fonnum, Johnsen and Hassel, 1997). This is said to be due to the tendency of astrocytes and not neurons to take up and utilize acetate for cellular metabolism (Wyss *et al.*, 2011). The specificity of FC and FAC for astrocytes is assumed but not conclusively proven and therefore, results using this technique should be interpreted with caution in the absence of additional supporting evidence.

In the presence of FAC, both ST-evoked EPSC amplitude and spontaneous EPSC frequency are reduced in NTS neurons that project to the ventrolateral medulla (VLM) (Accorsi-Mendonça *et al.*, 2013). This tonic, astrocytic contribution to synaptic transmission is likely mediated by release of ATP since antagonism

of P2X purinergic receptors with the broad-spectrum antagonist iso-PPADS recapitulates the effect of FAC, but the two do not have additive effects (Accorsi-Mendonça *et al.*, 2013). Furthermore, an increase in extracellular ATP observed in this study following ST-stimulation was reduced by FAC.

Evidence also suggests that astrocytes can restrain neuronal excitability directly in NTS neurons; astrocyte inhibition with FAC reduces the NTS neuronal A-type potassium current (IK_A) (Accorsi-Mendonca *et al.*, 2015). Under normal conditions, this outward potassium current present at the beginning of the initial depolarisation acts to restrain neuronal action potential threshold and firing. While the underlying mechanism has not yet been fully explored in the NTS, in the hypothalamus IK_A is inhibited when astrocytic glutamate uptake is reduced due to activation of extra-synaptic NMDA-Rs (Naskar and Stern, 2014). In postsynaptic neurons, ST-evoked AMPA EPSC amplitude is lower from brain slices in the presence of FAC while ST-evoked NMDA EPSC amplitude is greater (Accorsi-Mendonça, Bonagamba and Machado, 2019). This demonstrates that astrocytes provide tonic neuromodulation which has inverse effects on signalling via the two main types of ionotropic glutamate receptor.

A second mechanism by which astrocytes may support ST-NTS neurotransmission is by active supply of the metabolite lactate (Nagase *et al.*, 2014). As discussed above (section **1.2.1**), it has been proposed that in the brain, glucose is the main fuel source for astrocytes which metabolise this fuel to lactate. Astrocyte-derived lactate is then shuttled via monocarboyxlate transporters (MCTs) to neurons where it is metabolised to pyruvate and used to fuel the TCA cycle (Pellerin *et al.*, 1998; Pellerin and Magistretti, 2012). When MCTs are pharmacologically inhibited with 4-CIN, phloretin or D-lactate in rat NTS brain slices, the amplitude of ST-evoked neuronal EPSCs is reduced. Since this effect

is rescued by providing extracellular lactate it was concluded that ST-NTS synaptic fidelity is reliant on lactate from astrocytes transported through MCTs on astrocytes and neurons (Nagase *et al.*, 2014).

A further mechanism by which astrocytes may modulate ST-NTS neurotransmission is by regulating synaptic glutamate availability. In the NTS astrocytic glutamate reuptake appears to be essential for normal synaptic function (Matott *et al.*, 2016; Matott, Kline and Hasser, 2017; Yamamoto and Mifflin, 2018). Pharmacological blockade of both EAAT1 and EAAT2 with DL-*threo*-β-benzyloxyaspartic acid (TBOA) elevates synaptic glutamate as evidenced by NTS neuronal depolarisation and action potential firing, and increased spontaneous EPSCs (Matott *et al.*, 2016). Furthermore, in NTS neurons ST-evoked EPSCs are reduced by TBOA suggesting released glutamate is not being returned to the presynaptic terminal or that excess glutamate is activating presynaptic mGlu-Rs and suppressing transmission by negative feedback (Matott *et al.*, 2016). These effects can be recapitulated by dihydrokainate (DHK), an EAAT2 blocker (Matott, Kline and Hasser, 2017; Yamamoto and Mifflin, 2018). In combination with immunohistochemical evidence (Chounlamountry and Kessler, 2011), this indicates that EAAT2 is the primary glutamate transporter responsible for glutamate reuptake and recycling at the ST-NTS synapse (Matott, Kline and Hasser, 2017; Yamamoto and Mifflin, 2018).

Taken together, this combined evidence from a number of independent research groups shows that astrocytes support synaptic transmission in the NTS by buffering and recycling synaptic glutamate (Matott *et al.*, 2016; Matott, Kline and Hasser, 2017; Yamamoto and Mifflin, 2018), shuttling lactate to neurons (Nagase *et al.*, 2014) and providing tonic purinergic neuromodulation (Accorsi-Mendonça

et al., 2013; Accorsi-Mendonca *et al.*, 2015) (**Figure 1.5.1**). Interestingly, astrocytes are also able to directly detect vagal glutamate release (McDougal, Hermann and Rogers, 2011). This raises the possibility that astrocytes modulate their functions in response to increased vagal input making them key integrators of information at this important integrative site. To date this has not been investigated in the context of the systemic regulation of energy homeostasis.

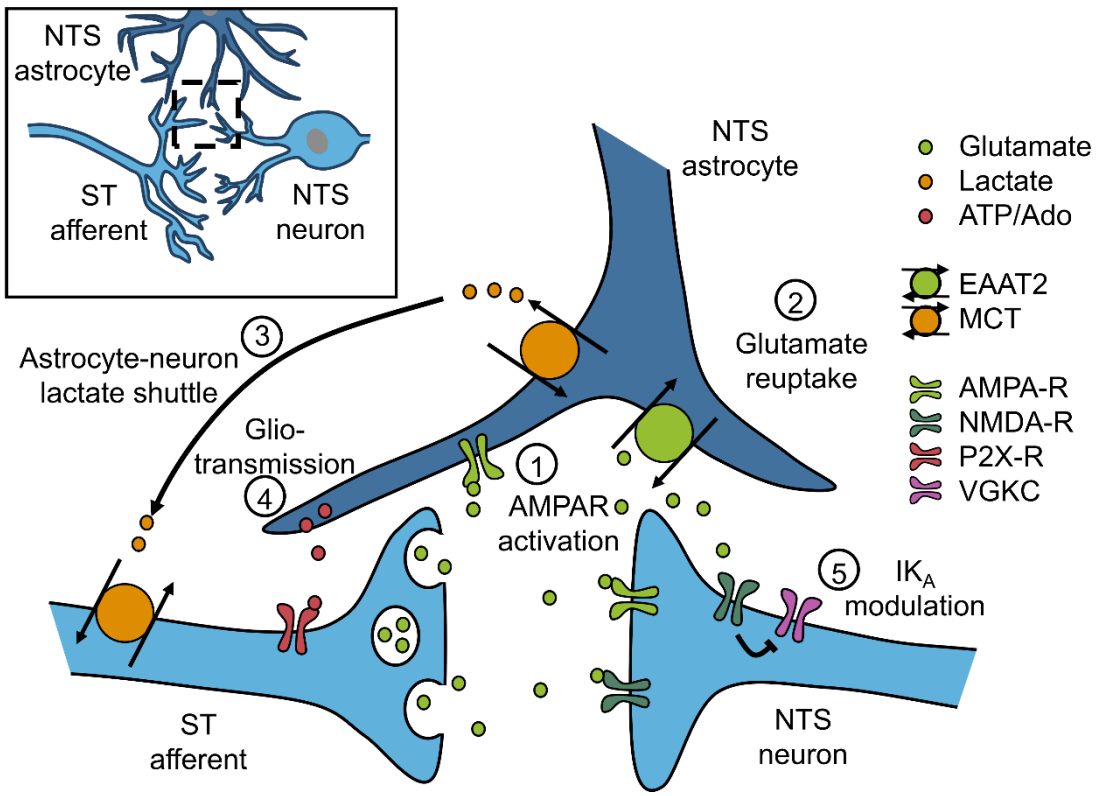

Figure 1.5.1 | A simplified schematic of astrocyte modulation of synaptic transmission in the NTS. (1) Astrocytes respond to synaptic glutamate *via* AMPA-receptors (AMPA-R) expressed on the cell surface. (2) Astrocytes clear glutamate from the synapse to restrain neuronal firing and maintain presynaptic glutamate levels *via* EAAT2. (3) Astrocytes provide fuel to neurons in the form of lactate in order to maintain fidelity of synaptic transmission. (4) Astrocytes provide tonic modulation to synaptic transmission in the form of purinergic gliotransmission (release of ATP which may be converted to adenosine in the synaptic cleft). (5) By controlling extracellular glutamate levels astrocytes may modulate the presence of the NMDA-R regulated a-type potassium current (IK_A) which restrains action potential firing. Abbreviations: Ado = adenosine, ATP = adenosine triphosphate, EAAT2 = excitatory amino acid transporter 2, MCT = monocarboxylate transporter, NTS= nucleus of the solitary tract, ST = solitary tract, VGKC = voltage gated potassium channel.

1.5.2 | Physiological and environmental stimuli modulate the morphology of NTS astrocytes

In hypothalamus and other brain areas, expression of GFAP and astrocyte morphology is dynamic (Hirrlinger *et al.*, 2006; N. Chen *et al.*, 2016; Zhang *et al.*, 2017; Li *et al.*, 2020). This is also true of the NTS. Notably within the NTS of rats, astrocytes are smaller, have a simpler morphology and greater overlapping domains than other brainstem autonomic nuclei (SheikhBahaei *et al.*, 2018).

Several studies have reported that NTS GFAP expression, commonly measured using immunoreactivity, is modulated by different experimental stimuli (**Table 1.5.1**). For example, hypoxic conditions for 1 to 24 hours induced either by inhalation of ozone gas or low oxygen air increase GFAP immunoreactivity and astrocyte ensheathment of synapses within the caudal NTS in rats and mice (Araneda *et al.*, 2008; Tadmouri, Champagnat and Morin-Surun, 2014; Chounlamountry *et al.*, 2015; Stokes *et al.*, 2017; De La Zerda *et al.*, 2018). This effect may be secondary to activation of microglia since inhibition of microglia with minocycline attenuates the GFAP response to hypoxia (Stokes *et al.*, 2017). Taken together this suggests that caudal NTS astrocytes are responsive to low oxygen are may be involved in mediating the central response to hypoxia (see **section 1.5.3**).

In addition, NTS GFAP expression is regulated in a diverse range of disease models associated with inflammation (**Table 1.5.1**) (Ebel, Torkilsen and Ostrowski, 2017; Tsai *et al.*, 2017; Fernandes-Junior *et al.*, 2018; Melo *et al.*, 2019). In these studies, the authors report autonomic dysfunction phenotypes coincident with increased NTS GFAP immunoreactivity. Correlational evidence does not reveal whether this observed astrocyte plasticity is a cause of, a

consequence of or unrelated to the physiological phenotypes displayed by these models.

In addition to those outlined above, a number of other studies have shown dynamic regulation of NTS astrocytes (Jacquin *et al.*, 2000; Biondo *et al.*, 2004; Alonso *et al.*, 2007; Wu, Howell and Palmiter, 2008; Hermann and Rogers, 2009; Bartel, 2012; Hardy *et al.*, 2018; Machaalani *et al.*, 2019). While not discussed here, these are summarised in **Table 1.5.1**. Thus, taken together these studies show that GFAP expression is highly plastic in the NTS and is regulated by a myriad of stimuli. Future studies are needed to address the physiological consequences of this GFAP regulation, if/how NTS astrocytes differentiate between stimuli of different modalities, and how this mechanistically relates to other astrocyte functions.

Stimulus	Outcome	Species	Ref
Ozone inhalation (3 hours)	Greater VEGF expression in NTS astrocytes than normoxic controls, increased branching	Rat	(Araneda *et al.*, 2008)
Ozone inhalation (24 hours)	Greater glial coverage of synapses in NTS compared with untreated controls	Rat	(Chounlamountry *et al.*, 2015)
10% Oxygen inhalation	Greater NTS GFAP immunoreactivity (1 and 6 hours, compared with normoxic controls)	Mouse	(Tadmouri *et al.*, 2014)
10% Oxygen inhalation	Greater GFAP immunoreactivity in NTS (4 and 24 hours, compared with normoxic controls)	Rat	(Stokes *et al.*, 2017)
10% Oxygen inhalation	Greater GFAP immunoreactivity in NTS after 10 days compared with normoxic controls	Rat	(De La Zerda *et al.*, 2018)
TAA injection (liver damage model)	Greater number of GFAP expressing cells in NTS compared with vehicle injected controls	Rat	(Tsai *et al.*, 2017)
Lateral ventricle STZ (neurodegeneration model)	Greater S100b immunoreactivity in commisural NTS compared with vehicle injected controls	Rat	(Ebel *et al.*, 2017)
Intrastriatal 6-OHDA injection (Parkinsonian model)	Lower GFAP immunoreactivity in NTS after 60 days compared with shorter durations	Rat	(Fernandes-Junior *et al.*, 2018)
Two-kidney 1-clip hypertension	Greater number of GFAP-positive pixels in NTS than in normotensive controls	Rat	(Melo *et al.*, 2019)

Isoproterenol induced water drinking	No difference in GFAP immunoreactivity in NTS	Rat	(Hardy *et al.*, 2018)
Age	Greater GFAP immunoreactivity in NTS of aged (24 months) than young (6 months)	Rat	(Hardy *et al.*, 2018)
Prenatal (E11 or E16) X-irradiation	Greater number of GFAP expressing cells in NTS at P7-14 for E11 irradiated pups	Rat	(Jacquin *et al.*, 2000)
Prenatal cigarette smoke inhalation	No difference in GFAP immunoreactivity in NTS compared with non-exposed pups	Mouse	(Machaalani *et al.*, 2019)
Sudden infant death syndrome	Greater GFAP-positive cell density in NTS from SIDS victims than age-matched controls	Human	(Biondo *et al.*, 2004)
Chronic morphine treatment	Greater GFAP-positive cell density in NTS than vehicle treated	Rat	(Alonso *et al.*, 2007)
AgRP neuron ablation	Greater number of GFAP-positive pixels in NTS than control mice	Mouse	(Wu *et al.*, 2008)
DVC tumor necrosis factor-α treatment	Greater c-FOS expression by NTS astrocytes than vehicle injected controls	Rat	(Hermann and Rogers, 2009)
Unilateral chorda tympani nerve crush	Greater GFAP immunoreactivity in rostral NTS compared with uninjured controls	Mouse	(Bartel, 2012)

Table 1.5.1 | Summary of studies which have examined impact of experimental manipulations on NTS astrocyte immunoreactivity and/or

morphology. 6-OHDA = 6-hydroxy-dopamine, AgRP = agouti-related protein, DVC = dorsal vagal complex, E = embryonic day, GFAP = glial fibrillary acidic protein, NTS = nucleus of the solitary tract, P = postnatal day, SIDS = sudden infant death syndrome, STZ = streptozotocin, TAA = thioacetamide, VEGF = vascular endothelial growth factor.

1.5.3 | Regulation of cardiorespiratory physiology by NTS astrocytes

In addition to regulating food intake, the most caudal portion of the NTS is the initial CNS detector of cardiovascular parameters (Machado, 2001; Accorsi-Mendonça and Machado, 2013). Specifically, peripheral baroreceptors in the aortic arch detect increases in arterial pressure and increase vagal tone into the NTS (Min *et al.*, 2019). This NTS signal drives a corresponding decrease in heart rate and arterial pressure. This process is known as the baroreflex. The NTS also receives input from peripheral chemosensors which monitor blood O_2 allowing for compensatory homeostatic chemoreflex responses to deviations in O_2 or CO_2 (Accorsi-Mendonça and Machado, 2013).

In a rat model of hypertension GFAP immunoreactivity is elevated in the caudal NTS (Melo *et al.*, 2019), suggesting an astrocytic component to the physiological response. Indeed, functional work involving pharmacological manipulation of NTS astrocytes has shown this to be the case. Saporins are toxic agents that, in their unconjugated form, selectively kill astrocytes when delivered to the rat NTS (Lin *et al.*, 2013). This ablation has severe consequences for cardiovascular function: lowering of 1) baroreflex sensitivity, 2) cardiopulmonary reflex sensitivity and 3) chemoreflex sensitivity. This suggests loss of correct physiological integration of peripheral cues by the NTS in these animals (Lin *et al.*, 2013). Rats with NTS astrocyte ablation show large variations in arterial pressure also indicative of poor cardiovascular reflex control. Critically, these rats show damage to their myocardium and in some cases die due to sudden cardiac arrest (Lin *et al.*, 2013). This failure of central cardiovascular control appears to be mediated by a loss of glutamate sensitivity since cardiovascular responses to NTS delivery of glutamate receptor agonists, AMPA and NMDA, are attenuated in NTS saporin treated rats (Talman, Dragon and Lin, 2017).

Recent evidence from a manuscript preprint posted on the server bioRxiv (therefore as yet not peer-reviewed), shows that astrocytes may fine-tune the baroreflex in rats (Mastitskaya *et al.*, 2019). The study utilised an adeno-associated viral (AAV) vector approach which allowed for TeLC to be selectively expressed by NTS astrocytes *in vivo*. This blocks vesicular release from astrocytes, but in contrast to saporin ablation spares the metabolic and structural functions of these cells. In awake rats expressing TeLC in NTS astrocytes the sensitivity of the baroreflex to spontaneous changes in arterial pressure is reduced compared to those expressing a control construct. Furthermore, in anaesthetised rats delivery of the $P2Y_1$ antagonist MDS-2500 to the NTS also increases baroreflex response initiated by the α_1-adrenergic receptor agonist phenylephrine (Mastitskaya *et al.*, 2019). As with some other NTS mediated physiological responses (discussed below), this suggests that under normal conditions astrocytes modulate baroreflex sensitivity via purinergic signalling.

In line with their role in integrating activity at the ST-NTS synapse, glutamate reuptake and recycling by NTS astrocytes is crucial for cardiovascular function. Blockade of all EAATs (by TBOA) or only EAAT2 (by DHK) causes cardiac depression and reduced baroreflex response to phenylephrine in rats (Matott *et al.*, 2016; Matott, Kline and Hasser, 2017; Yamamoto and Mifflin, 2018). This effect is blocked by an AMPA-R antagonist suggesting that under normal conditions NTS astrocytes sequester synaptic glutamate in order to regulate NTS neuronal activity and resulting output from DMX neurons to the cardiorespiratory system (Matott, Kline and Hasser, 2017; Yamamoto and Mifflin, 2018).

Under hypoxic conditions, chemoreflex responses are engaged which initiate compensatory increases in respiratory and heart rate. This effect persists even when animals are returned to normoxia, suggesting some central adaptation to

the low oxygen environment (Powell and Fu, 2008). In rats and mice, NTS astrocytes respond to the initial phase of hypoxia with an increase in GFAP immunoreactivity within 1-24 hours (Tadmouri, Champagnat and Morin-Surun, 2014; Stokes *et al.*, 2017). At the synaptic level, sustained hypoxia causes adaptations in the rat NTS: increased postsynaptic excitability mediated by decreased expression of IK_A and greater amplitude NMDA and AMPA currents evoked by ST stimulation (Accorsi-Mendonca *et al.*, 2015; Accorsi-Mendonça, Bonagamba and Machado, 2019). Importantly, inhibition of astrocytes with FAC recapitulates these effects in brain slices from hypoxia naïve rats, suggesting that reduced astrocyte modulation of synaptic transmission may be an adaptive mechanism to increase neuronal sensitivity and drive respiration in sustained hypoxia. In support of this, treatment with FAC produces no further decrease in IK_A, NMDA or AMPA currents in brain slices from rats which received sustained hypoxia, indicating a ceiling effect (Accorsi-Mendonca *et al.*, 2015; Accorsi-Mendonça, Bonagamba and Machado, 2019).

Together these studies illustrate the necessity for tight control of synaptic glutamate in the NTS to maintain cardiorespiratory function, and the importance of astrocytes in this process. Furthermore, the published studies on adaptation to hypoxia suggest that astrocytes adapt to compensate for changes physiological need.

1.5.4 | Regulation of blood glucose and the counter-regulatory response by NTS astrocytes

Orchestrated in part by the brain, the counter-regulatory response to hypoglycaemia (CRR) is initiated when blood glucose falls below the normal euglycemic range and is a multifaceted hormonal and neuronal response to restore blood glucose. The NTS is thought to be a critical site for the central

glucose detection and initiation of the CRR (Ritter *et al.*, 2011). Activation of a subpopulation NTS neurons in response to low glucose drives compensatory feeding and hepatic glucose production (Ritter *et al.*, 2011; Boychuk *et al.*, 2019; Aklan *et al.*, 2020).

In rat brain slices, 40% of NTS astrocytes increase their $[Ca^{2+}]_i$ in response to low extracellular glucose (0.1 mM) or the non-metabolisable glucose analogue 2-deoxyglucose (2-DG; a glucoprivic agent) indicating the glucose-sensitivity of these cells (McDougal, Hermann and Rogers, 2013). Delivery of 2-DG directly into the 4V increases blood glucose in anaesthetised rats; indicating that local reductions in brainstem glucose level are sufficient to drive compensatory changes in glucose homeostasis (Rogers, Ritter and Hermann, 2016). This blood glucose elevation is blocked by general inhibition of NTS astrocyte activity using FC delivered to the 4V or more specifically by the A1 adenosine-receptor antagonist DPCPX. This indicates that astrocyte-derived adenosine is a component in the detection and response to this glucoprivic stimulus (Rogers, Ritter and Hermann, 2016).

Of critical importance to the CRR are a subpopulation (around 20%) of NTS^{TH} neurons. In brain slices from mice, the Ca^{2+} response of NTS^{TH} neurons to 2-DG is abolished by pre-treatment with either FC or the broad spectrum P2 purinergic receptor antagonist suramin (Rogers *et al.*, 2018). The glucose transporter GLUT2 is a proposed glucose sensing protein and accordingly blockade of GLUT2 with quercetin abolishes astrocyte Ca^{2+} responses to low extracellular glucose and 2-DG in rat brain slices (Rogers *et al.*, 2019). Consequently, it appears that NTS astrocytes are glucose sensors that in hypoglycaemic conditions relay this signal to, and/or enhance intrinsic glucose sensitivity of

NTS^{TH} neurons via purinergic gliotransmission in order to drive the appropriate CRR.

Therefore, it appears that in concert with glucose-inhibited NTS neurons, astrocytes in the NTS are involved in sensing low tissue glucose levels. Indeed the temporal response in rat and mouse brain slices suggests that NTS astrocytes are a primary detector of low glucose and may enhance responses of NTS^{TH} neurons to low glucose at least in this experimental paradigm (McDougal, Hermann and Rogers, 2013; Rogers *et al.*, 2018).

1.5.5 | Regulation of food intake by NTS astrocytes

There is a large body of evidence implicating NTS neurons in the integration of viscerosensory signals from the stomach and gastrointestinal tract, including encoding of satiety and meal termination (see **Section 1.2.2.1**). A role for astrocytes in this process has only recently began to be investigated. Reiner and colleagues investigated astrocytes as components of the GLP1 signalling system (Reiner *et al.*, 2016). As discussed above, NTS^{PPG} neurons are the sole source of brain GLP1 while GLP1-R is distributed at restricted sites throughout the brain (Llewellyn-Smith *et al.*, 2011; Cork *et al.*, 2015; Holt, Richards, *et al.*, 2019). Both chemogenetic activation of NTS^{PPG} neurons and direct delivery of GLP1 to the brain reduce food intake (Turton *et al.*, 1996; Gaykema *et al.*, 2017; Shi *et al.*, 2017; Holt, Richards, *et al.*, 2019).

In rats, peripheral or 4V injection of a fluorescent GLP1-R agonist (fluoro-exendin-4) revealed binding to GLP1-Rs on both NTS neurons and astrocytes, an effect that is reduced by pre-treatment with a GLP1-R antagonist (Reiner *et al.*, 2016). This is further supported by the finding that exendin-4 causes an increase in $[Ca^{2+}]_i$ in 40% of NTS astrocytes in rat brain slices. Critically, NTS pre-treatment

with FC abolishes the inhibitory effect of exendin-4 directly delivered to the NTS on food intake. Taken together, these data suggest that NTS astrocytes are a component of the central GLP1 satiety system, although the molecular mechanism by which they exert their effects has not been fully investigated (Reiner *et al.*, 2016).

Although fluoro-exendin-4 binds to astrocytes in the rat NTS (Reiner *et al.*, 2016), observations from a transgenic mouse line expressing green fluorescent protein in GLP1-R expressing cells indicate no labelling of NTS astrocytes (Cork *et al.*, 2015). It remains to be demonstrated whether the contrasting results of Reiner *et al* and Cork *et al* reflect a species difference or are the result of two different methodological approaches to visualise the cellular location of the GLP1-R, but raises the possibility that astrocytes may play this important role in rats but not mice.

Using very similar methodology, a second study has shown that LepRb mRNA is expressed by NTS astrocytes in rats (Stein *et al.*, 2020). Pretreatment of the NTS with FC attenuates the feeding suppression induced by delivery of leptin directly into this brain region (Stein *et al.*, 2020). Again however, mice expressing a fluorescent protein (tdTomato) in LepRb expressing cells do not show labelling of astrocytes (Garfield *et al.*, 2012). Similar to the GLP1-R distribution this may represent a true species difference or a contrast in methodology (direct detection by *in situ* hybridisation compared with indirect labelling of cells with a fluorescent protein).

Further support for a key role of NTS astrocytes in the control of feeding comes from a series of studies on endozepines. NTS astrocytes (and tanycyte like cells of the AP known as vagliocytes (Dallaporta *et al.*, 2010)) express

octadecaneuropeptide (ODN) (Guillebaud *et al.*, 2017), ODN is an endozepine cleaved from acyl-CoA-binding protein (ACBP) which acts to suppress food intake (Garcia de Mateos-Verchere *et al.*, 2001). Delivery of ODN into the 4V suppresses food intake in rats and induces c-FOS expression in the NTS (Guillebaud *et al.*, 2017). Thus, under normal conditions it is possible that NTS astrocytes and vagliocytes may secrete ODN to regulate food intake. Indeed, in the ARC, astrocytes release ACBP (cleaved extracellularly to ODN), which activates ARC^{POMC} neurons to suppress appetite *via* its G-protein coupled receptor ODN-GPCR (Bouyakdan *et al.*, 2019).

Evidence generated by these studies suggest that NTS astrocytes can modulate the effects of two endogenous satiety signals but their involvement has not yet been conclusively demonstrated.

1.6 | Summary and Statement of Aims

To summarise, food intake is under potent control by the brain with respect to generation of a strong hunger signal and subsequent suppression of that signal in response to food intake (satiety). The key brain area mediating satiety is the NTS, given its connectivity from the gut and outputs to higher brain centres including the midbrain and hypothalamus where hunger and satiety signals converge. Astrocytes are an active element of neural circuits and modulate the functions of neurons directly and by altering the synaptic microenvironment. Astrocytes in the ARC are regulated by feeding state and their activation serves to modulate the firing of hunger-driving ARC^{AgRP} neurons. In the NTS, astrocytes are involved in synaptic transmission and regulation of cardiorespiratory physiology in addition to being regulated by various internal states. Despite the well-established role of the NTS in mediating satiety and the evidence that astrocytes in this nucleus are dynamically regulated there has yet to be a

description of the response of these cells to deviations in food intake. Furthermore, while genetic techniques have been applied to ARC astrocytes to demonstrate their ability to modulate appetite this same methodology has not been used to study NTS astrocytes and food intake.

To this end, the studies described in this thesis address three main aims:

1) Identify the responses of NTS astrocytes to short and long term deviations in food intake or energy balance

2) Assess the consequence of astrocyte activation on food intake and related behaviours

3) Examine potential mechanisms of astrocyte-neuron communication in the NTS with relevance to food intake

At the core of these aims is the following overarching hypothesis: NTS astrocytes sense increases in food intake in the form of vagal and non-vagal cues entering the brain after a large meal and in turn, alter their function to excite NTS neurons that signal satiety in order to drive a corresponding decrease in food intake.

Chapter 2

Materials and Methods

2.1 | Key Materials

Antibodies		
Reagent or Resource	**Source or Supplier**	**Identifier**
Mouse anti-GFAP	Merck	MAB360
Goat anti-mCherry	Origene	AB0081
Rabbit anti-NeuN	Abcam	Ab104225
Rabbit anti-c-FOS	Cell Signalling	2250s
Donkey anti-mouse AlexaFluor 568	Invitrogen	A10037
Donkey anti-mouse AlexaFluor 488	Invitrogen	A21202
Donkey anti-rabbit AlexaFluor 488	Invitrogen	A21206
Donkey anti-goat AlexaFluor 594	Invitrogen	A11058

Table 2.1.1 | Summary of antibodies used in the described studies. GFAP = glial fibrillary acidic protein. NeuN = neuronal nuclear protein.

Viral Vectors		
Reagent or Resource	**Source or Supplier**	**Identifier**
AAV5/2-hGFAP-hM3Dq_mCherry	ETH Zurich Viral vector facility	V97
AAV5/2-hGFAP-mCherry	Vigene Bioscience	N/A
AAV5/2-hGFAP-hM4Di_mCherry	ETH Zurich Viral vector facility	V103

Table 2.1.2 | Summary of viral vectors used in the described studies. AAV = adeno associated viral vector. hGFAP = human GFAP promoter.

Chemicals		
Reagent or Resource	**Source or Supplier**	**Identifier**
Paraformaldehyde	Sigma Aldrich	P6148
Sucrose	Melford	S0809
Sodium Chloride	Sigma Aldrich	S7653
Sodium Phosphate Dibasic	SAFC	A702X
Sodium Phosphate Monobasic	Sigma Aldrich	RDD007
Triton X-100	Sigma Aldrich	T8787
Normal Donkey Serum	Sigma Aldrich	566460
Fluoroshield mounting medium with DAPI	AbCam	ab104139
Clozapine-N-Oxide (CNO)	Tocris Bioscience	4936
Sodium Pentobarbital	Animal Care	Pentoject
Ketamine Hydrochloride	Covetrus	Narketan
Medetomidine	Covetrus	Domitor
Atipamezole	Covetrus	Antisedan
Buperonorphine	Covetrus	Vetergesic
0.9% Saline for injection	Aquapharm	#1
Carprofen	Covetrus	Rimadyl
D-Glucose	Sigma Aldrich	G8270
Cholecystokinin Octapeptide, Sulphated	Tocris Bioscience	1166/1
Lithium Chloride	Sigma	L4408
N-methyl-D-aspartate	Tocris Bioscience	0114
D-serine	Tocris Bioscience	0226
Dihydrokainic acid	Tocris Bioscience	0111
Potassium chloride	Sigma Aldrich	P9333
Sodium bicarbonate	Sigma Aldrich	S5761
Magnesium sulphate	Sigma Aldrich	M7506
Calcium chloride	Sigma Aldrich	21115
Sucrose	Sigma Aldrich	S7903
Potassium phosphate	Sigma Aldrich	P5655
Potassium gluconate	Sigma Aldrich	G4500

EGTA	Sigma Aldrich	E3889
HEPES	Sigma Aldrich	H3375
Magnesium chloride	Sigma Aldrich	442615-M
ATP	Sigma Aldrich	A1852
GTP	Sigma Aldrich	G8877

Table 2.1.3 | Summary of chemicals used in the described studies.

Mouse strains		
Reagent or Resource	**Source or Supplier**	**Identifier**
C57BL6/J	University of Exeter Colony (Originally Charles River)	N/A
C57BL6/J	Charles River	N/A
TH-EGFP	Washington State University Colony	MGI:3774290
Mouse chow		
Standard Chow	LabDiet	EURodent diet [5LF2]
High Fat Chow	TestDiet	D12492

Table 2.1.4 | Summary of mouse strains and mouse diets used in the described studies.

Software		
Reagent or Resource	**Source or Supplier**	**Identifier**
Leica Acquisition Suite X	Leica	LASX
FIJI	National Instituites for Health (Schindelin *et al* 2012)	N/A
Ethovision XT	Noldus	N/A
MATLAB	Mathworks	R2019a
MC_Rack	Multichannel Systems	N/A
pClamp	Molecular Devices	10.3
Clampfit	Molecular Devices	N/A
Mini analysis program	Synaptosoft Inc.	N/A
Prism 8	Graph Pad	N/A
Inkscape	Inkscape.org	N/A

Table 2.1.5 | Summary of software used in the described studies.

Equipment		
Reagent or Resource	**Source or Supplier**	**Identifier**
Sledge Microtome	Bright Instruments	8000
Upright Microscope	Leica	DM 4000
Confocal Microscope	Leica	DMi8
Stereotaxic Frame	David Kopf Instruments	N/A
Injection controller	Neurostar	N/A
Injection syringe	Hamilton	Neuros
Injection controller	Word Precision Instruments	UMP3
Conditioned Place Aversion Chamber	University of Bristol Workshop	N/A
Vibrotome	Leica	VT1200
Sapphire Vibratome Blade	Delaware Diamond Knives	N/A
Perforated multi-electrode array	Multichannel Systems	60Pmea 100/30iR-Ti-gr
MEA interface and amplifier	Multichannel Systems	MEA1060
Amplifier	Molecular Devices	Axopatch 700B
Digitiser	Molecular Devices	Digidata 1440A
Concentric bipolar stimulating electrode	FHC incorporated	50 µm internal diameter
Stimulator	AMPI	Isoflex stimulator

Table 2.1.6 | Summary of equipment used in the described studies.

2.2 | Mice

All animal studies performed in the UK were conducted in accordance with the UK Animals in Scientific Procedures Act 1986 (ASPA) and study plans were approved by the Institutional Animal Welfare and Ethical Review Body at the University of Bristol and/or Exeter. Experiments performed at Washington State University, USA were conducted with the approval of the Institutional Animal Care and Use Committee and in accordance with the US Public Health Service Policy on Human Care and Use of Laboratory Animals and the National Institutes of Health Guide for the Care and Use of Laboratory animals.

Adult (age > 8 weeks) male C57BL6/J mice (Charles River or University of Exeter Colony) were used for all experiments unless stated otherwise. All mice were individually housed at least 4 days prior to experiments and maintained on a 12:12 light-dark cycle at 22 ± 2 °C, with unlimited access to standard laboratory rodent diet (EURodent diet [5LF2], LabDiet, UK) and water unless otherwise stated. Each cohort of mice used to generate data in specific figures is described in **table 2.2.1**.

Strain	Number	Sex	Source	Procedure	Figures
C57BL6/J	9	Male	University of Exeter Colony	12 hour high fat chow feeding and standard chow controls, IHC	3.3.1 a, b, 3.3.2 - 3.3.4, 3.3.10
C57BL6/J	10	Male	University of Exeter Colony	12 hour high fat chow feeding and standard chow controls, IHC	3.3.1 a, b, 3.3.2
C57BL6/J	10	Male	University of Exeter Colony	12 hour fasting and standard chow controls, IHC	3.3.5, 3.3.6, 3.3.10
C57BL6/J	9	Male	University of Exeter Colony	13 week high fat chow feeding and standard chow controls, IHC	3.3.7 - 3.3.9, 3.3.10
C57BL6/J	12	Male	Charles River	DVC virus injection of AAV-GFAP-hM3Dq or mCherry controls, feeding assays, fast-induced refeed, conditioned place aversion, home cage activity monitoring, tail flick assay, IHC	4.3.1 - 4.3.13, 4.3.15 - 4.3.17
C57BL6/J	7	Male	Charles River	Conditioned place aversion, lithium chloride	4.3.10, 4.3.11
C57BL6/J	7	Male	University of Exeter Colony	DVC virus injection of AAV-GFAP-hM3Dq or mCherry controls, feeding assays, fast-induced refeed, IHC	4.3.14
C57BL6/J	12	Male	University of Exeter Colony	DVC virus injection of AAV-GFAP-hM4Di or mCherry controls, feeding assays, fast-induced refeed, IHC	4.3.18 - 4.3.22
C57BL6/J	10	Male	University of Exeter Colony	12 hour high fat chow feeding and standard chow controls, slice electrophysiology	3.3.1 c-e, 5.3.1 - 5.3.11
TH-EGFP	12	Female	Washington State University Colony	Slice electrophysiology	5.3.12 - 5.3.14

Table 2.2.1 | Description of mice used for each experiment. AAV = adeno-associated viral vector, GFAP = glial fibrillary acidic protein, IHC = immunohistochemistry.

2.3 | Methods used in Chapter 3

2.3.1 | Dark-phase high-fat feeding studies

Two independent cohorts of male C57BL6/J mice (16 weeks) were individually housed for 4-5 days. In the experimental group, standard chow (LabDiet) was substituted for high-fat chow (TestDiet) at lights off on the test day. Control mice were maintained on standard chow. 12-14 hours later mice were euthanized within two hours of lights on by intraperitoneal (i.p.) injection of sodium pentobarbital (1.6 g/kg) and transcardially perfused with 0.9% NaCl (Saline) containing heparin followed by 4% paraformaldehyde (PFA) in 0.01M phosphate buffered saline (PBS). Brains were post-fixed for 4-6 hours in 4% PFA PBS before being transferred to 30% sucrose in PBS. These brains were then removed from sucrose and stored at -80 °C until used for histology (see **Section 2.3.4** below).

2.3.2 | Dark-phase fasting studies

A cohort of male C57BL6/J mice (16 weeks) were individually housed for 4-5 days. In the experimental group, food was removed from the cage at lights off on the test day. Control mice were maintained on standard chow. 12-14 hours later mice were euthanized within two hours of lights on, perfused and brains stored as described above (**Section 2.3.1**).

2.3.3 | Diet induced obese studies

A cohort of male C57BL6/J mice (12 weeks) were assigned to receive either standard chow (LabDiet) or high fat chow (TestDiet). These mice were fed this diet for 13 weeks and body weight was measured weekly. At the end of the feeding period mice were euthanized within two hours of lights on, perfused and brains stored as described above (**Section 2.3.1**).

2.3.4 | GFAP immunohistochemistry

For the brains collected in the above studies (**Sections 2.3.1, 2.3.2, 2.3.3**) 30 µm coronal sections of the brainstem were taken with a freezing sledge microtome (Bright Instruments) in 4 series, i.e. each section in a series was 120 µm apart. One series was washed (3x 5 minute washes) in 0.01M PBS then incubated in blocking solution (0.01M PBS containing 0.3% Triton X-100 and 5% normal donkey serum [NDS]) for 1 hour at room temperature. These sections were then incubated in mouse-anti glial fibrillary acidic protein (GFAP; Merck) diluted 1:5000 in carrier solution (0.01M PBS containing 0.3% Triton X-100 and 1% NDS) overnight at 4 °C. Sections were then warmed to room temperature before being washed (8x 5 minute washes) in 0.01M PBS. Sections were incubated in donkey anti-mouse AlexaFluor 568 (Invitrogen) diluted 1:500 in 0.1M PBS containing 0.3% Triton X-100 for 1 hour at room temperature. Sections were then washed (8x 5 minute washes) in 0.01M PBS, mounted on to glass slides and cover slipped with mounting medium with DAPI (AbCam). A separate set of sections was stained following this protocol but with the primary antibody substituted for carrier solution to assess non-specific staining (**Figure 2.3.1 a**).

2.3.5 | Image acquisition and analysis

Images for cell counting were acquired at 10X magnification on a fluorescence microscope (Leica). One image with the NTS in the field of view was acquired for sections corresponding to -7.08 mm from Bregma to -8 mm from Bregma in a brain atlas (Paxinos and Franklin, 2001). The number of GFAP expressing cells was counted using the cell counting plugin in FIJI (Schindelin *et al.*, 2012) and the mean number of cells per section calculated for each animal. For regional analysis the NTS was sub-divided as follows: rostral = Bregma -7.08mm - -7.2mm, postremal = Bregma -7.32mm - -7.64mm, caudal = Bregma -7.76mm - -

8mm and the mean number of GFAP expressing cells per section binned into these divisions.

Images for morphological analysis were acquired at 20X magnification on a confocal microscope (Leica). Z-stacks were acquired for two pNTS sections per mouse. GFAP-immunoreactive cells in these images were marked with coloured dots using the cell counter plugin in FIJI, the original image was removed so only dots were visible to represent each cell then 5 of these cells were randomly selected for tracing. Semi-automated tracing was performed using the simple neurite tracer FIJI plugin (now known as SNT) (Ferriera *et al.*, 2014). The number of processes per cell were counted and Sholl analysis was performed to give the Sholl profile and enclosing radius of each cell (**Figure 3.3.3**). The investigator was blinded to the diet of the mice during immunohistochemical staining, image acquisition and analysis.

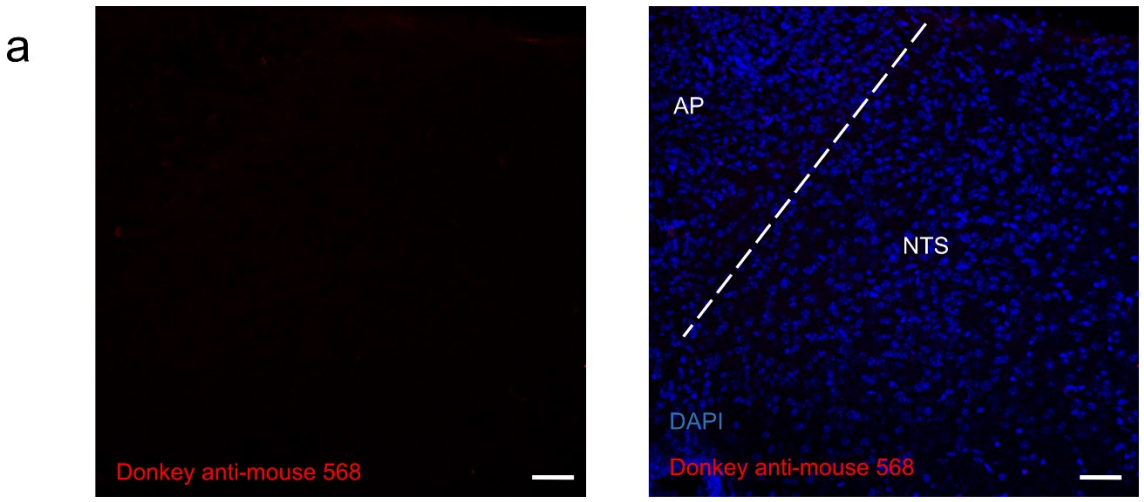

Figure 2.3.1 | Demonstration of specificity of anti-mouse AlexaFluor 568 secondary antibody binding. Representative images of NTS sections stained in the absence of the primary antibody and stained with the secondary donkey anti-mouse AlexaFluor 568. Left: 568 nm channel alone, Right: 568 nm channel with DAPI co-stain. AP = area postrema, NTS = nucleus of the solitary tract. Scale bars = 50 μm.

2.4 | Methods used in Chapter 4

2.4.1 | AAV vector injection

Initial injections were made at four sites across the NTS to ensure efficient targeting (mice described in **Sections 4.3.1 – 4.3.13 and 4.3.15 – 4.3.17**). Mice (8 – 12 weeks) were injected with adeno-associated viral (AAV) vectors to target the dorsal vagal complex (DVC). Mice were deeply anaesthetized with an i.p. injection of ketamine (70 mg/kg) and medetomidine (0.5 mg/kg) and placed in a stereotaxic frame (David Kopf Instruments) with the nose angled down by 20°. An incision from the occiput to the nape of the neck was made, the muscles were parted, and the atlanato-occipital membrane incised to expose the surface of the brainstem. Injections were made from a pulled glass pipette attached to an injection system (Neurostar) mounted on the stereotaxic frame at an angle of 35° relative to vertical, tip facing rostral. The pipette was inserted 400 µm lateral to the midline at the level of calamus scriptorius to a depth of 1mm. Four AAV injections of 180 nl were made bilaterally at angled depths of 1 mm, 750 µm, 500 µm and 250 µm, respectively, at a rate of 100 nl/minute. Mice were injected with either AAV5/2-hGFAP-hM3Dq_mCherry (ETH Zurich Viral Vector Facility) or AAV5/2-hGFAP-mCherry (Vigene Bioscience). The pipette was left in place for 1 minute after each injection. Following injection, the pipette was removed from the brain, the muscles were apposed with a loose suture and the skin sutured to allow the wound to heal. Mice were injected with atipamezole (1 mg/kg i.p) and buprenorphine (0.1 mg/kg subcutaneous) for anesthetic reversal and analgesia, respectively, and were transferred to a heated cage to recover. Following surgery mice were individually housed for the duration of the experiment.

For subsequent experiments, injections were made at a single site in the pNTS to restrict viral spread. These mice are those described in **Sections 4.3.14 and**

4.3.18 – 4.3.22. Surgery was identical to those described above except that injections were made from a syringe (Hamilton) connected to an injection controller (World Precision Instruments). This syringe was inserted 200 µm lateral to the midline at the level of calamus scriptorius to a depth of 500 µm. Bilateral injections of 180 nl were made at a rate of 100 nl/minute. Mice were injected with, AAV5/2-hGFAP-hM3Dq_mCherry (ETH Zurich Viral Vector Facility), AAV5/2-hGFAP-hM4Di_mCherry (ETH Zurich Viral Vector Facility), or AAV5/2-hGFAP-mCherry (Vigene Bioscience) The syringe was left in place for 2 minutes following the injection. In addition to the analgesia described above these mice received an injection of carprofen (5 mg/kg subcutaneous) the following morning.

All mice were allowed at least 3 weeks to recover from surgery and were individually housed before any experiments were performed.

2.4.2 | Immunohistochemistry of AAV injected mice

Mice received clozapine-N-oxide (CNO; 0.3 - 1 mg/kg i.p.) during the first 4 hours of the light phase and had food removed from the cage. 2-3 hours later mice were transcardially perfused and brains stored as described above (**Section 2.3.2**). 30 µm coronal sections containing the brainstem, midbrain and hypothalamus were taken with a freezing sledge microtome (Bright Instruments) in 4 series, i.e. each section in a series was 120 µm apart. NTS sections from one series were washed (3x 5 minute washes) in 0.01M PBS then incubated in blocking solution (0.01M PBS containing 0.3% Triton X-100 and 5% normal donkey serum [NDS]) for 1 hour at room temperature. These sections were then incubated in goat anti-mCherry (Origene) diluted 1:1000 in carrier solution (0.01M PBS containing 0.3% Triton X-100 and 1% NDS) overnight at 4 °C. Sections were then warmed to room temperature before being washed (8x 5 minute washes) in 0.01M PBS. Sections were incubated in donkey anti-goat AlexaFluor 594 (Invitrogen) diluted 1:500 in

0.1M PBS containing 0.3% Triton X-100 for 1 hour at room temperature. Sections were then washed (8x 5 minute washes) in 0.01M PBS and incubated in mouse anti-GFAP (Merck) 1:5000 in carrier solution overnight at 4 °C. Sections were then warmed to room temperature before being washed (8x 5 minute washes) in 0.01M PBS. Sections were incubated in donkey anti-mouse AlexaFluor 488 (Invitrogen) diluted 1:500 in 0.1M PBS containing 0.3% Triton X-100 for 1 hour at room temperature. Sections were then washed (8x 5 minute washes) and mounted on to glass slides and cover slipped with mounting medium with DAPI (AbCam).

NTS sections from a second series were stained in the same fashion but with rabbit anti-NeuN (AbCam) and donkey anti-rabbit AlexaFluor 488 (Invitrogen) replacing mouse anti-GFAP and donkey anti-mouse AlexaFluor 488, respectively.

Hypothalamus, midbrain and brainstem sections from a third series were stained with rabbit anti-c-FOS (Cell Signalling) and donkey anti-rabbit AlexaFluor 488 (Invitrogen).

A separate set of sections was stained in parallel following this protocol but with the primary antibody substituted for carrier solution to assess non-specific staining of AlexaFluor 488 tagged secondary antibodies (**Figure 2.4.1 a, b**).

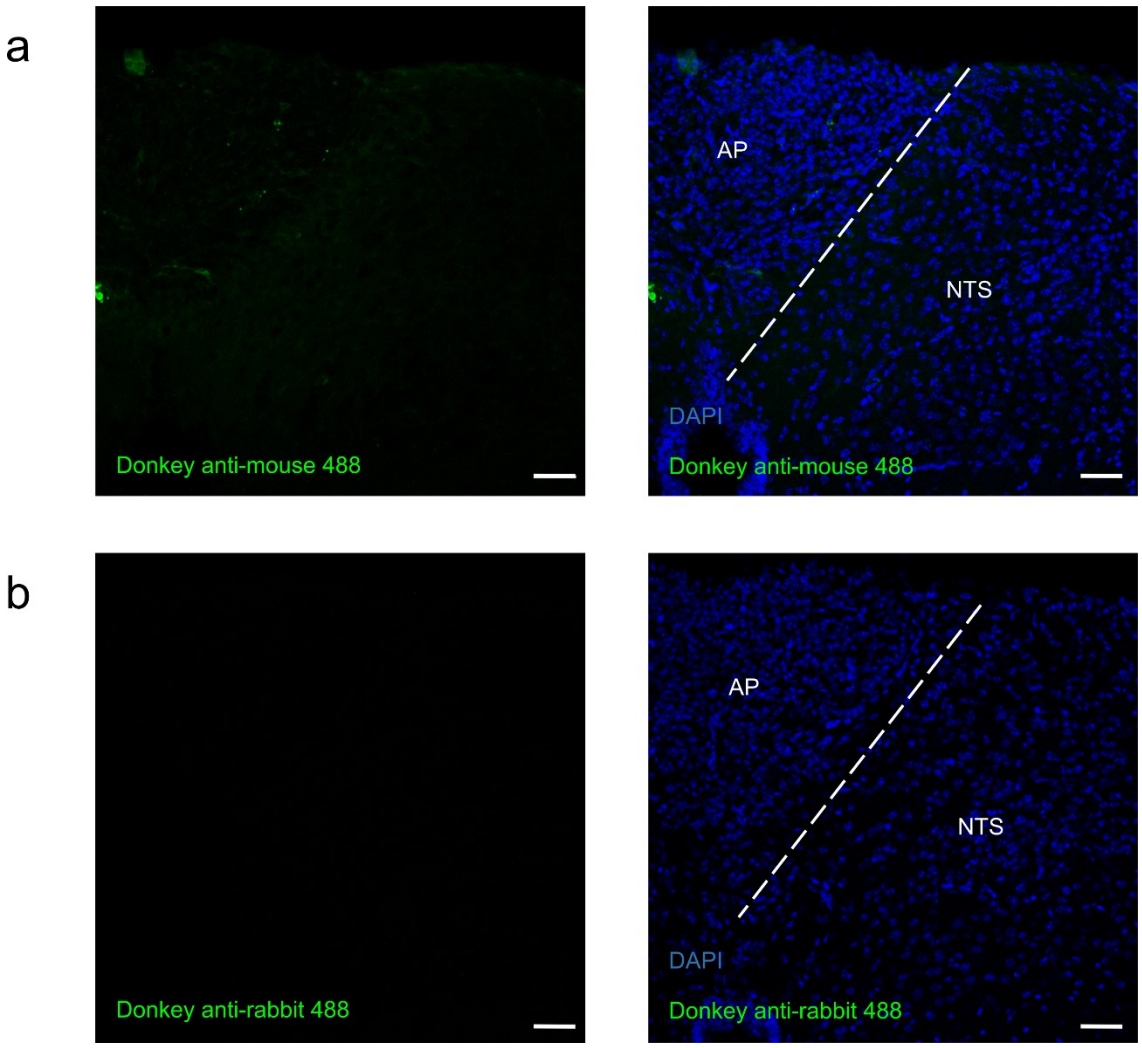

Figure 2.4.1 | Demonstration of specificity of anti-mouse and anti-rabbit AlexaFluor 488 secondary antibody binding. Representative images of NTS sections stained in the absence of the primary antibody and stained with **a**, the secondary donkey anti-mouse AlexaFluor 488 or **b**, the secondary donkey anti-mouse AlexaFluor 488. Left: 488 nm channel alone, Right: 488 nm channel with DAPI co-stain. AP = area postrema, NTS = nucleus of the solitary tract. Scale bars = 50 µm.

2.4.3 | AAV injection mapping

The AAV vectors used contained a sequence encoding mCherry to enable visualization of the viral transduction and spread. The distribution of mCherry immunoreactivity was manually mapped relative to corresponding sections in a mouse brain atlas (Paxinos and Franklin, 2001). The area of transduction was quantified using FIJI. To display this (**Figure 4.3.2**), transparent shapes (each one representing the spread in a single animal) were overlaid on a scale diagram of the NTS; where colours appear darkest is where the greatest overlap of transduction between mice occurred.

2.4.4 | Validating AAV transduction of astrocytes

Sections double stained for GFAP and mCherry-immunoreactivity or NeuN and mCherry-immunoreactivity were imaged on a confocal microscope (Leica) at 20X magnification. The total number of GFAP and NeuN expressing cells in the field of view and the number of each cell type also expressing mCherry were counted with the cell counter plugin in FIJI.

2.4.5 | Validating DREADD activation of astrocytes

Morphological analysis of NTS astrocytes from CNO treated mice was performed as described above (**Section 2.3.5**).

2.4.6 | c-FOS quantification

Sections stained for c-FOS immunoreactivity containing the paraventricular nucleus of the hypothalamus (Bregma -0.94 mm), lateral parabrachial nucleus (Bregma -5.02 mm) and pNTS (Bregma -7.56 mm) were imaged under 20X magnification with a confocal microscope (Leica). The number of c-FOS expressing cells within each brain region were manually counted using the cell counter plugin in FIJI.

In some experiments only the pNTS was imaged for c-FOS quantification.

2.4.7 | Dark phase food intake measurements

Mice were acclimatised to experimenter handling and i.p. injections for at least 4 days. On test days mice received saline (i.p.) 15 – 30 minutes prior to the onset of the dark phase. Food intake was manually measured by the investigator at 2, 4, 6, 12 and 24 hours after lights off (under red light illumination where necessary). In some experiments food weight was also measured at 1 hour after lights off. Body weight was measured either at 6 or 8 hours after lights-off. The following day mice received an injection of CNO (0.3 – 1 mg/kg i.p.) 15-30 minutes prior to the onset of the dark phase. Food intake and body weight were again measured at the same time points.

2.4.8 | Fast induced re-feeding experiments

Body weight of mice was measured prior to fasting. To fast the mice, all food was removed from cages at the beginning of the dark phase. Subsequently, 15-30 minutes prior to the onset of the light-phase mice received an injection of CNO (0.3-1 mg/kg i.p.) under red light illumination. At the onset of the light-phase food was returned to cages and intake was measured 1, 2, 4, 6, 8, 12 and 24 hours after lights on. In some experiments body weight was measured a second time, 8 hours after lights on. In some experiments mice received a second injection of saline or cholecystokinin (CCK) (3.5 µg/kg i.p.) concurrently with food being reintroduced. In these experiments food intake was also measured 30 minutes after reintroduction.

2.4.9 | Conditioned place aversion

For conditioned place aversion testing an apparatus consisting of two distinct chambers joined by a clear plastic external corridor was used (University of Bristol

Workshop; **Figure 4.3.10**). The left chamber had horizontal black and white stripes on the walls and a perforated floor, and the right chamber had vertical black and white stripes on the walls and a floor with horizontal grating. A counter-balanced paradigm was used to test conditioned place aversion. On the first day mice were given 20 minutes of free access to explore the whole apparatus. This session was recorded using a video camera and used to determine initial location preferences. On the second day (conditioning 1), mice were assigned to receive either CNO (0.3 mg/kg i.p.) or an equivalent volume of saline 15 minutes prior to being placed in either the left or right chamber for 45 minutes, with the access to the external corridor and second chamber blocked. On the third day (conditioning 2) mice received the opposite treatment with their access restricted to the alternate chamber, compared to the second day. These sessions were recorded and used to measure locomotion following injection of CNO or saline. On the fourth/final day mice were given free access to the whole apparatus for 30 minutes. Again, this session was recorded and used to determine conditioned preference. Recorded sessions were analyzed offline using Ethovision XT tracking software (Noldus). An independent cohort of C57BL6/J mice underwent the same conditioning protocol with the known aversive agent lithium chloride (LiCl, 150 mg/kg i.p. diluted in saline) as a positive control, replacing CNO as the experimental stimulus.

2.4.10 | Home cage food seeking

Individually housed mice were injected with CNO (0.3 mg/kg i.p.) 15 minutes prior to the beginning of the dark phase and their home cage placed under a video camera with food removed from the hopper and two pieces of food placed on the cage floor in the far corner from the nest. The activity was then recorded for 3 hours and food intake at 3 hours was measured. Recorded sessions were

analyzed offline using Ethovision XT tracking software (Noldus) with a 6 cm^2 zone centered around the pellets termed the 'food zone' and 4 cm x 3 cm zone centered around the water bottle spout termed the 'spout zone'.

2.4.11 | Tail flick test

Individually housed mice were restrained by scruffing and the distal end of the tail submerged into 52 °C water. This induces a characteristic 'tail flick' escape response (Malmberg and Bannon, 2001) and the latency from submersion to this response was recorded. Three 'baseline' measurements were made separated by 15 minutes before an injection of CNO (0.3 mg/kg i.p.). Following injection, measurements were made at 15 minute intervals for 1 hour.

2.5 | Methods used in Chapter 5: Mutli-electrode array (MEA) recordings

2.5.1 | Solutions

Molecule	**Concentration (mM)**
NaCl	124
KCl	3
$NaHCO_3$	24
NaH_2PO_4	1.25
$MgSO_4.7H_2O$	1
$CaCl_2$	2
D-Glucose	10

Table 2.5.1 | Concentrations of molecules in the 10mM Glucose artificial cerebrospinal fluid (aCSF).

Molecule	Concentration (mM)
NaCl	124
KCl	3
$NaHCO_3$	24
NaH_2PO_4	1.25
$MgSO_4.7H_2O$	1
$CaCl_2$	2
D-Glucose	5
Sucrose	5

Table 2.5.2 | Concentrations of molecules in the 5mM Glucose artificial cerebrospinal fluid (aCSF).

Molecule	Concentration (mM)
Sucrose	189
D-Glucose	3
$NaHCO_3$	24
KCl	1.25
$MgSO_4.7H_2O$	1
$CaCl_2$	0.1
NaH_2PO_4	1.25

Table 2.5.3 | Concentrations of molecules in the slicing solution.

2.5.2 | Coronal NTS slice preparation

Mice were individually housed for at least 4 days prior to experiment and food intake was monitored daily. The day before the brain slices were made, mice were either maintained on standard chow or provided with high fat chow immediately prior to lights off. 12 hours later (at lights on) mice were culled by cervical dislocation. The brain was quickly removed, cut in the coronal plane at roughly –3.4 mm from Bregma and the rostral surface glued to the stage of a cutting chamber. The chamber was filled with ice cold, oxygenated, cutting

solution and mounted on a vibrotome (Leica). 300 µm coronal slices were taken with a stainless steel blade and slices containing the NTS were transferred to 10 mM glucose aCSF at room temperature.

In these animals the stomachs were also dissected out and weighed. Stomach contents were then emptied and the empty stomach was weighed and subtracted from the full stomach weight to calculate the mass of stomach contents.

After at least an hour, a slice was placed in a perforated MEA (pMEA) recording chamber (Multichannel Systems) where the electrodes were arranged in a 6 x 10 configuration separated by 100 µm. The slices was oriented such that the NTS was located on the electrode array and held down by a harp. 5 mM glucose aCSF heated to 33 ˚C was continuously perfused into the chamber from a top flow controlled by a peristaltic pump and a bottom flow controlled by a suction pump. The flow rate was 2.5 ml/minute. To aid analysis, images were acquired *in situ* of the array and of the slice positioned on the array. After 30 minutes of acclimatisation the recording began (**Figure 5.3.3**). Resting activity was recorded for 20 minutes before 30 µM N-methyl-D-aspartate (NMDA) in aCSF was perfused into the chamber for 10 minutes. Then aCSF containing 30 µM NMDA and 50 µM D-serine was perfused for 10 minutes. Following this, aCSF was perfused in the bath for 10 minutes (washout) and then the recording was concluded. Data were acquired at a sample rate of 50 kHz using the MC_Rack system (Multichannel Systems) and raw data was stored for offline analysis.

2.5.3 | Data processing and analysis

Raw data from the recordings were filtered (high-pass filter 200 Hz, second-order Butterworth; the data were not low-pass filtered) then thresholded in MC_Rack (Multichannel systems) to extract spikes from the recordings. The threshold used

was -16 µV as at this threshold spiking activity could be clearly separated from noise and non-spiking electrical activity. These thresholded data were then processed in MATLAB (Mathworks) using a modified script originally written by Dr Jon Brown (University of Exeter) and a bespoke script for discarding channels. Channels were considered to have meaningful spiking activity and considered in statistical analysis if they met the following criteria; 1, a resting firing rate of > 1Hz OR 2, a > 2-fold increase in firing rate between resting and NMDA AND 3, more than 300 spikes during the whole recording period AND 4 located in the NTS. For suitable channels meeting these criteria mean firing rates were calculated during the final 180s of each period of the recording and extracted to Prism for statistical analysis. To generate heatmaps the approximate x and y coordinates of each electrode were calculated relative to the central canal. These were plotted as a scatter plot with the colour of each point reflective of the firing rate of that electrode (**Figure 5.3.6, 5.3.8**). These plots were generated using a bespoke MATLAB script.

2.6 | Methods used in Chapter 5: Whole cell patch clamp recordings

2.6.1 | Solutions

Molecule	**Concentration (mM)**
NaCl	125
KCl	3
$NaHCO_3$	25
KH_2PO_4	1.2
$MgSO_4$	1.2
$CaCl_2$	2
D-Glucose	10

Table 2.6.1 | Concentrations of molecules in the external artificial cerebrospinal fluid (aCSF).

Molecule	Concentration (mM)
NaCl	10
K gluconate	130
EGTA	11
HEPES	10
$MgCl_2.6H_2O$	2
$CaCl_2$	1
ATP	2
GTP	0.2
D-glucose	To osmolarity (297-300 mosM)

Table 2.6.2 | Concentrations of molecules in the internal recording pipette solution.

2.6.2 | Horizontal NTS slice preparation

Female TH-EGFP mice (maintained on a C57BL6/J background) (Matsushita *et al.*, 2002) aged 8-12 weeks were anesthetised with 4% isofluorane and killed by thoracic pressure. The hindbrain was quickly removed and placed in ice cold, oxygenated aCSF. The cerebellum was removed and a small wedge of tissue trimmed from the ventral surface of the hindbrain to correctly orient the ST and NTS in the cutting plane. The ventral surface tissue was then glued to the stage of a cutting chamber and submerged in ice cold oxygenated aCSF and the cutting chamber was mounted on a vibrotome (Leica). Under magnification and illumination the dura and blood vessels were removed from the dorsal surface of the hindbrain to expose the NTS. Small horizontal sections were taken with a sapphire blade (Delaware Diamond Knives) until the ST was clearly visible at the brain surface. Then a 250 μm thick slice was taken and immediately transferred to the recording chamber of a patch clamp rig. The slice was weighed down with a harp and perfused with room temperature aCSF for 1 hour.

2.6.3 | Whole cell patch clamp electrophysiology

Following the acclimatisation period, the inflow heater was turned on and the slice was perfused with 33 °C aCSF. A bipolar concentric stimulating electrode (FHC incorporated) was placed on the ST (**Figure 5.3.10**). Pulled pipettes (tip resistance 3-5 mΩ) were filled with internal solution and mounted onto the headstage. Cells were identified within 200 µm of the obex and were selected by the presence of EGFP fluorescence. Upon formation of a gigaohm seal and break in, cells were recorded in voltage clamp configuration and held at a membrane potential of -60 mV. Recordings were made using a protocol of 6 second sweeps consisting of a 1 second rest period followed by 10 ST stimulations (50 Hz) then the remainder of the sweep. A run consisted of 10 sweeps with no intersweep interval. This protocol was continuous for the whole experimental period. The stimulus intensity was increased until clear evoked EPSCs were visible, if no evoked EPSCs were observed the cell was not recorded from further. Cells were recorded for 10 minutes in aCSF then 10 minutes in a bath perfusion 100 µM DHK before a 10 minute washout period. Control cells were recorded the same but with aCSF instead of DHK perfused through the drug delivery system. Data were acquired with pClamp (Molecular Devices) and stored for offline analysis.

2.6.4 | Data analysis

For measurements of evoked EPSC amplitude, files from the final minute of each recording epoch were loaded in Clampfit (Molecular Devices) and the difference between the holding current and the peak (trough) of the evoked EPSC were measured. The mean of 10 sweeps was calculated and used for statistical analysis.

For measurements of spontaneous and asynchronous EPSCs the final 3 minutes of each recording epoch was loaded into Mini analysis program (Synaptosoft Inc.)

for event detection. The cumulative number of events in 100 ms bins was calculated for 30 sweeps and used for statistical analysis.

2.7 | Statistical analysis

Data are presented as mean ± SEM where appropriate with the exception of non-normally distributed MEA data which are shown in violin plots and data are presented as median ± interquartile range. Data for all experiments were analysed in Prism 7 (Graph Pad) and the appropriate statistical tests conducted. Graphs were generated in Prism or MATLAB, representative images were prepared in FIJI, representative electrophysiology traces were prepared in MATLAB and figures were prepared in Inkscape (inkscape.org).

Chapter 3

Response of NTS astrocytes to short- and long-term deviations in energy balance

3.1 | Introduction

Astrocytes in specific nuclei of the hypothalamus, including the arcuate nucleus (ARC), contribute to inflammation in both diet induced and genetic obesity in rats and mice (Thaler *et al.*, 2012; Buckman *et al.*, 2013). This is best characterised by greater expression of the cytoskeletal glial fibrillary acidic protein (GFAP) and increased branching of the primary (GFAP immunoreactive) processes. Inflammatory signalling in astrocytes increases susceptibility to obesity (Zhang *et al.*, 2017) while preventing astrocyte NF-κB signalling can be protective against weight gain (Douglass *et al.*, 2017; Zhang *et al.*, 2017). Taken together it appears that hypothalamic astrocyte inflammation in experimental models of obesity is a maladaptive response and serves to exacerbate weight gain, possibly by impairing the function of appetite governing hypothalamic circuits (Horvath *et al.*, 2010).

Hypothalamic astrocyte activation in response to high fat chow ingestion occurs in two distinct phases (Thaler *et al.*, 2012; Balland and Cowley, 2017). The initial phase occurs within the first 24 hours of high fat chow intake and appears to contribute to the homeostatic response to increased food intake since inhibiting astrocyte inflammatory signalling increases initial hyperphagia on a high fat diet (Buckman *et al.*, 2015). However with continued intake (four weeks or more) a second phase of astrocyte activation emerges (Thaler *et al.*, 2012; Balland and Cowley, 2017). Therefore it appears the acute activation of astrocyte inflammatory pathways is a mechanism to reduce food intake following hyperphagia while following continued high fat feeding, prolonged activation is detrimental to energy balance processing.

ARC astrocytes are bi-directionally regulated by food intake. In addition to showing changes in activity in response to nutritional excess associated with high

fat feeding (as described above), fasting and chronic i.c.v leptin infusion (which reduces food intake) cause increases in GFAP and altered morphology of arcuate astrocytes in mice and rats (Fuente-Martín *et al.*, 2012; N. Chen *et al.*, 2016; Zhang *et al.*, 2017). Given that neurons in the ARC can differentially mediate hunger and satiety it is likely that this acute astrocyte activation similarly serves to mediate food intake and restore energy levels in the face of fasting. In support of this, the outcome of direct ARC astrocyte activation using chemogenetics has differing effects depending on the energy state of the mouse, appearing to balance ARC neural circuit activity towards energy homeostasis (Yang, Qi and Yang, 2015; N. Chen *et al.*, 2016).

In addition to this established ARC astrocyte plasticity, there have been numerous demonstrations that GFAP expression and astrocyte morphology in the nucleus of the solitary tract (NTS) is dynamic and regulated in different experimental settings (**Table 1.4.1**). Despite the accepted role of the NTS in controlling food intake, and ARC astrocytes being regulated by energy state, the response of NTS astrocytes to perturbations in energy balance has not been reported.

3.2 | Aims and hypotheses

In this chapter we aimed to characterise the response of NTS astrocytes, as assessed by GFAP immunoreactivity and morphology, to deviations in food intake. To measure this cellular response to energy state, mice were fasted for 12-14 hours or fed high fat chow for 12-14 hours or 13 weeks. We then measured the number and morphology of GFAP expressing astrocytes in the NTS, with a specific focus of those at the level of the area postrema since that is where stomach-innervating vagal afferents terminate (Williams *et al.*, 2016; Han *et al.*, 2018; Bai *et al.*, 2019).

Given that the NTS is considered to be principally concerned with meal termination (Grill and Hayes, 2012), we first hypothesised that NTS astrocytes would show greater GFAP immunoreactivity and morphological complexity in the acute high fat group as compared with the standard chow fed controls.

Secondly, given that NTS astrocytes are capable of sensing low tissue glucose, we hypothesised that this process would drive astrocyte activation, detectable by our measurements, in fasted mice.

Finally, given the profound astrocyte alterations seen in the hypothalamus of diet induced obese (DIO) mice (Buckman *et al.*, 2013), we expected to see similar changes in the NTS.

3.3 | Results

3.3.1 | High fat chow induced acute hyperphagia in mice

The response of mice to high fat chow availability is stereotypical and well characterised (Buckman *et al.*, 2015; Douglass *et al.*, 2017). It consists of two phases, an initial hyperphagia followed by homeostatic reductions in food intake to compensate for the increased caloric content of the food. Thus, short term hyperphagia can be reliably induced by providing mice with high fat chow for a short duration. To allow us to investigate the response of NTS astrocytes to increased food intake we allowed mice to eat high fat chow for 12-14 hours during the dark phase before either perfusion fixation or cervical dislocation. Control animals were maintained on standard chow. High fat chow fed mice tended to eat a greater mass of food but this did not reach statistical significance (**Figure 3.3.1 a**, 3.31 ± 0.16 vs 3.62 ± 0.14 g, p = 0.16, unpaired t-test). Given the greater caloric density of the diet, high fat chow fed mice did however consume a greater number of calories than those on standard chow (**Figure 3.3.1 b**, 10.53 ± 0.51 vs

18.48 ± 0.74 kcal, $p < 0.0001$, unpaired t-test). In mice that were sacrificed by cervical dislocation, the contents of the stomach were measured and were found to be far greater in high fat chow fed mice compared with standard chow fed controls (**Figure 3.3.1 c, d,** 0.45 ± 0.07 vs 1.20 ± 0.22 g, $p < 0.0001$, unpaired t-test). As anticipated, the contents of the stomach correlated positively with the caloric intake (**Figure 3.3.1 e**, $r^2 = 0.87$, $p < 0.0001$ from zero) showing that mice on a high fat chow eat more calories and have prolonged gastric distention. These results demonstrate that this is a valid paradigm for stimulating hyperphagia and activating signals, including gastric distension that are relayed to the NTS.

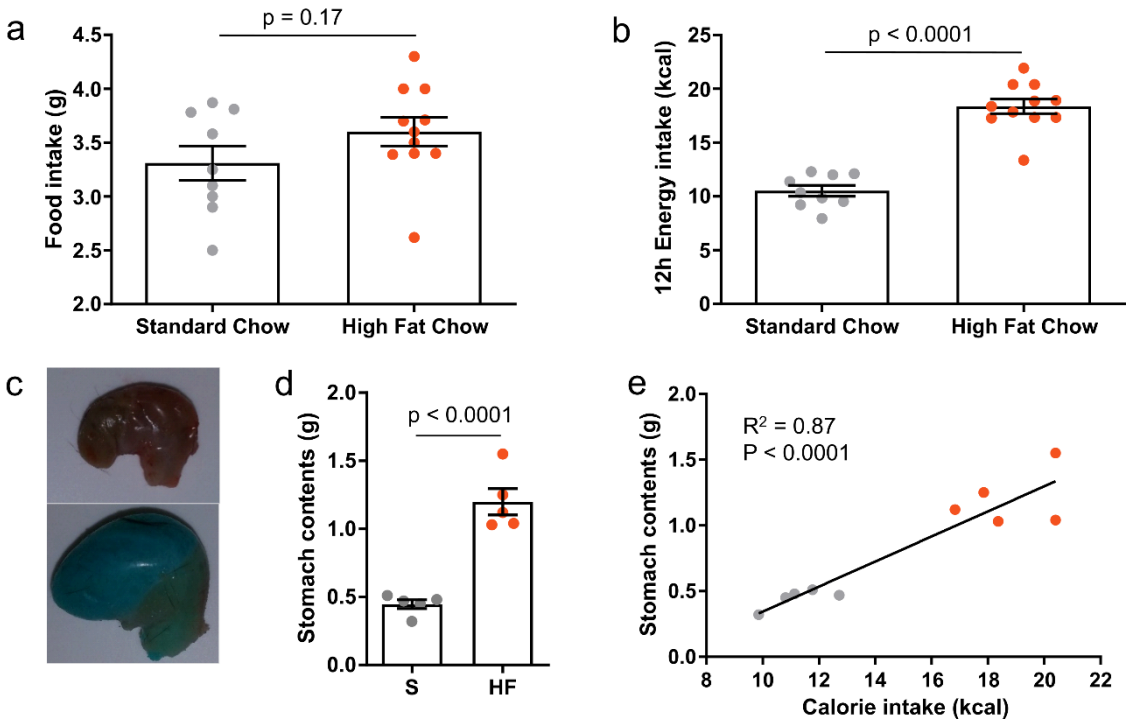

Figure 3.3.1 | High fat chow feeding induced hyperphagia in mice. **a,** Food intake during the 12-14 hour period prior to perfusion of mice fed standard chow and high fat chow (n = 9-10 mice per group, 3.31 ± 0.16 vs 3.62 ± 0.14 g; p = 0.16, unpaired t-test). **b**, Energy intake during the 12 – 14 hour period prior to perfusion of mice fed standard chow and high fat chow (n= 9 – 10 mice per group, 10.53 ± 0.51 vs 18.48 ± 0.74 kcal; p < 0.0001, unpaired t-test). **c,** Stomachs dissected from mice fed either standard chow (top) or high fat chow (bottom). **d,** Stomach contents of mice fed either standard chow (S) or high fat chow (HF) (n = 5 mice per group, 0.45 ± 0.07 vs 1.20 ± 0.22 g; p < 0.0001, unpaired t-test). **e,** Relationship between the energy intake and stomach contents in mice fed either standard chow or high fat chow (n = 5 mice per group, r^2 = 0.87, p < 0.0001 different from zero).

3.3.2 | High fat chow hyperphagia increased the number of GFAP immunoreactive astrocytes in the postremal NTS

In order to assess the impact of high fat chow induced hyperphagia on NTS astrocyte reactivity, we used immunohistochemistry against GFAP. In the NTS of high fat chow fed mice there was a striking increase in GFAP immunoreactivity (**Figure 3.3.2 a, b**). When quantified by counting the number of GFAP immunoreactive (GFAP+) cells across the rostro-caudal extent of the NTS, there were a greater number of GFAP+ cells per section in high fat chow fed mice when compared with standard chow controls (**Figure 3.3.2 c,** 43.09 ± 8.19 vs 67.90 ± 7.47 cells, $p = 0.038$, unpaired t-test). Binning the counts into rostral (rNTS), postremal (pNTS) and caudal (cNTS) subdivisions of the NTS revealed that the difference between diet groups was greatest, and statistically significant at the level of the NTS proximal to the area postrema (**Figure 3.3.2 d,** $p = 0.037$, two-way analysis of variance [ANOVA] with Sidak's post-hoc test).

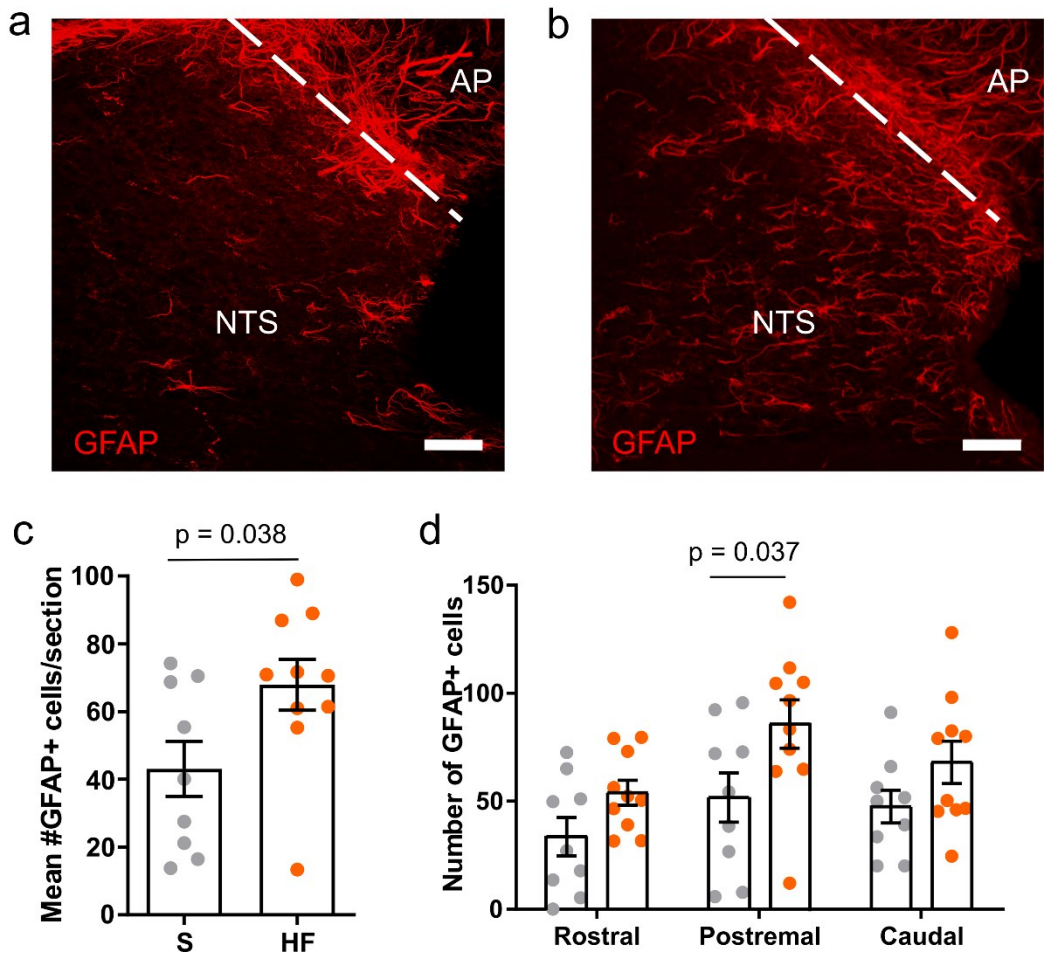

Figure 3.3.2 | High fat chow induced hyperphagia increased the number of GFAP immunoreactive astrocytes in the postremal NTS. a, Representative maximum projection confocal image of glial fibrillary acidic protein (GFAP) immunostaining from a standard chow fed mouse. **b,** Representative maximum projection confocal image of GFAP immunostaining from a high fat chow fed mouse. **c,** Mean number of GFAP immunoreactive (GFAP+) cells from tissue sections of the NTS from standard (S) and high fat chow fed (HF) mice (n = 9-10 mice per group, 43.09 ± 8.19 vs 67.9 ± 7.47 cells, p = 0.038, unpaired t-test). **d,** Number of GFAP+ cells within anatomical subdivisions of the NTS from standard and high fat chow fed mice (n=9-10 mice per group, Two-way ANOVA, food, p = 0.0018, $F_{(1,51)} = 10.81$, rostrocaudal position, p = 0.034, $F_{(2,51)} = 3.63$, interaction, p = 0.7, $F_{(2,51)} = 0.36$, Sidak's post-hoc test). AP = area postrema, GFAP = glial fibrillary acidic protein, NTS = nucleus of the solitary tract. Scale bars = 50 μm.

3.3.3 | High fat chow induced hyperphagia increased the morphological complexity of GFAP immunoreactive astrocytes in the postremal NTS

Given that GFAP makes up intermediate filaments of the astrocyte cytoskeleton, changes in its expression can result in changes to cytoskeletal morphology. To assess whether this was the case in our experiment, pNTS astrocytes from a subset of mice were randomly selected for morphological analysis by an investigator blinded to the experimental groups. Selected cells were 'traced' (digitally reconstructed using simple neurite tracer FIJI) to yield a 3 dimensional digital object on which to make measurements (**Figure 3.3.3 a-c**) (Ferriera *et al.*, 2014). Sholl analysis was used to quantify the morphological complexity of these traced cells (Sholl, 1953; Ferriera *et al.*, 2014). In this analysis, concentric rings of increasing radius (3 μm increments) were drawn around the cell's soma (**Figure 3.3.3 d**). The number of times processes of the cell intersect a given ring was quantified and plotted to give the Sholl profile of the cell (**Figure 3.3.3 e**). A cell with greater morphological complexity will give a greater "Sholl profile".

Sholl analysis revealed that astrocytes from the pNTS of high fat chow fed mice had a greater morphological complexity than those from standard chow fed controls (**Figure 3.3.4 a**). In addition, these cells had a greater number of processes than those from standard chow fed controls (**Figure 3.3.4 b,** 6.78 ± 0.41 vs 8.62 ± 0.38 processes per cell, $p = 0.0017$, unpaired t-test). Analysis of the mean enclosing radius (the farthest radius from the soma where a process intersects with the Sholl circle) showed no difference between the groups (**Figure 3.3.4 c**, 22.50 ± 1.02 vs 24.47 ± 1.12 μm, $p = 0.20$, unpaired t-test). Taken together, this suggests that astrocytes upregulate GFAP to form more processes rather than to extend existing ones. Representative traces from one mouse per group are shown (**Figure 3.3.4 d, e**).

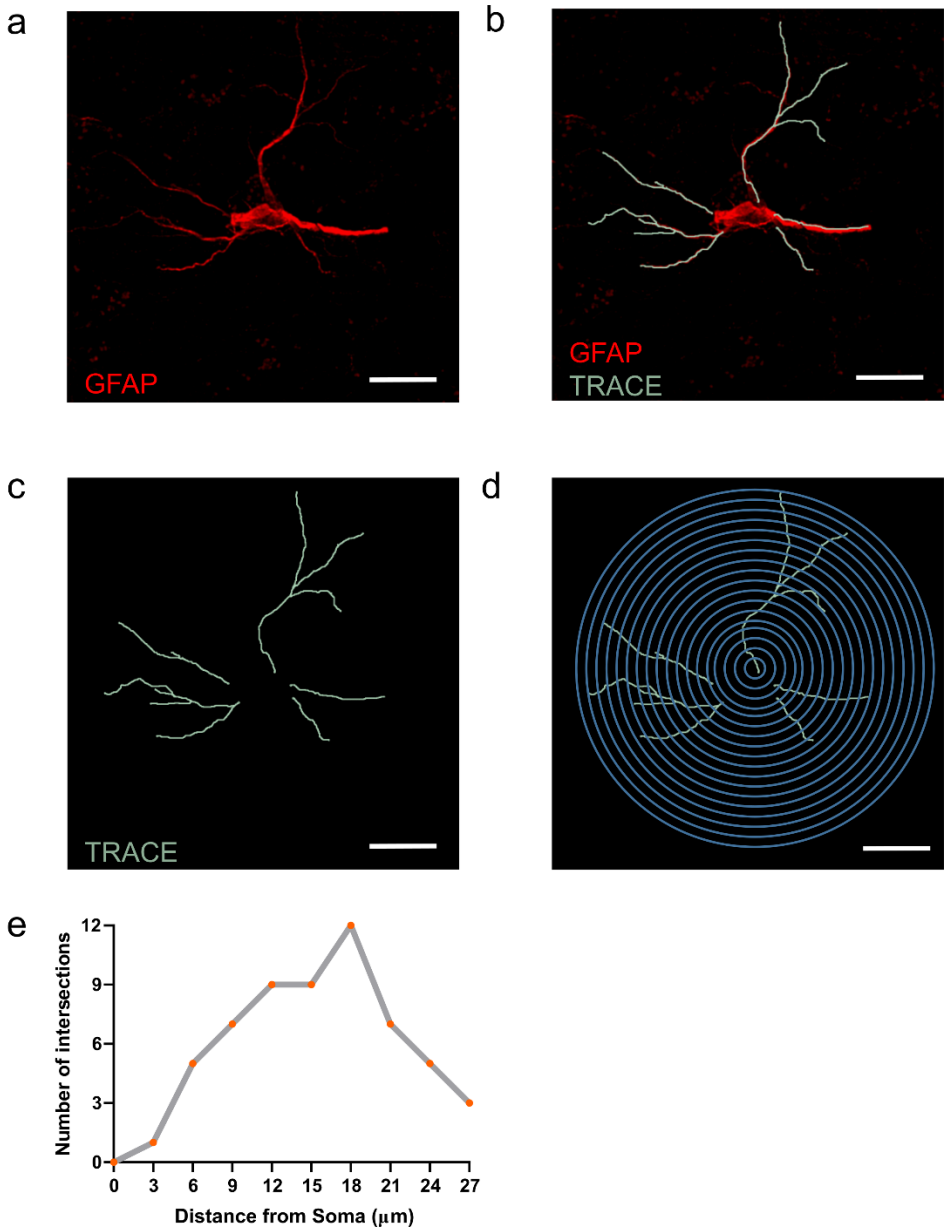

Figure 3.3.3 | Sholl analysis permits quantitative analysis of GFAP immunoreactive astrocyte morphological complexity. a, Maximum projection image of GFAP immunoreactivity from a single astrocyte. Note: this image is to clearly display the tracing and analysis and is not representative of the images used for statistical analysis in subsequent figures. **b**, Tracing results from Simple Neurite Tracer overlaid with the GFAP immunoreactivity of the selected cell. **c**, Tracing results from Simple Neurite Tracer. **d**, Sholl radii used for analysis overlaid with tracing results from Simple Neurite Tracer. **e**, Sholl profile of the selected cell. Scale bars = 10 µm.

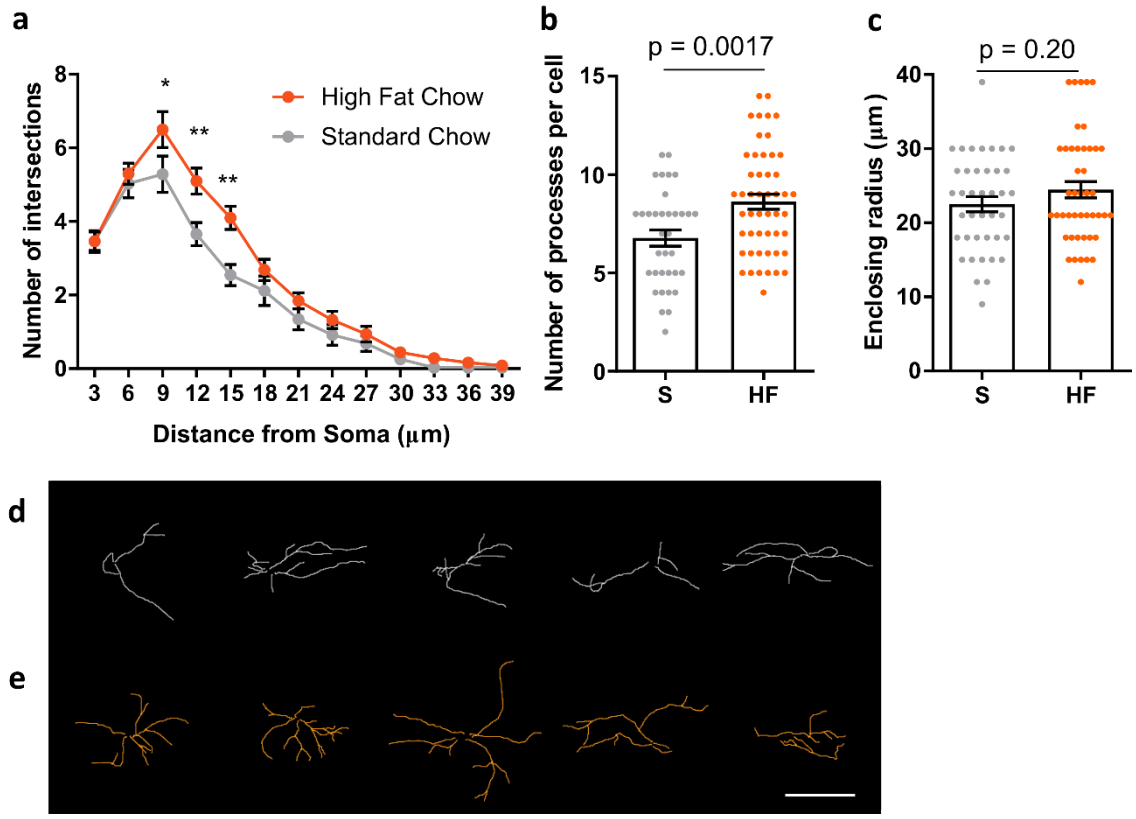

Figure 3.3.4 | High fat chow induced hyperphagia increased the morphological complexity of GFAP immunoreactive astrocytes in the pNTS. a, Mean Sholl profile of postremal NTS GFAP+ astrocytes of standard and high fat chow fed mice (n = 35-50 cells from 4-5 mice per group, Two-way ANOVA, food, $p < 0.0001$, $F_{(1,1079)} = 23.24$, distance from soma, $p < 0.0001$, $F_{(12,1079)} = 108.3$, interaction, $p = 0.04$, $F_{(12,1079)} = 1.83$, Sidak's post-hoc test). **b,** Number of processes of individual pNTS GFAP+ astrocytes from standard (S) and high fat chow fed (HF) mice (n = 35-50 cells from 4-5 mice per group, 6.77 ± 0.41 vs 8.62 ± 0.38 processes, $p = 0.0017$, unpaired t-test). **c,** Enclosing radius of individual pNTS GFAP+ astrocytes from standard (S) and high fat chow fed (HF) mice (n = 35-50 cells from 4-5 mice per group, 22.50 ± 1.02 vs 24.47 ± 1.12 µm, $p = 0.20$, unpaired t-test) **d**, Representative traces of five astrocytes from a standard chow fed mouse. **e,** Representative traces of five astrocytes from a high fat chow fed mouse. Scale bar = 25 µm. * = $p < 0.05$, ** = $p < 0.01$.

3.3.4 | Overnight fasting did not increase the number of GFAP immunoreactive astrocytes in the NTS

NTS astrocytes have been implicated in signalling negative energy balance, namely hyperglycaemia induced by 2-deoxyglucose (McDougal *et al.*, 2013; McDougal, Hermann and Rogers, 2013; Rogers *et al.*, 2018). Astrocytes of the ARC have also been shown to be activated by a 24 hour fast (N. Chen *et al.*, 2016). We examined NTS astrocyte activation using the same criteria as above (**3.3.2 & 3.3.4**) in mice that had been fasted overnight for 12 to 14 hours and compared it to those maintained on standard chow. In some of the standard chow fed control mice there was very low GFAP immunoreactivity relative to the fasted mice, however others were comparable to fasted mice (**Figure 3.3.5 a, b**). Due to this variation there was no significant difference overall in the number of GFAP+ cells per tissue section between the two groups (**Figure 3.3.5 c**, 49.09 ± 17.29 vs 71.17 ± 6.41 cells; $p = 0.27$, unpaired t-test). When the cell counts were binned by rostrocaudal position there were no statistically significant differences between the groups in the rNTS, pNTS or cNTS (**Figure 3.3.5 d**, two-way ANOVA with Sidak's post-hoc test).

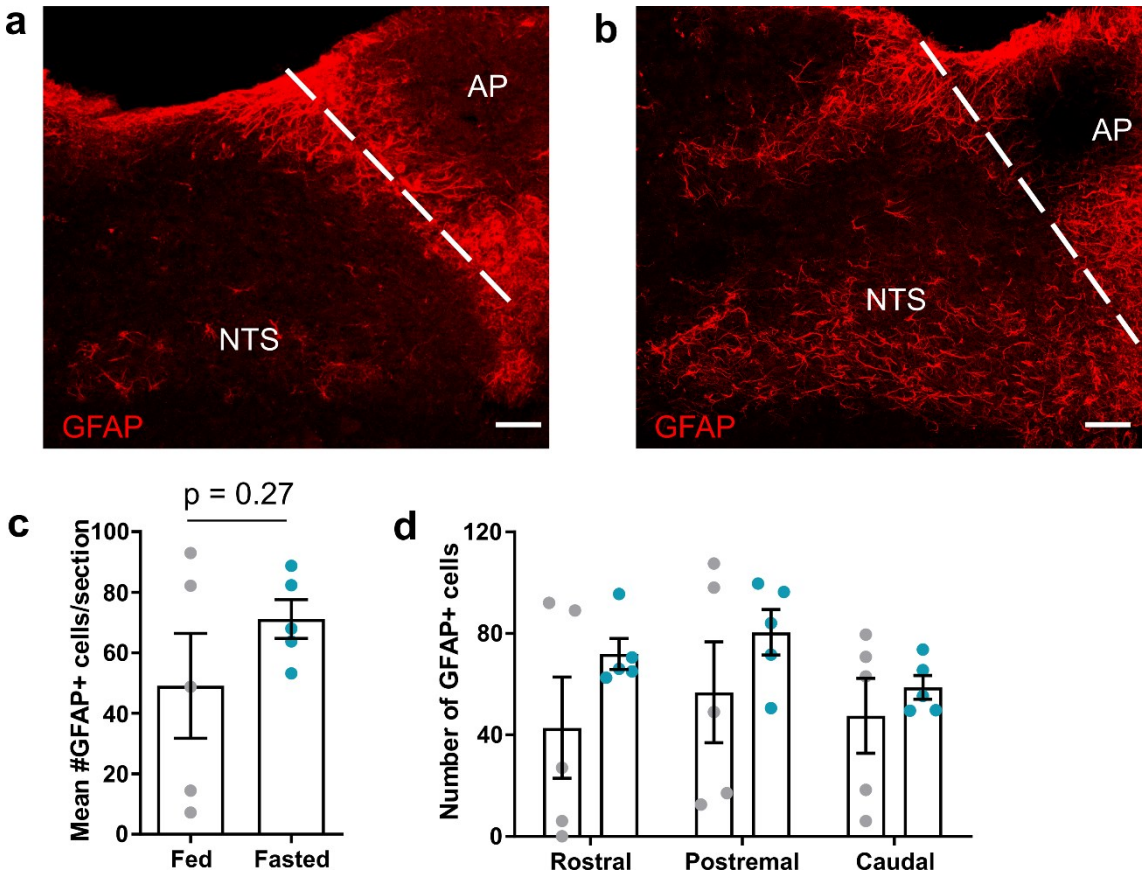

Figure 3.3.5 | Overnight fasting did not change the number of GFAP immunoreactive astrocytes in the NTS. **a,** Representative maximum projection confocal image of GFAP immunostaining from a standard chow fed mouse. **b,** Representative maximum projection confocal image of GFAP immunostaining from a fasted mouse. **c,** Mean number of GFAP+ cells from tissue sections of the NTS from standard chow fed and fasted mice (n = 5 mice per group, 49.09 ± 17.29 vs 71.17 ± 6.41 cells, p = 0.27, unpaired t-test). **d,** Number of GFAP+ cells within anatomical subdivisions of the NTS from standard chow fed and fasted mice (n = 5 mice per group, Two-way ANOVA, fast, p = 0.072, $F_{(1,24)}$ = 3.55, rostrocaudal position, p = 0.52, $F_{(2,24)}$ = 0.67, interaction, p = 0.81, $F_{(2,24)}$= 0.22, Sidak's post-hoc test, p > 0.05 for all comparisons). AP = area postrema, GFAP = glial fibrillary acidic protein, NTS = nucleus of the solitary tract. Scale bars = 50 µm

3.3.5 | Overnight fasting increased the morphological complexity of pNTS GFAP immunoreactive astrocytes

Sholl analysis showed that astrocytes in the pNTS of fasted mice had greater morphological complexity than those from standard chow control mice (**Figure 3.3.6 a**). These cells had a greater number of processes in the pNTS of fasted mice when compared to standard chow fed control mice (**Figure 3.3.6 b**, 5.82 ± 0.31 vs 7.44 ± 0.40; p = 0.0018, unpaired t-test). There was no difference in the mean enclosing radius between the two groups (**Figure 3.3.6 c**, 24.18 ± 0.91 vs 25.86 ± 0.98 µm; p = 0.21, unpaired t-test). This indicates that in fasted mice, astrocytes in the pNTS send out more processes without extending existing processes. Representative traces from one mouse per group are shown (**Figure 3.3.6 d, e**).

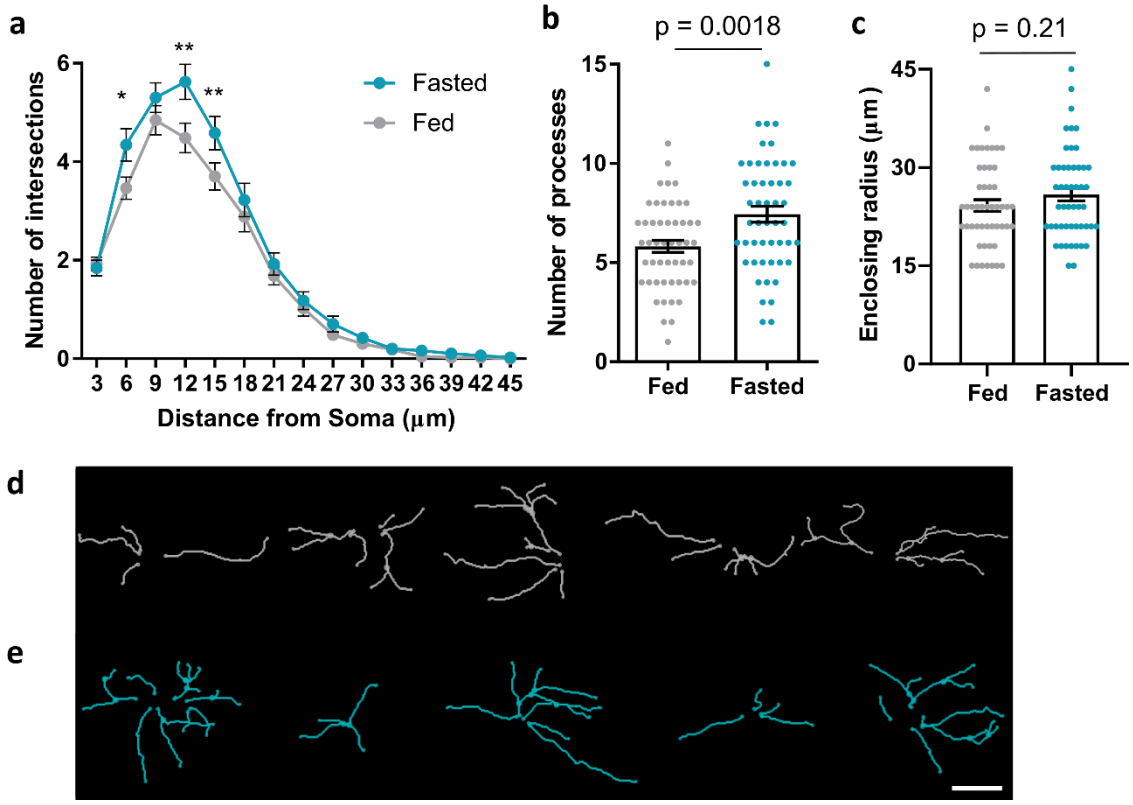

Figure 3.3.6 | Overnight fasting increased the morphological complexity of GFAP immunoreactive astrocytes in the pNTS. a, Mean Sholl profile of postremal NTS GFAP+ astrocytes of standard chow fed and fasted mice (n = 50 cells from 5 mice per group, Two-way ANOVA, fast, $p < 0.0001$, $F_{(1,1470)}=17.41$, distance from soma, $p < 0.0001$, $F_{(14,1470)}=178.7$, interaction, $p = 0.058$, $F_{(14,1470)}=1.66$, Sidak's post-hoc test). **b,** Number of processes of individual pNTS GFAP+ astrocytes from standard chow fed and fasted mice (n = 50 cells from 5 mice per group, 5.82 ± 0.31 vs 7.44 ± 0.40 processes, $p = 0.0018$, unpaired t-test). **c,** Enclosing radius of individual pNTS GFAP+ astrocytes from standard and high fat chow fed mice (n = 50 cells from 5 mice per group, 24.18 ± 0.91 vs 25.86 ± 0.98 µm, $p = 0.21$, unpaired t-test) **d**, Representative traces of five astrocytes from a standard chow fed mouse. **e,** Representative traces of five astrocytes from a fasted mouse. Scale bar = 25 µm. * = $p < 0.05$, ** = $p < 0.01$.

3.3.6 | Prolonged consumption of a high fat diet results in greater body weight

To assess the effects of long-term deviations from energy balance we fed mice either high fat chow or standard chow for 13 weeks. Mice on a high fat chow quickly developed an increased body weight relative to the start of the experiment and greater body weight relative to standard chow fed controls (**Figure 3.3.7 a, b**, Week 13 body weight 30.45 ± 1.20 vs 45.88 ± 1.78 g; $p < 0.0001$, two-way ANOVA with Sidak's post-hoc test). Owing to this greater weight gain this cohort of mice were determined to be DIO.

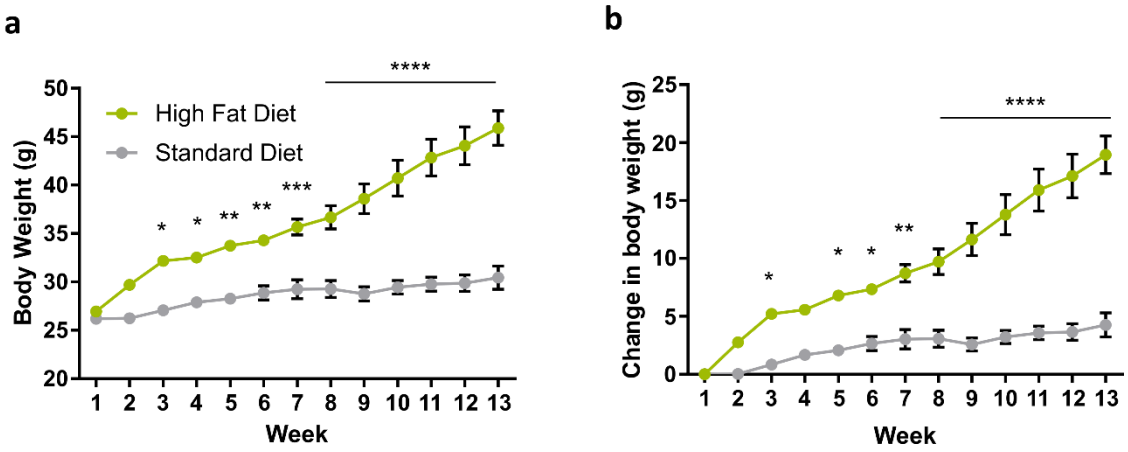

Figure 3.3.7 | 13 weeks of high fat diet intake increased body weight in mice. **a,** Mean body weight of standard chow and high fat chow fed mice over the duration of the feeding period (n = 4-5 mice per group, two-way ANOVA, diet, $p < 0.0003$, $F_{(1,7)} = 42.99$, week, $p < 0.0001$, $F_{(12,84)} = 50.56$, interaction, $p < 0.0001$, $F_{(12,84)} = 20.78$, Sidak's post-hoc test). **b**, Mean change in body weight of standard chow and high fat chow fed mice over the duration of the feeding period (n = 4-5 mice per group, two-way ANOVA, diet, $p < 0.0002$, $F_{(1,7)} = 49.43$, week, $p < 0.0001$, $F_{(12,84)} = 50.56$; interaction, $p < 0.0001$, $F_{(12,84)}=20.78$, Sidak's post-hoc test). * = $p < 0.05$, ** = $p < 0.01$, *** = $p < 0.001$, **** = $p < 0.0001$.

3.3.7 | GFAP immunoreactivity in the NTS was not increased in mice after 13-weeks of consumption of a high fat diet

After 13 weeks on either a high fat diet or standard chow (control), mice were perfused and tissue sections stained for GFAP. There was no clear difference in GFAP immunoreactivity between either of the groups (**Figure 3.3.8 a, b**). Indeed, when the number of GFAP+ cells was quantified across the whole NTS there was no significant difference in the number of GFAP+ cells per tissue section between the groups (**Figure 3.3.8 c**, 98.42 ± 13.57 vs 98.85 ± 5.92 cells; p = 0.98, unpaired t-test). When these cell counts were binned by rostrocaudal region there were no statistically significant differences between the groups in the rNTS, pNTS or cNTS (**Figure 3.3.8 d,** two-way ANOVA with Sidak's post-hoc test). This shows that within the NTS the response to a long term high fat diet is distinct from the response to the initial intake. Of note, the baseline number of GFAP+ cells in the standard chow fed group was elevated over numbers seen in acute experiments. This is likely due to the age of the animals since they were 3 months older (the length of the diet) than mice used in acute experiments. It has been documented that in the NTS and the brain in general that GFAP mRNA and immunoreactivity increases with age (Nichols *et al.*, 1993; Hardy *et al.*, 2018).

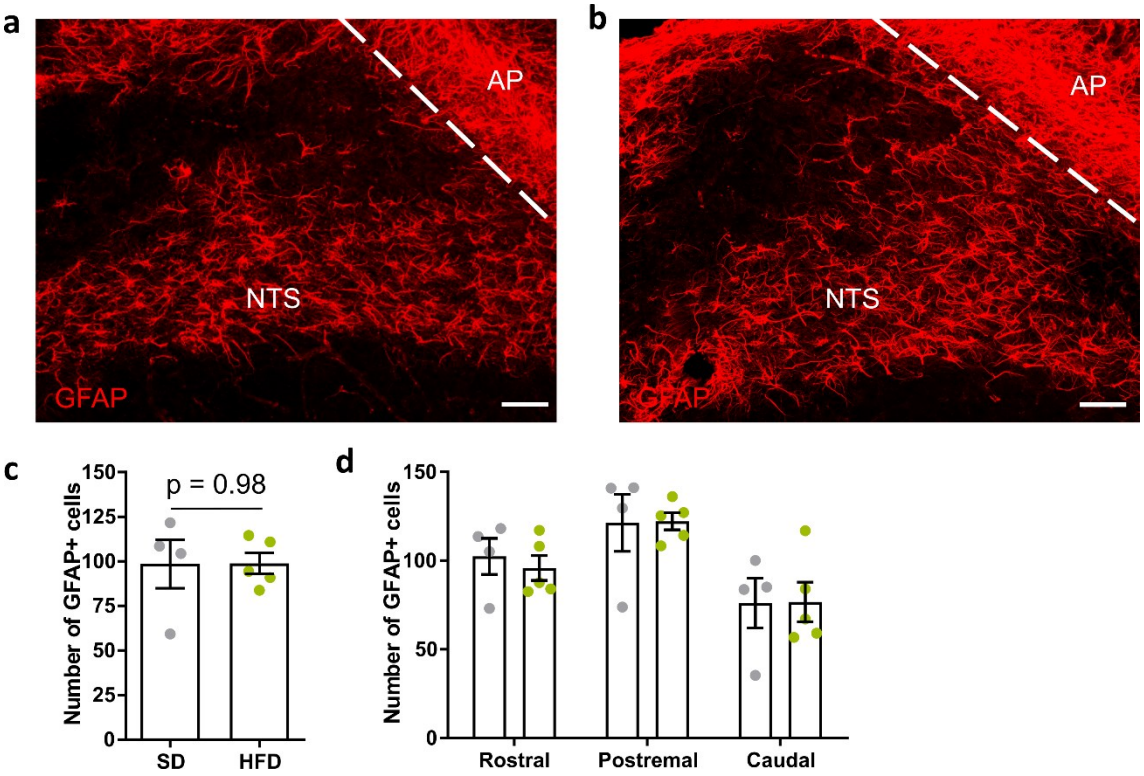

Figure 3.3.8 | 13 weeks of high fat diet intake did not change the number of GFAP immunoreactive astrocytes in the NTS. **a,** Representative maximum projection confocal image of NTS GFAP immunostaining from a standard chow fed mouse. **b,** Representative maximum projection confocal image of NTS GFAP immunostaining from a 13 week high fat chow fed mouse. **c,** Mean number of GFAP+ cells from tissue sections from the NTS of standard diet (SD) and 13 week high fat diet (HFD) fed mice (n = 4-5 mice per group, 98.42 ± 13.57 vs 98.85 ± 5.92 cells, p = 0.98, unpaired t-test). **d,** Number of GFAP+ cells within anatomical subdivisions of NTS from standard and high fat chow fed mice (n = 4-5 mice per group, Two-way ANOVA, diet, p = 0.85, $F_{(1,21)}$ = 0.04, rostrocaudal position, p = 0.002, $F_{(2,21)}$ = 9.03, interaction, p = 0.93, $F_{(2,21)}$ = 0.08, Sidak's post-hoc test, p > 0.05 for all comparisons). AP = area postrema, GFAP = glial fibrillary acidic protein, NTS = nucleus of the solitary tract. Scale bars = 50 µm.

3.3.8 | 13 week consumption of a high fat diet increased the process number and maximum process length of pNTS astrocytes

Morphological tracing and Sholl analysis of randomly selected pNTS astrocytes showed no significant difference in the Sholl profile between the groups (**Figure 3.3.9 a**). However, these cells did have a greater number of processes in the DIO mice when compared with the standard chow group (**Figure 3.3.9 b,** 5.93 ± 0.36 vs 7.36 ± 0.41 processes per cell; p = 0.012, unpaired t-test). Furthermore, the enclosing radius of these cells was greater in DIO mice compared with standard chow fed mice (**Figure 3.3.9 c**, 29.55 ± 1.04 vs 33.00 ± 1.21 μm; p = 0.037, unpaired t-test). This indicates that despite not observing a difference in Sholl profile, these cells did have subtle morphological alterations, namely more processes and longer processes. Representative traces from one animal per group are shown (**Figure 3.3.9 d,e**).

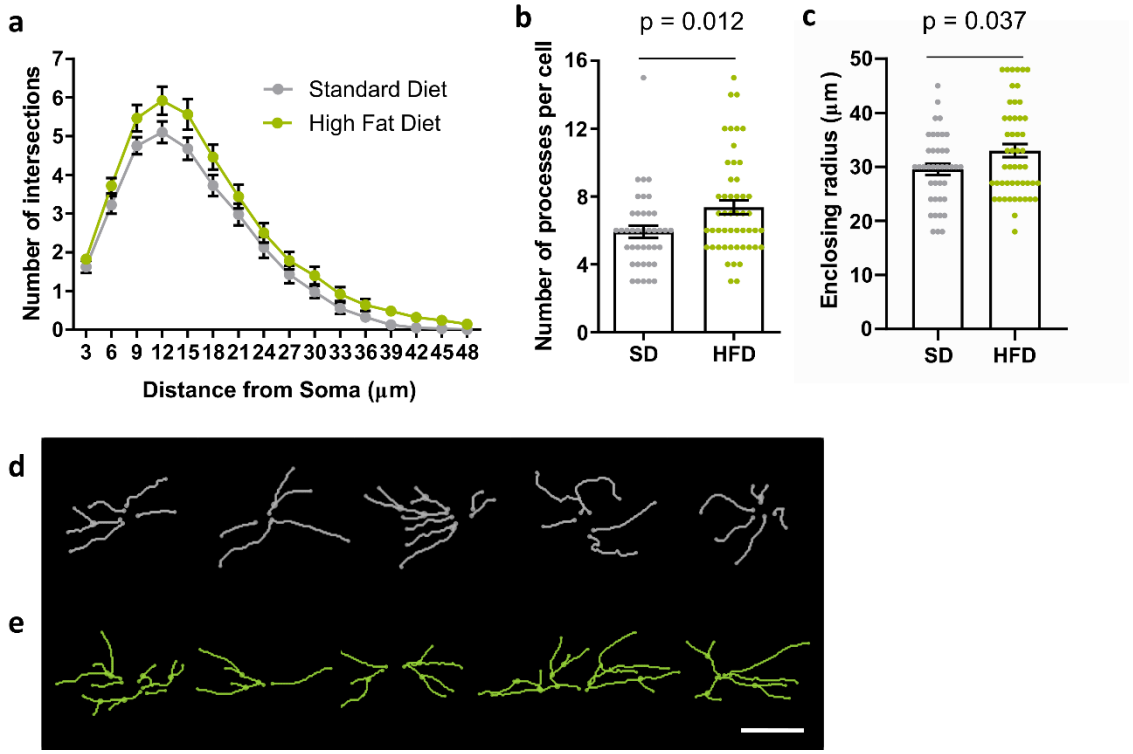

Figure 3.3.9 | 13 weeks of high fat diet intake increased the number of processes and enclosing radius of GFAP immunoreactive astrocytes in the pNTS. **a,** Mean Sholl profile of postremal NTS GFAP+ astrocytes of standard diet and 13 week high fat diet fed mice (n = 40-50 cells from 4-5 mice per group, Two-way ANOVA, Diet, $p < 0.0001$, $F_{(1,1408)} = 30.46$; Distance from soma, $p < 0.0001$, $F_{(15,1408)} = 146.7$; interaction, $p = 0.94$, $F_{(15,1408)} = 1.66$; Sidak's post-hoc test, $p > 0.05$ for all comparisons). **b,** Number of processes of individual pNTS GFAP+ astrocytes from standard diet (SD) and 13 week high fat diet (HFD) fed mice (5.93 ± 0.36 vs 7.36 ± 0.41 processes, n = 40-50 cells from 4-5 mice per group, $p = 0.012$, unpaired t-test). **c,** Enclosing radius of individual pNTS GFAP+ astrocytes from standard diet and 13 week high fat diet (HFD) fed mice (29.55 ± 1.04 vs 33.00 ± 1.21 µm, n = 50 cells from 5 mice per group, $p = 0.037$, unpaired t-test) **d**, Representative traces of five astrocytes from a standard diet fed mouse. **e,** Representative traces of five astrocytes from a 13 week high fat diet mouse. Scale bar = 25 µm.

3.3.9 | Using nested analysis to evaluate the effect of mouse on cellular morphology

In the morphological analyses presented above we use individual cells as data points. This does not meet the assumptions of the statistical tests used since each cell is not truly independent and the experimental manipulation (i.e. the diet) is applied to the mouse making mouse the experimental unit (Lazic, Clarke-Williams and Munafò, 2018). To account for this we used a nested (or hierarchical) statistical analysis which allows cells to be grouped by the mouse they belong to. This analysis showed that, when accounting for the influence of which replicate the cell originated from there was a significantly greater amount of processes per cell in the overnight high fat chow fed group compared to standard chow fed controls (**Figure 3.3.10 b**). The same was true of the fasted group when compared to their standard chow fed controls (**Figure 3.3.10 e**). There was no statistically significant difference in process number between cells from 13 week high fat diet fed mice and their standard chow fed controls (**Figure 3.3.10 h**).

Applying this analysis to the Sholl profile was not possible since two-way nested analysis is not possible. Instead we compared the sum of the number of Sholl intersections for each cell between groups with mouse as a nested variable. None of these comparisons reached statistical significance (**Figure 3.3.10 a, d, g**). This may mean that variation between mice in a group accounts for the difference or alternatively that by reducing the dimensionality of the data our measurements are less sensitive.

Finally nested analysis of enclosing radius showed there was no statistically significant differences between any of the experimental groups and their respective controls (**Figure 3.3.10 c, f, i**).

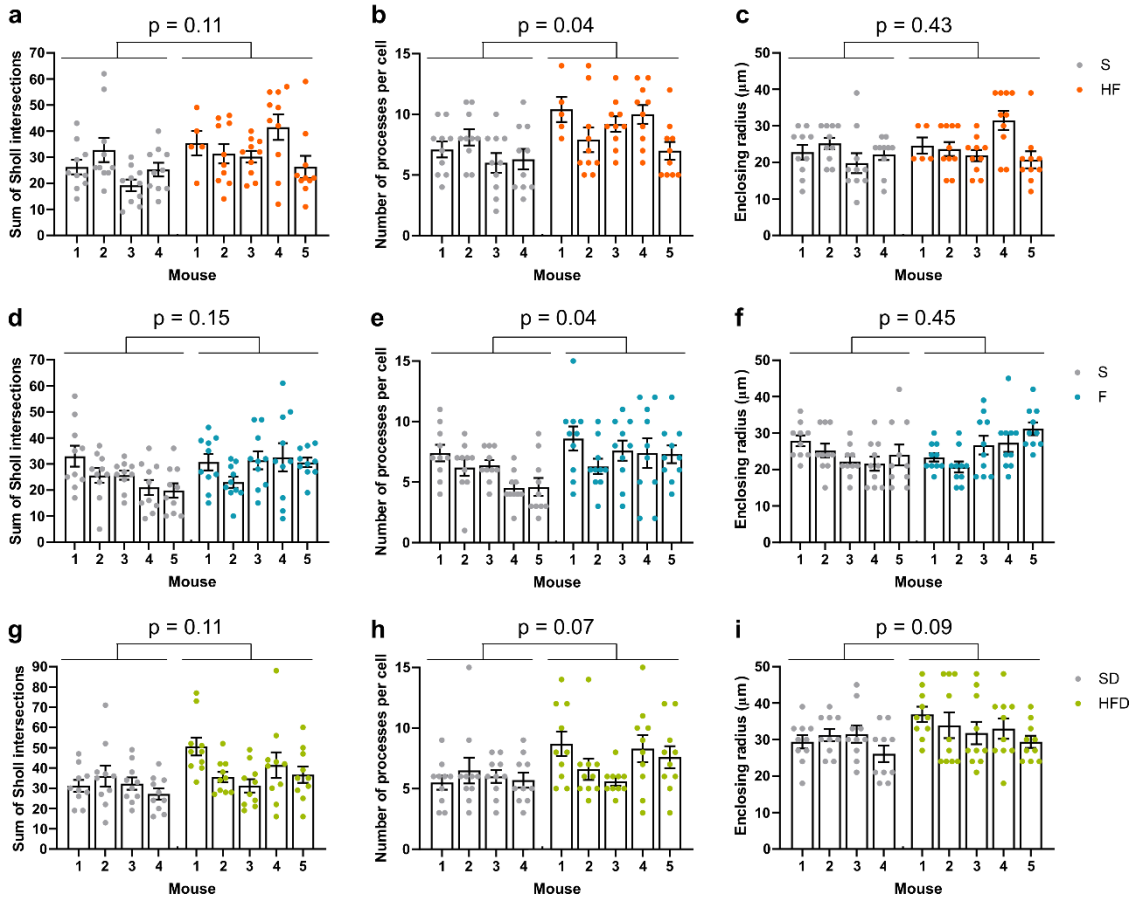

Figure 3.3.10 | Morphological analysis with mouse as a nested variable. **a,** Sum of Sholl intersections for pNTS GFAP+ astrocytes of standard chow and overnight high fat chow fed mice with mouse as a nested variable (n = 35-50 cells from 4-5 mice per group, nested t-test, p = 0.11). **b,** Number of processes per cell for pNTS GFAP+ astrocytes of standard chow and overnight high fat chow fed mice with mouse as a nested variable (n = 35-50 cells from 4-5 mice per group, nested t-test, p = 0.04). **c,** Enclosing radius for pNTS GFAP+ astrocytes of standard chow and overnight high fat chow fed mice with mouse as a nested variable (n = 35-50 cells from 4-5 mice per group, nested t-test, p = 0.43). **d,** Sum of Sholl intersections for pNTS GFAP+ astrocytes of standard chow and overnight fasted mice with mouse as a nested variable (n = 50 cells from 5 mice per group, nested t-test, p = 0.15). **e,** Number of processes per cell for pNTS GFAP+ astrocytes of standard chow and overnight fasted mice with mouse as a nested

variable (n = 50 cells from 5 mice per group, nested t-test, p = 0.04). **f,** Enclosing radius for pNTS GFAP+ astrocytes of standard chow and overnight fasted mice with mouse as a nested variable (n = 50 cells from 5 mice per group, nested t-test, p = 0.45). **g,** Sum of Sholl intersections for pNTS GFAP+ astrocytes of standard chow and 13 weeks high fat diet fed mice with mouse as a nested variable (n = 40-50 cells from 4-5 mice per group, nested t-test, p = 0.11). **h,** Number of processes per cell for pNTS GFAP+ astrocytes of standard chow and 13 weeks high fat diet mice with mouse as a nested variable (n = 40-50 cells from 4-5 mice per group, nested t-test, p = 0.04). **i,** Enclosing radius for pNTS GFAP+ astrocytes of standard chow and 13 weeks high fat diet mice with mouse as a nested variable (n = 40-50 cells from 4-5 mice per group, nested t-test, p = 0.43).

3.4 | Discussion

In this chapter we have shown that in the mouse NTS, GFAP+ astrocytes show morphological alterations in response to dietary perturbations. In particular, the hyperphagia following presentation of high fat chow drove an increase in the number of GFAP+ astrocytes in the pNTS which manifested as an increase in branching of GFAP+ astrocyte processes. Less consistent was the response to overnight fasting; there was no statistically significant difference in the number of GFAP+ NTS astrocytes observed between fed and fasted animals but there was a difference in the cellular morphology, potentially suggestive of functional changes in astrocytes. Finally, prolonged intake of a high fat diet induced weight gain but had no effect on the number of GFAP+ NTS astrocytes. We did however observe subtle changes in the morphology of these cells, which again may reflect subtle changes in astrocyte function.

3.4.1 | Comparisons between NTS and hypothalamic astrocyte responses to energy balance manipulation

In the hypothalamus, glial alterations are seen following all three of the manipulations presented in this chapter; fasting, acute and chronic high fat feeding. In mice and rats fed a high fat diet there is an immediate (24 – 72 hours) increase in GFAP mRNA, immunoreactivity and protein quantity in the mediobasal hypothalamus (Thaler *et al.*, 2012; Buckman *et al.*, 2015). We show here that this is true of the NTS at an even shorter latency from food intake (12 – 14 hours). In the ARC, fasting induces greater GFAP expression and morphological complexity of GFAP+ astrocyte processes (Fuente-Martín *et al.*, 2012; N. Chen *et al.*, 2016). The morphological reorganization also occurs in the NTS although in the absence of detectable increases in GFAP immunoreactivity. Finally, it is well documented that diet-induced obesity resulting from

consumption of a high fat diet increases GFAP expression and alters morphological organisation of astrocytes throughout the hypothalamus (Thaler *et al.*, 2012; Buckman *et al.*, 2013). The brainstem response in this case appears to be distinct since we did not observe any changes in the number of GFAP+ cells and only observed subtle morphological differences.

Of note, three studies that inhibit inflammatory nuclear factor kappa b (NF-κB) signalling in all GFAP-expressing astrocytes report feeding phenotypes, namely, increased initial intake of a high fat diet following initial exposure, resistance to the obesity phenotype when already on a high fat diet and protection from metabolic dysfunction and weight gain on a high fat diet (Buckman *et al.*, 2015; Douglass *et al.*, 2017; Zhang *et al.*, 2017). Although these studies attribute the observed effects to ARC astrocytes, the contribution of NTS astrocytes identified here as responsive to high fat diet intake cannot be ruled out.

3.4.2 | Comparisons to other stimuli shown to modify NTS astrocyte GFAP expression or morphology

In mice and rats, inhalation of either ozone gas or low oxygen air results in greater NTS GFAP immunoreactivity and astrocyte branching within 24 hours (Araneda *et al.*, 2008; Tadmouri, Champagnat and Morin-Surun, 2014; Stokes *et al.*, 2017; De La Zerda *et al.*, 2018). This observed increase in GFAP is reduced when microglia are inhibited with minocycline, indicating a cross talk between these two cell populations (Stokes *et al.*, 2017). We did not measure microglia number or morphology in our acute studies, but it is possible that communication between these two glial cell classes contributes to astrocyte activation and downstream effects on feeding.

3.4.3 | Evidence for physiological consequences of astrocyte reorganisation

The consequences of the observed NTS astrocyte morphological plasticity are of particular interest for further study. In the magnocellular nuclei of the hypothalamus (the supraoptic nucleus [SON] and the magnocellular division of the paraventricular hypothalamic nucleus [PVH_M]), astrocytes display a remarkable process plasticity in response to physiological stimuli (Theodosis *et al.*, 2004). In these nuclei, oxytocinergic (OXT) neurons project to the hypophyseal circulation to initiate and control parturition, lactation and fluid homeostasis. During physiological states when the activity of these neurons is required, for example lactation, the processes of neighbouring astrocytes retract from the cell bodies and dendrites of OXT neurons (Theodosis *et al.*, 2004). This has numerous consequences on the synaptic function of these neurons.

The reduced astrocyte presence in the synapse leads to elevations of extracellular K^+ (Coles and Poulain, 1991). This decreases the outward electrochemical gradient for K^+ and thus increases neuronal excitability and the burst firing pattern required for lactation. Secondly, glutamate clearance is decreased, leading to elevated extrasynaptic glutamate and concurrent reduction of presynaptic release by negative feedback (Oliet, Piet and Poulain, 2001). Increased extracellular space can also facilitate greater volume transmission (Piet *et al.*, 2004). Finally, reduced glial coverage of somata and dendrites allows for more synapses to contact the neurons (Theodosis *et al.*, 2004). Together, the plasticity of astrocyte processes modulates the firing of OXT neurons and their downstream physiological/behavioural functions (Oliet and Bonfardin, 2010).

In our experiment we performed morphological analysis on GFAP+ processes. As GFAP is an intermediate filament protein constituent of the astrocyte cytoskeleton, in reality what we observe using this method only represents

around 10% of the total cell volume (Shigetomi *et al.*, 2013). Astrocytes consist of large GFAP+ processes and far finer GFAP- processes. In conditions that increase hypothalamic GFAP+ morphological complexity (fasting, high fat diet, NF-κB activation), finer GFAP- processes labelled by Golgi staining retract (Zhang *et al.*, 2017). When activated in this fashion it appears that astrocytes may retract their finer processes to increase the number and complexity of larger GFAP+ processes.

This suggests that in our experiment, particularly in the 12 hour high fat chow fed mice, that the astrocytes ramify and possibly retract processes from synapses in a fashion analogous to those of the SON and PVH_M. This would need to be conclusively demonstrated in future studies by repeating the nutritional manipulations followed by Golgi staining (or other methods to label the wider extent of fine astrocyte processes). If this were to be confirmed, there could be several significant impacts on neuronal communication in the NTS. Firstly, this may result in increased extracellular K^+ which can increase NTS neuron excitability by modulation of the A-type K^+ current (Accorsi-Mendonca *et al.*, 2015). Secondly, it likely increases synaptic glutamate through reduced glutamate reuptake which in the NTS also increases neuronal activity and autonomic outflow from the NTS (Matott *et al.*, 2016; Matott, Kline and Hasser, 2017; Yamamoto and Mifflin, 2018). The predicted increase in extracellular space may allow for greater volume transmission of neuromodulators e.g. serotonin and acetylcholine which excite NTS^{TH} neurons (Cui, Roberts, Zhao, Zhu, *et al.*, 2012; Page, Zhu and Appleyard, 2018). Finally, it may allow ultrastructural remodelling of synapses onto NTS neurons, increasing vagal influence over these neurons.

3.4.4 | Opposing stimuli generate similar responses

Somewhat paradoxical is our finding that bidirectional acute changes in energy balance (12 hour high fat chow and fasting) both induce morphological changes in NTS astrocytes. This is also observed in the ARC which is home to both orexigenic ARC^{AgRP} and anorexigenic ARC^{POMC} neuronal populations (Buckman *et al.*, 2015; N. Chen *et al.*, 2016). What remains to be investigated is the degree of heterogeneity exhibited by ARC astrocytes: does an individual astrocyte respond to both fasting and feeding? Or are there distinct populations of fasting-responsive and feeding-responsive astrocytes?

To date, the majority of evidence suggests the NTS predominantly contains anorexigenic neurons but there is some evidence that a subset of NTS^{TH} neurons can stimulate glucoprivic feeding (Aklan *et al.*, 2020). It is possible that the changes are most pronounced in two sub-populations of astrocytes. Ca^{2+} imaging from NTS slices shows that ~40% of astrocytes respond to low glucose or 2-deoxyglucose while ~40% respond to the GLP1-R receptor agonist exendin-4 (McDougal *et al.*, 2013; Reiner *et al.*, 2016). What has not been demonstrated is whether these are two distinct populations of astrocytes whose activation may serve to drive opposing physiological responses. This could be clarified by exposing slices to each condition (0.1 mM glucose and exendin-4) sequentially and measuring single-cell $[Ca^{2+}]_i$ responses to identify if individual NTS astrocytes bidirectionally respond to these opposing energy cues.

3.4.5 | Potential signals that activate NTS astrocytes

In these studies, acute high fat chow induced hyperphagia caused the greatest change in NTS GFAP immunoreactivity and morphology of GFAP+ processes. The signals underlying induction of these changes are not clear from our results but several possibilities exist.

NTS astrocytes are able to directly sense glutamate release from the vagus nerve *via* Ca^{2+}-permeable AMPA receptors on their cell surface (McDougal, Hermann and Rogers, 2011; Accorsi-Mendonça *et al.*, 2013). Opening of these receptors allows Ca^{2+} into the cell which acts at ryanodine receptors to liberate Ca^{2+} from intracellular stores, thus further increasing intracellular Ca^{2+} (McDougal, Hermann and Rogers, 2011).

Moreover, astrocytes of the NTS and wider brainstem are responsive to endocrine cues including the GLP1-R agonist exendin-4, leptin and ghrelin (Reiner *et al.*, 2016; Marina *et al.*, 2017; Stein *et al.*, 2020). This raises the possibility that NTS astrocytes may integrate and summate synaptic and endocrine signals of satiety. However, neither LepRb nor GLP1-R fluorescent reporter mice show labelling of NTS astrocytes (Garfield *et al.*, 2012; Cork *et al.*, 2015). Additionally astrocytes do not show increased p-STAT3 activation in response to leptin injection (Ellacott, Halatchev and Cone, 2006). Because of these discrepancies, the endocrine sensing function of NTS astrocytes *in vivo* in mice remains to be convincingly demonstrated.

In the fasted animals it is possible that NTS astrocytes were activated by low blood glucose since overnight fasting depletes liver glycogen and lowers blood glucose in mice (Ayala *et al.*, 2010). Some NTS astrocytes have been shown to be directly glucose sensitive and involved in mounting the counter regulatory response to hypoglycaemia (Marty *et al.*, 2005; McDougal *et al.*, 2013; Rogers, Ritter and Hermann, 2016; Rogers *et al.*, 2018). Therefore, it is possible that low glucose may have contributed to astrocyte changes observed in this instance. Additionally, the pancreatic islet cells can activate vagal neurons by release of 5-HT and thus direct synaptic signalling from vagal sensory neurons innervating pancreatic islets may also play a role in this activation (Makhmutova *et al.*, 2019).

Finally, in DIO mice we did not detect a difference in the number of astrocytes or the Sholl profile. This is in contrast to the ARC where astrocyte activation accompanies general tissue inflammation and microglial activation in DIO mice and rats (Zhang *et al.*, 2008; Thaler *et al.*, 2012). It is possible that this chronic astrocyte activation is driven by tissue inflammation in the hypothalamus. It has not yet been investigated whether markers of inflammation are present in the NTS of DIO mice but if not then this may explain the observed difference. Alternatively, this may indicate a loss of sensitivity in the activation mechanism induced by 12 hours high fat chow potentially contributing to continued caloric excess by impairing this proposed satiety mechanism.

We did not measure meal patterning or food intake in our study since the mice were group housed. The high fat chow is more energy dense than standard chow and DIO mice may eat less food by mass than the standard diet fed controls but a greater number of calories. This could result in less gastric distention, potentially resulting in low gut to brain vagal signalling. If this is the main driver of NTS astrocyte activation in the short term high fat paradigm then this may explain the lack of effect in the DIO paradigm.

3.5 | Conclusion

To conclude we have identified that NTS astrocytes respond with morphological changes robustly in response to short term intake of a high fat chow suggesting that similarly to their ARC counterparts, they may mediate physiological responses to increases in food intake (i.e. corresponding decreases in food intake). In addition, we observed an unexpected morphological change in the NTS astrocytes of fasted mice, potentially mediated by hypoglycaemia. Finally, only very subtle alterations in astrocyte morphology were observed in diet

induced obese mice which may reflect changes in the eating behaviour of these animals, but this would need to be confirmed with further studies.

Investigating the consequence of this morphological NTS astrocyte activation for subsequent food intake will clarify their role in energy homeostasis circuitry.

Chapter 4

Chemogenetic control of DVC astrocytes and effects on energy homeostasis

4.1 | Introduction

Within the last fifteen years, neuroscience research has undergone a revolution with the rapid advances in technologies for direct manipulation and monitoring of genetically defined neural cell types in awake, behaving animals (Sternson and Roth, 2014; Adamantidis *et al.*, 2015; Roth, 2016; Luo, Callaway and Svoboda, 2018). This has allowed, with an unprecedented level of precision, the generation of causal evidence for the contributions of populations of neural cells to a wide range of specific behaviours.

As discussed in **section 1.1.2.1**, a number of populations of nucleus of the solitary tract (NTS) neurons have been interrogated in this fashion. Chemogenetic stimulation of NTS neurons with designer receptors exclusively activated by designer drugs (DREADDs) has been shown to predominantly suppress food intake when activated but also with some evidence for modulation of blood glucose control, endogenous analgesia and the rewarding/aversive nature of food (Zhan *et al.*, 2013; Cerritelli *et al.*, 2016; D'Agostino *et al.*, 2016, 2018; Roman, Derkach and Palmiter, 2016; Alhadeff *et al.*, 2017; Shi *et al.*, 2017; Roman, Sloat and Palmiter, 2017; Han *et al.*, 2018; Boychuk *et al.*, 2019; Holt, Richards, *et al.*, 2019; Cheng *et al.*, 2020).

In addition to neurons, optogenetic and chemogenetic methodologies have been applied to non-neuronal cells to show causality in their function (Bang, Kim and Lee, 2016). From these studies, the utility of the Gq-coupled DREADD (hM3Dq) and ligand clozapine-N-oxide (CNO) to drive increased $[Ca^{2+}]_i$ and modulate local neurons and alter behaviour has been established (Bonder and McCarthy, 2014; N. Chen *et al.*, 2016; Martin-Fernandez *et al.*, 2017; Adamsky *et al.*, 2018; Durkee *et al.*, 2019). Due to this, we will henceforth refer to stimulation of astrocyte Gq-

GCPR signalling by this hM3Dq-CNO method as chemogenetic activation of astrocytes.

Using this methodology, diverse roles of astrocytes in numerous brain regions have been elucidated. For example, in the nucleus accumbens (NAc) core, chemogenetic activation of astrocytes suppresses ethanol and cocaine seeking following abstinence (Bull *et al.*, 2014; Scofield *et al.*, 2015). Along with corroborating evidence this suggests that NAc astrocyte hypoactivity can bias rats towards relapse (Scofield *et al.*, 2016). Chemogenetic activation of astrocytes in the CA1 region of the hippocampus induces synaptic plasticity and strengthens contextual and fear memories, an effect that is not observed when CA1 neurons are chemogenetically activated (Adamsky *et al.*, 2018). In contrast, chemogenetic activation of astrocytes in the central extended amygdala (CeA) reduces conditioned fear learning, suggesting distinct roles for astrocytes in different circuits contributing to the same behaviour (Martin-Fernandez *et al.*, 2017). Thus, chemogenetic activation of astrocytes is established for studying their role as circuit elements that modulate behaviour.

In the context of the regulation of energy homeostasis, of particular interest are a handful of studies examining the effect of chemogenetic manipulation of astrocytes in the arcuate nucleus (ARC) on feeding behaviour. The first study from Yang and colleagues showed that activation of ARC astrocytes with hM3Dq and CNO produced a modest decrease in baseline food intake during the dark phase and an increase during the light phase. Furthermore, they showed that this activation reduced the orexigenic action of ghrelin while potentiating the anorexic effect of leptin. Finally, they used complementary methodology and claimed to demonstrate that chemogenetic ‘inhibition’ of astrocytes with the Gi-coupled DREADD (hM4Di) and CNO produced opposing effects to activation on hormonal

but not baseline food intake (Yang, Qi and Yang, 2015). Despite the bidirectional effect observed in this study, the ability of hM4Di to inhibit astrocyte signalling remains to be demonstrated (Durkee *et al.*, 2019). The second study from Chen and colleagues published shortly after the work of Yang *et al*, used similar methodology and also reported a modest increase in feeding during the light phase (N. Chen *et al.*, 2016). Recently, detailed meal pattern analysis revealed that stimulation of hM4Di in ARC astrocytes increased meal size and duration without an effect on total food intake (Nuzzaci *et al.*, 2020). This effect was coincident with reduced astrocytic contact onto ARC^{POMC} neurons. It therefore appears that chemogenetic modulation of ARC astrocytes is sufficient to alter food intake at baseline and modulate hormone-induced feeding.

4.2 | Aims and hypothesis

The aim of the experiments in this chapter were to validate the use of hM3Dq to activate NTS astrocytes and to characterise the subsequent effects on behaviour and neural circuit activation. We hypothesised that applying this chemogenetic methodology to astrocytes in the NTS and wider dorsal vagal complex (DVC) would reduce food intake by exciting neighbouring appetite-suppressing neurons. Given that other functions have been demonstrated to be regulated by NTS neurons, we postulated that this manipulation would also have other effects on other physiological functions: those involved in endogenous analgesia (NTS^{POMC}) (Cerritelli *et al.*, 2016). Finally, we hypothesized that activating Gi-coupled signalling in DVC astrocytes, putatively inhibiting astrocyte activity, would potentiate re-feeding after a fast and reduce the appetite-suppressive effect of cholecystokinin (CCK).

4.3 | Results

4.3.1 | A viral-genetic strategy for chemogenetic activation of DVC astrocytes

In order to ascertain the consequences of NTS astrocyte activation on feeding behaviour we utilized DREADDs. Adeno-associated viral (AAV) vectors containing single stranded RNA encoding either the hM3Dq receptor fused to the fluorescent reporter mCherry under the GFAP promoter or identical vectors containing mCherry only were used (**Figure 4.3.1 a**). The mCherry only AAV vectors were used as controls to enable any impact of the surgical procedure, injection of viral vector and/or CNO treatment on behaviour to be observed. The AAV vectors were delivered to the NTS by stereotactic surgery (**Figure 4.3.1 b**). Following surgery, immunoreactivity for the reporter mCherry confirmed successful injection and transduction (**Figure 4.3.1 c**). This indicates the utility of this strategy for delivery of viral vectors to the NTS. Given that infection was not limited to the NTS and instead consistently covered the extent of the DVC and to a varying degree neighbouring nuclei (**Figure 4.3.1 c**), these mice are subsequently referred to as DVC::GFAP^{hM3Dq} and DVC::GFAP^{mCherry} mice for AAV-hM3Dq_mCherry and AAV-mCherry injected mice, respectively.

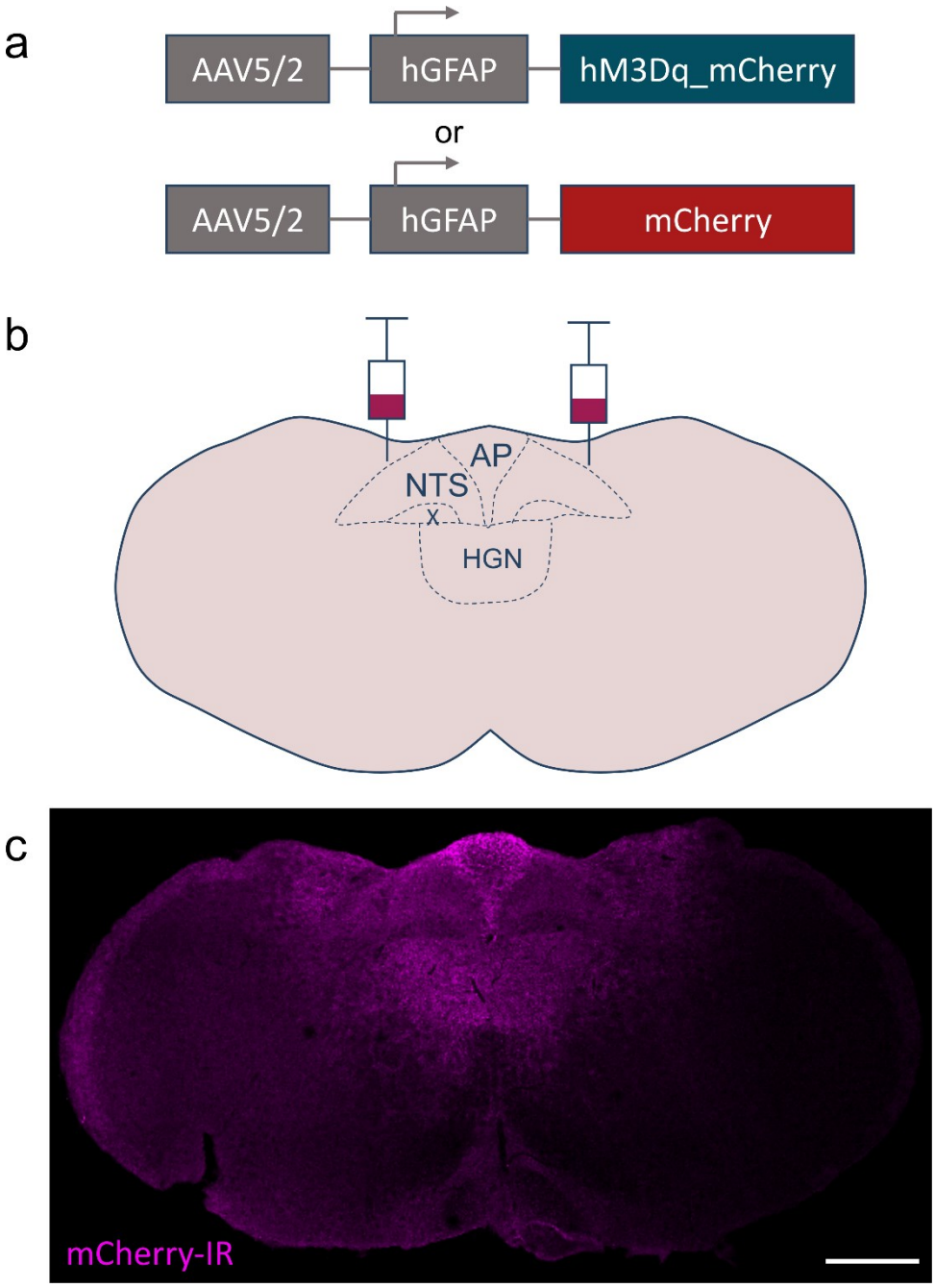

Figure 4.3.1 | Strategy for chemogenetic control of DVC astrocytes. a, Schematic of viral vectors used to create DVC::GFAP^{hM3Dq} and DVC::GFAP^{mCherry} mice. **b,** Schematic showing anatomy of target region. **c,** Representative section showing immunoreactivity (IR) against hM3Dq_mCherry in and around the DVC. AP = area postrema, HGN = hypoglossal nucleus, NTS = nucleus of the solitary tract, X = dorsal motor nucleus of the vagus. Scale bar = 500 μm.

4.3.2 | Quantification of viral infection

In the first cohort of mice an injection protocol using four injections per side was used. This resulted in a wide infection of the dorsal portion of the caudal brainstem. In these mice the caudal NTS (cNTS) and postremal (pNTS) were reliably transduced with hM3Dq_mCherry (**Figure 4.3.2 a, b**). The transduction in the rostral NTS (rNTS) was more variable with only 50% of mice showing mCherry immunoreactivity at Bregma -7.08 (**Figure 4.3.2 c**). The transduction of neighbouring nuclei was variable between mice.

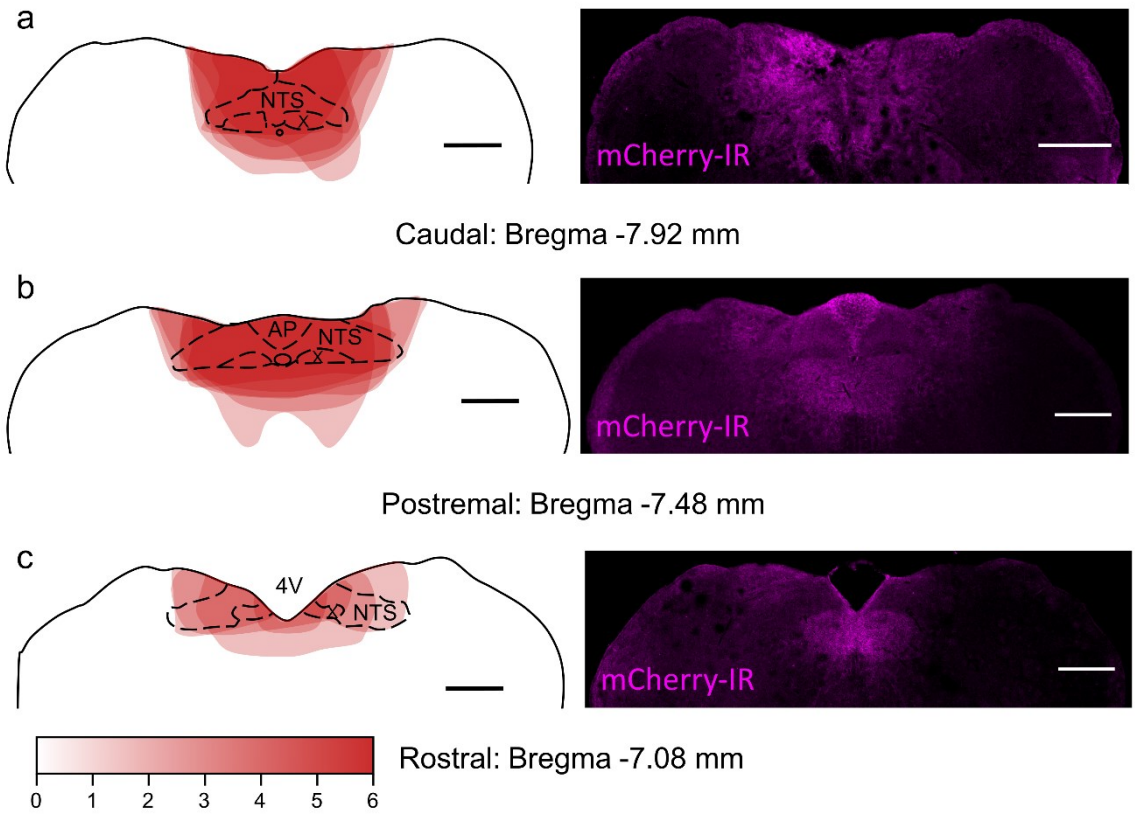

Figure 4.3.2 | AAV vector spread in individual DVC::GFAP^{hM3Dq} mice. a, Left, quantification of mCherry immunoreactivity from DVC::GFAP^{hM3Dq} mice (n = 6) in the caudal DVC (Bregma -7.92 mm). Right, representative image of mCherry immunoreactivity in the caudal DVC. **b,** Left, quantification of mCherry immunoreactivity from DVC::GFAP^{hM3Dq} mice (n = 6) in the postremal DVC (Bregma -7.48 mm). Right, representative image of mCherry immunoreactivity in the postremal DVC. **c,** Left, quantification of mCherry immunoreactivity from DVC::GFAP^{hM3Dq} mice (n = 6) in the rostral DVC (Bregma -7.08 mm). Right, representative image of mCherry immunoreactivity in the rostral DVC. Brightness 6 = six mice had mCherry IR in this region. 4V = fourth ventricle, AP = area postrema, NTS = nucleus of the solitary tract, X = dorsal motor nucleus of the vagus. Scale bars = 500 µm.

4.3.3 | Cell type specificity of viral infection

Double-immunohistochemistry was used to examine the cell type transduced by the viral injections. mCherry immunoreactivity revealed a ‘honeycomb’ pattern in the DVC where very fine glial processes were labelled but staining was absent from certain cell bodies. When quantified it was seen that 91.2% of GFAP immunoreactive cells were mCherry immunoreactive (**Figure 4.3.3 a**). Since GFAP labels primary processes while hM3Dq_mCherry is a receptor expressed on the cell surface the patterns of staining were distinct but were seen to associate with one another and were easily distinguished from GFAP-negative mCherry-negative cell bodies (putative neurons). In contrast, 0.2% of NeuN immunoreactive cells were mCherry immunoreactive (**Figure 4.3.3 b**). This indicates that appropriate cell type specificity was achieved.

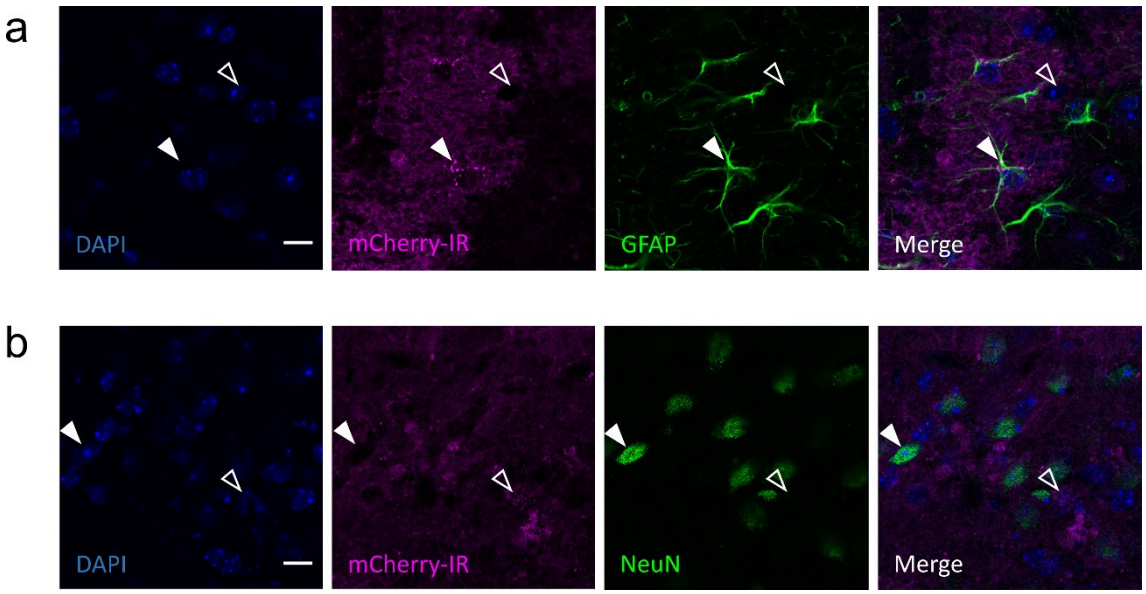

Figure 4.3.3 | Expression of hM3Dq_mCherry in DVC astrocytes. a, Immunoreactivity for GFAP and mCherry in a DVC::GFAP^{hM3Dq} mouse. Closed arrow shows a GFAP-positive cell, open arrow shows a GFAP-negative putative neuron. 91.5 ± 1.6% of GFAP-positive cells had mCherry immunoreactivity (242 of 265 cells from n = 4 mice). **b**, Immunoreactivity for NeuN and mCherry in a DVC::GFAP^{hM3Dq} mouse. Closed arrow shows a NeuN-positive cell, open arrow shows a NeuN-negative putative astrocyte. 0.2 ± 0.2% of NeuN-positive cells had mCherry immunoreactivity (1 of 509 cells from n = 4 mice). Scale bars = 25 μm.

4.3.4 | Chemogenetic activation of DVC astrocytes induced morphological plasticity

In previous experiments we had used GFAP immunoreactivity and morphology as an indicator of astrocyte activation. To assess the utility of hM3Dq to activate DVC astrocytes mice were injected with the ligand CNO (0.3 mg/kg intraperitoneal [i.p.]) and perfused 2-3 hours later. Immunohistochemistry for GFAP showed greater GFAP immunoreactivity in DVC::GFAP^{hM3Dq} mice when compared with DVC::GFAP^{mCherry} mice (**Figure 4.3.4 a, b**). When the cells were traced, Sholl analysis showed that randomly selected pNTS astrocytes from DVC::GFAP^{hM3Dq} mice had greater morphological complexity when compared with those from DVC::GFAP^{mCherry} mice (**Figure 4.3.4 c**). These cells had a greater number of processes in DVC::GFAP^{hM3Dq} mice than DVC::GFAP^{mCherry} mice (**Figure 4.3.4 d**, 6.14 ± 0.29 vs 7.88 ± 0.43 processes; p = 0.0015, unpaired t-test). In addition, these cells had a greater enclosing radius in DVC::GFAP^{hM3Dq} mice than DVC::GFAP^{mCherry} mice (**Figure 4.3.4 e**, 25.29 ± 1.02 vs 30.30 ± 1.41 µm; p = 0.0063, unpaired t-test). This indicates that our strategy indeed induced activation of DVC astrocytes when stimulated with CNO (0.3 mg/kg i.p.).

Given that multiple cells from the same mouse were taken as individual data points (discussed in more detail in **section 3.3.9**), this analysis was repeated including the mouse as a nested variable (**Figure 4.3.4 h-j**). These analyses did not reach statistical significance indicating that all mice do not contribute equally to the observed difference in **figures 4.3.4 c-e** and suggesting that the morphological alterations induced by chemogenetic activation of DVC astrocytes were not uniform across mice.

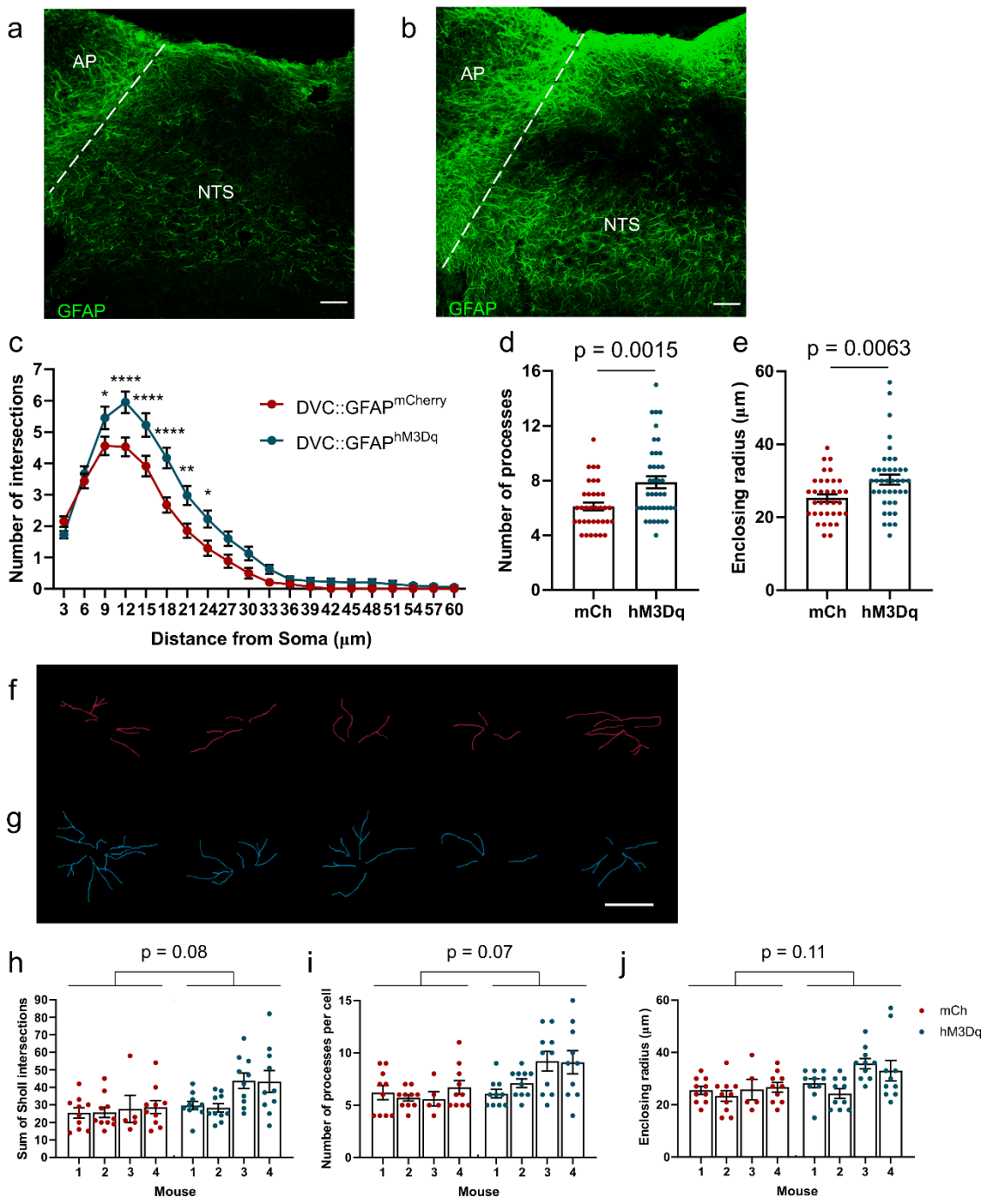

Figure 4.3.4 | Chemogenetic activation increased morphological complexity of DVC astrocytes. DVC::GFAP^{mCherry} and DVC::GFAP^{hM3Dq} were injected with CNO (0.3 mg/kg i.p.) and perfused 2-3 hours later. **a**, Representative GFAP immunoreactivity from a DVC::GFAP^{mCherry} mouse. **b**, Representative GFAP immunoreactivity from a DVC::GFAP^{hM3Dq} mouse. **c**, Sholl profile of pNTS astrocytes of DVC::GFAP^{mCherry} and DVC::GFAP^{hM3Dq} mice (n = 35-40 cells from 4 mice per group, Two-way ANOVA, DREADD, $p < 0.0001$, $F_{(1,1440)} = 63.05$,

Distance from soma, $p < 0.0001$, $F_{(19,1440)} = 167.0$, interaction, $p < 0.0001$, $F_{(19,1440)} = 3.49$, Sidak's post-hoc test). **d**, Number of processes of individual pNTS astrocytes of DVC::GFAP^{mCherry} and DVC::GFAP^{hM3Dq} mice (n = 35-40 cells from 4 mice per group, 6.14 ± 0.29 vs 7.88 ± 0.43, p = 0.0015, unpaired t-test). **e**, Enclosing radius of individual pNTS astrocytes of DVC::GFAP^{mCherry} and DVC::GFAP^{hM3Dq} mice (n = 35-40 cells from 4 mice per group, 25.29 ± 1.02 vs 30.30 ± 1.41 µm, p = 0.0063, unpaired t-test). **f**, Representative traces of 5 cells from a DVC::GFAP^{mCherry} mouse. **g**, Representative traces of 5 cells from a DVC::GFAP^{hM3Dq} mouse. **h**, Sum of Sholl intersections of pNTS astrocytes of DVC::GFAP^{mCherry} and DVC::GFAP^{hM3Dq} mice with mouse as a nested variable (n = 35-40 cells from 4 mice per group, nested t-test, p = 0.08). **i**, Number of processes for pNTS astrocytes of DVC::GFAP^{mCherry} and DVC::GFAP^{hM3Dq} mice with mouse as a nested variable (n = 35-40 cells from 4 mice per group, nested t-test, p = 0.07). **j**, Enclosing radius for pNTS astrocytes of DVC::GFAP^{mCherry} and DVC::GFAP^{hM3Dq} mice with mouse as a nested variable (n = 35-40 cells from 4 mice per group, nested t-test, p = 0.11). Scale bars in **a** and **b** = 50 µm. Scale bar in **g** = 25 µm. * = $p < 0.05$, ** = $p < 0.01$, **** = $p < 0.0001$.

4.3.5 | Chemogenetic activation of DVC astrocytes suppressed food intake

Our aim was to understand the consequences of NTS/DVC astrocyte activation on food intake. To this end, mice were individually housed and habituated to experimenter handling and i.p. injections. On the first test day DVC::GFAP^{hM3Dq} and DVC::GFAP^{mCherry} mice had i.p. injections of saline (vehicle) at the beginning of the dark phase and their food intake was monitored for 24 hours. The following day the mice had CNO (1 mg/kg i.p.) and their food intake was again measured. In DVC::GFAP^{hM3Dq} mice, CNO produced a robust suppression of food intake when compared with saline. This was evident from the cumulative food intake (**Figure 4.3.5 a**) and the rate of food intake (**Figure 4.3.5 b**). In contrast, in DVC::GFAP^{mCherry} mice there was no difference in either cumulative food intake (**Figure 4.3.5 c**) or the rate of food intake (**Figure 4.3.5 d**). This shows that chemogenetic activation of DVC astrocytes, but not the ligand CNO alone, suppressed food intake in mice.

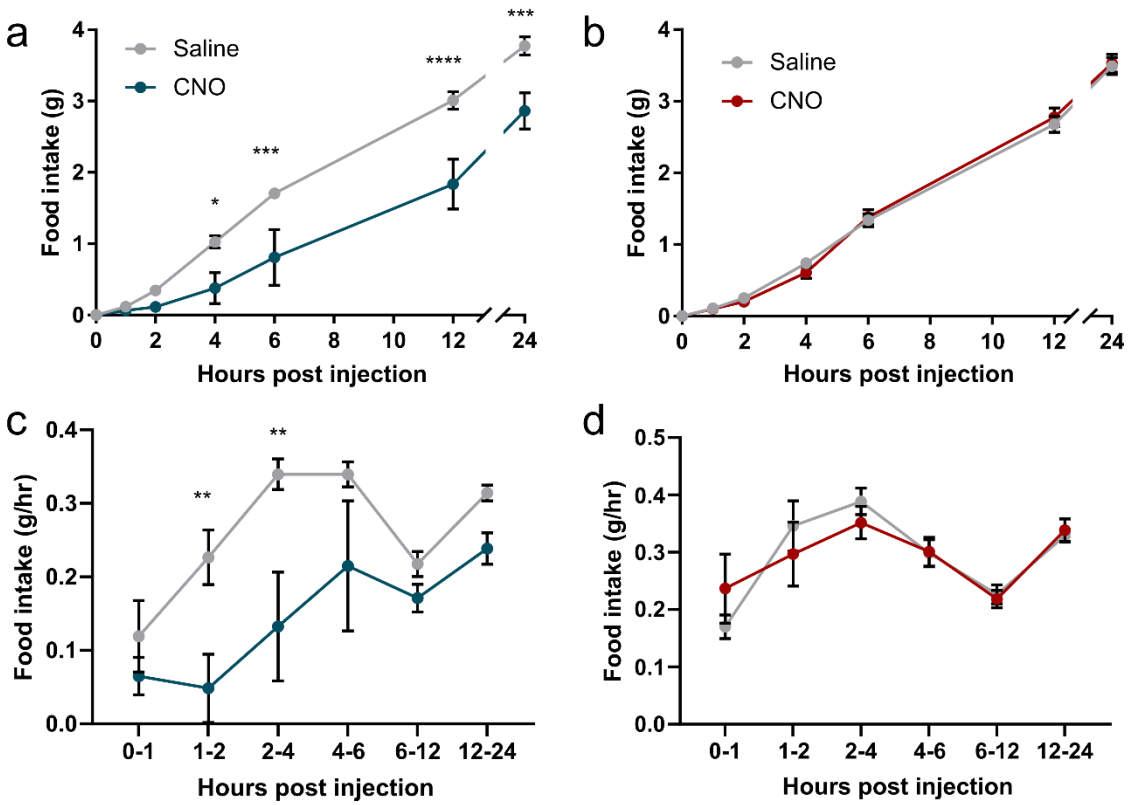

Figure 4.3.5 | Chemogenetic activation of DVC astrocytes suppressed food intake. a, Cumulative food intake of DVC::GFAP^{hM3Dq} mice following injection of saline or CNO (1 mg/kg i.p.) (n = 6 mice, Two-way repeated measure [RM] ANOVA, CNO, p = 0.03, $F_{(1,5)}$ = 8.97, Time, p < 0.0001, $F_{(5,25)}$ = 278.5, interaction, p = 0.002, $F_{(5,25)}$ = 5.44, Sidak's post-hoc test). **b**, Cumulative food intake of DVC::GFAP^{mCherry} mice following injection of saline or CNO (1 mg/kg i.p.) (n = 6 mice, Two-way RM ANOVA, CNO, p = 0.98, $F_{(1,5)}$ > 0.0005, Time, p < 0.0001, $F_{(5,25)}$ = 508.4, interaction, p = 0.53, $F_{(5,25)}$ = 0.84, Sidak's post-hoc test, p > 0.05 for all comparisons). **c**, Rate of food intake of DVC::GFAP^{hM3Dq} mice following injection of saline or CNO (1 mg/kg i.p.) (n = 6 mice, Two-way RM ANOVA, CNO, p = 0.03, $F_{(1,5)}$ = 8.52, Time, p < 0.0001, $F_{(5,25)}$ = 10.78, interaction, p = 0.14, $F_{(5,25)}$= 1.86, Sidak's post-hoc test). **d**, Rate of food intake of DVC::GFAP^{mCherry} mice following injection of saline or CNO (1 mg/kg i.p.) (n = 6 mice, Two-way RM ANOVA, CNO, p = 0.84, $F_{(1,5)}$ = 0.04, Time, p < 0.0002, $F_{(5,25)}$ = 7.32, interaction,

$p = 0.17$, $F_{(5,25)} = 1.72$, Sidak's post-hoc test, $p > 0.05$ for all comparisons). * = $p < 0.05$, ** = $p < 0.01$, *** = $p < 0.001$, **** = $p < 0.0001$.

4.3.6 | Expression of hM3Dq outside the DVC did not account for the effect of CNO on food intake

Reporter expression was consistent within the DVC but varied in nuclei outside the DVC between mice. This allowed us to examine the relationship between the transduced area at the rostrocaudal level of the pNTS and the magnitude of CNO-induced feeding suppression in DVC::GFAP^{hM3Dq} mice. Given that the DVC was reliably transduced in all mice (**Figure 4.3.6 a, b**), a larger transduction area represents greater extra-DVC hM3Dq expression. A linear regression analysis of this relationship revealed no relationship between the size of the transduced area and the effect of CNO injection on food intake in the DVC::GFAP^{hM3Dq} mice (**Figure 4.3.6 c**). This suggests that the transduction of neighbouring nuclei is unlikely to account for the effect on food intake.

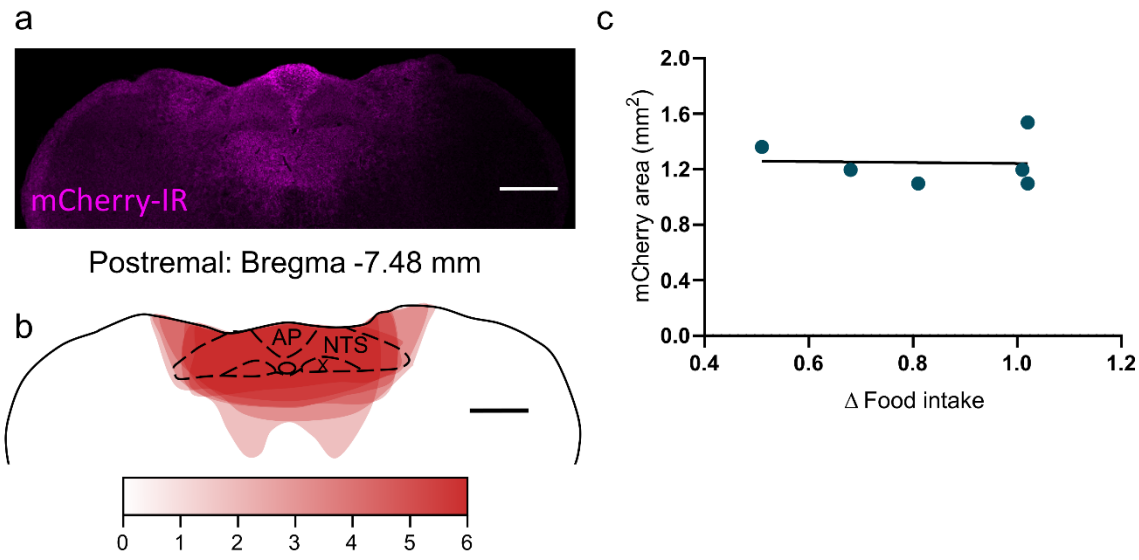

Figure 4.3.6 | Expression of hM3Dq outside the DVC did not account for the effect of CNO on food intake. a, Representative image showing expression of hM3Dq_mCherry in the pNTS of a DVC::GFAP^{hM3Dq} mouse. **b**, Quantification of mCherry immunoreactivity from DVC::GFAP^{hM3Dq} mice (n = 6) in the postremal DVC (Bregma -7.48 mm). **c,** Relationship between transduced area of postremal section (Bregma -7.48 mm) and the CNO-induced reduction of food intake (calculated as control food intake (saline) minus CNO food intake 4 hours post injection) (Linear regression slope = -0.04, not significantly different from zero p = 0.93). Brightness 6 = six mice had mCherry IR in this region. 4V = fourth ventricle, AP = area postrema, NTS = nucleus of the solitary tract, X = dorsal motor nucleus of the vagus. Scale bars = 500 μm.

4.3.7 | Chemogenetic activation of DVC astrocytes reproducibly suppressed food intake

To ascertain whether repeated CNO injections would continue to suppress food intake, the experiment was repeated in the same mice 4 weeks later. Again, CNO injection at the beginning of the dark phase suppressed food intake in DVC::GFAP^{hM3Dq} mice (**Figure 4.3.7 a, b**) but not DVC::GFAP^{mCherry} mice (**Figure 4.3.7 c, d**). This shows that the effect could be reliably produced allowing for further experiments.

Furthermore, body weight measured at 8 hours post injection was significantly lower on the CNO day than the saline day in DVC::GFAP^{hM3Dq} mice (**Figure 4.3.7 e**, 28.81 ± 0.68 vs 27.21 ± 0.58 g; p = 0.003, paired t-test) but was unchanged in DVC::GFAP^{mCherry} mice (**Figure 4.3.7 f**, 29.46 ± 0.36 vs 29.52 ± 0.36 g; p = 0.79, paired t-test). This shows that chemogenetic DVC astrocyte activation suppressed food intake resulting in loss of body weight. This suggests that chemogenetic activation of DVC astrocytes did not stimulate compensatory changes in energy expenditure to maintain body weight.

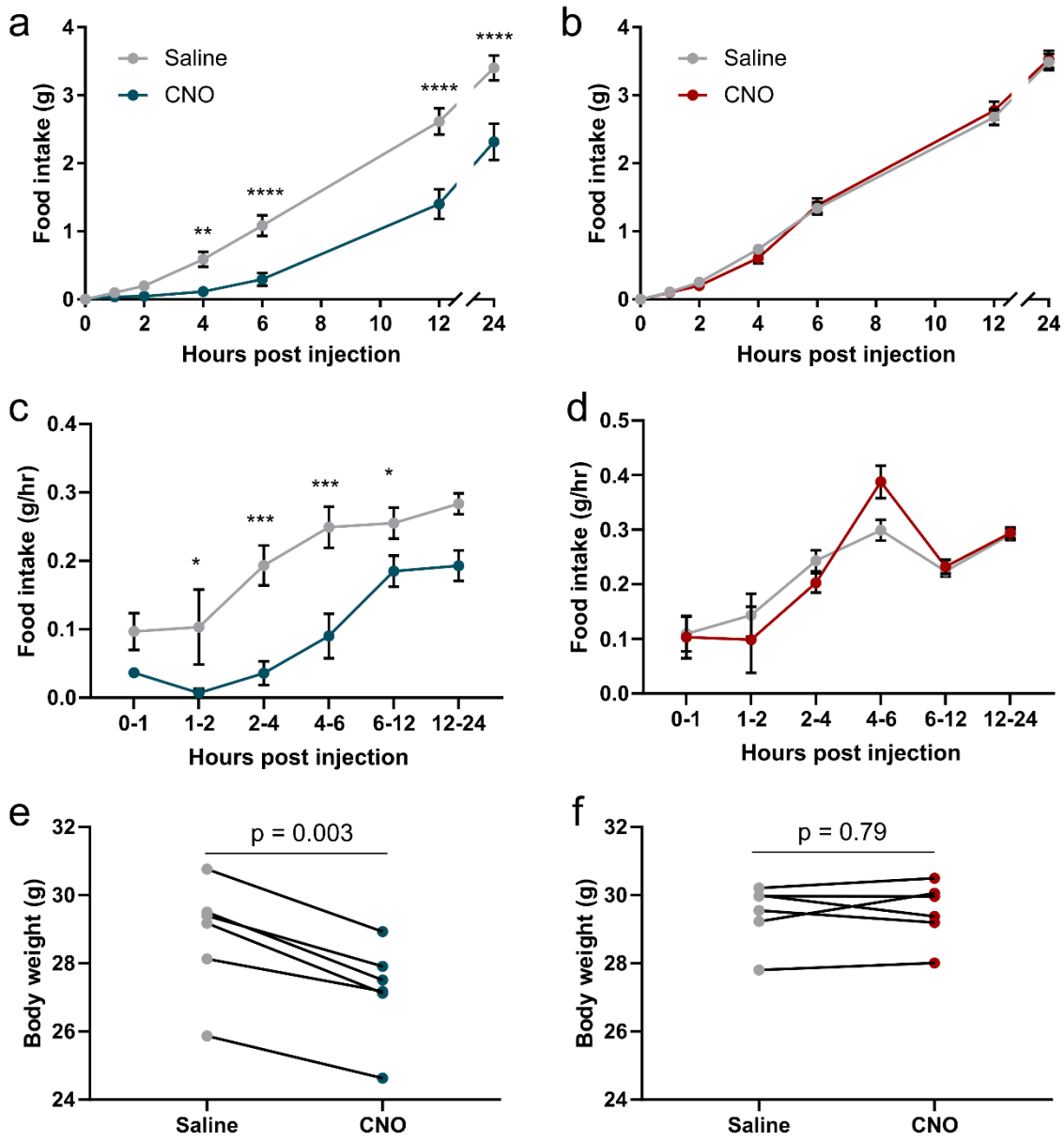

Figure 4.3.7 | Chemogenetic activation of DVC astrocytes reproducibly suppressed food intake. a, Cumulative food intake of DVC::GFAP^{hM3Dq} mice following injection of saline or CNO (1 mg/kg i.p.) (n = 6 mice, Two-way RM ANOVA, CNO, p = 0.0018, $F_{(1,5)}$ = 36.18, Time, p < 0.0001, $F_{(5,25)}$ = 178.5, interaction, p < 0.0001, $F_{(5,25)}$ = 15.16, Sidak's post-hoc test). **b**, Cumulative food intake of DVC::GFAP^{mCherry} mice following injection of saline or CNO (1 mg/kg i.p.) (n = 6 mice, Two-way RM ANOVA, CNO, p = 0.99, $F_{(1,5)}$ < 0.0002, Time, p < 0.0001, $F_{(5,25)}$ = 682.4, interaction, p = 0.41, $F_{(5,25)}$ = 1.044, Sidak's post-hoc test, p > 0.05 for all comparisons). **c**, Rate of food intake of DVC::GFAP^{hM3Dq} mice

following injection of saline or CNO (1 mg/kg i.p.). **d**, Rate of food intake of DVC::GFAP^{mCherry} mice following injection of saline or CNO (1 mg/kg i.p.) (n = 6 mice, Two-way RM ANOVA, CNO, $p = 0.95$, $F_{(1,5)} = 0.005$, Time, $p < 0.0001$, $F_{(5,25)} = 18.85$, interaction, $p = 0.17$, $F_{(5,25)} = 1.69$, Sidak's post-hoc test, $p > 0.05$ for all comparisons). **e**, Body weight measured 8 hours after lights off in DVC::GFAP^{hM3Dq} mice after injection of saline or CNO (1 mg/kg i.p.) (n = 6 mice, 28.81 ± 0.68 vs 27.21 ± 0.58 g, $p = 0.003$, paired t-test). **f**, Body weight measured 8 hours after lights off in DVC::GFAP^{mCherry} mice after injection of saline or CNO (1 mg/kg i.p.) (n = 6 mice, 29.46 ± 0.36 vs 29.52 ± 0.36 g, $p = 0.79$, paired t-test). * = $p < 0.05$, ** = $p < 0.01$, *** = $p < 0.001$, **** = $p < 0.0001$.

4.3.8 | Chemogenetic activation of DVC astrocytes suppressed food intake at a lower dose of CNO

It is recommended that CNO is used at the lowest effective dose to minimise potential off-target effects (Roth, 2016). With this in mind, we sought to investigate the effect on food intake in DVC::GFAP^{hM3Dq} mice of treatment with the lowest dose of CNO shown to effectively activate astrocytes: 0.3 mg/kg (N. Chen *et al.*, 2016). Repeating the experiment as above with 0.3 mg/kg CNO produced identical effects namely reduced cumulative food intake (**Figure 4.3.8 a**), rate of food intake (**Figure 4.3.8 c**) and body weight (**Figure 4.3.8 e**, 28.89 ± 0.69 vs 27.93 ± 0.55g, p = 0.016, paired t-test) relative to saline. Similarly, there were no effects in DVC::GFAP^{mCherry} mice (**Figure 4.3.8 b, d, f**). Direct comparison of both doses showed a similar magnitude of food intake suppression relative to saline in DVC::GFAP^{hM3Dq} mice (**Figure 4.3.8. g, h**). Since the effect size of this lower dose was comparably to the higher one, 0.3 mg/kg CNO i.p. was used for subsequent chemogenetic activation experiments except for **Section 4.3.13**.

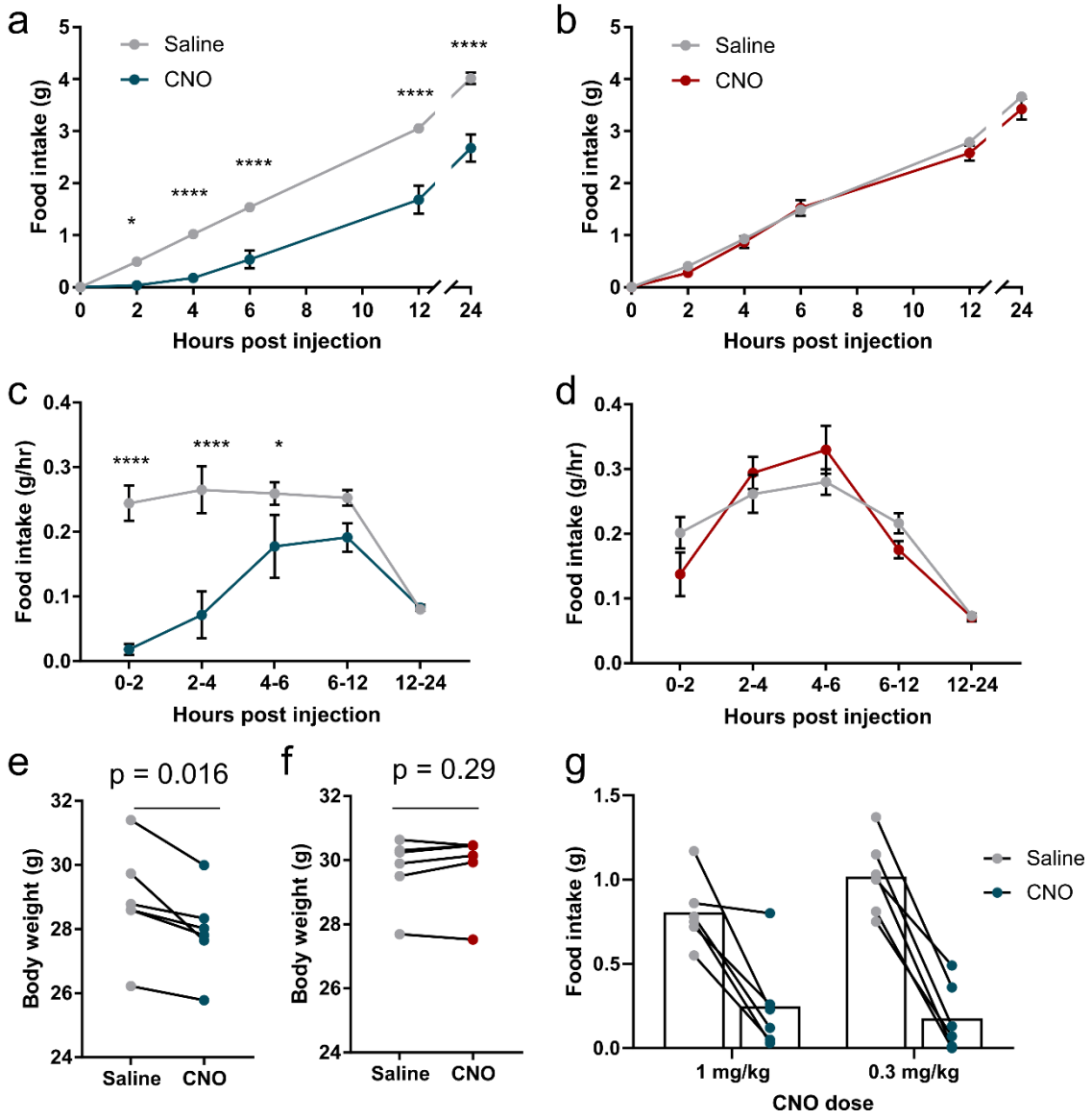

Figure 4.3.8 | Chemogenetic activation of DVC astrocytes with 0.3 mg/kg CNO suppressed food intake. a, Cumulative food intake of DVC::GFAP^{hM3Dq} mice following injection of saline or CNO (0.3 mg/kg i.p.) (n = 6 mice, Two-way RM ANOVA, CNO, p = 0.0007, $F_{(1,5)}$ = 55.7, Time, p < 0.0001, $F_{(5,25)}$ = 331.3, interaction, p < 0.0001, $F_{(5,25)}$ = 15.64, Sidak's post-hoc test). **b**, Cumulative food intake of DVC::GFAP^{mCherry} mice following injection of saline or CNO (0.3 mg/kg i.p.) (n = 6 mice, Two-way RM ANOVA, CNO, p = 0.33, $F_{(1,5)}$ = 1.15, Time, p < 0.0001, $F_{(5,25)}$ = 506.7, interaction, p = 0.18, $F_{(5,25)}$ = 1.65, Sidak's post-hoc test, p > 0.05 for all comparisons). **c**, Rate of food intake of DVC::GFAP^{hM3Dq} mice following injection of saline or CNO (0.3 mg/kg i.p.) (n = 6 mice, Two-way RM

ANOVA, CNO, p = 0.0009, $F_{(1,5)}$ = 49.15, Time, p = 0.0001, $F_{(4,20)}$ = 9.94, interaction, p < 0.0001, $F_{(4,20)}$ = 11.07, Sidak's post-hoc test). **d**, Rate of food intake of DVC::GFAP^{mCherry} mice following injection of saline or CNO (0.3 mg/kg i.p.) (n = 6 mice, Two-way RM ANOVA, CNO, p = 0.76, $F_{(1,5)}$ = 0.10, Time, p < 0.0001, $F_{(4,20)}$ = 29.57, interaction, p = 0.07, $F_{(4,20)}$ = 2.56, Sidak's post-hoc test, p > 0.05 for all comparisons). **e**, Body weight measured 8 hours after lights off in DVC::GFAP^{hM3Dq} mice after injection of saline or CNO (0.3 mg/kg i.p.) (n = 6 mice, 28.89 ± 0.69 vs 27.93 ± 0.55g, p = 0.016, paired t-test). **f**, Body weight measured 8 hours after lights off in DVC::GFAP^{mCherry} mice after injection of saline or CNO (0.3 mg/kg i.p.) (n = 6 mice, 29.59 ± 0.43 vs 29.83 ± 0.47g, p = 0.29, paired t-test). **g**, 4 hour food intake in DVC::GFAP^{hM3Dq} mice following injection with different doses of CNO or corresponding volumes of saline (n = 6 mice). * = p < 0.05, **** = p < 0.0001.

4.3.9 | Chemogenetic activation of DVC astrocytes suppressed food intake following an overnight fast

Hunger is a very strong behavioural motivator and is able to overcome other behavioural stimuli including drive to sleep, chronic pain, anxiety and reproductive instincts (Burnett *et al.*, 2016; Padilla *et al.*, 2016; Alhadeff *et al.*, 2018; Goldstein *et al.*, 2018; X.-Y. Li *et al.*, 2019). However, strong satiety signals are sufficient to suppress food intake even in mice that are given access to food after fasting (Essner *et al.*, 2017). To assess whether this was the case for chemogenetic DVC astrocyte activation, DVC::GFAP^{hM3Dq} and DVC::GFAP^{mCherry} mice were fasted for 12 hours during the dark phase. 15-30 minutes prior to lights on mice received CNO (0.3 mg/kg i.p.) and food was returned at lights on. Cumulative food intake during re-feeding after this fast was lower in DVC::GFAP^{hM3Dq} mice when compared with DVC::GFAP^{mCherry} (**Figure 4.3.9 a**). The rate of food intake in DVC::GFAP^{hM3Dq} mice was far lower than DVC::GFAP^{mCherry} within the first hour (**Figure 4.3.9 b**). Body weight had returned to pre-fasting levels in DVC::GFAP^{mCherry} mice 8 hours after re-introduction while in DVC::GFAP^{hM3Dq} mice weight regain was lower (**Figure 4.3.9 c**, 99.51 ± 0.65 vs 95.24 ± 1.47 %, $p = 0.024$ unpaired t-test). This shows that even in the presence of a strong homeostatic drive to feed, DVC astrocyte activation is sufficient to reduce food intake.

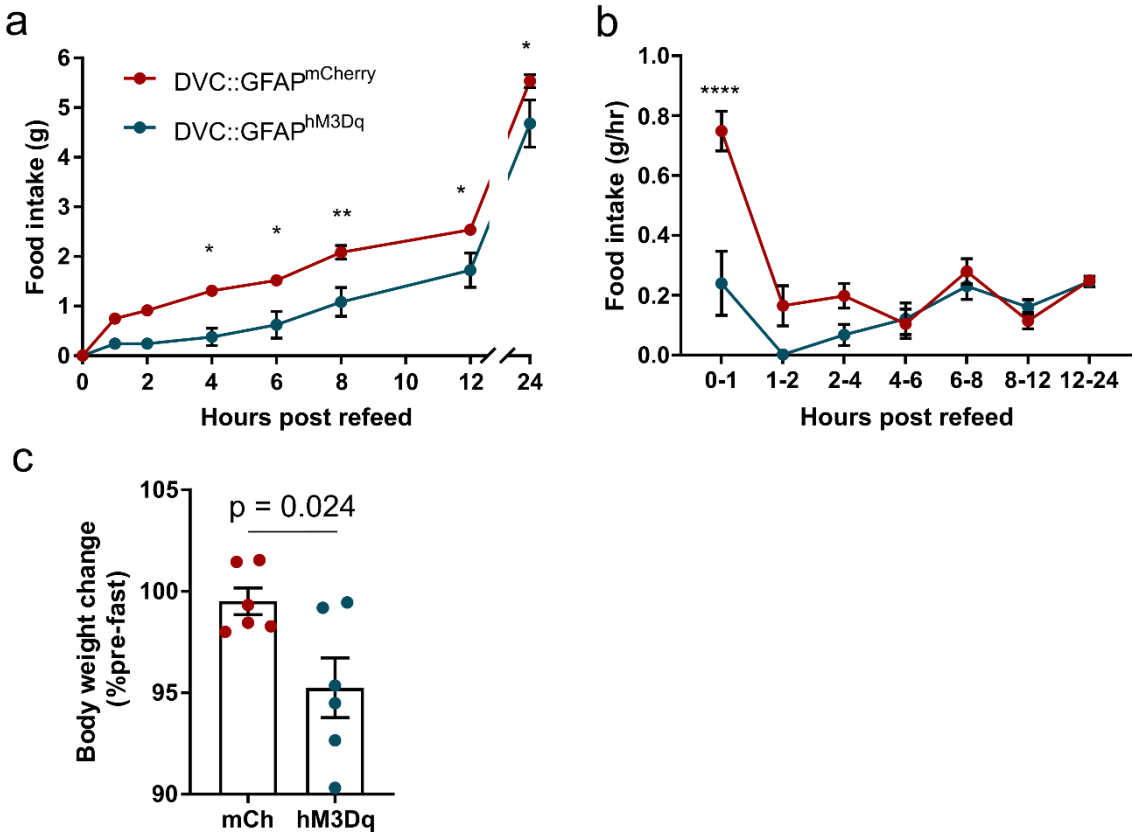

Figure 4.3.9 | Chemogenetic activation of DVC astrocytes suppressed food intake during re-feeding after a 12 hour fast. DVC::GFAP^{mCherry} and DVC::GFAP^{hM3Dq} mice were fasted for 12 hours during the dark phase then injected with CNO 30 minutes prior to reintroduction of food at the onset of the light phase. **a**, Cumulative food intake (n = 6 mice per group, Two-way ANOVA, DREADD, p = 0.01, $F_{(1,10)}$ = 10.03, Time, p < 0.0001, $F_{(7,70)}$ = 310.5, interaction, p = 0.0053, $F_{(7,70)}$ = 3.20, Sidak's post-hoc test). **b**, Rate of food intake (n = 6 mice per group, Two-way ANOVA, DREADD, p = 0.007, $F_{(1,10)}$= 11.4, Time, p < 0.0001, $F_{(6,60)}$ = 18.55, interaction, p < 0.0001, $F_{(6,60)}$ = 8.35, Sidak's post-hoc test). **c**, Body weight (% of pre-fasting weight) 8 hours after refeeding (n = 6 mice per group, 99.51 ± 0.65 vs 95.24 ± 1.47 %, p = 0.024 unpaired t-test). * = p < 0.05, ** = p < 0.01, **** = p < 0.0001.

4.3.10 | Chemogenetic activation of DVC astrocytes did not induce conditioned place aversion

Strong satiety signals and malaise inducing agents can evoke negative affective states (e.g. nausea) (Maniscalco and Rinaman, 2018). To probe the affective salience of chemogenetic DVC astrocyte activation and CNO alone, we performed a conditioned place aversion (CPA) assay in DVC::GFAP^{hM3Dq} and DVC::GFAP^{mCherry} mice using CNO as a conditioning stimulus (**Figure 4.3.10 a**). On the initial day mice in either group showed no preference for either chamber. Mice were then conditioned with one trial in each chamber after injection of either CNO (0.3 mg/kg i.p.) or saline in a randomised, counterbalanced fashion (i.e. across the group the order of saline or CNO and the chamber to which each stimulus was conditioned was varied to control for drug order or chamber effects). Following conditioning, DVC::GFAP^{hM3Dq} mice did not show a preference or aversion for the CNO paired chamber over the saline one (**Figure 4.3.10 b, c**), indicating that DVC astrocyte activation is not sufficient to induce CPA in this paradigm. Secondly, DVC::GFAP^{mCherry} mice did not show a preference or aversion for the CNO paired chamber indicating that CNO alone is not sufficient to induce CPA (**Figure 4.3.10 b, d**).

As a positive control, we conditioned a separate cohort of mice using lithium chloride (LiCl [150 mg/kg i.p.]) as a stimulus. LiCl has been shown to be aversive in longer conditioning paradigms (3-4 sessions) (Le Merrer *et al.*, 2011; Longoni *et al.*, 2011; Sanjakdar *et al.*, 2015; T. Zhang *et al.*, 2019) but following our protocol it did not cause mice to avoid the LiCl-paired chamber (**Figure 4.3.10 f**). This limits the conclusions we can draw from our chemogenetic conditioning experiments.

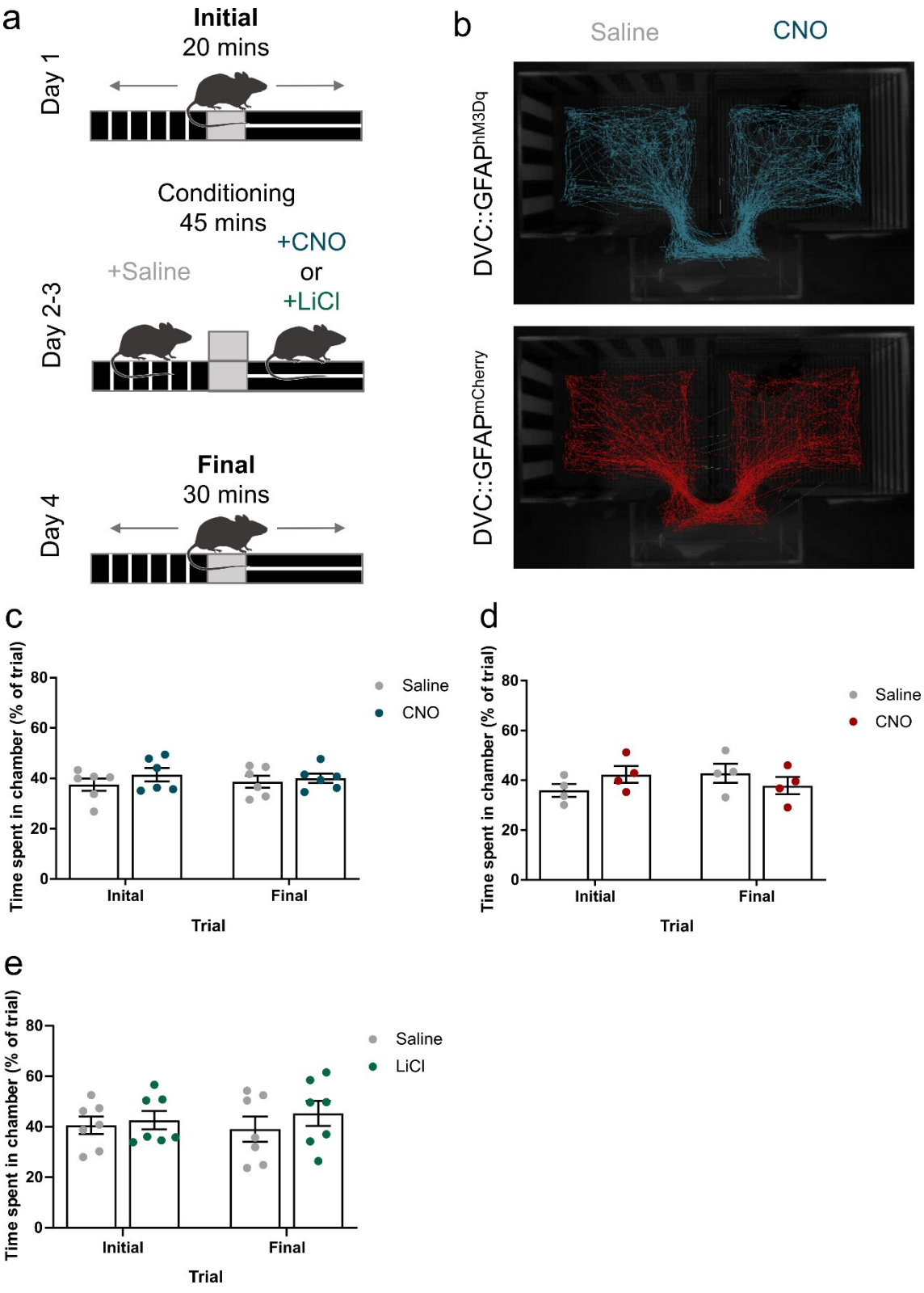

Figure 4.3.10 | Chemogenetic activation of DVC astrocytes did not induce conditioned place aversion. a, Schematic of the conditioning protocol. **b,** Representative tracks of a DVC::GFAP^{hM3Dq} (top, blue) and a DVC::GFAP^{mCherry} (bottom, red) mouse during the final trial. **c,** Percentage of the trial spent in the

saline- and CNO-paired chamber before (initial) and after (final) conditioning sessions in DVC::GFAP^{hM3Dq} mice (n = 6 mice, Two-way RM ANOVA, CNO, p = 0.32, $F_{(1,10)}$ = 1.09, Conditioning, p = 0.96, $F_{(1,10)}$ = 0.002, interaction, p = 0.57, $F_{(1,10)}$ = 0.35, Sidak's post-hoc test, p > 0.05 for all comparisons). **d,** Percentage of the trial spent in the saline- and CNO-paired chamber before and after conditioning sessions in DVC::GFAP^{mCherry} mice. (n = 4 mice, Two-way RM ANOVA, CNO, p = 0.76, $F_{(1,6)}$ = 0.10, Conditioning, p = 0.78, $F_{(1,6)}$ = 0.08, interaction, p = 0.23, $F_{(1,6)}$ = 1.81, Sidak's post-hoc test, p > 0.05 for all comparisons). **e,** Percentage of the trial spent in the saline- and LiCl-paired chamber before and after conditioning sessions. (n = 7 mice, Two-way RM ANOVA, LiCl, p = 0.48, $F_{(1,12)}$ = 0.54, Conditioning, p = 0.8, $F_{(1,12)}$ = 0.06, interaction, p = 0.38, $F_{(1,12)}$ = 0.82, Sidak's post-hoc test, p > 0.05 for all comparisons).

4.3.11 | Chemogenetic activation of DVC astrocytes did not acutely effect locomotion

A second indicator of malaise in mice is reduced locomotion. We were able to assess this by examining the distance travelled during the 45 minute conditioning trials (i.e. 15 minutes after mice had been injected with CNO or saline) of our CPA paradigm (**Figure 4.3.11 a**). This analysis showed no significant difference in distance travelled between saline and CNO trials in DVC::GFAP^{hM3Dq} mice (**Figure 4.3.11 b**, 10260 ± 1101 vs 7501 ± 1183 cm, p = 0.18, paired t-test). Furthermore, CNO did not alter locomotion in DVC::GFAP^{mCherry} mice (**Figure 4.3.11 c**, 9773 ± 991.1 vs 9870 ± 896.3 cm, p = 0.94, paired t-test).

Finally, in this experiment LiCl (150 mg/kg i.p.) did reduce distance travelled compared with saline (**Figure 4.3.11 d**, 6316 ± 360.9 vs 3261 ± 343.4 cm, p = 0.007, paired t-test) thus indicating that this measure is sensitive to acute malaise and suggesting chemogenetic DVC astrocyte activation suppresses food intake independent of malaise, but further work would be required to conclusively demonstrate this.

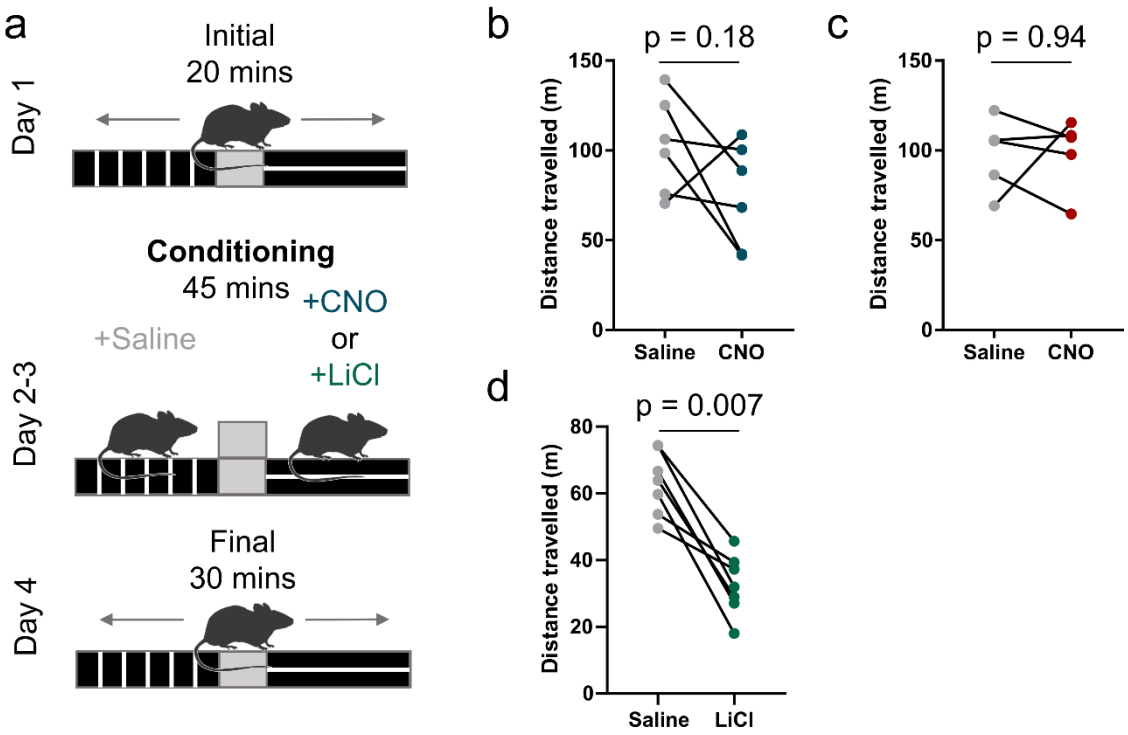

Figure 4.3.11 | Chemogenetic activation of DVC astrocytes did not suppress locomotion. **a**, Schematic of the conditioning protocol. **b**, Distance travelled during conditioning sessions for DVC::GFAP^{hM3Dq} mice (n = 6 mice, 10260 ± 1101 vs 7501 ± 1183 cm, p = 0.18, paired t-test). **c**, Distance travelled during conditioning sessions for DVC::GFAP^{mCherry} mice (n = 5 mice, 9773 ± 991.1 vs 9870 ± 896.3 cm, p = 0.94, paired t-test). **d**, Distance travelled during conditioning sessions in mice injected with saline or LiCl (n = 7 mice, 6316 ± 360.9 vs 3261 ± 343.4 cm, p = 0.007, paired t-test).

4.3.12 | Chemogenetic activation of DVC astrocytes reduced food seeking independent of locomotion and drinking

To observe the behaviour of mice during DVC astrocyte activation we placed mice in their home cages under a video camera. Food was removed from the hopper and two pellets were placed in the far side of the cage from the nest (**Figure 4.3.12 a**). Mice were injected with CNO at the beginning of the dark phase, returned to their home cage and recorded for 3 hours. During the 3 hour period food intake was lower in DVC::GFAP^{hM3Dq} mice compared with DVC::GFAP^{mCherry} mice (**Figure 4.3.12 b**, 0.79 ± 0.10 vs 0.21 ± 0.14 g, p = 0.028, unpaired t-test). During this same time period DVC::GFAP^{hM3Dq} mice entered the food zone fewer times than DVC::GFAP^{mCherry} mice (**Figure 4.3.12 c**, 118.3 ± 12 vs 30.67 ± 15.38 entries, p = 0.011, unpaired t-test). Analysing the first hour in 10 minute bins revealed that the DVC::GFAP^{mCherry} mice immediately began eating as evidenced by the number of entries to the zone in the first 10 minutes while DVC::GFAP^{hM3Dq} mice did not (**Figure 4.3.12 d**). The relationship between food intake and the number of food zone entries revealed a strong positive correlation indicating this is a reliable metric for assessing food seeking behaviour rather than general exploration or unrelated entries to the zone (**Figure 4.3.12 e**, R^2 = 0.98, p = 0.0002). Between groups there was no difference in the total time spent moving (**Figure 4.3.12 f**, 1518 ± 147.4 vs 1100 ± 536.2 seconds, p = 0.49, unpaired t-test), the total distance travelled (**Figure 4.3.12 g**, 11801 ± 1809 vs 10147 ± 5158 cm, p = 0.78, unpaired t-test) or the entries to the water spout zone (**Figure 4.3.12 h**, 82 ± 8.67 vs 61 ± 30.66 entries, p = 0.55, unpaired t-test). This indicates the effects of DVC astrocyte activation on food intake are independent of locomotion or fluid intake. Additionally, it suggests that DVC::GFAP^{hM3Dq} mice

have a reduced drive to eat following CNO injection given that food seeking is lower and zone entries correlate with intake.

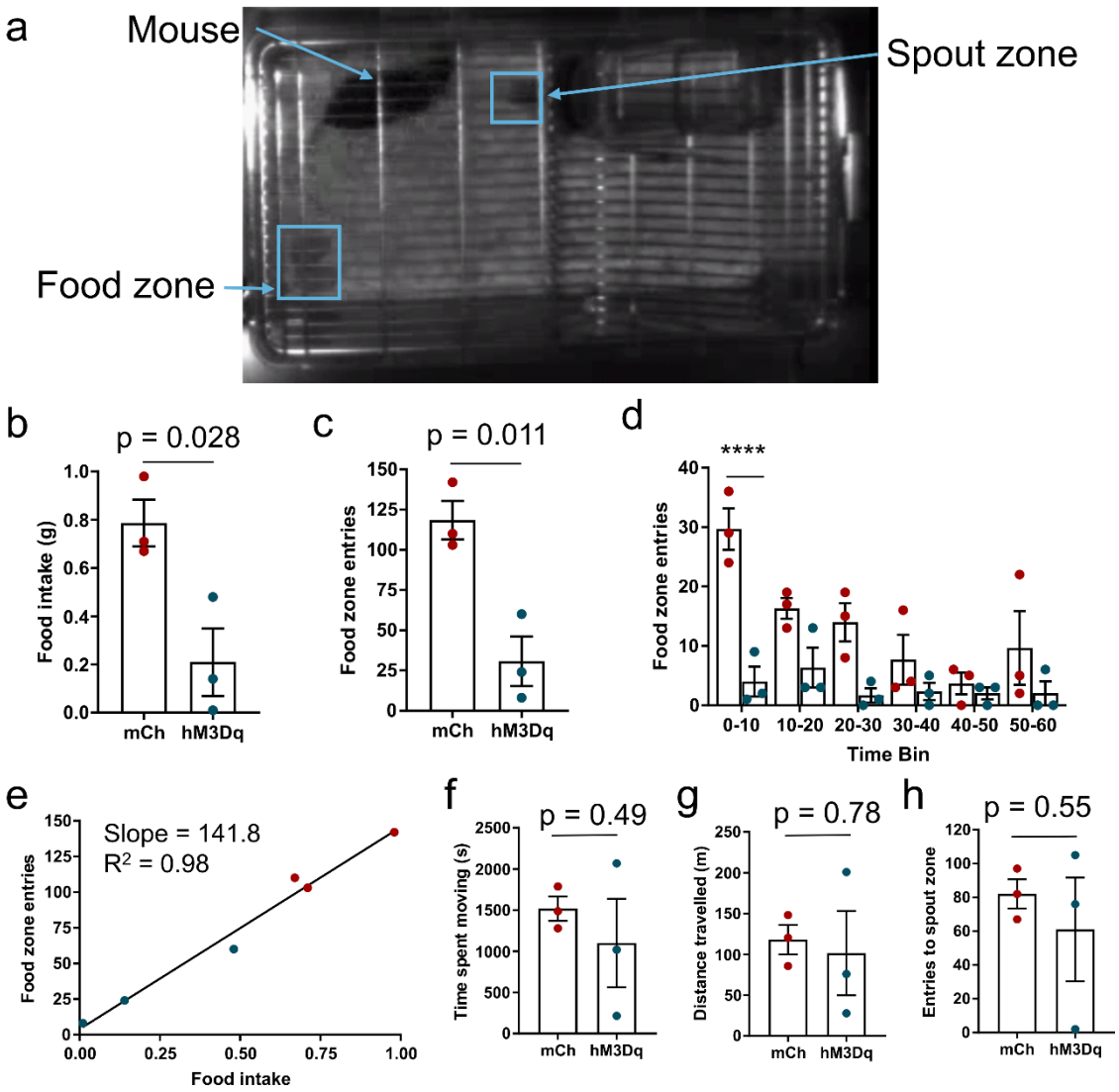

Figure 4.3.12 | Chemogenetic activation of DVC astrocytes suppressed food seeking independent of locomotion or drinking. a, Image of the recording set up indicating the home cage, food zone, spout zone and mouse. **b**, Food intake during the 3 hour recording period (n = 3 mice per group, 0.79 ± 0.10 vs 0.21 ± 0.14 g, p = 0.028, unpaired t-test). **c**, Food zone entries during the 3 hour recording period (n = 3 mice per group, 118.3 ± 12 vs 30.67 ± 15.38 entries, p = 0.011, unpaired t-test). **d**, Food zone entries during the first hour of the recording period in 10 minute bins (n = 3 mice per group, Two-way ANOVA, DREADD, p = 0.0052, $F_{(1,4)} = 30.81$, Time, p < 0.0019, $F_{(5,20)} = 5.74$, interaction, p < 0.013, $F_{(5,20)} = 3.85$, Sidak's post-hoc test). **e**, Relationship between total food intake and total

entries to the food zone (linear regression slope = 141.8, significantly non-zero p = 0.0002). **f**, Time spent moving during the 3 hour recording period (n = 3 mice per group, 1518 ± 147.4 vs 1100 ± 536.2 seconds, p = 0.49, unpaired t-test). **g**, Distance travelled during the 3 hour recording period (n = 3 mice per group, 11801 ± 1809 vs 10147 ± 5158 cm, p = 0.78, unpaired t-test). **h**, Spout zone entries during the 3 hour recording period (n = 3 mice per group, 82 ± 8.67 vs 61 ± 30.66 entries, p = 0.55, unpaired t-test). **** = p < 0.0001.

4.3.13 | Chemogenetic activation of DVC astrocytes is not analgesic

A population of NTS neurons expressing pro-opiomelanocortin (NTS^{POMC}) have been shown to produce analgesia when chemogenetically activated (Cerritelli *et al.*, 2016). To assess whether these neurons were potentially recruited in our manipulation we compared tail flick responses to 51 °C water immersion in DVC::$GFAP^{mCherry}$ and DVC::$GFAP^{hM3Dq}$ before and after CNO (1 mg/kg i.p.). There were no significant differences between the groups either at baseline (before CNO injection) or at any of the measured points (15 minute intervals for 60 minutes after CNO injection) in the raw withdrawal latency (**Figure 4.3.13 a**). To remove the influence of baseline differences between animals all values were also plotted as a percentage of each mouse's own baseline measurement. This confirmed that there was no difference in the withdrawal latency between DVC::$GFAP^{mCherry}$ and DVC::$GFAP^{hM3Dq}$ mice (**Figure 4.3.13 b**). This suggests that DVC astrocyte activation is again selective for feeding rather than a general activation of NTS circuitry.

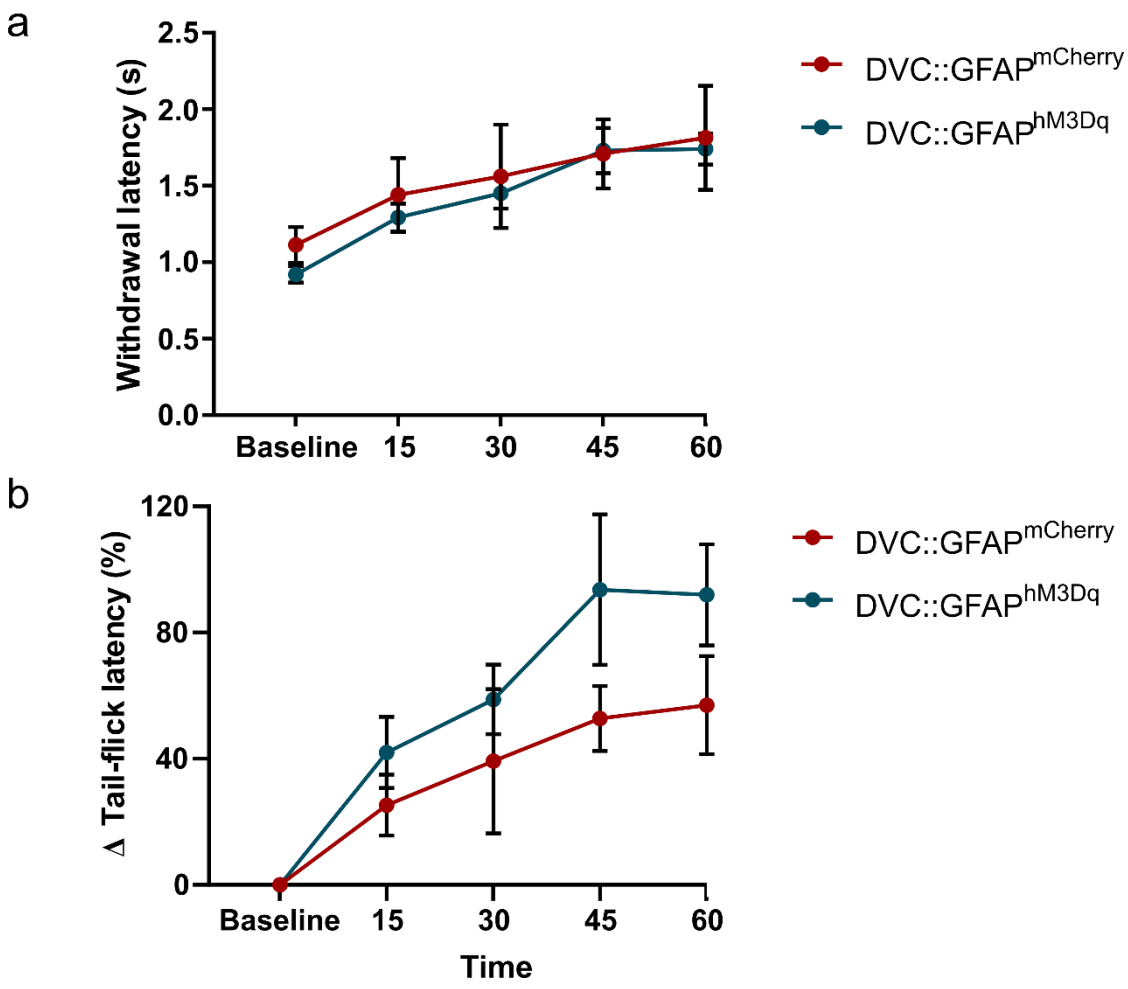

Figure 4.3.13 | Chemogenetic activation of DVC astrocytes did not increase tail-flick latency. a, Raw latency to withdraw the tail from 51 °C water before (baseline) and at 15 minute intervals after CNO (1 mg/kg i.p.) (n = 6 mice per group, Two-way ANOVA, DREADD, p = 0.68, $F_{(1,10)}$= 0.18, Time, p < 0.0001, $F_{(4,40)}$= 11.74, interaction, p = 0.93, $F_{(4,40)}$= 0.21, Sidak's post-hoc test, p > 0.05 for all comparisons). **b**, Normalised latency to withdraw the tail from 51 °C water at 15 minute intervals after CNO (1 mg/kg i.p.) (n = 6 mice per group, Two-way ANOVA, DREADD, p = 0.13, $F_{(1,10)}$= 2.80, Time, p < 0.0001, $F_{(4,40)}$= 13.42, interaction, p = 0.47, $F_{(4,40)}$= 0.91, Sidak's post-hoc test, p > 0.05 for all comparisons). Data collected by Dr Fiona Holmes, University of Bristol.

4.3.14 | Chemogenetic activation of DVC astrocytes reduced nocturnal feeding and refeeding after a fast in mice with restricted viral transduction

The experiments described above were from a cohort of mice that received angled AAV vector injections at four sites across the NTS which resulted in spread through the DVC. In an attempt to further restrict the virus expression, we generated a second cohort of DVC::GFAP^{hM3Dq} mice and DVC::GFAP^{mCherry} controls that received only one injection per side (**Figure 4.3.14 a-c**). In these mice injection with CNO (0.3 mg/kg i.p.) reduced cumulative food intake (**Figure 4.3.14 d**), rate of food intake (**Figure 4.3.14 e**) and refeeding after a 12 hour fast (**Figure 4.3.14 f, g**) with a similar magnitude and duration when compared with the previous cohort. This lower AAV vector injection volume was used for the experiments described below with the exception of c-FOS immunohistochemistry in **Figures 4.3.15, 4.3.16** and **4.3.17** which was performed on the original cohort.

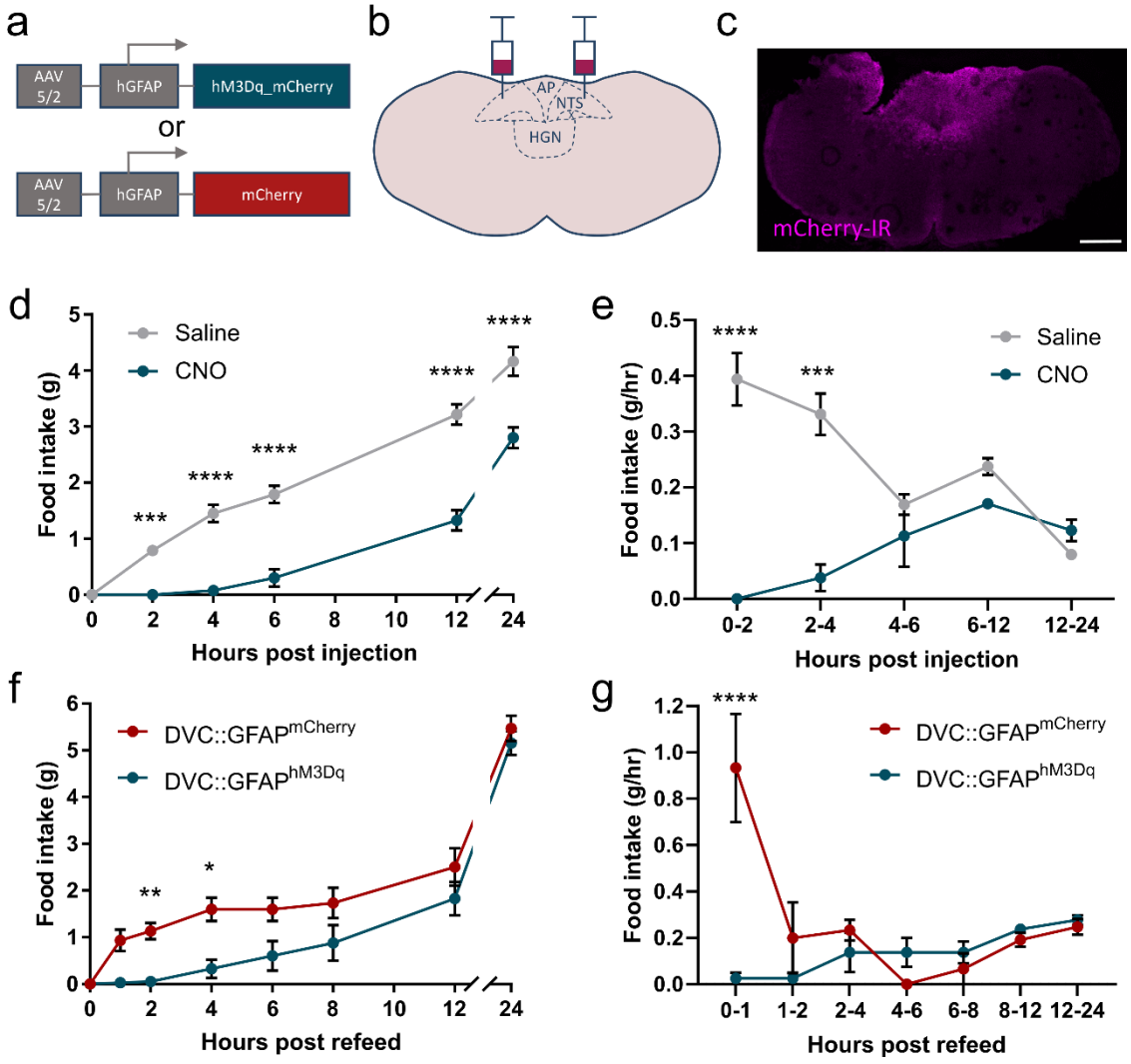

Figure 4.3.14 | Lower AAV vector injection volume is still sufficient to suppress feeding. a, Schematic of viral vectors used to create DVC::GFAP^{hM3Dq} and DVC::GFAP^{mCherry} mice. **b,** Schematic showing anatomy of target region. **c,** Representative section showing immunoreactivity against hM3Dq_mCherry in and around the DVC. DVC::GFAP^{hM3Dq} mice were injected i.p. with saline or CNO (0.3 mg/kg) 30 minutes prior to the beginning of the dark-phase. **d,** Cumulative food intake (n = 4 mice, Two-way RM ANOVA, CNO, $p < 0.0001$, $F_{(1,18)} = 335.1$, Time, $p < 0.0001$, $F_{(5,18)} = 112.0$, interaction, $p < 0.0001$, $F_{(5,18)} = 18.64$, Sidak's post-hoc test). **e,** Rate of food intake (n = 4 mice, Two-way RM ANOVA, CNO, $p = 0.0036$, $F_{(1,3)} = 69.45$, Time, $p = 0.0019$, $F_{(4,12)} = 8.25$, interaction, $p < 0.0001$, $F_{(4,12)} = 16.03$, Sidak's post-hoc test). DVC::GFAP^{mCherry} and DVC::GFAP^{hM3Dq}

mice were fasted for 12 hours during the dark phase then injected i.p. with CNO (0.3 mg/kg) 30 minutes prior to reintroduction of food at the onset of the light phase. **f,** Cumulative food intake (n = 3-4 mice per group ,Two-way ANOVA, DREADD, $p = 0.038$, $F_{(1,5)} = 7.818$, Time, $p < 0.0001$, $F_{(7,35)} = 168.0$, interaction, $p = 0.026$, $F_{(7,35)} = 2.67$, Sidak's post-hoc test). **g,** Rate of food intake (n = 3-4 mice per group, Two-way ANOVA, DREADD, $p = 0.029$, $F_{(1,5)} = 9.29$, Time, $p = 0.0001$, $F_{(6,30)} = 6.73$, interaction, $p < 0.0001$, $F_{(6,30)} = 11.21$, Sidak's post-hoc test). * = $p < 0.05$, ** = $p < 0.01$, **** = $p < 0.0001$. AP = area postrema, HGN = hypoglossal nucleus, NTS = nucleus of the solitary tract, X = dorsal motor nucleus of the vagus. Scale bar = 500 µm. * = $p < 0.05$, ** = $p < 0.01$, *** = $p < 0.001$, **** = $p < 0.0001$.

4.3.15 | Chemogenetic activation of DVC astrocytes induced c-FOS immunoreactivity in the NTS and AP

Immunoreactivity for the immediate early gene product c-FOS as a marker of cellular activation was assessed to quantitate the extent of DVC activation in DVC::GFAP^{hM3Dq} and DVC::GFAP^{mCherry} mice. To this end, DVC::GFAPhM3Dq and DVC::GFAPmCherry mice were injected with CNO 2-3 hours prior to perfusion fixation followed by immunohistochemistry for c-FOS.

There was greater c-FOS immunoreactivity in the NTS and AP of DVC::GFAP^{hM3Dq} than DVC::GFAP^{mCherry} mice following injection of CNO (0.3 mg/kg i.p.) (**Figure 4.3.15 a-c**). Reflective of this, there were more c-FOS immunoreactive cells in the NTS of DVC::GFAP^{hM3Dq} mice than DVC::GFAP^{mCherry} mice (**Figure 4.3.15 d**, 29 ± 5 vs 113.7 ± 19.6 cells, p = 0.002, unpaired t-test). This was also true for the AP where there were more c-FOS immunoreactive cells in DVC::GFAP^{hM3Dq} mice than DVC::GFAP^{mCherry} mice (**Figure 4.3.15 e**, 11.8 ± 3.2 vs 63.2 ± 17.2 cells, p = 0.014, unpaired t-test). This shows that activation of DVC astrocytes stimulates neighbouring neurons.

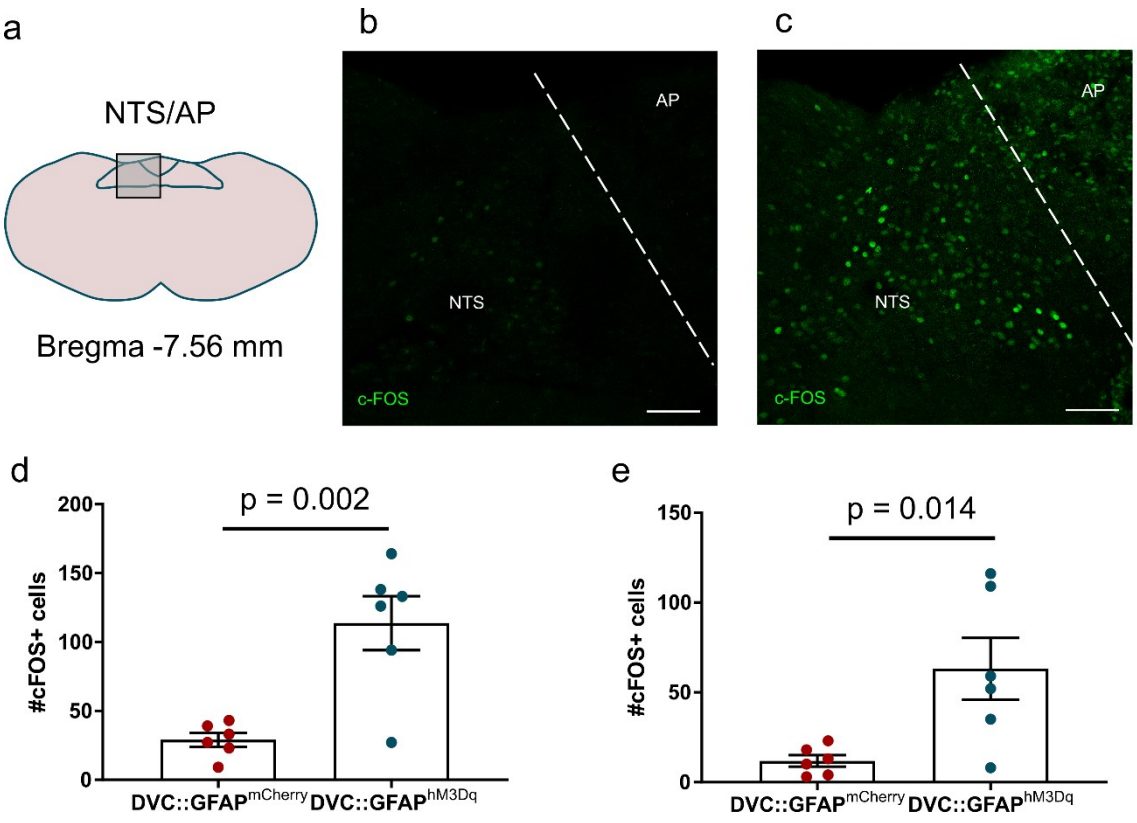

Figure 4.3.15 | Chemogenetic activation of DVC astrocytes induced c-FOS immunoreactivity in the NTS and AP. a, Diagram showing region of interest for imaging and cell counting. **b**, Representative image from a DVC::GFAP^{mCherry} mouse. **c**, Representative image from a DVC::GFAP^{hM3Dq} mouse. **d**, Number of c-FOS immunoreactive cells in the NTS of DVC::GFAP^{mCherry} and DVC::GFAP^{hM3Dq} mice perfused 2-3 hours after injection of CNO (0.3 mg/kg i.p.) (n = 6 mice per group, 29 ± 5 vs 113.7 ± 19.6 cells, p = 0.002, unpaired t-test). **e**, Number of c-FOS immunoreactive cells in the AP of DVC::GFAP^{mCherry} and DVC::GFAP^{hM3Dq} mice perfused 2-3 hours after injection of CNO (0.3 mg/kg i.p.) (n = 6 mice per group, 11.8 ± 3.2 vs 63.2 ± 17.2 cells, p = 0.014, unpaired t-test). AP = area postrema, NTS = nucleus of the solitary tract. Scale bars = 50 μm.

4.3.16 | Chemogenetic activation of DVC astrocytes induced c-FOS immunoreactivity in the lPBN

Since circuits controlling food intake are distributed across the brain, changes in food intake require long-range neuronal communication. Astrocytes do not project outside their resident brain nuclei and therefore we hypothesised that activation of DVC astrocytes was increasing the activity of local neurons and signalling to downstream circuits. The lateral parabrachial nucleus (lPBN) has been identified as a major projection target of satiety signalling NTS neurons and its role in meal termination is well described (Carter *et al.*, 2013; Campos *et al.*, 2016; Roman, Derkach and Palmiter, 2016; Palmiter, 2018). Consistent with our hypothesis there was greater c-FOS immunoreactivity in the lPBN of DVC::GFAP^{hM3Dq} than DVC::GFAP^{mCherry} mice following injection of CNO (0.3 mg/kg) (**Figure 4.3.16 a-c**). Reflective of this, there were more c-FOS immunoreactive cells in the lPBN of DVC::GFAP^{hM3Dq} mice than DVC::GFAP^{mCherry} mice (**Figure 4.3.16 d**, 17.5 ± 4.49 vs 89.33 ±11.08 cells, p = 0.0001, unpaired t-test). This shows that chemogenetic activation of DVC astrocytes recruits local neurons to excite downstream nuclei involved in meal termination and satiety.

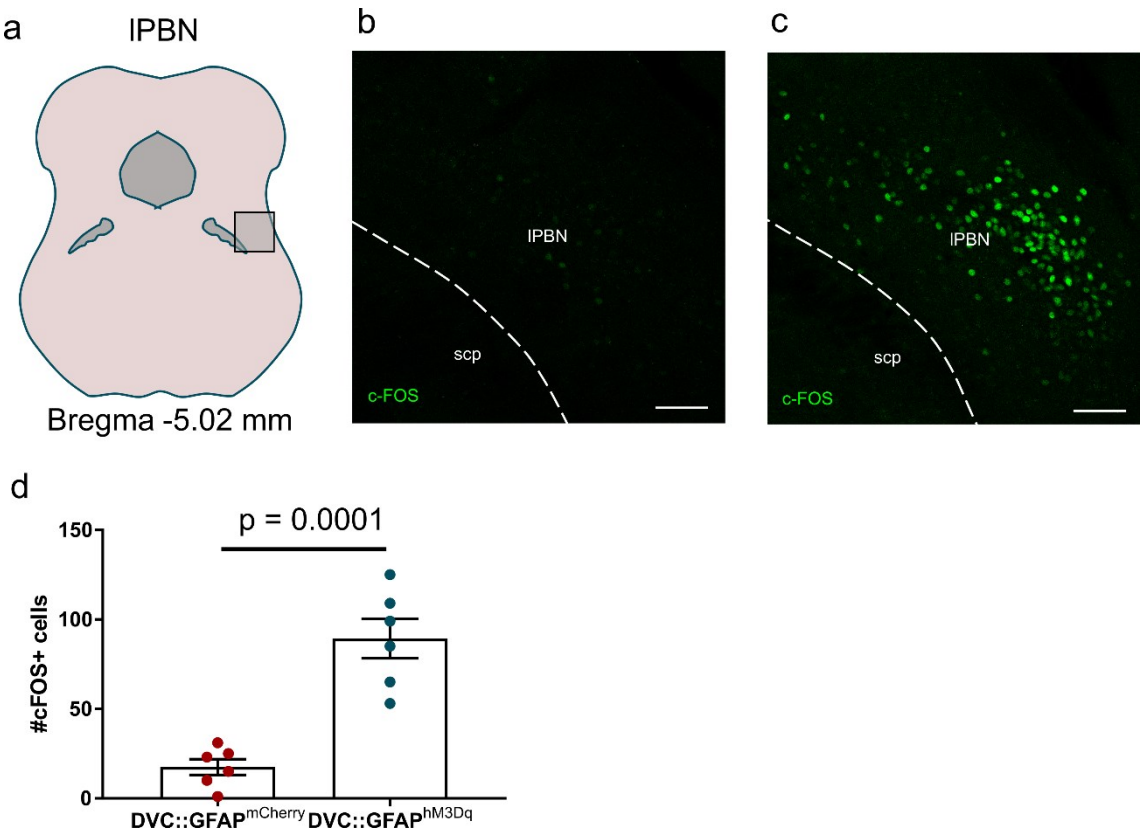

Figure 4.3.16 | Chemogenetic activation of DVC astrocytes induced c-FOS immunoreactivity in the lPBN. **a**, Diagram showing region of interest for imaging and cell counting. **b**, Representative image from a DVC::GFAP^{mCherry} mouse. **c**, Representative image from a DVC::GFAP^{hM3Dq} mouse. **d**, Number of c-FOS immunoreactive cells in the lPBN of DVC::GFAP^{mCherry} and DVC::GFAP^{hM3Dq} mice perfused 2-3 hours after injection of CNO (0.3 mg/kg i.p.) (n = 6 mice per group, 17.5 ± 4.49 vs 89.33 ±11.08 cells, p = 0.0001, unpaired t-test). lPBN = lateral parabrachial nucleus, scp = superior cerebellar peduncle. Scale bars = 50 µm.

4.3.17 | Chemogenetic activation of DVC astrocytes did not induce c-FOS immunoreactivity in the PVH

The paraventricular nucleus of the hypothalamus (PVH) is a second major projection target of satiety signalling NTS neurons (Rinaman, 2010; D'Agostino *et al.*, 2016). There was no difference in c-FOS immunoreactivity in the PVH between DVC::GFAP^{hM3Dq} and DVC::GFAP^{mCherry} mice following injection of CNO (0.3 mg/kg) (**Figure 4.3.17 a-c**). Reflective of this, there was no statistically significant difference in the number of c-FOS immunoreactive cells in the PVH of DVC::GFAP^{hM3Dq} mice and DVC::GFAP^{mCherry} mice (**Figure 4.3.17 d**, 75.5 ± 12.05 vs 77.33 ± 8.58 cells, p = 0.9, unpaired t-test). However, in DVC::GFAP^{mCherry} mice PVH c-FOS immunoreactivity was greater than in the lPBN and DVC possibly due to the stress of injection/preparation for perfusion (Füzesi *et al.*, 2016). This may occlude detection of c-FOS induced by chemogenetic activation of DVC astrocytes due to the high baseline.

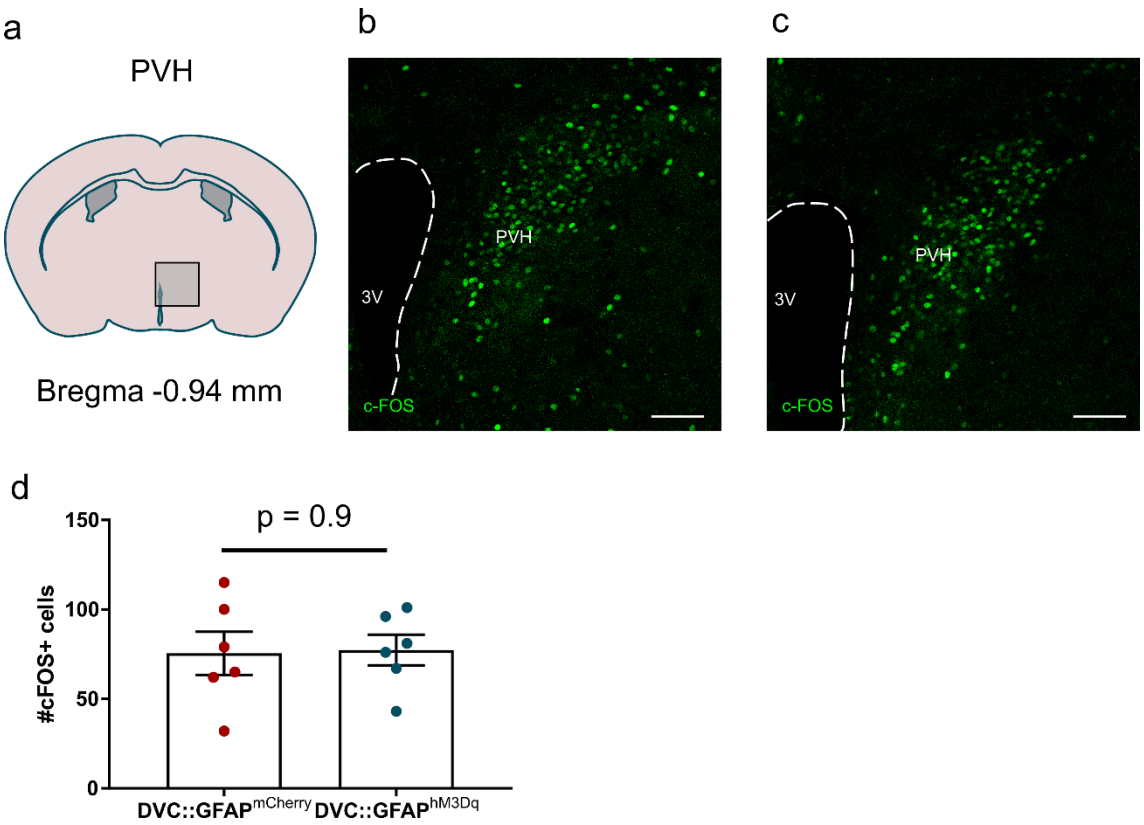

Figure 4.3.17 | Chemogenetic activation of DVC astrocytes did not induce c-FOS immunoreactivity in the PVH. a, Diagram showing region of interest for imaging and cell counting. **b**, Representative image from a DVC::GFAP^{mCherry} mouse. **c**, Representative image from a DVC::GFAP^{hM3Dq} mouse. **d**, Number of c-FOS immunoreactive cells in the PVH of DVC::GFAP^{mCherry} and DVC::GFAP^{hM3Dq} mice perfused 2-3 hours after injection of CNO (0.3 mg/kg i.p.) (n = 6 mice per group, 75.5 ± 12.05 vs 77.33 ± 8.58 cells, p = 0.9, unpaired t-test). 3V = third ventricle, PVH = paraventricular nucleus of the hypothalamus. Scale bars = 50 μm.

4.3.18 | Stimulation of Gi-GPCR signalling in DVC astrocytes did not alter nocturnal food intake in DVC::GFAP^{hM4Di} mice

The 'inhibitory' DREADD hM4Di hyperpolarises neurons and inhibits neurotransmitter release (Roth, 2016). Its effect when expressed in astrocytes is unknown but it has been successfully used to potentiate the feeding effects of ghrelin and blunt the effects of leptin when expressed on ARC astrocytes (Yang, Qi and Yang, 2015). Opposing effects were observed with hM3Dq in this paper suggesting that this DREADD did indeed inhibit ARC astrocytes (Yang, Qi and Yang, 2015). Stimulation of hM3Dq but not hM4Di induced expression of c-FOS in astrocytes showing hM4Di does not activate ARC astrocytes, at least at the level of gene expression (Yang, Qi and Yang, 2015). A systematic investigation of hM3Dq and hM4Di in hippocampal and cortical astrocytes however showed that both DREADDs stimulated astrocyte $[Ca^{2+}]_i$ increases, although by distinct intracellular mechanisms (Durkee *et al.*, 2019).

We aimed to determine the effect of hM4Di in DVC astrocytes and to this end generated a cohort of DVC::GFAP^{hM4Di} mice using one injection of AAV-GFAP-hM4Di_mCherry per side (**Figure 4.3.18 a-c**). A cohort of DVC::GFAP^{mCherry} mice were generated as a control group. To assay the effect of astrocyte Gi-GPCR signalling on feeding we measured food intake from the beginning of the dark phase after injection of saline or CNO (0.3 mg/kg i.p.) and found there was no difference in the cumulative food intake (**Figure 4.3.18 d**) or rate of food intake (**Figure 4.3.18 f**) in DVC::GFAP^{hM4Di}. Correspondingly, there was no difference in body weight measured 6 hours after injection of saline or CNO (**Figure 4.3.18 h**, 26.85 ± 0.90 vs 27.00 ± 0.89 g, p = 0.33, paired t-test). The same was true of DVC::GFAP^{mCherry} mice although a slight reduction in cumulative food intake appeared to be induced by CNO at 12 and 24 hours post-injection which had not

been observed in any of the previous 4 experiments where food intake was measured (**Figure 4.3.18 e, g, i**).

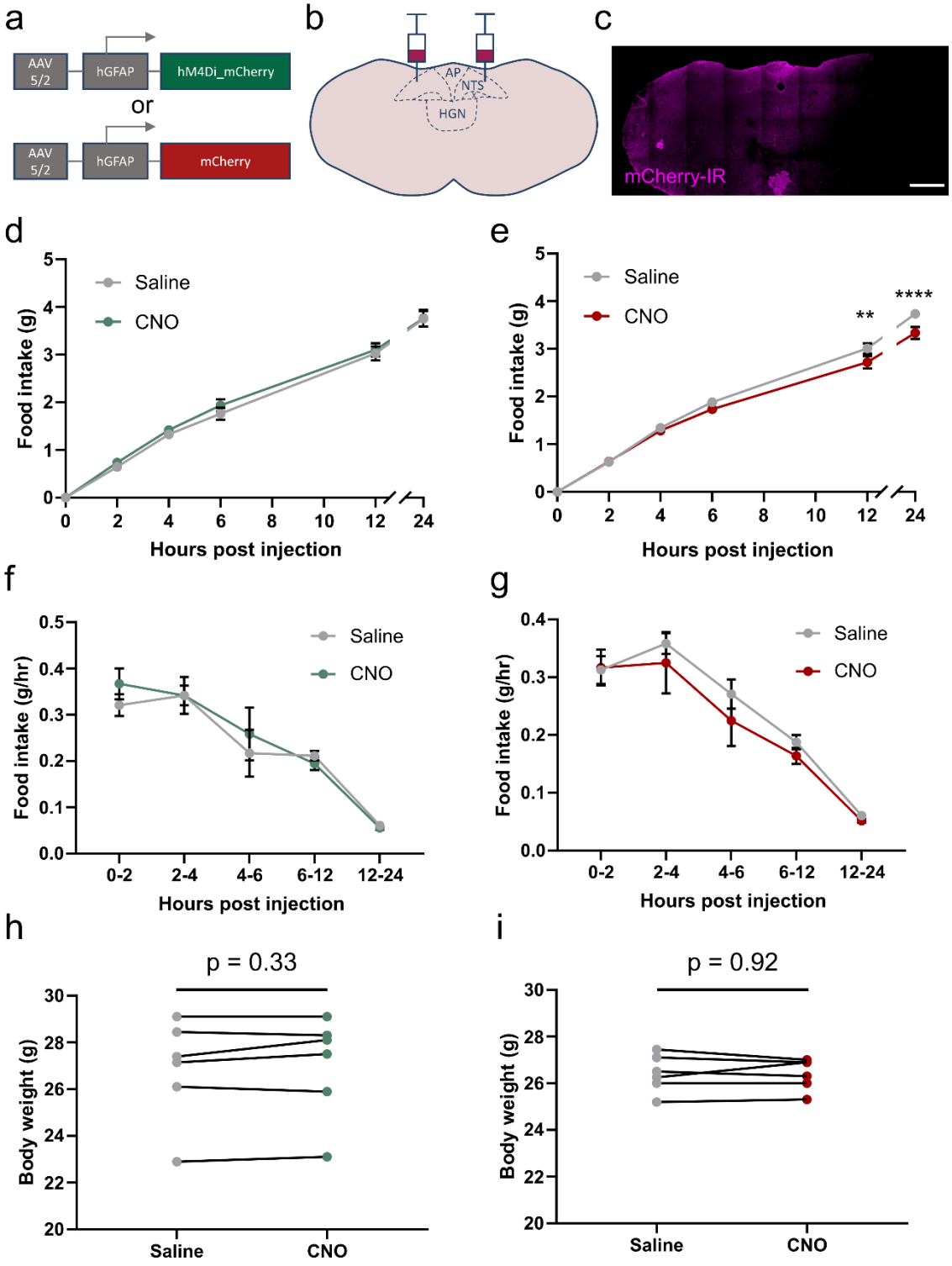

Figure 4.3.18 | Stimulation of Gi-GPCR signalling in DVC astrocytes did not increase food intake. a, Schematic of viral vectors used to create DVC::GFAP^{hM4Di} and DVC::GFAP^{mCherry} mice. **b,** Schematic showing anatomy of target region. **c,** Representative section showing immunoreactivity against hM4Di_mCherry in and around the DVC. **d**, Cumulative food intake of

DVC::GFAP^{hM4Di} mice following injection of saline or CNO (0.3 mg/kg i.p.) (n = 6 mice, Two-way RM ANOVA, CNO, p = 0.40, $F_{(1,5)}$ = 0.83, Time, p < 0.0001, $F_{(5,25)}$ = 482.8, interaction, p = 0.78, $F_{(5,25)}$ = 0.49, Sidak's post-hoc test, p > 0.05 for all comparisons). **e**, Cumulative food intake of DVC::GFAP^{mCherry} mice following injection of saline or CNO (0.3 mg/kg i.p.) (n = 6 mice, Two-way RM ANOVA, CNO, p = 0.17, $F_{(1,5)}$ = 2.54, Time, p < 0.0001, $F_{(5,25)}$ = 689.8, interaction, p = 0.0023, $F_{(5,25)}$ = 5.109, Sidak's post-hoc test). **f**, Rate of food intake of DVC::GFAP^{hM4Di} mice following injection of saline or CNO (0.3 mg/kg i.p.) (n = 6 mice, Two-way RM ANOVA, CNO, p = 0.41, $F_{(1,5)}$ = 0.80, Time, p < 0.0001, $F_{(4,20)}$ = 23.42, interaction, p = 0.74, $F_{(4,20)}$ = 0.48, Sidak's post-hoc test, p > 0.05 for all comparisons). **g**, Rate of food intake of DVC::GFAP^{mCherry} mice following injection of saline or CNO (0.3 mg/kg i.p.) (n = 6 mice, Two-way RM ANOVA, CNO, p = 0.15, $F_{(1,5)}$ = 2.81, Time, p < 0.0001, $F_{(4,20)}$ = 22.89, interaction, p = 0.86, $F_{(4,20)}$ = 0.32, Sidak's post-hoc test, p > 0.05 for all comparisons). **h**, Body weight measured 6 hours after lights off in DVC::GFAP^{hM4Di} mice after injection of saline or CNO (0.3 mg/kg i.p.) (26.85 ± 0.90 vs 27.00 ± 0.89 g, n = 6 mice; p = 0.33, paired t-test). **i**, Body weight measured 6 hours after lights off in DVC::GFAP^{mCherry} mice after injection of saline or CNO (0.3 mg/kg i.p.) (26.42 ± 0.32 vs 26.40 ± 0.27 g, n = 6 mice; p = 0.92, paired t-test). AP = area postrema, HGN = hypoglossal nucleus, NTS = nucleus of the solitary tract, X = dorsal motor nucleus of the vagus. Scale bar = 500 µm. ** = p < 0.01, **** = p < 0.0001.

4.3.19 | A greater dose of CNO did not alter feeding behaviour in DVC::GFAP^{hM4Di} mice

It is unclear from the literature whether CNO has a similar efficacy at hM3Dq and hM4Di. To ensure we were not missing an effect by using a low dose of CNO we repeated the feeding study with a higher dose (1 mg/kg i.p.). These studies yielded almost identical results; there was no difference in the cumulative food intake (**Figure 4.3.19 a**) or rate of food intake (**Figure 4.3.19 c**) in DVC::GFAP^{hM4Di} mice. Again, there was no difference in body weight when measured 6 hours after injection (**Figure 4.3.19 e**) in DVC::GFAP^{hM4Di} mice. In DVC::GFAP^{mCherry} mice there was no major effect, although again a slightly reduced cumulative food intake was observed at 24 hours post-injection,, although paradoxically smaller than with a lower dose of CNO (**Figure 4.3.19 b, d, f**).

To ensure we were not missing an effect in subsequent experiments and since no major effects were observed in DVC::GFAP^{mCherry} mice, 1 mg/kg i.p. CNO was used for subsequent hM4Di experiments.

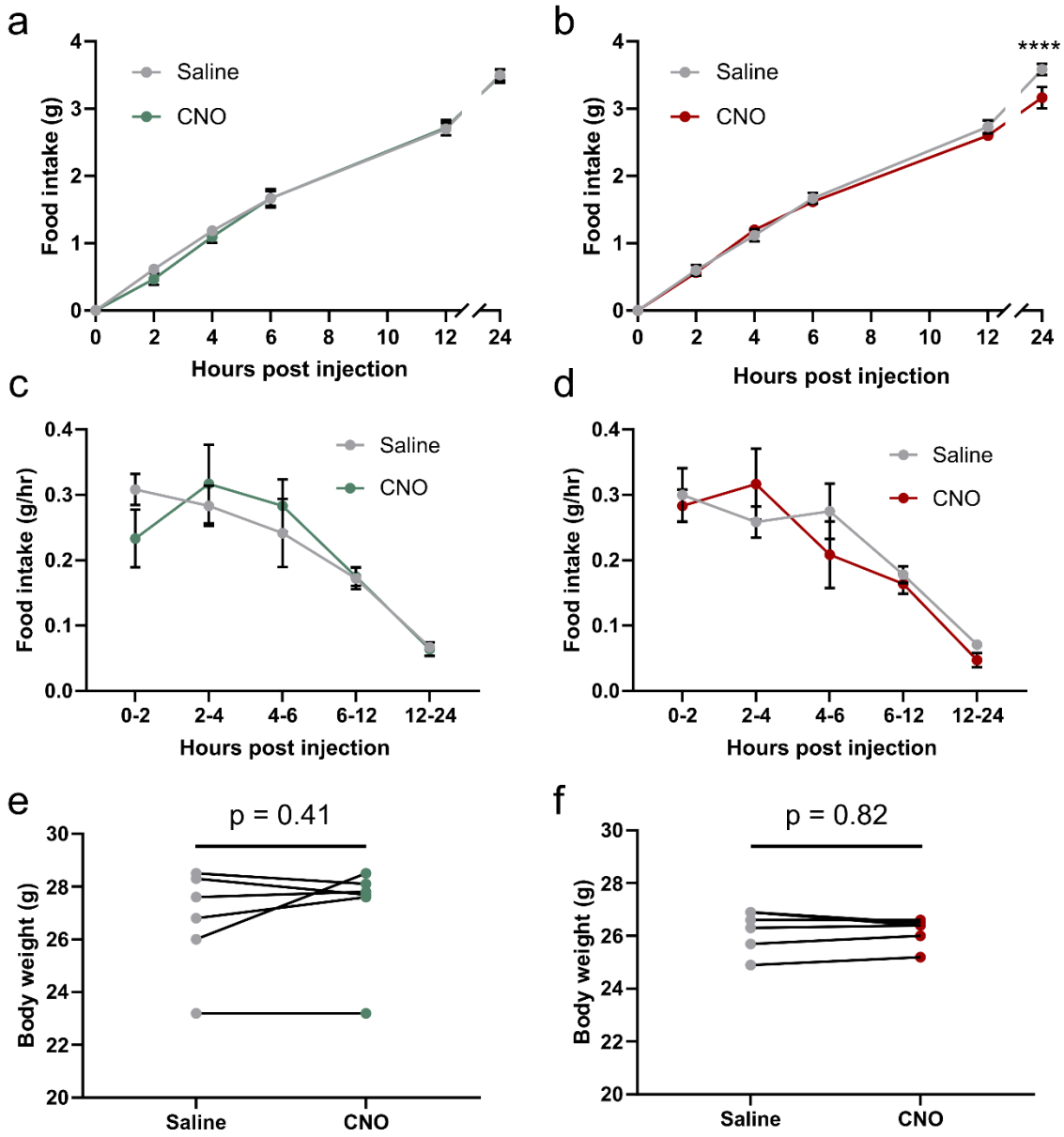

Figure 4.3.19 | Stimulation of Gi-GPCR signalling in DVC astrocytes with 1 mg/kg CNO did not increase food intake. **a**, Cumulative food intake of DVC::GFAP^{hM4Di} mice following injection of saline or CNO (1 mg/kg i.p.) (n = 6 mice, Two-way RM ANOVA, CNO, p = 0.62, $F_{(1,5)} = 0.29$, Time, p < 0.0001, $F_{(5,25)} = 382.9$, interaction, p = 0.51, $F_{(5,25)} = 0.88$, Sidak's post-hoc test, p > 0.05 for all comparisons). **b**, Cumulative food intake of DVC::GFAP^{mCherry} mice following injection of saline or CNO (1 mg/kg i.p.) (n = 6 mice, Two-way RM ANOVA, CNO, p = 0.18, $F_{(1,5)} = 2.50$, Time, p < 0.0001, $F_{(5,25)} = 458.6$, interaction, p = 0.002, $F_{(5,25)} = 4.98$, Sidak's post-hoc test). **c**, Rate of food intake of DVC::GFAP^{hM4Di}

mice following injection of saline or CNO (1 mg/kg i.p.) (n = 6 mice, Two-way RM ANOVA, CNO, $p > 0.99$, $F_{(1,5)}<0.0001$, Time, $p < 0.0001$, $F_{(4,20)} = 10.59$, interaction, $p = 0.41$, $F_{(4,20)} = 1.05$, Sidak's post-hoc test, $p > 0.05$ for all comparisons). **d**, Rate of food intake of DVC::GFAP^{mCherry} mice following injection of saline or CNO (1 mg/kg i.p.) (n = 6 mice, Two-way RM ANOVA, CNO, $p = 0.08$, $F_{(1,5)} = 4.86$, Time, $p < 0.0001$, $F_{(4,20)} = 14.46$, interaction, $p = 0.52$, $F_{(4,20)} = 0.83$, Sidak's post-hoc test, $p > 0.05$ for all comparisons). **e**, Body weight measured 6 hours after lights off in DVC::GFAP^{hM4Di} mice after injection of saline or CNO (1 mg/kg i.p.) (26.73 ± 0.80 vs 27.15 ± 0.80, $p = 0.41$, paired t-test). **f**, Body weight measured 6 hours after lights off in DVC::GFAP^{mCherry} mice after injection of saline or CNO (1 mg/kg i.p.) (26.22 ± 0.32 vs 26.18 ± 0.21, $p = 0.82$, paired t-test). **** = $p < 0.0001$.

4.3.20 | Stimulation of Gi-GPCR signalling in DVC astrocytes did not affect refeeding after a 12 hour fast in DVC::GFAP^{hM4Di} mice

It is possible that regular nocturnal feeding does not engage NTS satiety signalling to a large degree since inhibition of specific populations of NTS neurons often does not affect normal feeding (D'Agostino *et al.*, 2018; Holt, Richards, *et al.*, 2019; Cheng *et al.*, 2020). Thus, to stimulate a large amount of feeding in a short period of time and subsequent activation of satiety pathways (Wu *et al.*, 2014), we fasted DVC::GFAP^{hM4Di} mice for 12 hours during the dark phase. Prior to lights on they received an injection of CNO (1 mg/kg i.p.) followed by an injection of saline (see **4.3.21** below) and had food intake measured periodically for 24 hours. During re-feeding after a fast there was no difference in cumulative food intake between DVC::GFAP^{hM4Di} and DVC::GFAP^{mCherry} mice (**Figure 4.3.20 a**). There was also no difference between groups in rate of food intake (**Figure 4.3.20 b**). This suggests that stimulation of Gi-GPCRs on DVC astrocytes does not impair satiety signalling driven by voracious refeeding following a fast. It is possible however that the mice are consuming as much food as physically possible in this paradigm however given that our cumulative food intake is approximately the same as that seen in mice refed after a 36 hour fast, indicating a potential celling effect (Wu *et al.*, 2014).

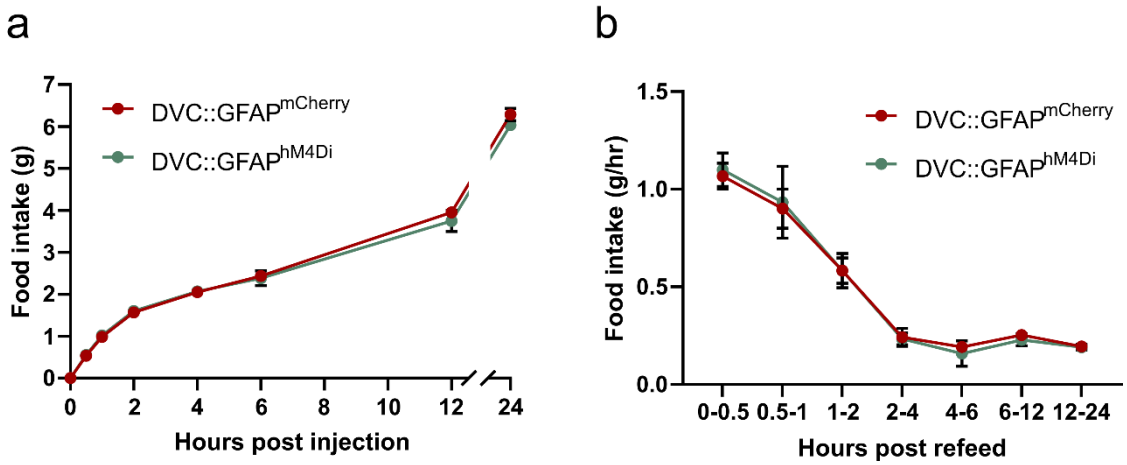

Figure 4.3.20 | Stimulation of Gi-GPCR signalling in DVC astrocytes did not increase food intake after a 12 hour fast. DVC::GFAP^{mCherry} and DVC::GFAP^{hM4Di} mice (n = 6/group) were fasted for 12 hours during the dark phase then injected with CNO (1 mg/kg i.p.) 30 minutes prior to reintroduction of food at the onset of the light phase. **a**, Cumulative food intake (n = 6 mice per group, Two-way ANOVA, DREADD, p = 0.65, $F_{(1,10)}$ = 0.22, Time, p < 0.0001, $F_{(7,70)}$ = 960.2, interaction, p = 0.66, $F_{(7,70)}$ = 0.76, Sidak's post-hoc test, p > 0.05 for all comparisons). **b**, Rate of food intake (n = 6 mice per group, Two-way ANOVA, DREADD, p = 0.98, $F_{(1,10)}$ < 0.0001, Time, p < 0.0001, $F_{(6,60)}$ = 51.02, interaction, p < 0.99, $F_{(6,60)}$ = 0.06, Sidak's post-hoc test, p > 0.05 for all comparisons).

4.3.21 | Stimulation of Gi-GPCR signalling in DVC astrocytes attenuated cholecystokinin-induced satiety

CCK is a peptide released from enteroendocrine cells in the digestive system following a meal. It acts on CCK receptors on vagal sensory neurons to stimulate signalling to the NTS and suppress further food intake and therefore is a vagally-mediated satiety signal. We wanted to assess whether Gi-GPCR signalling in DVC astrocytes would impair vagally-mediated satiety. As such, mice were fasted overnight and injected with CNO (1 mg/kg i.p.) followed by either saline (data shown above, **Section 4.3.20**) or CCK (3.5 µg/kg i.p.). As expected, CCK suppressed refeeding after a fast in DVC::GFAP^{mCherry} mice as evidenced by reduced cumulative food intake (**Figure 4.3.21 b**) and reduced rate of food intake within the first hour (**Figure 4.3.21 d**). This was also true of DVC::GFAP^{hM4Di} mice although the magnitude of reduction in cumulative food intake was lower (**Figure 4.3.21 a**) and the suppression of food intake rate had a shorter duration (**Figure 4.3.21 c**). Comparison between the two groups of mice showed that while cumulative food intake was lower 4 hours after refeeding in DVC::GFAP^{mCherry} mice, this was not the case in DVC::GFAP^{hM4Di} mice (**Figure 4.3.21 e, f**). This is potentially suggestive of reduced effect of CCK in DVC::GFAP^{hM4Di} mice.

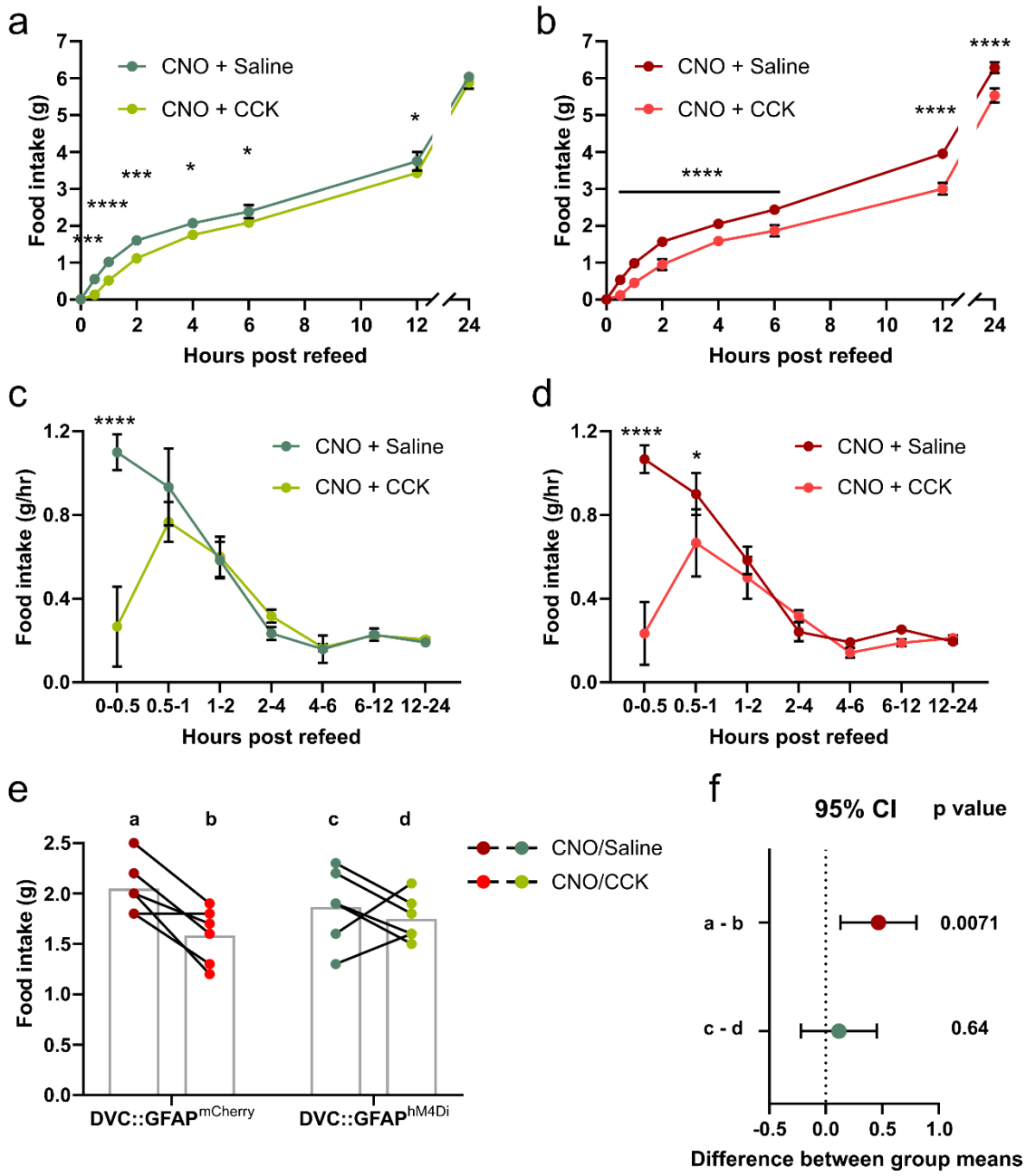

Figure 4.3.21 | Stimulation of Gi-GPCR signalling in DVC astrocytes attenuated CKK-induced satiety after a 12 hour fast. DVC::GFAP^{mCherry} and DVC::GFAP^{hM4Di} mice were fasted for 12 hours during the dark phase then injected with CNO (1 mg/kg i.p.) 30 minutes prior to the onset of the light phase. At the onset of the light phase mice were injected with saline or CKK (3.5 µg/kg i.p.) and food was returned to the cages. **a**, Cumulative food intake of DVC::GFAP^{hM4Di} mice (n = 6 mice, Two-way RM ANOVA, CCK, $p = 0.007$, $F_{(1,5)} = 19.34$, Time, $p < 0.0001$, $F_{(7,35)} = 645.7$, interaction, $p = 0.01$, $F_{(7,35)} = 3.10$,

Sidak's post-hoc test). **b**, Cumulative food intake of DVC::GFAP^{mCherry} mice (n = 6 mice, Two-way RM ANOVA, CCK, p = 0.002, $F_{(1,5)}$ = 38.36, Time, p < 0.0001, $F_{(7,35)}$ = 814, interaction, p < 0.0001, $F_{(7,35)}$ = 11.72, Sidak's post-hoc test). **c**, Rate of food intake of DVC::GFAP^{hM4Di} mice (Two-way RM ANOVA, CCK, p = 0.0054, $F_{(1,5)}$ = 11.4, Time, p < 0.0001, $F_{(6,30)}$ = 15.14, interaction, p < 0.0001, $F_{(6,30)}$ = 8.06, Sidak's post-hoc test). **d**, Rate of food intake of DVC::GFAP^{mCherry} mice (Two-way RM ANOVA, CCK, p = 0.0013, $F_{(1,5)}$ = 41.54, Time, p < 0.0001, $F_{(6,30)}$ = 13.2, interaction, p < 0.0001, $F_{(6,30)}$ = 17.31, Sidak's post-hoc test). **e**, 4 hour cumulative food intake after a 12 hour fast in DVC::GFAP^{mCherry} and DVC::GFAP^{hM4Di} mice following injection of CNO and either saline or CCK prior to refeeding. **f**, Difference between group means of the data in **e** for within group comparisons (n = 6 mice per group, One-way RM ANOVA, CCK, p = 0.024, Sidak's post-hoc test). Error bars show 95% confidence interval. * = p < 0.05, *** = p < 0.001, **** = p < 0.0001.

4.3.22 | Stimulation of Gi-GPCR signalling in DVC astrocytes did not induce c-FOS immunoreactivity in the NTS

To examine whether Gi-GPCR signalling in DVC astrocytes activated neighbouring neurons in the NTS, DVC::GFAP^{hM4Di} mice and DVC::GFAP^{mCherry} mice were injected with CNO (1 mg/kg) and perfused 2-3 hours later. Examination of c-FOS immunoreactivity showed very low levels which was comparable between the groups (**Figure 4.3.22 a-c**). Quantifying the number of c-FOS immunoreactive cells in the NTS showed there was no difference between the groups (**Figure 4.3.22 d**, n = 5 mice per group; 7.6 ± 4.23 vs 9.2 ± 2.50 cells, p = 0.75, unpaired t-test). This suggests that in contrast to stimulation with hM3Dq, stimulation of hM4Di in DVC astrocytes does not excite neighbouring neurons.

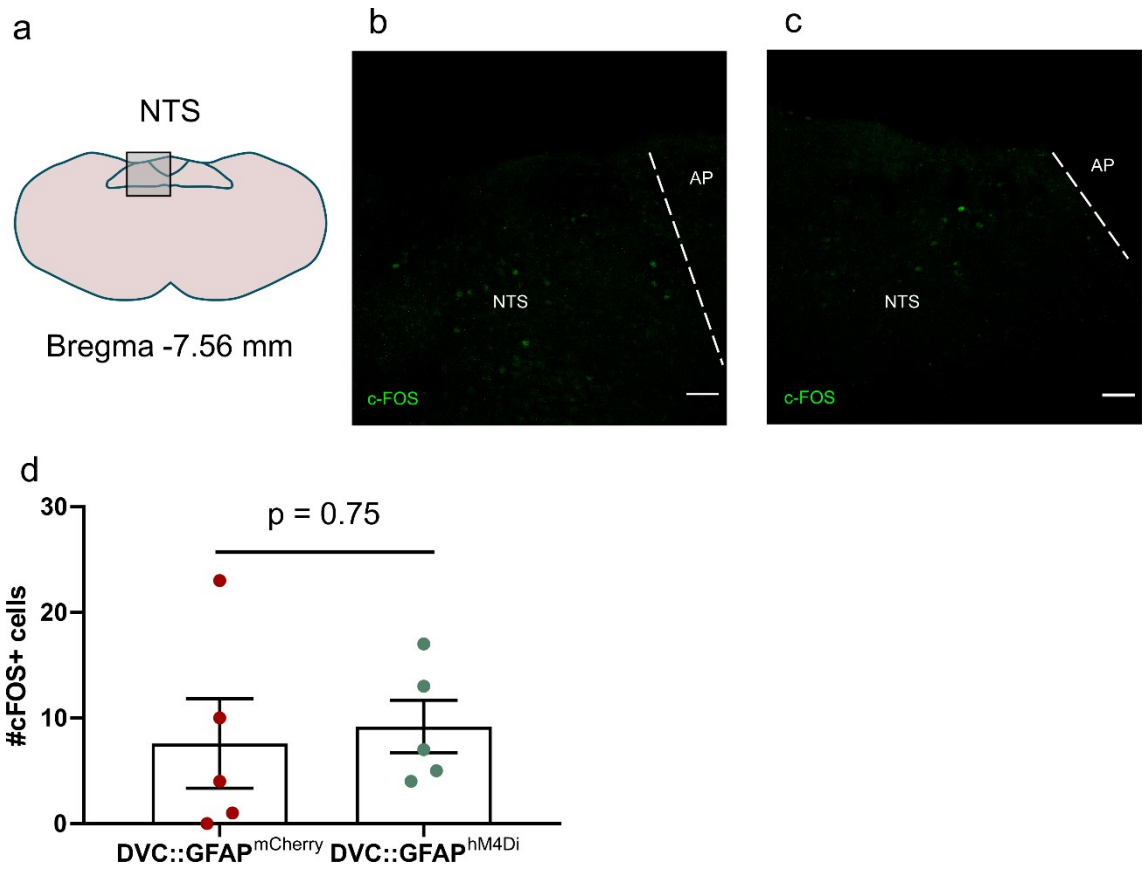

Figure 4.3.22 | Stimulation of Gi-GPCR signalling in DVC astrocytes did not induce c-FOS immunoreactivity in the NTS. a, Diagram showing region of interest for imaging and cell counting. **b**, Representative image from a DVC::GFAP^{mCherry} mouse. **c**, Representative image from a DVC::GFAP^{hM4Di} mouse. **d**, Number of c-FOS expressing cells in the NTS of DVC::GFAP^{mCherry} and DVC::GFAP^{hM4Di} mice perfused 2-3 hours after injection of CNO (0.3 mg/kg i.p.) (n = 5 mice per group, 7.6 ± 4.23 vs 9.2 ± 2.5 cells, p = 0.75, unpaired t-test). AP = area postrema, NTS = nucleus of the solitary tract. Scale bar = 50 μm.

4.4 | Discussion

In this chapter we have shown that DREADD-mediated activation of DVC astrocytes caused a potent, reversible decrease in food intake. This effect persisted even following a 12 hour fast and was independent of locomotion or endogenous analgesic effects and appears to be mediated by engagement of local and downstream neuronal circuits. We also showed that manipulation of Gi-GPCR related signalling did not recapitulate the effects of Gq-GPCR activation nor did it show any indication of inhibiting the astrocyte effect on nocturnal or fast-induced refeeding. There was however a modest attenuation of the satiating effect of CCK on refeeding after a fast.

4.4.1 | Comparisons to ARC astrocytes

ARC astrocytes have previously been implicated in the regulation of food intake. In the hypothalamus these glia are responsive to short-term energy imbalance, both fasting and acute high-fat feeding (Fuente-Martín *et al.*, 2012; Thaler *et al.*, 2012; Buckman *et al.*, 2015), and direct manipulation of their activity using DREADDs alters food intake (Yang, Qi and Yang, 2015; N. Chen *et al.*, 2016). Both studies using activating DREADDs in ARC astrocytes show a modest increase in food intake during the light-phase, when mice are not typically eating (Yang, Qi and Yang, 2015; N. Chen *et al.*, 2016). In contrast, it appears from our observations that chemogenetic DVC astrocyte activation has more pronounced effects on feeding with respect to the magnitude, direction and onset/duration of the response.

The less pronounced impact of chemogenetic modulation of ARC astrocytes on feeding behaviour in mice may be due, in part, to the fact that the ARC contains at least two neurochemically unique neuronal populations: ARC^{AgRP} and ARC^{POMC} neurons; the activation of which drives and inhibits feeding behaviour,

respectively (Aponte, Atasoy and Sternson, 2011; Krashes *et al.*, 2011). As the two neuronal populations are anatomically interspersed yet functionally opposite, chemogenetic activation of ARC astrocytes may result in modulation of the activity of both neuronal populations, making interpretation of the physiological impact on feeding complex. With respect to feeding, to date, neurons of the NTS have principally been implicated in satiety rather than hunger (Grill and Hayes, 2012), which may account for the more pronounced physiological effect consequent on local astrocytic activation.

4.4.2 | Potential mechanisms of astrocyte-neuron communication underlying the effects induced by chemogenetic activation of DVC astrocytes

We found that CNO treatment in DVC::GFAP^{hM3Dq} mice decreased food intake, yet the underlying molecular mechanisms by which this occurs remain to be resolved. Astrocytes can modulate the activity of neurons by mechanisms including altered glutamate transport and also via release of neuroactive molecules (e.g. glutamate, ATP, d-serine) (Panatier *et al.*, 2006; Gourine *et al.*, 2010; Araque *et al.*, 2014; Matott, Kline and Hasser, 2017; Papouin, Dunphy, *et al.*, 2017; Schwarz *et al.*, 2017). Critically, glutamatergic signalling is the principal mechanism for communication between the vagus and second order NTS neurons (Doyle and Andresen, 2001) and NTS astrocytes directly sense vagal glutamate release *via* Ca^{2+}-permeable AMPA receptors expressed on the cell membrane (McDougal, Hermann and Rogers, 2011). In the NTS, synaptic clearing of glutamate by astrocytes has been shown to restrain NTS neuronal firing and vagal outflow to cardiorespiratory organs (Matott, Kline and Hasser, 2017). As such, astrocyte glutamate transport can manipulate the firing rates of NTS neurons and alter output from the NTS.

In our study, it is unclear how (and indeed if) astrocyte Gq-GPCR activation may be linked to altered glutamate uptake; however previous reports have shown that altered morphology of astrocytes results in corresponding changes in glutamate uptake and neuronal excitability (Oliet, Piet and Poulain, 2001).

An additional potential mechanism of communication that could be important in mediating the effects seen is active gliotransmission (Araque *et al.*, 2014). Activation of a GPCR expressed on NTS astrocytes (protease activated receptors [PAR]) leads to increased activation of neurons by glutamate, possibly exocytosed by astrocytes (Vance, Rogers and Hermann, 2015). Given that antagonism of NMDA receptors in the NTS increases meal size (Treece *et al.*, 1998) it is possible that activation of these receptors by astrocyte-derived glutamate or D-serine would reduce food intake, but further study would be required to specifically test this.

4.4.3 | Absence of conditioned place aversion following chemogenetic DVC astrocyte activation or LPS conditioning

Given the reduction in food intake we observed, it was important to evaluate whether induction of malaise and/or aversion could be contributing to the effect seen, particularly as the DVC is implicated in mediating these responses in addition to satiety (Maniscalco and Rinaman, 2018). This is particularly important in light of the increase in c-FOS immunoreactivity observed in the lPBN of DVC::GFAP^{hM3Dq} mice after CNO treatment, which may indicate the activation of a NTS-lPBN pathway previously reported to reduce food intake through aversion/negative salience (Roman, Sloat and Palmiter, 2017). To do this we used a CPA assay utilizing a protocol previously used by the Pickering group to indicate aversive responses/negative salience in response to chemogenetic

activation of prefrontal cortex-projecting locus coeruleus neurons (LC^{PFC}) in rats (Hirschberg *et al.*, 2017).

We found that after one conditioning session per agent, CNO treatment in DVC::$GFAP^{hM3Dq}$ or DVC::$GFAP^{mCherry}$ mice did not induce CPA. However, since the known aversive LiCl agent was unable to induce CPA in this paradigm it suggests our assay was likely not sufficiently sensitive to detect/induce CPA in this context. As such, the affective properties of DREADD-mediated DVC astrocyte activation remain unclear. A longer protocol may have revealed an effect since 3 or 4 conditioning sessions with LiCl does induce CPA in mice (Le Merrer *et al.*, 2011; Longoni *et al.*, 2011; Sanjakdar *et al.*, 2015; T. Zhang *et al.*, 2019). We did however find that LiCl injection reduced locomotion during the conditioning trial while CNO treatment did not. This suggests LiCl acutely induces malaise, an effect that was not seen in the CNO treated mice.

Evidence suggests that satiety and aversion exist on a continuum, where in some cases aversion may be a manifestation of extreme satiety *e.g.* associated with excessive gastrointestinal distention (Maniscalco and Rinaman, 2018). As such, ability of an agent to induce CPA or conditioned taste aversion does not necessarily indicate that an effect is non-physiological. For example, exogenous CCK can induce satiety or aversion dependent on dose (Swerdlow *et al.*, 1983; West *et al.*, 1987; Moran, 2000). Our results suggest that that DREADD-mediated DVC astrocyte activation likely does not produce acute malaise, but its emotional salience remains unclear and further studies using a longer conditioning protocol or a conditioned taste aversion paradigm would be required to explore this.

4.4.4 | Does chemogenetic activation recapitulate physiological activity of NTS astrocytes

It is understood that astrocyte Ca^{2+} signalling is a very complex process of desynchronized events in independent microdomains of individual cells (Volterra, Liaudet and Savtchouk, 2014; Bindocci *et al.*, 2017). To date this has been best studied in forebrain astrocytes and evidence of microdomain signalling in the brainstem is lacking, although it likely exists. As such, sustained activation by a highly expressed GPCR, such as the hM3Dq in our studies, may yield supra-physiological levels of $[Ca^{2+}]_i$ and may disrupt the nuanced Ca^{2+}-code of microdomains. However, a number of studies utilizing Ca^{2+} imaging in somatic and major branches of astrocytes in the NTS and other brainstem nuclei have shown large, synchronized $[Ca^{2+}]_i$ elevations in response to a range of physiological stimuli. For example, work from the labs of Herrman and Rogers have shown that NTS astrocytes increase somatic Ca^{2+} in response to synaptic stimulation, PAR activation, GLP1-R activation, LepRb activation and low extracellular glucose (Hermann *et al.*, 2009; McDougal, Hermann and Rogers, 2011, 2013; McDougal *et al.*, 2013; Reiner *et al.*, 2016; Rogers *et al.*, 2018; Stein *et al.*, 2020). This suggests that this type of Ca^{2+} signal is physiologically relevant in these cells.

What is currently lacking is an understanding of the $[Ca^{2+}]$ dynamics of NTS astrocytes *in vivo* throughout the normal daily cycle of food intake. While deep-brain Ca^{2+} imaging is technically challenging it is a rapidly evolving field. Indeed the Ca^{2+} activity of neurons in brainstem respiratory regions have been monitored *in vivo* to assess their responses to low ambient oxygen (Bhandare, Huckstepp and Dale, 2019). This means that potentially it would be possible to apply similar methodology to study NTS astrocyte responses.

4.4.5 | Technical limitations of viral spread

One technical limitation which confounds the interpretation of the results presented in this chapter arises from the spread of hM3Dq expression beyond the limits of the NTS and DVC. Although we have taken some steps post-hoc to strengthen the inferences we can make, future work could examine the possibility of ensuring restricted expression to the NTS using a dual-recombinase strategy.

Cre-lox recombination is a two-component system that utilizes an enzyme, Cre, and a recognition site, locus of crossing over p1 (loxP). loxP sites oriented in the correct way around the sequence for a protein of interest can be inverted into the correct sequence in the presence of Cre to allow for production of the protein (Atasoy *et al.*, 2008; Cardin *et al.*, 2009; Sohal *et al.*, 2009). This method is called a double-inverted open reading frame (diORF). This is routinely used to direct tools for manipulation or monitoring of defined neural populations (e.g. DREADDs, opsins, GCaMP) by using Cre-driver mice expressing Cre in a defined cell type and crossing or viral injection with DREADD contained in a diORF.

A similar system Flp-FRT recombination exists (Kranz *et al.*, 2010). This system is almost identical to CRE-lox but uses the distinct recombinase Flippase (Flp) and recognition site fliappase recognition target (FRT). As such, these can be combined to further restrict expression of a knocked in effector to cells only expressing both recombinases.

NTS development is an area that has not received much attention although some details are known (Zhang and Ashwell, 2001). Noradrenergic neurons of the NTS have been shown to originate from the rhombomeres 3 and 5 marked by transcription factor Krox20 (Robertson *et al.*, 2013). As such, it is possible that a transcription factor exists to specify NTS fate. Crossing a mouse expressing Flp

under this putative transcription factor with the astrocyte-specific Aldh1l1-Cre mouse will yield offspring expressing Flp in NTS cells and Cre in astrocytes. Injection of a virus containing an inverted diORF-DREADD sequence downstream of a FRT-flanked STOP codon (AAV-FRT-STOP-FRT-diORF-hM3Dq_mCherry) into the DVC would result in expression of the DREADD exclusively in NTS astrocytes, thus achieving the spatial and cell type specificity required to refine and validate our studies.

4.4.6 | Specificity of CNO for hM-DREADDs

It was initially thought that CNO exerted its *in vivo* effects on DREADD receptors by directly binding to their ligand binding domain (Armbruster *et al.*, 2007; Roth, 2016). However, it has since been demonstrated that a second possible mechanism of action in rodents is the metabolism of CNO to clozapine which crosses the blood-brain barrier and binds to the DREADD (Gomez *et al.*, 2017). This raises the issue of off target effects of clozapine since it is an antagonist of D2 dopamine receptors. To account for this all of our chemogenetic manipulation experiments were performed in parallel with control mice expressing only mCherry. In these mice any off target effects of CNO or its metabolite clozapine would be detected.

4.4.7 | Factors underlying the differential effects of DVC::GFAP^{hM3Dq} and DVC::GFAP^{hM4Di} activation on feeding

At the time of the experiment it was assumed that hM4Di could reduce astrocyte activation by reducing transmitter release and lowering intracellular Ca^{2+}. This was supported by some evidence from a study showing activation of hM3Dq but not hM4Di on ARC astrocytes induces c-FOS immunoreactivity (Yang, Qi and Yang, 2015). However, it has now been demonstrated that in some brain regions, activation of Gi-coupled GPCRs, including hM4Di, increases $[Ca^{2+}]_i$ in astrocytes

(Durkee *et al.*, 2019). This is in contrast with its known inhibitory effects in neurons (Roth, 2016; Durkee *et al.*, 2019). With this knowledge it is surprising that ours, and other studies have not shown the same behavioural outcome with Gi and Gq coupled DREADDs (Yang, Qi and Yang, 2015; N. Chen *et al.*, 2016). However, the mechanisms of Gq and Gi activation are distinct and thus may have different downstream consequences (Durkee *et al.*, 2019). Therefore, in our studies it appears that the downstream astrocyte signalling pathways engaged result in distinct behavioural effects (either suppression of nocturnal food intake [hM3Dq] or no effect on nocturnal food intake but modulation of hormone induced satiety [hM4Di]).

4.5 | Conclusion

To summarise, in this chapter we describe the first genetic manipulation of astrocytes in the NTS and wider DVC and demonstrate that chemogenetic activation of these cells reduces nocturnal and fast-induced food intake. This activation is independent of effects on locomotion and endogenous analgesia while its emotional salience remains elusive. Chemogenetic activation of DVC astrocytes activates local neurons and those in the downstream lPBN as evidenced by c-FOS expression. Finally, stimulation of Gi-GPCR signalling in DVC astrocytes did not affect nocturnal or fast induced feeding but attenuated the satiating effect of CCK. This provides the first causal evidence that modulation of DVC astrocyte signalling can alter food intake and related behaviours.

Chapter 5

Electrophysiological interrogation of astrocyte neuromodulation in the NTS

5.1 | Introduction

To date, studies using electrophysiology to assay nucleus of the solitary tract (NTS) neurons have elucidated the features of these neurons in general and have characterised specific neurochemical populations (Doyle *et al.*, 2004; Appleyard *et al.*, 2005, 2007; Bailey *et al.*, 2008; Thek *et al.*, 2019). Neurons in the NTS receive glutamatergic input from vagal afferents fibres in the solitary tract (ST) which is modulated pre- and post-synaptically by a wide range of neurotransmitters and conditions (Cui, Li and Appleyard, 2011; Cui, Roberts, Zhao, Andresen, *et al.*, 2012; Cui, Roberts, Zhao, Zhu, *et al.*, 2012; Zhao *et al.*, 2015; Roberts *et al.*, 2017; Page, Zhu and Appleyard, 2018). Of interest to our studies have been those studies examining NTS astrocytes. An emergent theme in this literature is that, in the NTS, glutamate homeostasis and glutamatergic transmission are under the tight control of and modulated by astrocytes (Accorsi-Mendonça *et al.*, 2013; Lin *et al.*, 2013; Nagase *et al.*, 2014; Accorsi-Mendonca *et al.*, 2015; Matott *et al.*, 2016; Matott, Kline and Hasser, 2017; Talman, Dragon and Lin, 2017; Yamamoto and Mifflin, 2018; Accorsi-Mendonça, Bonagamba and Machado, 2019). In this chapter we investigate two potential mechanisms of glial modulation of neighbouring neurons in the NTS.

First, we examined whether NTS neurons are sensitive to D-serine, a known gliotransmitter, and whether this sensitivity was modulated by dietary state. D-serine is of interest since it is an endogenous co-agonist of NMDA receptors (NMDA-R) and either D-serine or glycine are necessary for channel opening. NTS neurons require NMDA-R for sustained activation under high frequency ST stimulation in *ex vivo* slices (Zhao *et al.*, 2015). This indicates the potential importance of this receptor in the integration of synaptic input from the periphery. Injection of NMDA-R antagonists into the NTS increases meal size in rats

implicating this receptor in controlling satiety (Treece *et al.*, 1998; Hung *et al.*, 2006). This is further supported by data showing that enhancing glycine availability in the NTS and wider dorsal vagal complex (DVC) by injection of glycine or chemical or genetic inhibition of its transporter decreases food intake in rats refeeding after a fast (Yue *et al.*, 2016).

In the hippocampus and hypothalamus NMDA-R excitation is potently modulated by D-serine derived from local astrocytes (Panatier *et al.*, 2006; Papouin, Dunphy, *et al.*, 2017; Adamsky *et al.*, 2018; Robin *et al.*, 2018). Combined, these data led us to hypothesise that NTS neurons would be sensitive to D-serine and this excitability would be modulated following physiological manipulations impacting activity of local astrocytes: 12 hour high fat chow intake, see **Chapter 3**. This experiment additionally afforded the opportunity to assess the population activity of NTS neurons following acute hyperphagia, something that had not previously been investigated.

Second, we examined the effects of blocking astrocyte glutamate uptake on synaptic integration in NTS neurons expressing tyrosine hydroxylase (NTS^{TH} neurons). These neurons were chosen since their chemogenetic activation reduces food intake (Roman, Derkach and Palmiter, 2016; Aklan *et al.*, 2020) and the features of their synaptic profile are very well described (Appleyard *et al.*, 2007) and subject to modulation by a wide variety of conditions (Cui, Li and Appleyard, 2011; Cui, Roberts, Zhao, Andresen, *et al.*, 2012; Cui, Roberts, Zhao, Zhu, *et al.*, 2012; Roberts *et al.*, 2017; Page, Zhu and Appleyard, 2018). Glutamate reuptake is a key function of astrocytes and blockade of transporters alters transmission across the ST→NTS synapse leading to cardiorespiratory depression, mediated by increased parasympathetic output (Matott *et al.*, 2016; Matott, Kline and Hasser, 2017; Yamamoto and Mifflin, 2018). We sought to build

upon and refine these studies by examining how inhibiting astrocyte glutamate transporters changes activity at the ST→NTSTH synapse which is known to mediate satiety (Appleyard *et al.*, 2007; Roman, Derkach and Palmiter, 2016; Aklan *et al.*, 2020).

5.2 | Aims and hypotheses

In the experiments described in this chapter we first aimed to assess the population response of NTS neuronal activity to high fat chow intake, exogenous application of NMDA-R agonists and whether the latter was regulated by the former. We hypothesised that multi-unit (MU) firing rate would be greater at rest in NTS slices from high fat chow fed mice than standard chow fed controls. We also hypothesised that the response to D-serine would be lower in slices from high fat fed mice indicative of higher D-serine availability at rest.

Secondly, we aimed to assess the contribution of astrocytic glutamate reuptake to synaptic integration of vagal cues in NTSTH neurons. We hypothesised that the amplitude of ST-evoked excitatory postsynaptic currents (EPSCs) would be reduced while the frequency of spontaneous EPSCs would be increased.

5.3 | Results

5.3.1 | Perforated Multi-Electrode Array allows population recording in the NTS

As discussed earlier (**Section 1.2.2.1**), the organisational logic of NTS neurochemical populations is not well understood compared to other brain regions (e.g. cortex, hippocampus, and cerebellum). Studies using targeted single-cell recordings in mice expressing fluorescent proteins in cell types of interest (Doyle *et al.*, 2004) have successfully characterised the electrophysiological features of numerous classes of NTS neuron (Appleyard *et*

al., 2005, 2007; Bailey *et al.*, 2008; Thek *et al.*, 2019). However, population level responses in NTS neuronal activity have not been studied.

Here, our interest was in observing changes in electrical activity of NMDA-responsive NTS neurons as a population across the nucleus, irrespective of neurochemical identity. To achieve unbiased recordings, we used a perforated multi-electrode array (pMEA) to record extracellular neural activity across the NTS in *ex vivo* slices. (**Figure 5.3.1 a**). This approach has recently been used to record activity in two hypothalamic nuclei and has certain advantages over single cell recordings (Hanna *et al.*, 2017, 2020). Namely, neuronal activity across a complex, neurochemically diverse brain area can be simultaneously recorded and the spatial positions of activity within the recorded section are known. Each electrode site (channel) allows the extracellular recording of neuronal activity. This multi-unit activity (MUA) includes voltage 'spikes' (indicative of neuronal action potential firing) and thus the combined firing rate of units (neurons) in the vicinity of the electrode is measured by recording the frequency of these spikes for a given channel (MU firing rate).

Arrays in a 6x10 electrode configuration provided sufficient coverage to record from the entire medial-lateral and dorsal-ventral extent of the NTS on a given side (**Figure 5.3.1 a-c**). For the experiment, slices were left to acclimatise on the MEA for half an hour before recording began. The baseline period was 20 minutes followed by bath application of NMDA for 10 minutes, NMDA + D-serine for the following 10 minutes and finally a 10 minute aCSF 'wash' period (**Figure 5.3.2 a, b**). Channels with MUA which was increased by bath application of 30 μM NMDA were judged to have active, viable cells in the vicinity of the recording electrode.

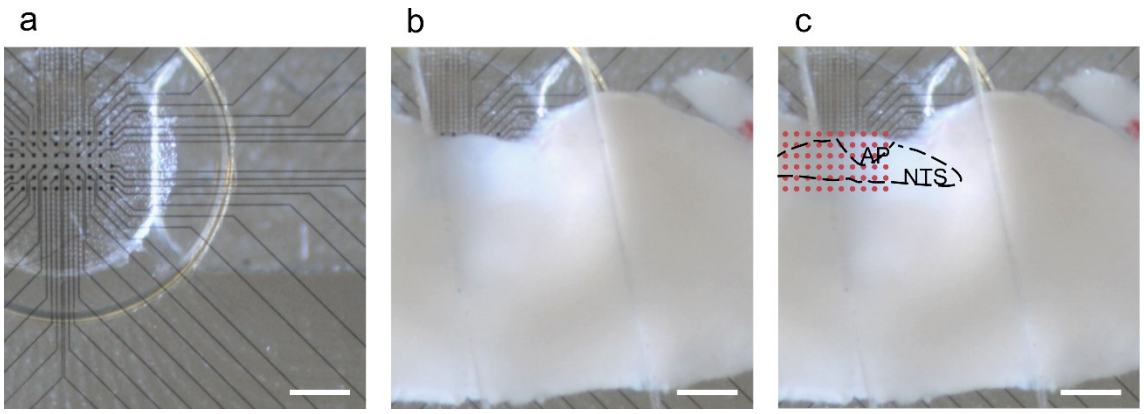

Figure 5.3.1 | pMEA recording set up for NTS. a, 6x10 array of electrodes (black dots). **b**, *ex vivo* NTS-containing brain slice on the pMEA in aCSF held down by a harp. **c**, annotated image showing positions of electrodes and atlas overlay to indicate electrode positions relative to the NTS. Scale bars = 500 µm. AP = area postrema, NTS = nucleus of the solitary tract.

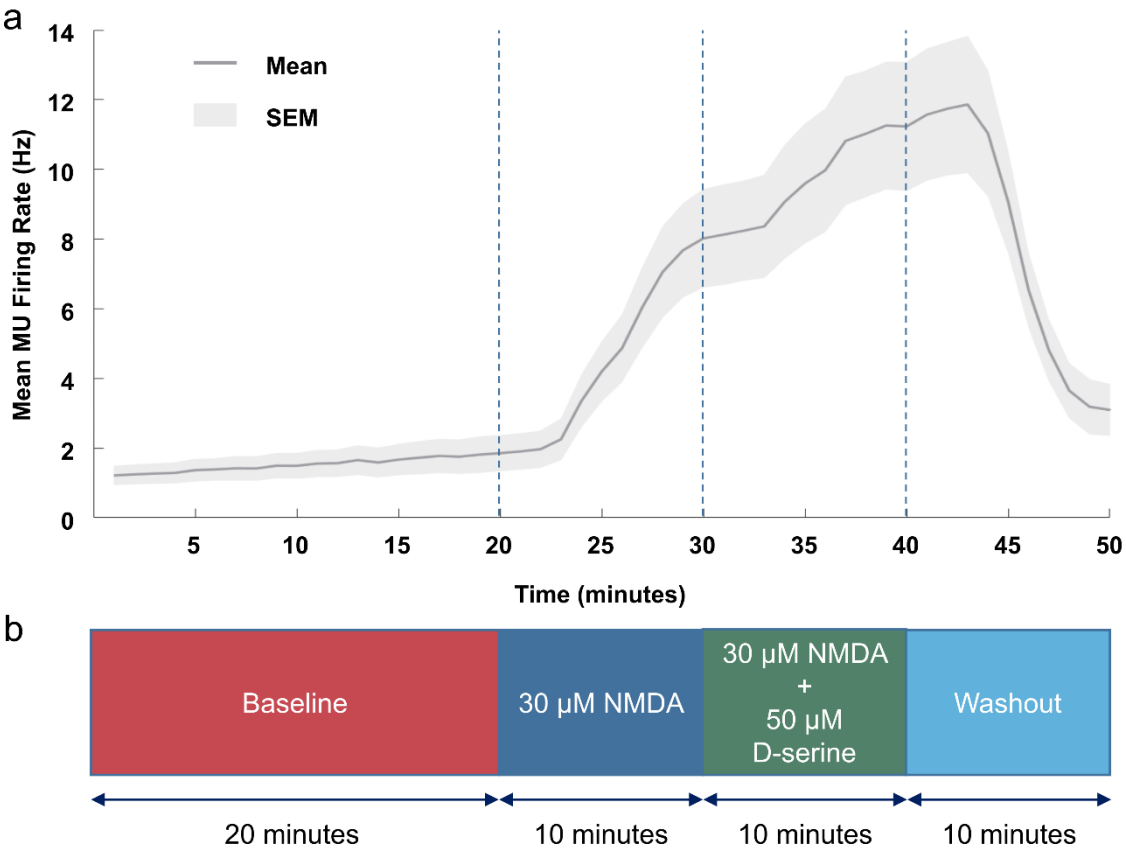

Figure 5.3.2 | Recording protocol and drug treatments. a, Representative firing rate of NMDA-responsive channels on a single pNTS slice during the recording (n = 34 channels from one slice, bin size = 1 minute). **b**, Schematic of recording protocol illustrating the different periods and durations of drug treatments. This schematic is aligned to the x-axis of **a**.

5.3.2 | High fat chow hyperphagia increased the firing rate of NTS channels at baseline

In order to assess the impact of high fat chow induced hyperphagia on NTS neuronal firing, 300μm coronal slices containing the NTS were obtained from mice fed either standard chow or high fat chow for 12 hours during the dark phase. As in previous experiments, mice fed a high fat chow for this period had a greater energy intake during the feeding period than those in the standard chow control group (**Figure 5.3.3 a,** 11.26 ± 0.48 vs 18.77 ± 0.71 kcal; $p < 0.0001$, unpaired t-test). Since these mice were not perfused the contents of the stomach were able to be accurately measured. Mice fed a high fat chow had greater stomach contents (by mass) at the end of the 12 hour feeding period than those in the standard chow control group (**Figure 5.3.3 b,** 0.45 ± 0.033 vs 1.20 ± 0.096 g; $p < 0.0001$, unpaired t-test).

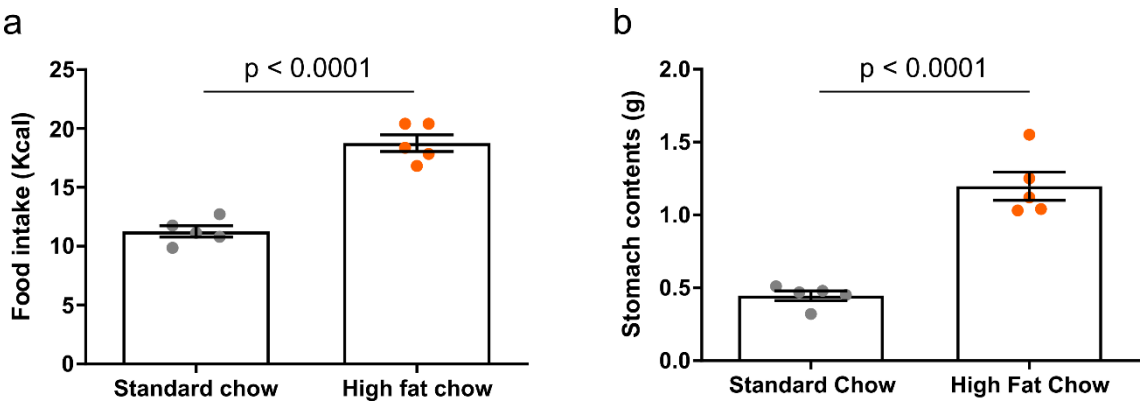

Figure 5.3.3 | Food intake and stomach contents of experimental mice. **a**, Energy intake during the 12 hour period prior to brain tissue collection of mice fed standard and high fat chow (11.26 ± 0.48 vs 18.77 ± 0.71 kcal; n= 5 mice/group $p < 0.0001$, unpaired t-test). **b**, Stomach contents of mice fed either standard chow or high fat chow (0.45 ± 0.033 vs 1.20 ± 0.096 g; n= 5 mice/group $p < 0.0001$, unpaired t-test) This panel is also shown in **Figure 3.3.1 d**.

Given the high dimensionality of this data (50000 samples/sec x 59 channels x 3000 seconds x 20 slices) an analytical pipeline was employed to aid in the extraction of relevant data (**Figure 5.3.4 a**). From the experiments we obtained 20 slice recordings (1,180 channels) from ten mice. 650 of these channels did not meet the inclusion criteria (based on channel location and activity) and were discarded from further analysis. Of the remaining 530 channels, baseline firing rate and response to drug applications were compared between feeding groups.

The mean baseline MU firing rate was greater on NTS channels in slices from high fat fed mice compared with standard chow fed controls (**Figure 5.3.5 a,** 0.12 ± 0.305 vs 0.3 ± 0.98 Hz; median ± interquartile range, $p < 0.0001$, Mann-Whitney test). These data, like other population recordings, are heavily skewed in the direction of low frequency (Buzsáki and Mizuseki, 2014). To better visualise the distribution and compare the differences the same data are also shown against a logarithmic^{10} y-axis (**Figure 5.3.5 b**).

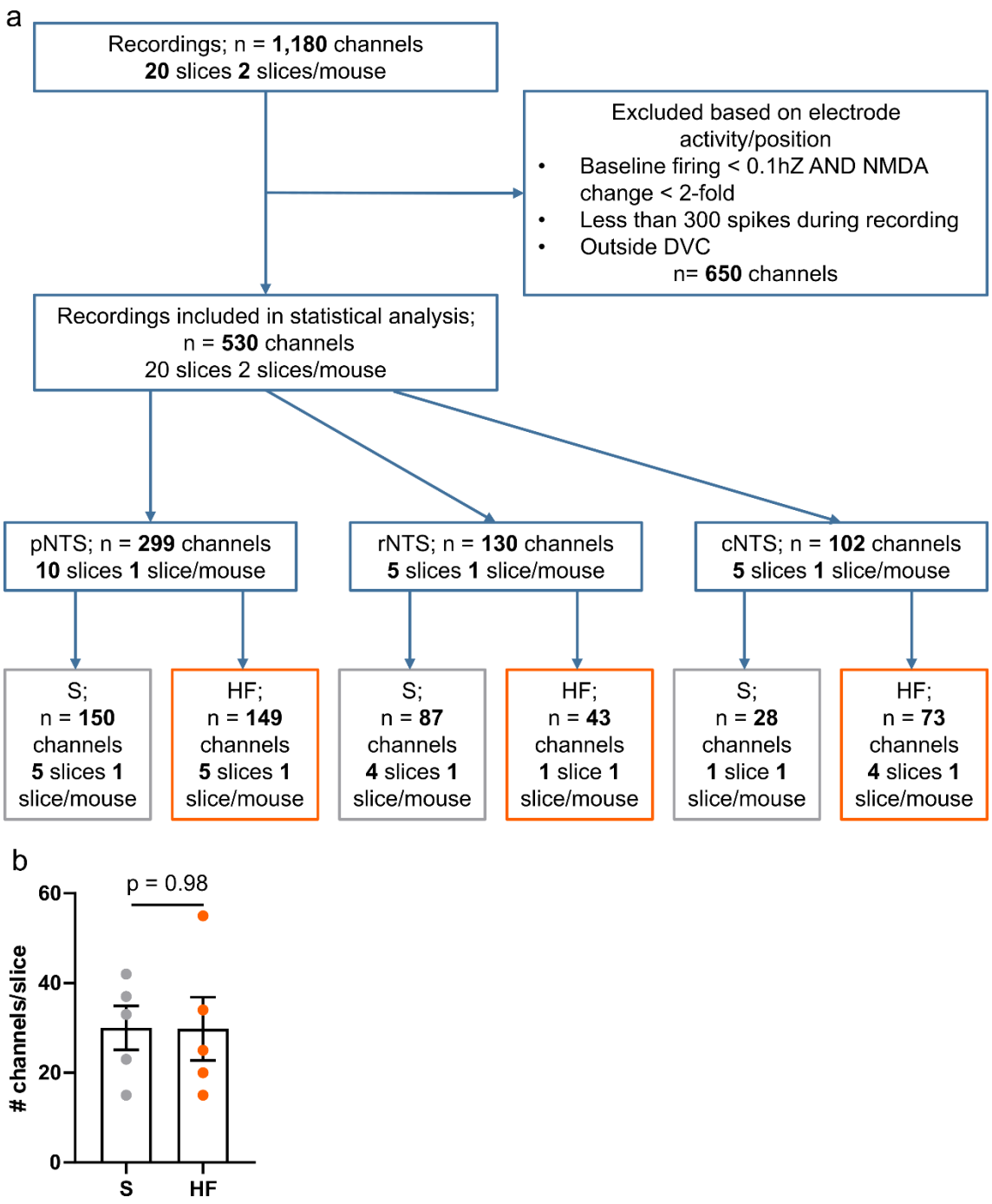

Figure 5.3.4 | Analysis pipeline for pMEA recordings. a, Flow chart for channel selection and grouping for further analysis. **b**, The number of pNTS channels per slice included in statistical analysis did not differ between groups (n = 5 slices, 30 ± 4.9 vs 29.8 ± 7 channels, p = 0.98, unpaired t-test). cNTS = caudal nucleus of the solitary tract, HF = high fat chow fed, pNTS = postremal nucleus of the solitary tract, rNTS = rostral nucleus of the solitary tract, S = standard chow fed.

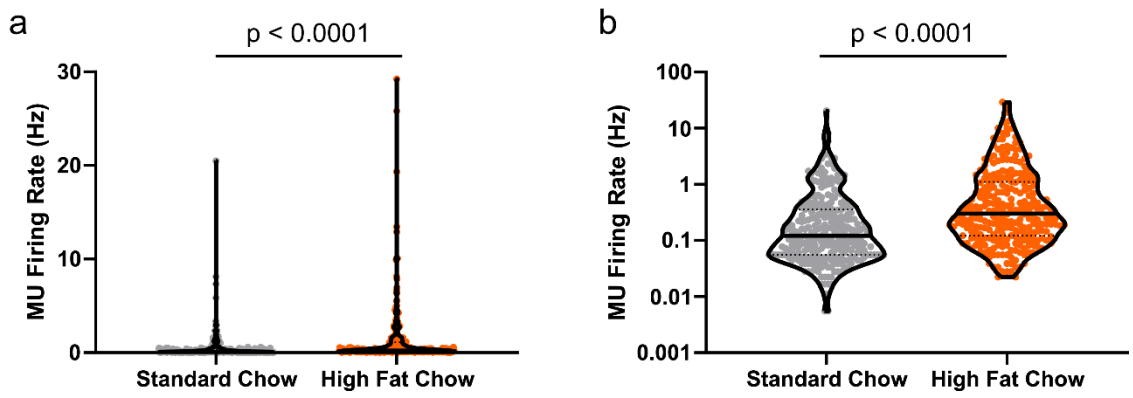

Figure 5.3.5 | Greater baseline MU firing rate of channels across the NTS from mice fed high fat chow for 12 hours compared to standard chow fed controls. a, Baseline MU firing rate of channels across the NTS of standard chow and high fat chow fed mice (0.12 ± 0.305 vs 0.3 ± 0.98 Hz, n = 265 channels/group from 10 slices from 5 mice/group, $p < 0.0001$, Mann-Whitney test). **b**, Baseline MU firing rate of channels across the NTS of standard chow and high fat chow fed mice displayed on a logarithmic scale. Data are presented as median ± interquartile range.

5.3.3 | High fat chow hyperphagia increased the firing rate of pNTS channels at baseline

In our previous experiment we found that the astrocyte GFAP-response to 12 hour intake of high fat chow was most pronounced in the postremal NTS (pNTS) (**Section 3.3.2**). In addition, the literature shows that this is the region in which most gut-innervating vagal afferents terminate and is where appetite regulating neurons are abundant (Grill and Hayes, 2012; Williams *et al.*, 2016; Han *et al.*, 2018; Bai *et al.*, 2019). Because of this, we focussed on the pNTS for further analysis. Of the recorded slices, 1 per animal covered the pNTS with an equal number of channels that met the inclusion criteria between mice in the different diet groups (**Figure 5.3.4 a**, n = 149-150, n = 5 slices per group, 1 slice per mouse). Although there was variation in the number of suitable channels per slice this variation was equal between the different diet groups (**Figure 5.3.4 b**). The baseline MU firing rate was greater in channels in the pNTS of mice fed a high fat chow than from standard chow fed mice (**Figure 5.3.6 a** 0.12 ± 0.34 vs 0.37 ± 1.15 Hz; median ± interquartile range, $p < 0.0001$, Mann-Whitney test). Again, the logarithmic plot is also shown (**Figure 5.3.6 b**). Since the MEA also gives spatial information (i.e. the electrode position is known) the approximate location of each electrode relative to the central canal was calculated and plotted with the colour of the point corresponding to firing rate for standard chow fed mice (**Figure 5.3.6 c**) and high fat chow fed mice (**Figure 5.3.6 d**). This shows that high fat chow intake for 12 hours elevates neuronal population activity in the NTS.

Since the experimental manipulation (the diet) was applied to mice and the activity of many channels was recorded simultaneously, the possibility of individual channels influencing one another means they are not truly independent samples (Lazic, Clarke-Williams and Munafò, 2018). To account for this the data

were also analysed with slice (or mouse since only one slice per mouse is used) as a nested variable. Since the data were not normally distributed the data were first transformed by $y=log(x)$ to allow for parametric statistical testing. This analysis (**Figure 5.3.6 e**) shows that elevated firing in high fat chow fed channels is statistically significant when the influence of slice is accounted for.

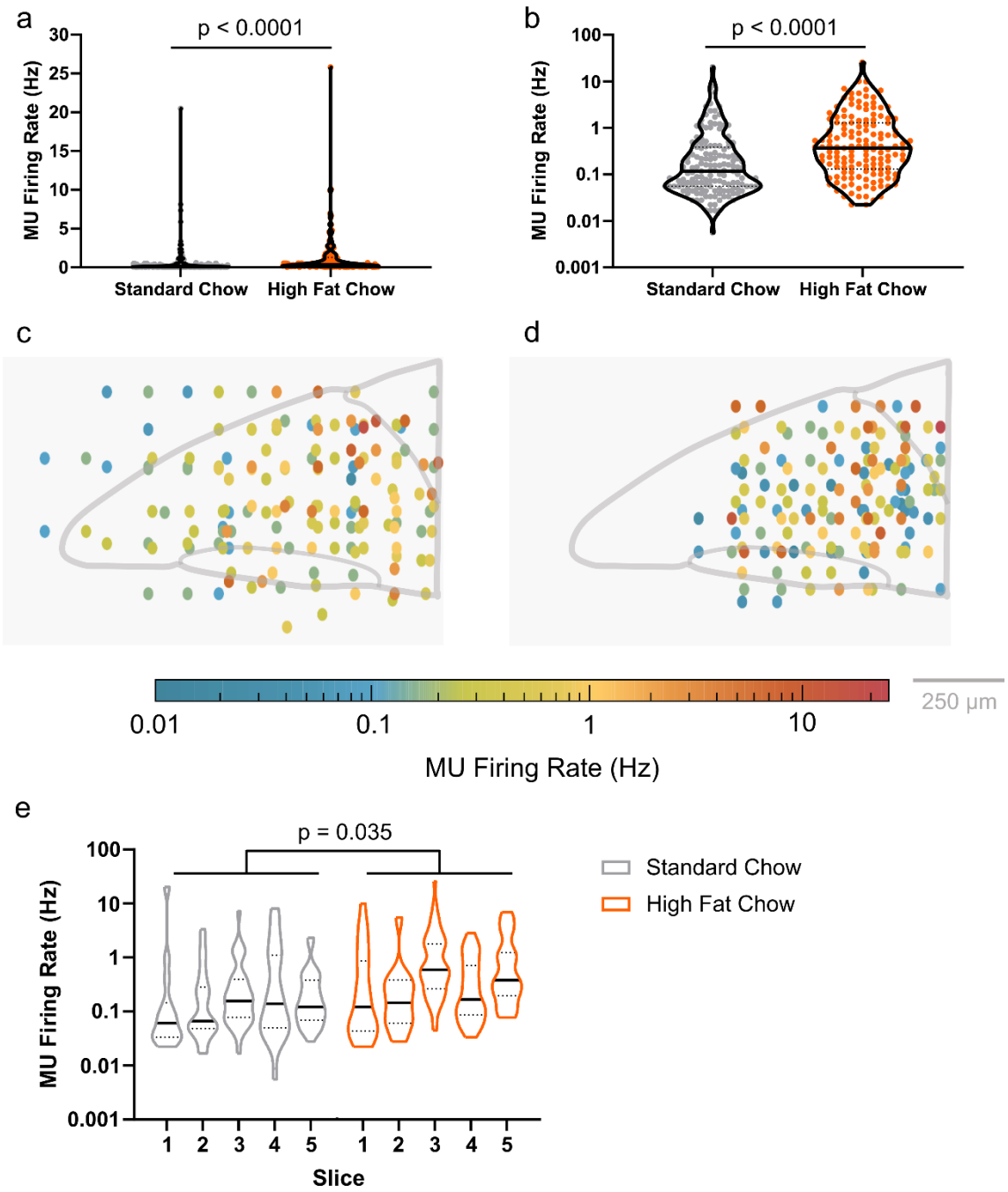

Figure 5.3.6 | Greater baseline MU firing rate of channels in the postremal NTS (pNTS) from mice fed a high fat chow for 12 hours compared to standard chow fed controls. a, Baseline MU firing rate of channels in the pNTS of standard chow and high fat chow fed mice (0.12 ± 0.34 vs 0.37 ± 1.15 Hz; n = 149-150 channels/group from 5 slices from 5 mice/group, $p < 0.0001$, Mann-Whitney test). **b**, Baseline MU firing rate of channels in the pNTS of standard chow and high fat chow fed mice against a logarithmic scale. **c**, Heat map showing approximate electrode locations and baseline MU firing rate for standard

chow fed mice (n = 150 channels from 5 slices from 5 mice). **d**, Heat map showing approximate electrode locations and baseline MU firing rate for high fat chow fed mice (n = 149 channels from 5 slices from 5 mice). **e**, Baseline MU firing rate with slice as a nested variable (n = 145-150 channels/group from 5 slices from 5 mice/group, p = 0.035, nested t-test on $y=log(x)$ transformed data). Data are presented as median ± interquartile range.

5.3.4 | Firing rate of channels in cNTS and rNTS at baseline

For each mouse, in addition to the pNTS slice, recordings were made from a second slice. The initial aim was to record from the caudal NTS (cNTS) but in situations where this slice was unsuitable, the rostral NTS (rNTS) was used. As with the pNTS the baseline MU firing rate of channels from the cNTS again indicated a greater firing rate in high fat chow fed mice than standard chow fed controls (**Figure 5.3.7 a, b**). Likewise, the baseline MU firing rate of channels from the rNTS indicate a greater firing rate in high fat chow fed mice than standard chow fed controls (**Figure 5.3.7 c, d**). By chance, the group sizes within the rNTS and cNTS recordings were unbalanced (See **Figure 5.3.4**). The data are not suitable for statistical hypothesis testing, particularly as in two groups (rNTS high fat chow and cNTS standard chow) all the data were obtained from a single mouse. As such, all subsequent analysis was only performed on the data obtained from pNTS slices.

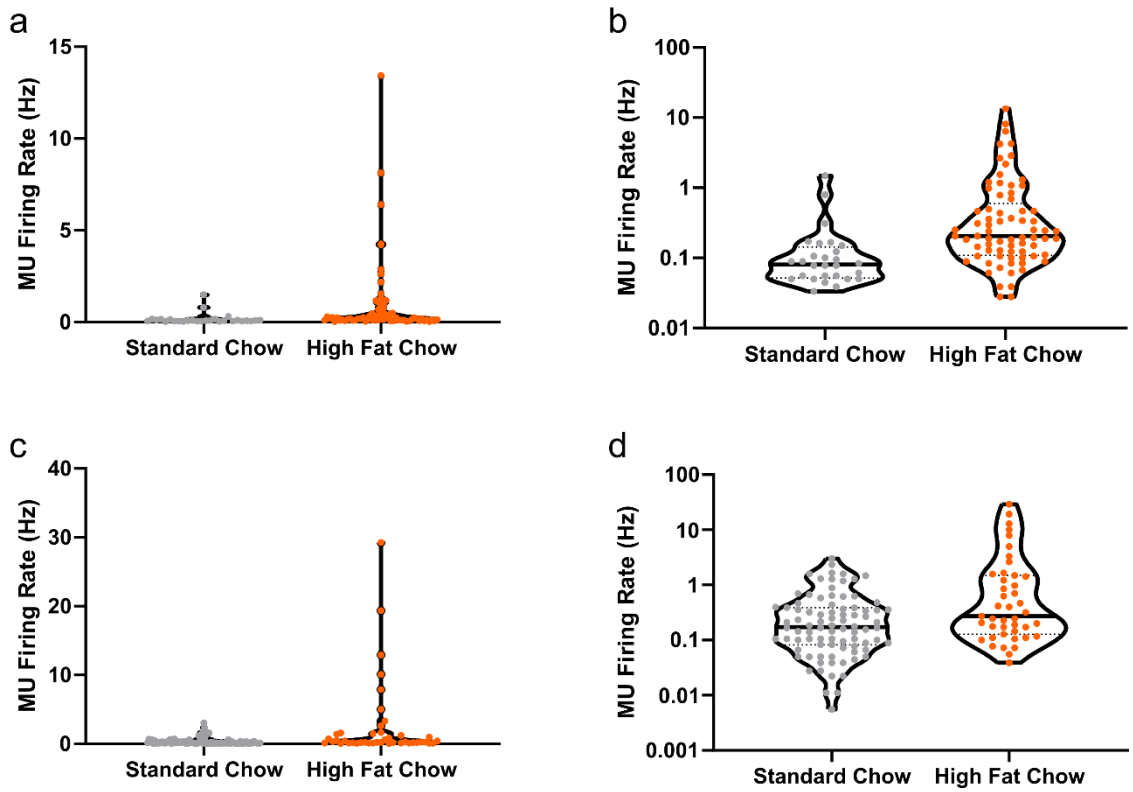

Figure 5.3.7 | Firing was greater in slices from high fat chow fed mice in the cNTS and rNTS. a, Baseline MU firing rate of channels in the cNTS of standard chow and high fat chow fed mice (n = 28 channels from 1 slice from 1 mouse [Standard Chow], n = 73 channels from 4 slices from 4 mice [High Fat Chow]). **b**, Baseline MU firing rate of channels in the cNTS of standard chow and high fat chow fed mice against a logarithmic scale. **c**, Baseline MU firing rate of channels in the rNTS of standard chow and high fat chow fed mice (n = 87 channels from 4 slices from 4 mice [Standard Chow], n = 43 channels from 1 slice from 1 mouse [High Fat Chow]). **d**, Baseline MU firing rate of channels in the rNTS of standard chow and high fat chow fed mice against a logarithmic scale. Data are presented as median ± interquartile range.

5.3.5 | NMDA increased MU firing rate in pNTS channels and this effect was potentiated by co-application of D-serine

In the hippocampus and hypothalamus, astrocytes gate the excitability of postsynaptic neurons by modulating extracellular D-serine levels and, by proxy, NMDA-mediated excitability since NMDA receptors rely on glutamate and a co-agonist (either D-serine or glycine) for activation (Panatier *et al.*, 2006; Papouin, Dunphy, *et al.*, 2017; Robin *et al.*, 2018). In order to ascertain whether D-serine could regulate neuronal activity in the pNTS, we tested the population response to application of D-serine in the presence of saturating concentrations of NMDA.

After baseline firing rates were established, agonists for the NMDA-R were added to the bath. In both feeding groups bath application of NMDA increased the MU firing rate (**Figure 5.3.8 a**). This effect was potentiated by the co-application of D-serine with NMDA (**Figure 5.3.8 a**). When the slice was returned to being perfused with aCSF (washout) MU firing rate decreased (**Figure 5.3.8 a**). Of note, the mean MU firing rate of channels in slices from high fat chow fed mice was higher than standard chow fed mice throughout the whole recording.

MU firing rates during the final 180 seconds of each application window were quantified for statistical analysis. In pNTS, channels in slices from standard chow fed mice there was a statistically significant increase in MU firing rate in the presence of NMDA relative to the baseline rate (**Figure 5.3.8 b, c**). In the presence of NMDA and D-serine there was a statistically significant increase in MU firing rate compared to the baseline rate and NMDA alone (**Figure 5.3.8 b, c**). This was also true of pNTS channels in slices from mice fed a high fat chow (**Figure 5.3.8 d, e**). This indicates that, as a population, NMDA responsive neurons in the NTS are sensitive to D-serine and identifies D-serine as a candidate gliotransmitter capable of exciting these neurons.

Analysis accounting for the slice as a nested variable showed that NMDA increased MU firing rate and NMDA + D-serine further increased this firing on channels from standard chow fed mice (**Figure 5.3.9 a**). The effect of NMDA was also observed in high fat fed mice although co-application of NMDA + D-serine did not further increase MU firing rate (**Figure 5.3.9 b**). This is potentially indicative of a differential response to D-serine in different slices from high fat chow fed mice.

Spike waveforms are shown from a representative recording (**Figure 5.3.10**). The shape of these waveforms is influenced by the proximity of a neuron to the recording electrode and ought to be stable throughout a recording. On the majority of these channels the waveform is the same shape between baseline (**Figure 5.3.10 a**) and drug treatments (**Figure 5.3.10 b**). This indicates that the same neurons are firing between the treatments. However, on some channels (e.g. channel 68) the waveform changes between the baseline and treatment periods which suggests a previously silent neuron has begun firing in response to drug treatment. Further analysis using principle component analysis and spike sorting could permit the separation of individual neurons in these instances.

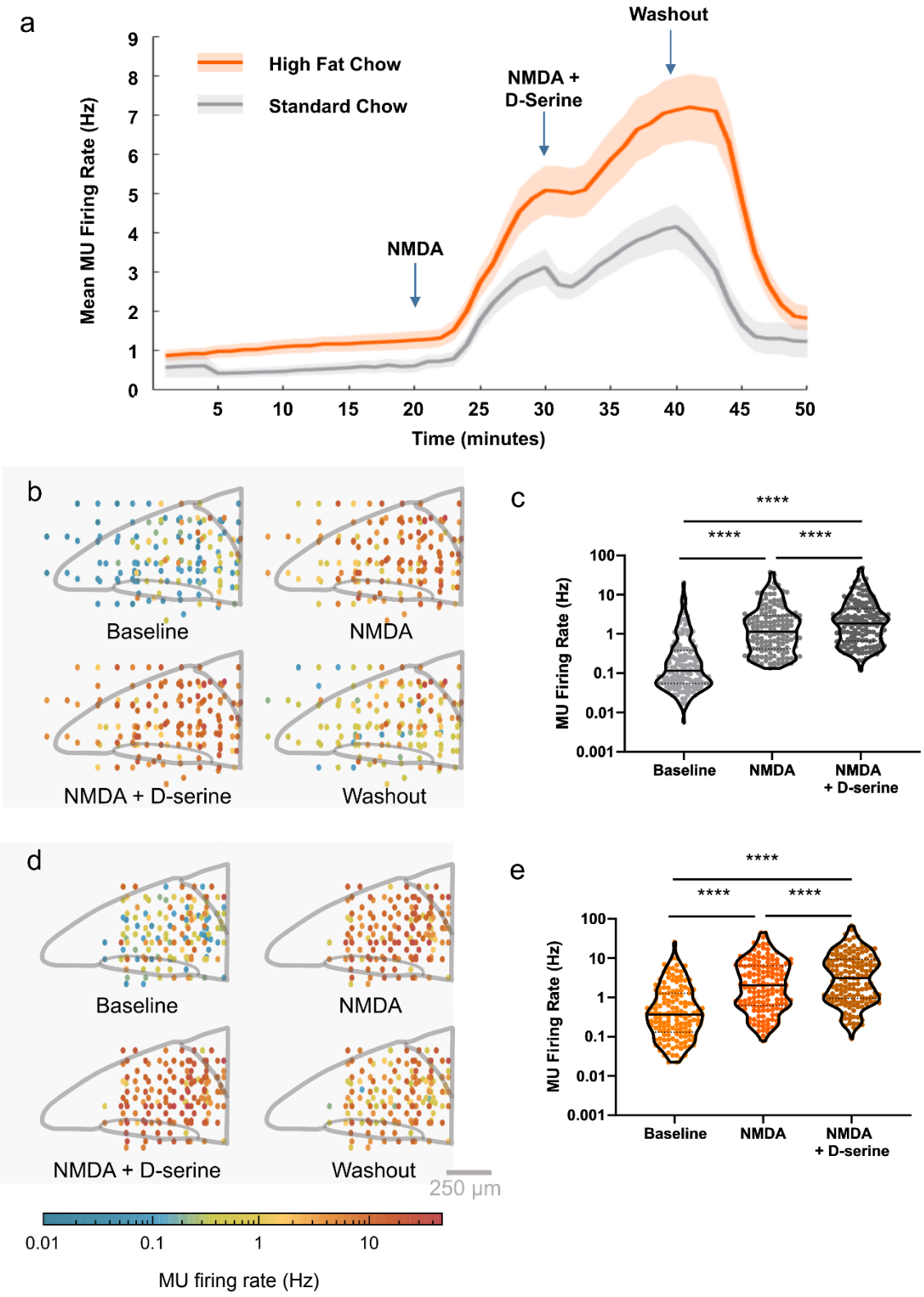

Figure 5.3.8 | Bath application of NMDA increases MU firing rate in the pNTS and this effect is potentiated by co-application of D-serine. a, Mean (± SEM) MU firing rate of pNTS channels from standard chow and high fat chow fed mice throughout the duration of recording (n = 149-150 channels/group from 5 slices

from 5 mice/group). **b**, Heat maps showing the approximate position and MU firing rate of channels in the pNTS of standard chow fed mice in the different drug windows. **c**, MU firing rate of channels in the pNTS of standard chow fed mice at rest, during bath application of NMDA and during bath application of NMDA + D-serine (n = 150 channels/group from 5 slices from 5 mice/group, Friedman test, $p < 0.0001$, Dunn's multiple comparisons test). **d**, Heat maps showing the approximate position and MU firing rate of channels in the pNTS of high fat chow fed mice in the different drug windows. **e**, MU firing rate of channels in the pNTS of high fat chow fed mice at rest, during bath application of NMDA and during bath application of NMDA + D-serine (n = 149 channels/group from 5 slices from 5 mice/group, Friedman test, $p < 0.0001$, Dunn's multiple comparisons test). **** = $p < 0.0001$. Data are presented as median ± interquartile range with the exception of panel **a**.

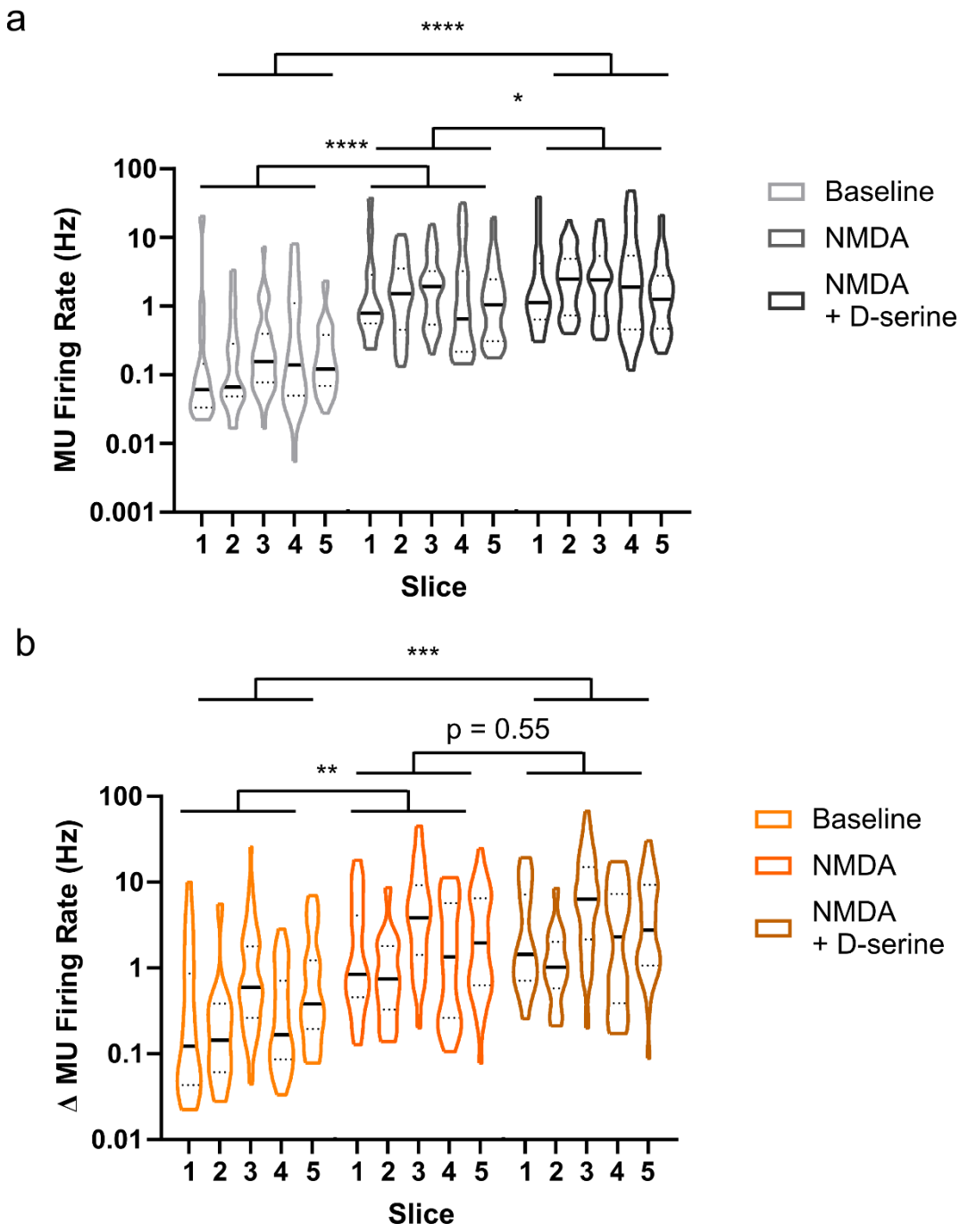

Figure 5.3.9 | NMDA-R agonists enhance MU firing in pNTS slices. a, MU firing rate of channels in the pNTS of standard chow fed mice at rest, during bath application of NMDA and during bath application of NMDA + D-serine with slice as a nested variable (n = 150 channels/group from 5 slices from 5 mice/group, nested One-way ANOVA performed on *y=log(x)* transform of data, $p < 0.0001$, $F_{(2,447)} = 150.9$ Tukey's multiple comparisons test). **b**, MU firing rate of channels in the pNTS of high fat chow fed mice at rest, during bath application of NMDA

and during bath application of NMDA + D-serine with slice as a nested variable (n = 149 channels/group from 5 slices from 5 mice/group, nested One-way ANOVA performed on *y=log(x)* transform of data, p = 0.0008, $F_{(2,12)}$ = 13.74, Tukey's multiple comparisons test). * = p < 0.05, ** = p < 0.01, *** = p < 0.001, **** = p < 0.0001.

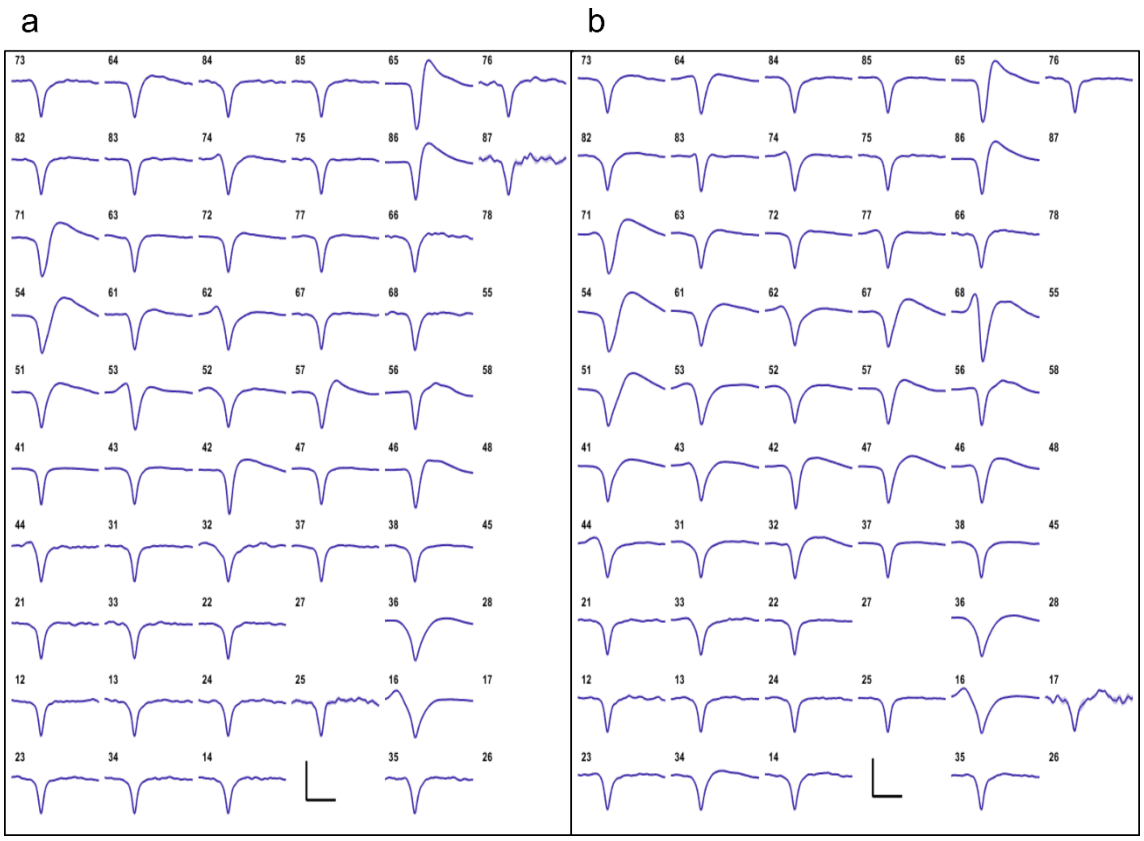

Figure 5.3.10 | Representative spike waveforms. a, Representative spike waveforms from a single pNTS slice during the baseline period. **b**, Representative spike waveforms from the same slice during the NMDA and NMDA + D-serine periods.

5.3.6 | In the pNTS channels from high fat chow fed mice showed greater responses to NMDA-R agonists

As mentioned above, D-serine and glycine are co-agonists for the NMDA-R. In order to examine the relative contributions of the glutamate site, the co-agonist site and whether these were regulated by nutritional state, we compared the relative changes in MU firing rate evoked by the different drug treatments between feeding groups.

The application of NMDA alone resulted in an increase in MU firing rate. Since this saturating concentration is assumed to activate all available NMDA-Rs, subtracting the NMDA MU firing rate from the baseline MU firing rate shows the residual 'glutamate capacity' (**Figure 5.3.11 a**). The glutamate capacity is indicative of the number of unbound glutamate NMDA-R sites and is inverse to baseline agonist (glutamate and D-serine) availability. There was no statistically significant difference in glutamate capacity between the two diet groups (**Figure 5.3.11 b**, 1.02 ± 2.16 vs 1.31 ± 4.04 Hz, median ± interquartile range, $p = 0.08$, Wilcoxon matched-pairs test). This suggests that there is no difference in the ambient glutamate and D-serine availability at rest between diet groups.

The co-application of NMDA and D-serine resulted in an increase in MU firing rate relative to NMDA alone in both diet groups. This saturating concentration is assumed to activate all of the co-agonist sites of NMDA-Rs (Papouin, Dunphy, *et al.*, 2017), thus subtracting the NMDA + D-serine MU firing rate from the NMDA MU firing rate shows the 'co-agonist capacity' (**Figure 5.3.11 a**). The co-agonist capacity is indicative of the number of unbound co-agonist NMDA-R sites and is inverse to baseline D-serine and glycine availability. Since astrocytes show morphological changes induced by the acute high fat chow stimulus we hypothesised that co-agonist capacity would be lower in this group than standard

chow fed, indicating elevated baseline D-serine levels in the NTS. The reverse was true, co-agonist capacity was greater in the high fat chow fed group suggesting that occupancy of the co-agonist site at rest is lower in this group (**Figure 5.3.11 c**, 0.48 ± 1.05 vs 0.9 ± 2.69 Hz, median ± interquartile range, p = 0.0005, Wilcoxon matched-pairs test).

Finally, indicative of total possible NMDA-R mediated MU firing, the maximum capacity was calculated by subtracting the NMDA + D-serine MU firing rate from the baseline MU firing rate (**Figure 5.3.11 a**). The maximum NMDA-R capacity was greater in the high fat chow fed group compared with the standard chow fed group (**Figure 5.3.11 d**, 1.65 ± 3.30 vs 2.20 ± 6.59 Hz, median ± interquartile range, p = 0.023, Wilcoxon matched-pairs test). This indicates that there is greater potential for NMDA-R excitability in slices from high fat fed mice compared with those fed standard chow. This suggests, in contrast to our hypothesis, that in fact the elevated baseline firing rate is not controlled by the increased availability of endogenous agonists for the NMDA-R, instead these channels are more excitable by NMDA-R agonism as indicated by the greater maximum NMDA-R capacity, suggesting perhaps that the number of receptors is upregulated in this condition.

When these agonist capacity analyses were repeated with the inclusion of slice as a nested variable none of the comparisons reached statistical significance (**Figure 5.3.11 e-g**). This indicates that observed differences in the above analyses may originate from differences between slices rather than a uniform effect of agonists in slices from different diet groups.

Overall, this study shows that independent of greater baseline MU firing rate, that MU activity in slices from high fat diet fed mice is more sensitive to combined

application of agonists for both the glutamate and co-agonist sites of the NMDA-R, which may reflect a difference in receptor number.

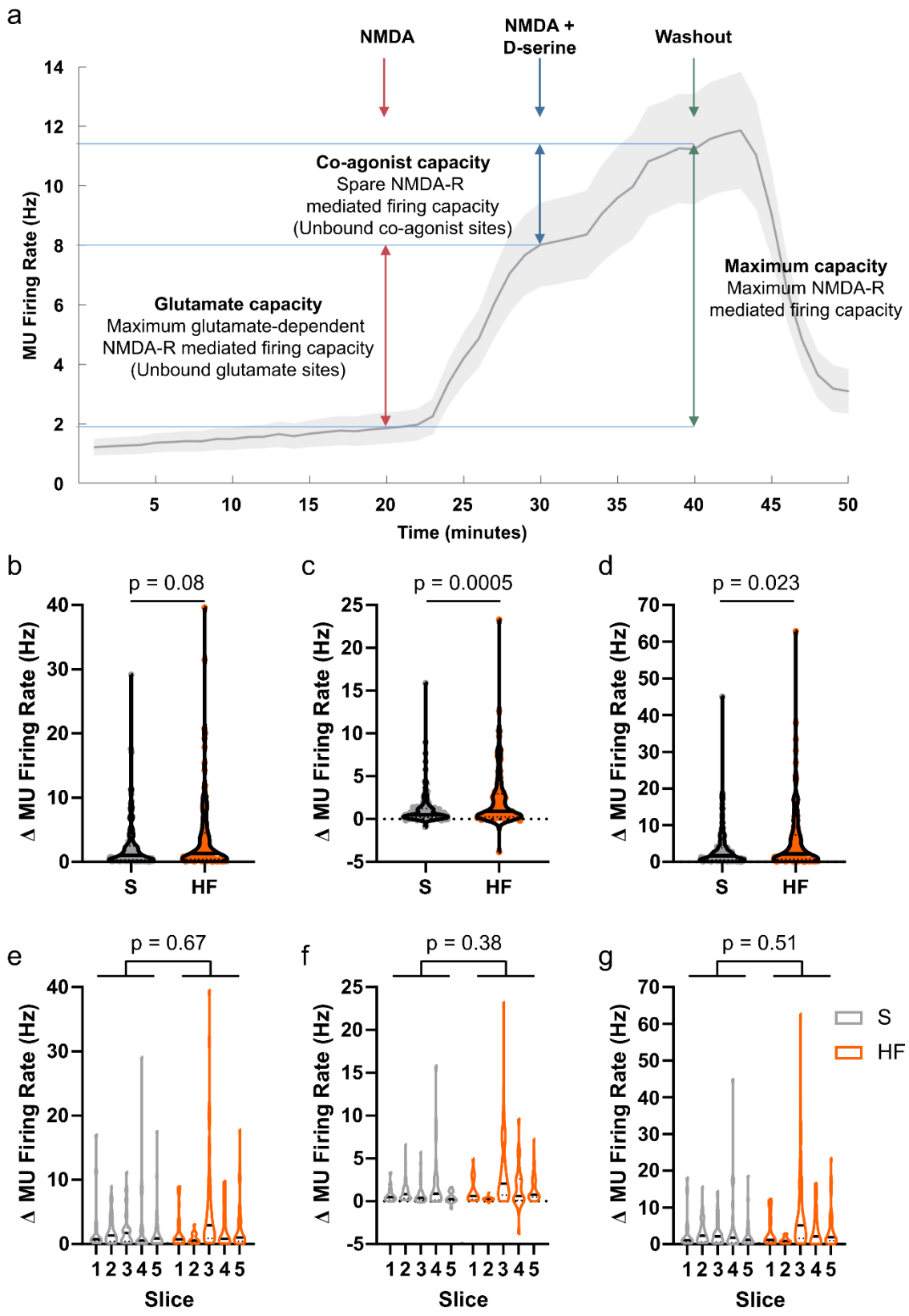

Figure 5.3.11 | Total capacity of NMDA-R mediated firing and co-agonist capacity of NMDA-R mediated firing are greater in pNTS channels from high fat chow fed mice. a, Schematic describing how the different components of

NMDA-dependent MU firing rate are calculated. **b**, Glutamate capacity (NMDA MU firing rate – baseline MU firing rate) of pNTS channels in slices from standard chow fed (S) and high fat chow fed (HF) mice (1.02 ± 2.16 vs 1.31 ± 4.04 Hz, n = 149-150 channels/group from 5 slices from 5 mice/group, p = 0.08, Wilcoxon matched-pairs test). **c**, Co-agonist capacity (NMDA + D-serine MU firing rate – NMDA MU firing rate) of pNTS channels in slices from S and HF fed mice (0.48 ± 1.05 vs 0.9 ± 2.69 Hz, n = 149-150 channels/group from 5 slices from 5 mice/group, p = 0.0005, Wilcoxon matched-pairs test). **d**, Maximum capacity (NMDA + D-serine MU firing rate – baseline MU firing rate) of pNTS channels in slices from S and HF fed mice (1.65 ± 3.30 vs 2.20 ± 6.59 Hz, n = 149-150 channels/group from 5 slices from 5 mice/group, p = 0.023, Wilcoxon matched-pairs test). **e**, Glutamate capacity (NMDA MU firing rate – baseline MU firing rate) of pNTS channels from S and HF fed mice with slice as a nested variable (n = 149-150 channels/group from 5 slices from 5 mice/group, p = 0.67, nested t-test). **f**, Co-agonist capacity (NMDA + D-serine MU firing rate – NMDA MU firing rate) of pNTS channels from S and HF fed mice with slice as a nested variable (n = 149-150 channels/group from 5 slices from 5 mice/group, p = 0.38, nested t-test). **g**, Maximum capacity (NMDA + D-serine MU firing rate – baseline MU firing rate) of pNTS channels from S and HF mice with slice as a nested variable (n = 149-150 channels/group from 5 slices from 5 mice/group, p = 0.51, nested t-test). All nested tests were performed on data transformed by $y=log(x)$. Data are presented as median ± interquartile range with the exception of panel **a**.

5.3.7 | Whole-cell patch clamp in the horizontal slice to investigate glial glutamate reuptake

In addition to gliotransmission, astrocytes can also modulate neuronal excitability by regulating extracellular glutamate levels. Since glutamate is the primary transmitter at the ST→NTS synapse this is a very important process. Indeed, in rats, pharmacological blockade of the primary glutamate transporter excitatory amino acid transporter 2 (EAAT2) increases parasympathetic output to the cardiovascular system in an AMPA-R dependent manner (Matott, Kline and Hasser, 2017; Yamamoto and Mifflin, 2018).

To examine the effects of EAAT2 blockade on appetite-suppressing neurons in the mouse brain we made whole cell patch clamp recordings of fluorescent cells in horizontal brainstem slices from mice expressing enhanced green fluorescent protein (EGFP) in TH cells (TH-EGFP mice). In this preparation the solitary tract is preserved which allows for its electrical stimulation (**Figure 5.3.12 a**). In addition, NTS^{TH} neurons can be visualised for patch clamp by their expression of EGFP (Appleyard *et al.*, 2007). We used a recording protocol where in the voltage clamp configuration, 'spontaneous' activity was recorded for 1 second followed by a 10 pulse @ 50 Hz stimulation train to measure 'evoked' activity. The remainder of the protocol (total length 6 seconds) was a measure of 'asynchronous' activity, a type of non-time locked, activity-dependent phenomenon observed at this synapse (Peters *et al.*, 2010; Wu, Fenwick and Peters, 2014). A representative trace from this protocol is shown in **Figure 5.3.12 b**.

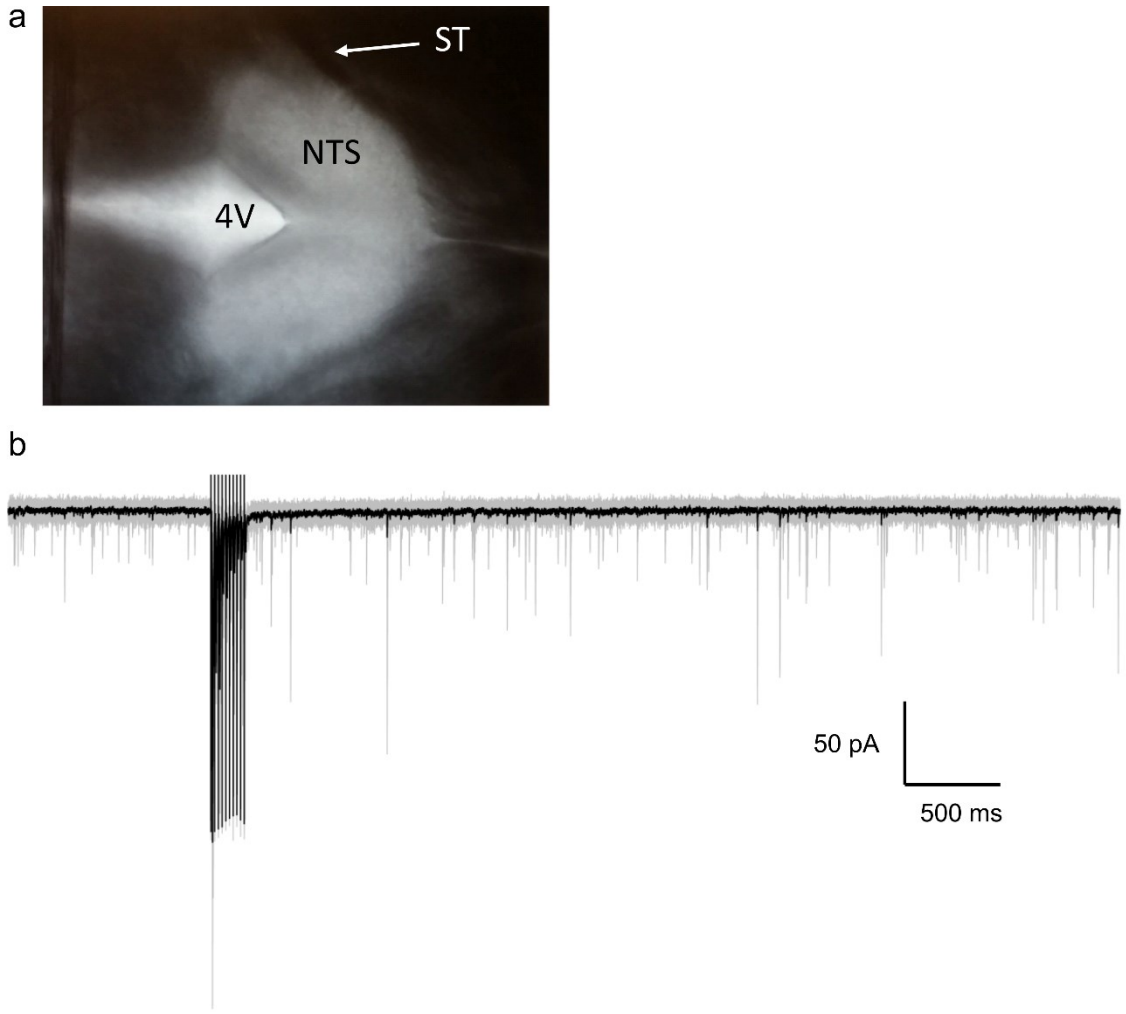

Figure 5.3.12 | Patch clamp recording in the horizontal brainstem slice. a, Example of a horizontal slice at 4X magnification. **b**, Representative trace from 10 sweeps of the recording protocol, mean of 10 sweeps in black, individual sweeps in grey. 4V = fourth ventricle, NTS = nucleus of the solitary tract, ST = solitary tract.

5.3.8 | DHK reduced the size of evoked EPSCs into NTS^{TH} neurons

The size of evoked EPSCs were measured in aCSF (baseline), dihydrokainic acid (DHK [100 μM]), and after being returned to aCSF (washout) (A representative trace from the baseline condition is shown in **Figure 5.3.13 a**). As previously observed (Appleyard *et al.*, 2007), NTS^{TH} neurons showed large time-locked EPSCs and frequency-dependent depression with repeated stimulation (**Figure 5.3.13 a**). Representative mean (of 10 sweeps) EPSCs from each condition are shown in **Figure 5.3.13 b**. Quantification of EPSC amplitude showed that the size of the first evoked EPSC was reduced by DHK (402.4 ± 88.43 vs 319.6 ± 87.37 pA) and did not recover with 10 minutes of washout (**Figure 5.3.13 c**). Importantly, in cells that were untreated but had aCSF fed through the drug delivery system for the same period, there was no change in evoked EPSC amplitude (**Figure 5.3.13 d**). Looking at the amplitude of the first EPSC over the whole recording period shows a step-wise decrease during the DHK period before plateau of this effect in the washout (**Figure 5.3.13 e**). This is suggestive of a true effect of DHK rather than a gradual 'run down' of the evoked response. There was no observed change in the ratio of $EPSC_2/EPSC_1$ (paired-pulse ratio) although this ratio was heterogeneous between cells which makes mechanistic conclusions difficult (**Figure 5.3.13 f**). Taken together this shows that inhibition of astrocyte glutamate transport reduces fidelity of communication between vagal afferents and NTS^{TH} neurons. This suggests that under normal conditions astrocyte glutamate transport contributes to sustaining this synaptic transmission.

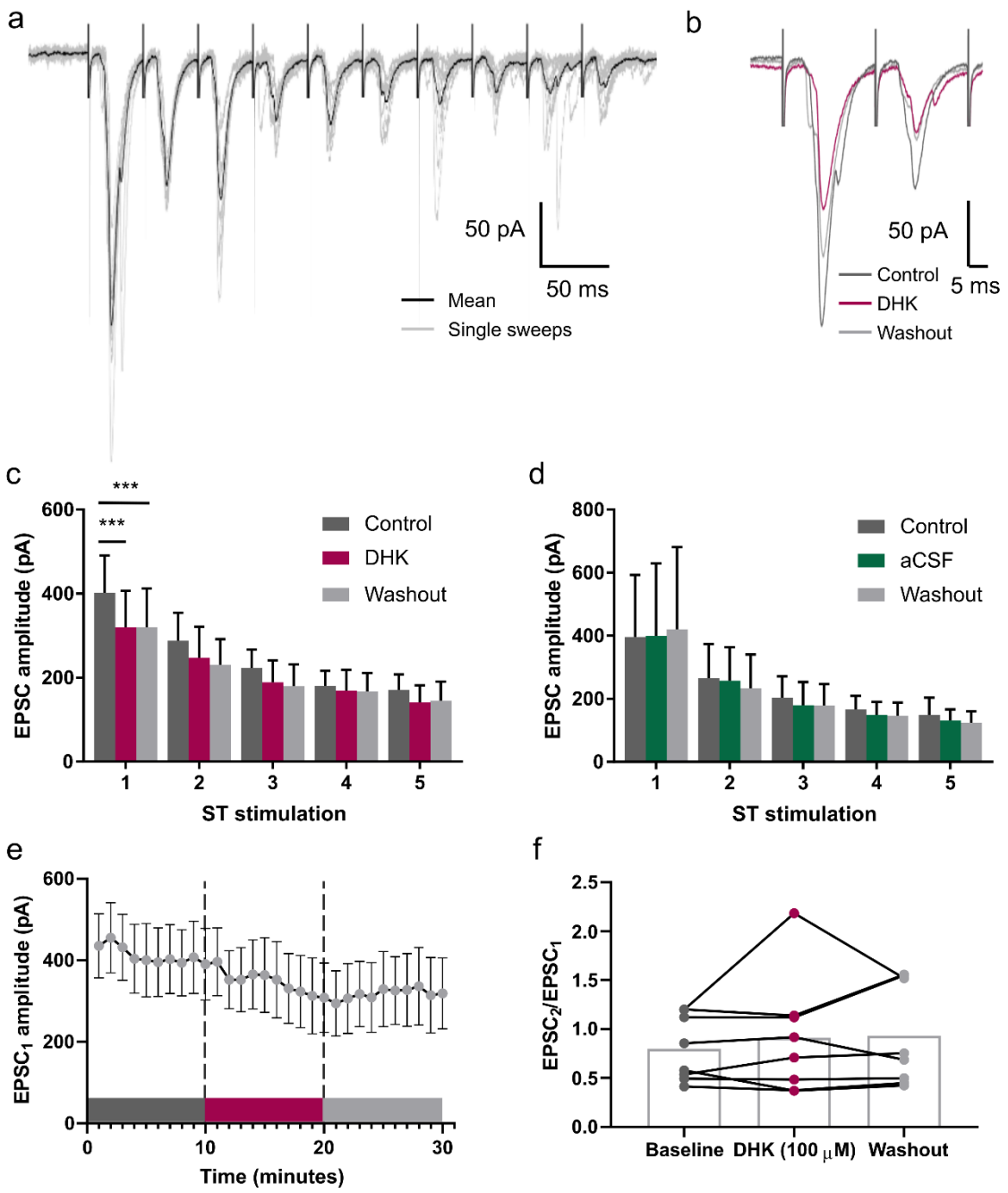

Figure 5.3.13 | Effect of DHK on evoked EPSCs in NTSTH neurons. a, Representative trace from 10 DHK sweeps (sweeps in grey, mean of 10 sweeps in black). **b**, Representative trace from 10 wash sweeps (sweeps in grey, mean of 10 sweeps in black). **c**, Evoked EPSC amplitude during baseline, DHK and wash (n = 8 cells from 5 mice, Two-way RM ANOVA, DHK, $p < 0.0001$, $F_{(2,70)} = 14.96$; Stimulation, $p = 0.17$, $F_{(4,35)} = 1.73$, interaction, $p = 0.28$, $F_{(8,70)} = 1.25$, Sidak's post-hoc test). **d**, Evoked EPSC during baseline, aCSF and washout (n

= 4 cells from 3 mice, Two-way RM ANOVA, aCSF, p = 0.32, $F_{(2,30)}$ = 1.20, Stimulation, p = 0.53, $F_{(4,15)}$ = 0.82, interaction, p = 0.83, $F_{(8,30)}$ = 0.52, Sidak's post-hoc test, p > 0.05 for all comparisons). **e**, Mean amplitude of $EPSC_1$ throughout the recording period (n = 8 cells from 5 mice). **f**, Paired pulse ratio in the final minute of each condition (n = 8 cells from 5 mice, One-way RM ANOVA, treatment, p = 0.48, $F_{(2,14)}$ = 0.76, Dunnet's post-hoc test, p > 0.05 for all comparisons). *** = P< 0.001.

5.3.9 | DHK did not affect the frequency of spontaneous or asynchronous EPSCs into NTS^{TH} neurons

The recording protocol also permitted recording of EPSCs outside of the stimulation window. A representative trace of this is shown in **Figure 5.3.14 a**. Note the increased EPSC frequency following stimulation, this is termed asynchronous release and is shown to be mediated by glutamate released from presynaptic terminals in an activity dependent fashion (Peters *et al.*, 2010). This quickly decays and EPSC frequency returns to baseline frequency. Quantification of cumulative EPSCs in 0.1s bins over 30 sweeps shows that DHK did not affect the spontaneous (prior to stimulation) or asynchronous (immediately after stimulation) EPSC frequency (**Figure 5.3.14 b**). Statistical analysis of the cumulative EPSCs in the time bins immediately before and immediately after stimulation showed that there was no difference in pre stimulation (i.e. spontaneous EPSC) or post stimulation (i.e. asynchronous EPSC) between aCSF and DHK (**Figure 5.3.14 c**). The amplitude of spontaneous and asynchronous EPSCs was decreased upon bath incubation with DHK (**Figure 5.3.14 d**). This suggests that, contrary to our hypothesis, the accumulation of glutamate in the synapse did not lead to increased spontaneous activation of postsynaptic receptors. However in agreement with the observed reduction in evoked EPSC amplitude, the amplitude of spontaneous and asynchronous EPSCs was reduced by DHK. This is potentially indicative of reduced presynaptic release of glutamate for a given release event.

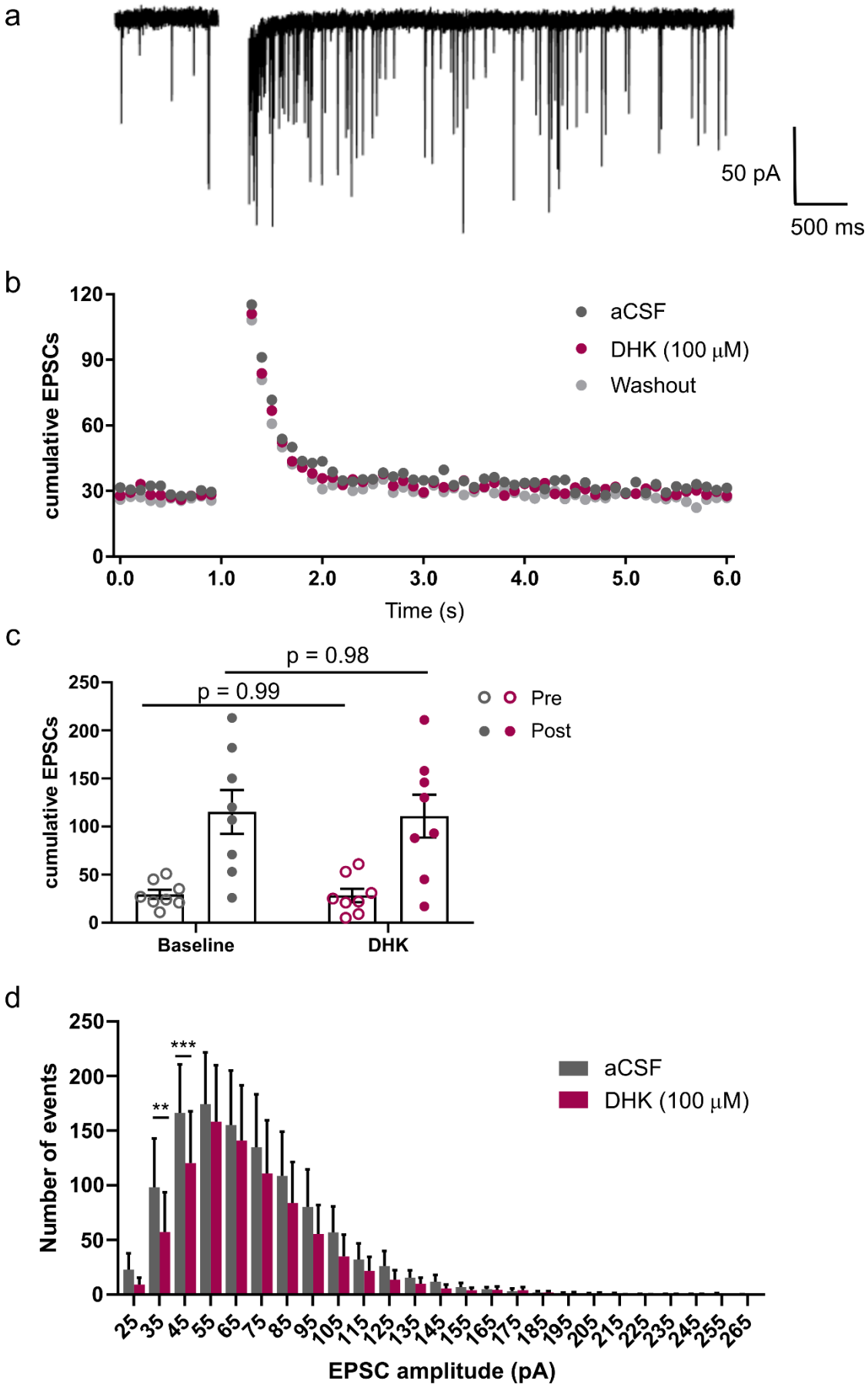
a
50 pA
500 ms
b
cumulative EPSCs
120
90
60
30
0
0.0
1.0
2.0
3.0
4.0
5.0
6.0
Time (s)
aCSF
DHK (100 μM)
Washout
c
cumulative EPSCs
250
200
150
100
50
0
p = 0.98
p = 0.99
Pre
Post
Baseline
DHK
d
Number of events
250
200
150
100
50
0
***
**
aCSF
DHK (100 μM)
25
35
45
55
65
75
85
95
105
115
125
135
145
155
165
175
185
195
205
215
225
235
245
255
265
EPSC amplitude (pA)

Figure 5.3.14 | DHK did not affect the frequency of spontaneous and asynchronous EPSCs in NTSTH neurons. **a**, Representative trace from a single sweep with the stimulation window omitted for clarity. **b**, Quantification of the cumulative number of EPSCs in 0.1 ms bins across 30 sweeps. **c**, Number of EPSC events in the bin immediately prior to stimulation (pre) or immediately following stimulation (post) at baseline and following bath application of DHK (n = 8 cells from 5 mice, Two-way RM ANOVA, Stimulation, $p < 0.0001$, $F_{(1,14)} = 28.29$, DHK, $p = 0.87$, $F_{(1,14)} = 0.025$, interaction, $p = 0.92$, $F_{(1,14)} = 0.01$, Sidak's post-hoc test). **d**, Frequency distribution of EPSC amplitudes across 30 sweeps. Bins are ± 5 pA. (n = 8 cells from 5 mice, Two-way RM ANOVA, Bin, $p < 0.0001$, $F_{(24,150)} = 5.3.22$, DHK, $p < 0.0001$, $F_{(1,150)} = 26.28$, interaction, $p = 0.04$, $F_{(1,14)} = 0.01$, Sidak's post-hoc test). ** = $p < 0.01$, *** = $p < 0.001$.

5.4 | Discussion

In this chapter we have used two different electrophysiological methods to interrogate two potential mechanisms of astrocyte-neuron communication in the NTS. First, we show that high fat chow intake results in greater MU activity in the NTS and that these neurons are able to sense exogenous D-serine. Second, we show that blockade of EAAT2 modulates the integration of vagal signals by NTS^{TH} neurons raising the possibility that this process may be plastic in the intact brain.

5.4.1 | Perforated Multi-Electrode Array allows population recording in the NTS

By utilising the pMEA we were able to record multi-unit activity at 59 sites across the NTS simultaneously. Despite this advantage, a certain level of detail is lost when compared with single cell recordings. For example, we were not able to separate individual units by spike sorting. Additionally. due to measuring extracellular spikes we could not use synaptic blockers and as such cannot distinguish between intrinsic excitability and network activity. Despite these limitations the study provides initial insight into the effects of feeding on multiunit activity in the NTS and response to exogenously applied ligands for NMDA-R in these conditions. Future studies could focus on understanding this phenomenon in greater detail, perhaps by single cell recording to ascertain whether increased firing following high fat chow intake is a function of greater intrinsic excitability, greater synaptic input or some combination of the two. Furthermore, by combining this preparation with direct manipulation of astrocytes (e.g. using chemogenetics), neuron-glia interactions may be better studied.

5.4.2 | Assessment of the differential contribution of NMDA-R agonist binding sites to MU firing rate

We analysed differences in MU activity between drug conditions in our pMEA experiment and compared these between the diet groups to infer the state of NMDA-R ligand binding in the baseline period. However, this analysis was dependent on some assumptions; that the capacity for NMDA-R-mediated excitability are the same and that the glutamate receptor number (both AMPA-R and NMDA-R) is roughly equivalent between groups. It appears that at least one of these assumptions is wrong, given that the maximum capacity for NMDA-R excitability is greater in mice from the high fat diet fed group. This suggests that perhaps there is an upregulation of NMDA-R which means not only are neurons in these slices more excited (i.e. greater baseline MU firing rate), but they have greater NMDA-R excitability (i.e. greater maximum NMDA-R capacity). This limits the inferences of baseline agonist availability we can draw from the glutamate capacity and co-agonist capacity analyses.

Another limitation of the study, alluded to above, is that it does not differentiate between the contribution of the different glutamate receptor subtypes to the effects seen. Addition of bath application of a specific NMDA-R antagonist at 40mins (i.e. NMDA + D-serine + NMDA-R antagonist) prior to wash out would have enabled the contribution of non-NMDA glutamatergic receptor activation to the baseline firing to be revealed and would also have provided additional confidence in the specificity of the effects seen. Future studies, e.g. using radioligand binding, could be used to specifically determine the impact of 12 hour high fat diet consumption on NTS ionotropic glutamate receptor expression.

5.4.3 | Mechanisms underlying EAAT2 blockade reducing evoked EPSC in NTSTH neurons

We found that bath application of DHK reduced the evoked EPSC resulting from ST stimulation in NTSTH neurons. We hypothesised that this was due to reduced glutamate being taken into the astrocyte and therefore not returned to the presynaptic neuron as glutamine. This could be tested by repeating the experiment and adding glutamine to the aCSF during DHK treatment to see if the effect is rescued. Alternatively, increased synaptic glutamate may activate presynaptic mGlu-Rs which reduce presynaptic glutamate release as a negative feedback mechanism (Oliet, Piet and Poulain, 2001). In future work this could also be further explored using specific inhibitors of mGlu-Rs. Similarly we found the amplitude of spontaneous and asynchronous EPSCs was reduced by DHK further suggesting reduced presynaptic glutamate release.

We did not observe a change in the paired-pulse ratio between conditions suggesting there was no change to presynaptic release probability. However, in contrast to other reports (Appleyard *et al.*, 2007; Yamamoto *et al.*, 2010), we saw heterogeneity in this parameter. Typically in NTS neurons the PPR is low indicating a high release probability upon first stimulation but this was variable in our sample.

The effect of DHK in NTSTH neurons in mice differs to that of unlabelled NTS neurons in rats. For example, Matott *et al* found that DHK treatment induced a slow inward current that we did not observe (Matott, Kline and Hasser, 2017). They also found that spontaneous EPSCs were greater in DHK than at baseline which we did not. However, in our study we were not recording true spontaneous EPSCs since we were stimulating every 6 seconds which potentially interferes with, or masks changes in spontaneous EPSCs.

In further contrast to our study, Matott *et al* found that evoked EPSC amplitude was not reduced by DHK. It is unclear whether the conflicting outcomes between our studies and those of Matott *et al* represents either a species difference, differences in stimulation protocol, or a specific feature of vagal afferents connected to NTS^{TH} neurons. This is intriguing since vagal afferents synapsing onto specific neuronal subtypes may have unique features masked in studies looking at unlabelled neurons. Both their study and ours found no change in the number of asynchronous events with DHK (Matott, Kline and Hasser, 2017).

Since we have shown that neuronal firing and astrocyte morphology are altered following dietary manipulation it would be of interest in future studies to examine the effect of diet on EAAT2 glutamate uptake in the NTS and downstream effects on synaptic integration in NTS^{TH} neurons. This could perhaps be achieved by whole-cell patch clamp recordings from NTS astrocytes in slices from standard chow and high fat chow fed mice in which EAAT2-dependent inward currents (indicative of transporter capacity) can be measured by focal application of D-aspartate (Huda, McCrimmon and Martina, 2013; Matott, Kline and Hasser, 2017).

5.5 | Conclusion

To conclude, in this chapter we have shown that MU neuronal activity is elevated in mice fed a high fat chow for 12 hours. This excitability may be mediated by greater sensitivity of neurons to endogenous NMDA-R agonists (i.e. glutamate and D-serine) possibly due to an increase in receptor number. Secondly, we have shown that synaptic integration of vagal glutamate is impaired in NTS^{TH} neurons when astrocyte EAAT2 is pharmacologically blocked. This suggests under normal conditions astrocyte EAAT2 glutamate uptake supports synaptic transmission from vagal afferents to these satiety signalling neurons. D-serine

gliotransmission and glutamate reuptake are two mechanisms by which astrocytes, activated after intake of high fat chow, may modulate neuronal signalling in the NTS to influence satiety.

Chapter 6

Conclusion and outlook

6.1 | Key findings and contributions to scientific knowledge

This project had three main aims:

1) Identify the responses of NTS astrocytes to short and long term deviations in energy balance

2) Assess the consequence of NTS/DVC astrocyte activation on food intake and related behaviours

3) Examine potential mechanisms of astrocyte-neuron communication in the NTS with relevance to food intake

The work presented in **Chapter 3** of this thesis addressed the first aim by manipulating the diet of mice and examining NTS GFAP immunoreactivity then using this to assess changes in astrocyte cytoskeletal morphology. We found that overnight feeding of high fat chow provided the largest change in these two parameters indicating a role for these astrocytes in response to energy excess. These studies build on an established literature. Crucially we provide the first link between a wealth of literature indicating that GFAP immunoreactivity and morphology of astrocytes is highly plastic in the NTS (**Table 1.1.1**) and the understanding that the NTS mediates gut to brain satiety signalling (Grill and Hayes, 2012). We achieved this by showing that in a condition of caloric excess and stomach distension, NTS GFAP immunoreactivity is greater and the cells have a more ramified morphology, indicative of cellular activation.

The second aim was addressed principally by direct chemogenetic activation of NTS astrocytes (and those in the surrounding DVC) and monitoring behavioural parameters in freely moving mice (**Chapter 4**). We found that activation of DVC astrocytes was sufficient to significantly reduce feeding under normal conditions and when drive to eat was enhanced after a prolonged fast. This was independent

of effects on locomotion or nociception. As such we provide the first causal evidence that NTS/DVC astrocyte activation reduces food intake and indeed the first described genetic manipulation of NTS astrocytes.

Finally, with respect to aim 3, we are the first to utilise *ex vivo* NTS slices with pMEA to allow for large scale recording of population activity. We show this is elevated in mice fed a high fat chow for 12 hours. The electrophysiological studies of **Chapter 5** represent some steps towards a mechanistic understand of astrocyte-neuron communication in the NTS in the context of nutritional manipulation but the ability to draw direct conclusions from these studies is limited and future work is required.

Taken together the evidence presented in this thesis is consistent with the overarching hypothesis that NTS astrocytes are activated following food intake and that the consequence of this activation is to reduce food intake by enhancing the activity of satiety signalling neurons (**Figure 6.1.1**).

Returning to our framework for central control of food intake (**Figure 1.1.3**) we have identified NTS astrocytes as a node within this circuit likely acting to regulate vagal signals of satiety within the NTS. In our experiments, this NTS astrocyte activation was artificially driven by hM3Dq but perhaps *in vivo* it is driven by vagal glutamate or hormones released in response to gastrointestinal distention and nutrients. Support for this comes from evidence presented in this thesis (**Chapter 3**) of astrocyte activation after acute high fat chow intake. NTS astrocyte activation appears to modulate NTS satiety signalling neurons either directly (via gliotransmitters) or indirectly (by modulating glutamate transport or presynaptic transmission) and results in suppression of food intake likely *via* excitation of downstream lPBN neurons (possibly including $lPBN^{CGRP}$ neurons). This appears

to intercept ARC^{AgRP} hunger signals since we also observed this effect in mice that were refed after a 12 hour fast.

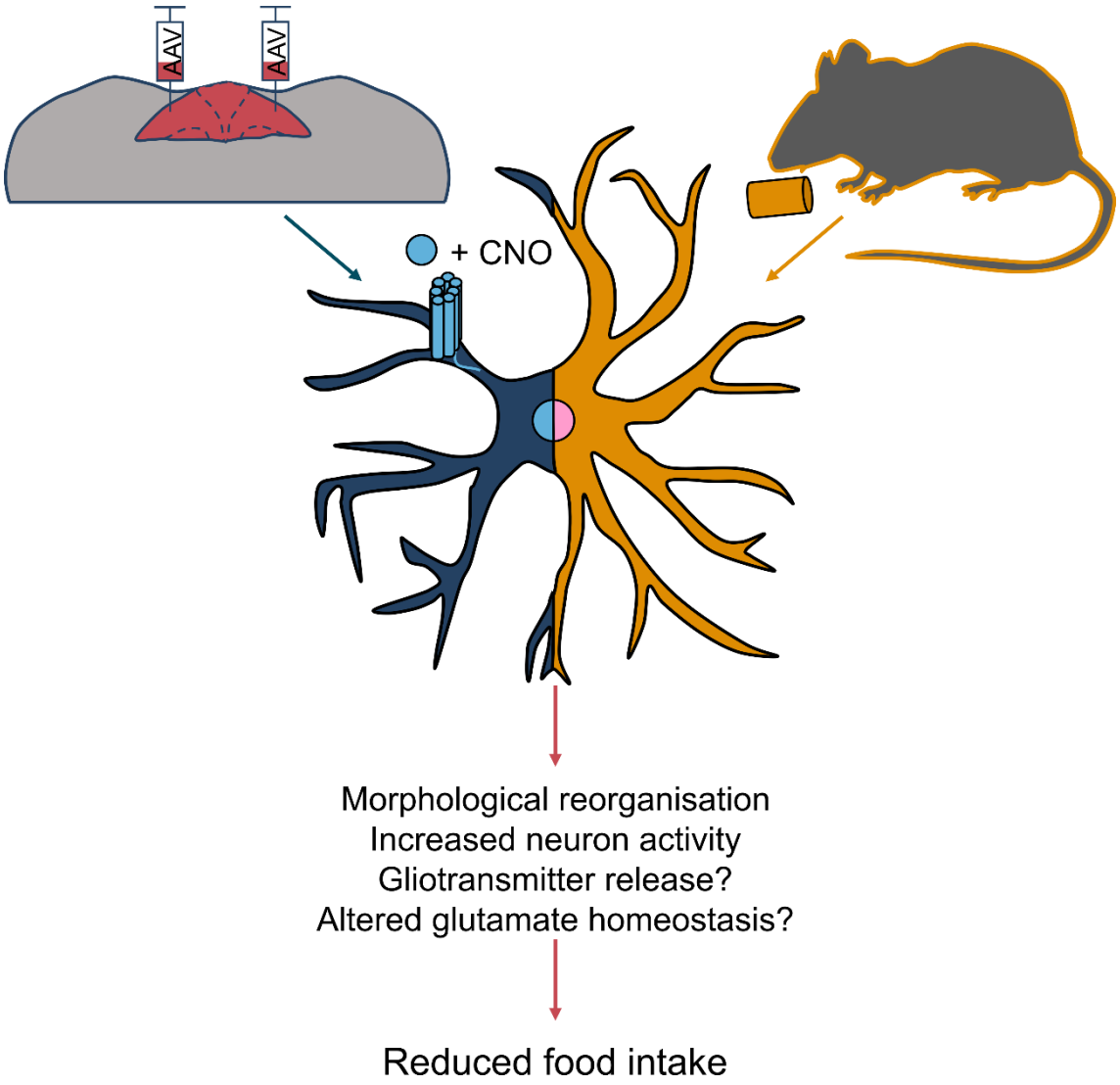

Figure 6.1.1 | Summary of the main findings of this thesis as they relate to the overarching hypothesis. Simplified diagrammatic representation of the key results. NTS astrocytes are activated by acute intake of a high fat chow or direct chemogenetic stimulation. This activation causes morphological reorganisation of GFAP-immunoreactive processes in both instances. Chemogenetic activation of NTS/DVC astrocytes decreases food intake by activation of NTS neurons. In high fat chow fed mice there is a coincident increase in NTS neuronal firing which accompanies astrocyte activation. The consequences of this are unclear but astrocytes may be activated by high fat diet in order to drive compensatory changes in food intake (i.e. decreased) by increasing the activity of neighbouring satiety signalling neurons.

6.2 | Core limitations of work

Since the specific technical limitations of each study are discussed within the results chapters, this section highlights key conceptual limitations of the work described in this thesis.

6.2.1 | Reliance on inducible manipulations to infer function

A limitation the work presented is that we have utilised an inducible manipulation in the form of hM3Dq and hM4Di in order to demonstrate the sufficiency of NTS/DVC astrocytes to modulate food intake. This provides crucial evidence to demonstrate the potential of these cells to be involved in satiety signalling and is a selective and reversible tool. However, in isolation, this approach is limited by the fact that the experimenter is inducing a specific type of activity in these cells which may not be in the range of its normal signalling repertoire. We arrive at an incomplete description of these cells since vital information is lacking on the activity throughout normal cycles of food intake and under experimental food manipulations *in vivo*. While we have been able to make inferences about this from *ex vivo* and *post-mortem* analyses, real time *in vivo* monitoring of astrocyte $[Ca^{2+}]_i$ dynamics would be needed to complete the picture.

Secondly, we demonstrated that chemogenetic activation of NTS/DVC astrocytes activated local and downstream neurons at the level of c-FOS expression. However, we did not further investigate the molecular/synaptic mechanism(s) by which chemogenetic activation of astrocytes exerts its effects on food intake. This was predominantly due to technical difficulties in preparing *ex vivo* brain slices from animals that had undergone virus injection surgery. Tissue scarring above the NTS where the dura had been removed made obtaining healthy intact slices very challenging. We were however able to examine two potential mechanisms

in non-virus injected mice using dietary manipulation and selective pharmacology (**Chapter 5**).

6.2.2 | Reliance on *ex vivo* and *post-mortem* measurements to infer real time activity

In **Chapter 3** and **Chapter 4** were able to show that in fixed brain sections from diet manipulated or chemogenetically manipulated mice that protein expression (GFAP and/or c-FOS) and cellular morphology were altered compared with control mice. From this we inferred that the cells had been activated by the experimental stimuli. However, using this indirect, end-point measure does not yield insight into the events leading up to this morphological change or its time course. For example, we are lacking information on the temporal relationship between food intake and $[Ca^{2+}]_i$ variation and the signalling events occurring between food intake and the astrocyte cytoskeletal reorganisation we observe. From the literature on ARC^{AgRP} neurons we now know that despite showing c-FOS expression and higher action potential firing in *ex vivo* slices (Takahashi and Cone, 2005), their true activity *in vivo* is far more dynamic across feeding behaviour (Betley *et al.*, 2015; Chen *et al.*, 2015; Mandelblat-Cerf *et al.*, 2015). Therefore, there is potentially a far richer picture of NTS astrocyte activity across food intake *in vivo* than our analyses permit us to measure.

Similarly, in **Chapter 5** we demonstrate that multi-unit firing activity is greater in the NTS of *ex vivo* brain slices from mice fed high fat chow for 12 hours when compared with slices from mice fed standard chow. This has the same limitations in that we are measuring an end point and the actual activity of cells in this brain region during feeding and the progression towards satiation remain unknown.

In both these analyses, since we are only able to make our measurements at a single time point we rely on a between subjects experimental design which comes at the expense of statistical power.

6.2.3 | Use of male mice

Except for the whole cell patch clamp electrophysiology recordings in **Chapter 5**, all the experiments described in this thesis were performed on male mice. In the field there is a growing appreciation of the importance of performing experiments on animals of both sexes (Karp *et al.*, 2017). Indeed, there is evidence that hypothalamic astrocytes show sexual dimorphism in rodents (Camandola, 2018) although the same has not yet been described for the NTS. In addition, there are well described sex differences in energy homeostasis in mice, including their weight gain and microglial response to feeding of high fat diet (Dorfman *et al.*, 2017; Wang and Xu, 2019). Designing experiments for both sexes however has its own complications since the experiment must be sufficiently powered to detect the main effect in the variable of interest and any potential effects of sex. As such the field has yet to reach a consensus on best practice (Karp *et al.*, 2017).

6.3 | Outstanding questions and future directions

The knowledge generated in this thesis raises some interesting points for further consideration and research. These fall into three broad categories: signal detection, signal processing and signal propagation.

6.3.1 | Signal detection: What are the cues that activate NTS astrocytes?

In **Chapter 3** we showed that intake of a high fat diet over 12 hours drove changes in protein immunoreactivity and cellular morphology indicative of cellular activation. This stimulus likely increases the release of glutamate from vagal afferents since these afferents are activated by physical distention and nutrient

content (Williams *et al.*, 2016; Bai *et al.*, 2019). Furthermore, ST stimulation causes glutamate release which is necessary for meal termination (Andresen and Yang, 1990; Treece *et al.*, 1998). In our experiment the stomachs of the high fat fed mice were fuller (by mass) and the nutritional content of the food ingested was greater. Since NTS astrocytes are closely involved in glutamatergic transmission at this synapse, both by expression of AMPA-R and EAAT2 (McDougal, Hermann and Rogers, 2011; Matott, Kline and Hasser, 2017) these nodes represent potential mechanisms by which increases in food intake may stimulate NTS astrocytes. For instance, activation of AMPA-R on NTS astrocytes by ST-stimulation causes an increase in $[Ca^{2+}]_i$, it is possible that this leads to downstream signalling that results in morphological plasticity in addition to other signalling like gliotransmission.

A second potential mechanism is the modulation of astrocyte activity by hormonal satiety signals. There is some suggestive evidence in the literature that NTS astrocytes increase $[Ca^{2+}]_i$ in response to leptin and GLP1 and that this activation modulates food intake (Reiner *et al.*, 2016; Stein *et al.*, 2020). Given that NTS^{PPG} neurons are activated by food intake and have local terminals in the NTS (Kreisler, Davis and Rinaman, 2014; Card *et al.*, 2018) it is possible that these neurons are the local source of GLP1 that act in part *via* astrocytes to inhibit food intake. Plasma leptin is elevated in mice fed a short term high fat diet (3 weeks) (Briggs *et al.*, 2014) and it is possible it is acutely elevated in our paradigm which may activate astrocyte Ca^{2+} signalling by its action at the LepRb on NTS astrocytes (Stein *et al.*, 2020). A very enticing possibility is the idea that astrocytes in fact integrate these hormonal and neuronal cues of satiety and modify their homeostatic function (e.g. glutamate reuptake) to promote a corresponding reduction of food intake.

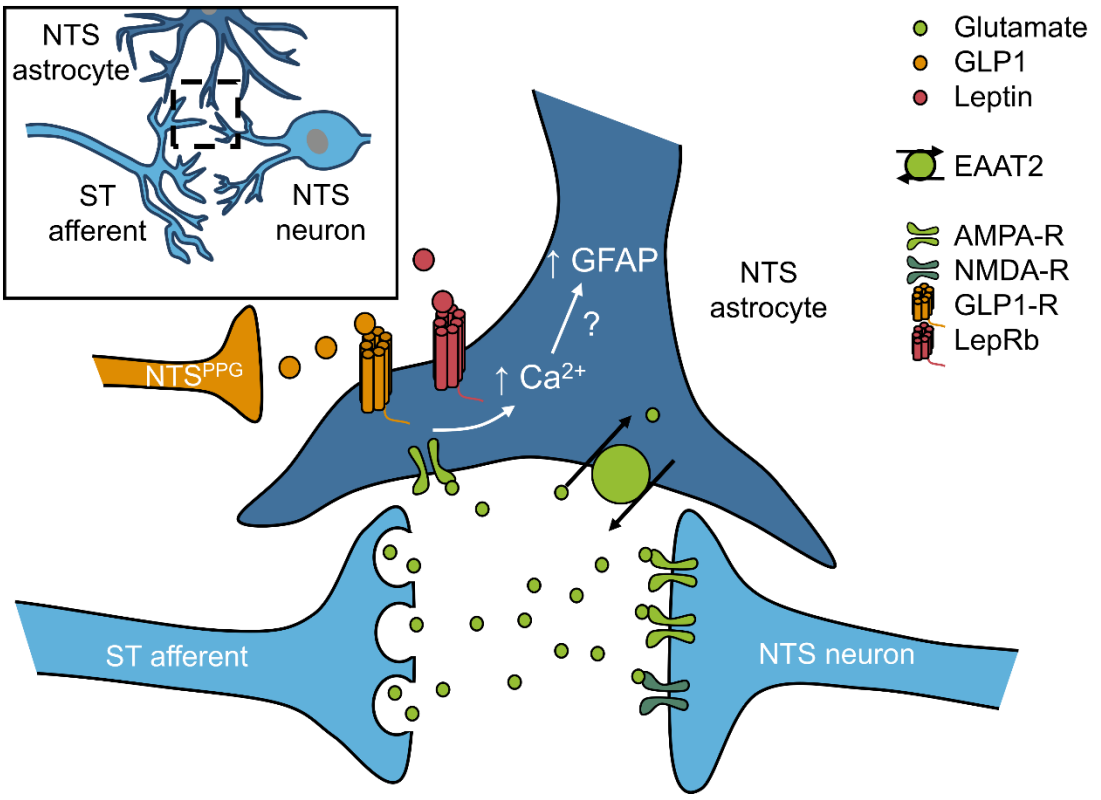

Figure 6.3.1 | Proposed signals leading to NTS astrocyte activation. Simplified diagrammatic representation of post-meal (post-prandial) satiety signals that may activate NTS astrocytes. Gut innervating vagal-sensory neurons are activated by GI stretch and nutrient content resulting in glutamate release in the NTS; this may activate AMPA-Rs on NTS astrocytes leading to $[Ca^{2+}]_i$ elevations. Secondly this may increase the activity of EAAT2, the main glutamate transporter in the NTS. NTS^{PPG} neurons are activated by food intake and may release GLP1 in the NTS, in turn this may activate GLP1-Rs on NTS astrocytes which has been shown to cause increased $[Ca^{2+}]_i$. Finally post-prandial leptin elevations may lead to greater leptin concentrations in the NTS; again activation of LepRb on NTS astrocytes leads to increased $[Ca^{2+}]_i$. While the link between $[Ca^{2+}]_i$ and morphological change is not clear it is likely that the two are related since stimulation of Gq-GPCR signalling in NTS astrocytes leads to morphological reorganisation. EAAT2 = excitatory amino acid transporter 2, GFAP = glial fibrillary acidic protein, GLP1 = glucagon-like peptide, GLP1-R =

glucagon-like peptide 1 receptor, LepRb = long form leptin receptor, NTS = nucleus of the solitary tract, PPG = preproglucagon, ST = solitary tract.

6.3.2 | Signal processing: What is the real time Ca^{2+} 'code' of NTS/DVC astrocytes and how does it relate to food intake?

As discussed above, while we were able to make inferences about astrocyte activity during feeding based on the effects of direct manipulation and end-point measures, the real time $[Ca^{2+}]_i$ dynamics of NTS/DVC astrocytes are unknown. In the literature, a series of studies have shown broad somatic $[Ca^{2+}]_i$ fluctuations in response to various pharmacological stimuli in mouse and rat brain slices indicating the presence of this signalling in NTS astrocytes (McDougal, Hermann and Rogers, 2011, 2013; Reiner *et al.*, 2016; Rogers *et al.*, 2018; Stein *et al.*, 2020) but the significance of this *in vivo* is not known. Future studies may make use of coincident advances in genetically encoded Ca^{2+} indicators (e.g. GCaMP) and deep-brain fluorescence recording (e.g. microendoscopy or fibre photometry) to record NTS/DVC astrocyte $[Ca^{2+}]_i$ dynamics *in vivo* in awake behaving mice (King *et al.*, 2020). As has been shown for ARC^{AgRP} neurons, this information is very valuable for understanding the functions of populations of cells as they relate to feeding behaviour (Betley *et al.*, 2015; Chen *et al.*, 2015).

6.3.3 | Signal propagation: How do astrocytes modulate vagal and NTS signalling to reduce food intake?

In **Chapter 4** we demonstrated that chemogenetic activation of DVC astrocytes reduced food intake and coincidentally induced activation of local neurons and downstream satiety circuits. In **Chapter 5** we began to investigate mechanisms of astrocyte neuromodulation using diet manipulation and pharmacology. However, it remains to be demonstrated how exactly activation of DVC astrocytes stimulates satiety signalling NTS neurons.

As discussed in detail in the individual chapter discussions, altered glial morphology changes the ability of astrocytes to perform their homeostatic

functions that maintain the synaptic microenvironment (Theodosis *et al.*, 2004). Thus, in conditions where astrocyte morphology is altered (high fat chow intake and chemogenetic activation in our studies), it is possible that homeostatic functions of astrocytes are disrupted. This could include modulation of glutamate availability at the synapse by altering the proximity of the glutamate transporter EAAT2 to synapses (Oliet, Piet and Poulain, 2001). In addition, the physical proximity of astrocytes to synapses can modulate diffusion of neuromodulators by volume transmission. Some of these modulators e.g. serotonin (5-HT) and acetylcholine, alter synaptic transmission across the ST→NTS synapse, ultimately acting to increase neuronal activity and suppress food intake (Cui, Roberts, Zhao, Zhu, *et al.*, 2012; D'Agostino *et al.*, 2018; Page, Zhu and Appleyard, 2018).

In addition to these homeostatic functions, astrocytes have been demonstrated to release gliotransmitters that modulate both the firing of postsynaptic neurons and presynaptic neurotransmitter release (Araque *et al.*, 2014). We have shown that NTS neurons are sensitive to D-serine and that this sensitivity may be modulated by nutritional state (**Chapter 5**). It is possible that activated astrocytes amplify glutamatergic vagal signals by releasing D-serine to increase postsynaptic excitability, a process well described in the CA1 region of the hippocampus (Papouin, Dunphy, *et al.*, 2017). Secondly, astrocyte-derived ATP and adenosine have been implicated in increasing neuronal excitability and supporting synaptic transmission in the NTS (Accorsi-Mendonça *et al.*, 2013; Rogers, Ritter and Hermann, 2016; Rogers *et al.*, 2018; Mastitskaya *et al.*, 2019). These purines are also candidate signalling molecules for mediating the effect of astrocyte activation on neighbouring neurons and downstream effects on food intake. These factors (homeostatic functions and gliotransmission) may work in

concert or independently of one another to exert the excitatory effect of astrocyte activation on neighbouring neurons (**Figure 6.3.2**).

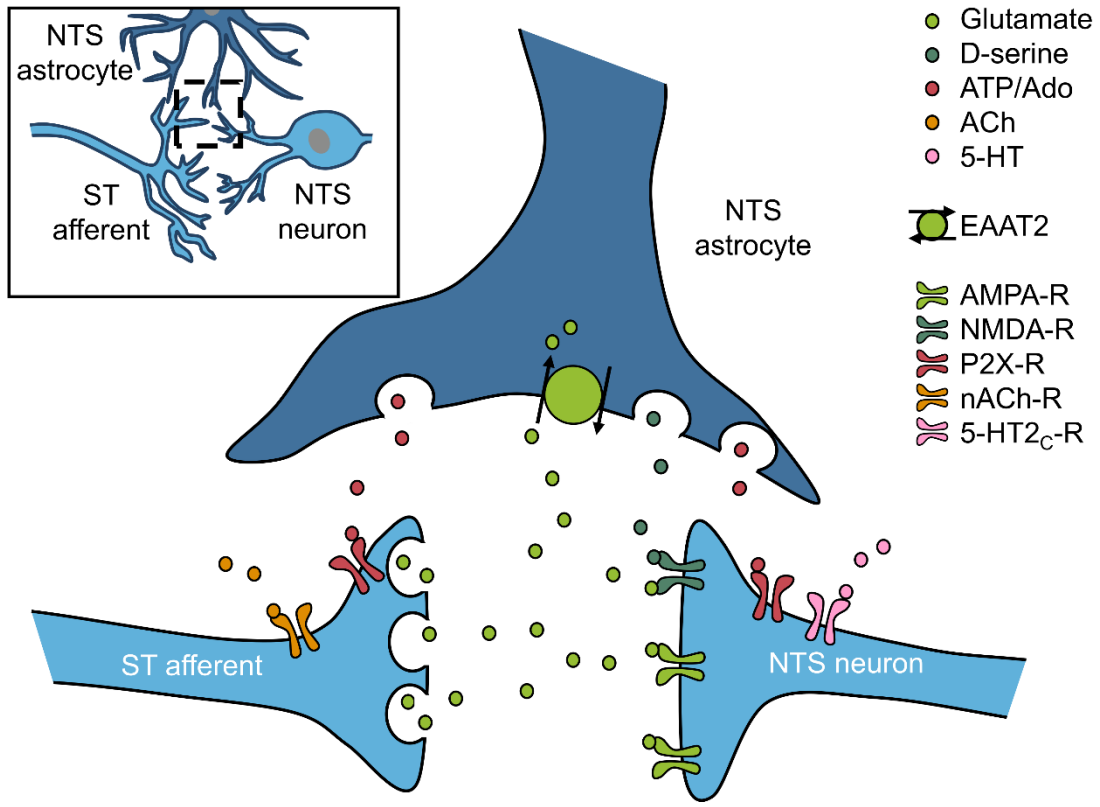

Figure 6.3.2 | Potential mechanisms of astrocyte-neuron communication in the NTS. Simplified diagrammatic representation of mechanisms by which astrocytes may excite neurons. By modulating their physical proximity to the synapse astrocyte glutamate transport can be increased or reduced. This may lead to greater levels of ambient glutamate which increases postsynaptic excitability. Reduced astrocyte ensheathment of synapses may be permissive for volume transmission of neuromodulators. Both ACh and 5-HT increase neuronal activity in the NTS by pre- and post-synaptic mechanisms, respectively, which reduces food intake. Astrocytes may also modulate neuronal excitability by the release of gliotransmitters. Astrocyte-derived D-serine could gate the excitability of post-synaptic NMDA-Rs. ATP released from astrocytes or its degraded form adenosine have been shown to mediate modulation of NTS neurons by P2X-R activation. 5-HT = serotonin, 5-HT_{2C}-R = serotonin receptor 2C, ACh = acetylcholine, Ado = adenosine, ATP = adenosine triphosphate, EAAT-2 =

excitatory amino acid transporter 2, nACh-R = nicotinic acetylcholine receptor, NTS = nucleus of the solitary tract, ST = solitary tract.

6.3.4 | Outstanding conceptual questions

In the field of astrocyte research it is still not definitively known how much of the documented astrocyte responses are due to true information processing and signal integration (Bazargani and Attwell, 2017) or whether these cells are simply responding to elevated metabolic demands of active local neurons (Xanthos and Sandkühler, 2014). For most of this discussion we have taken the former view driven by some key pieces of evidence. Firstly, astrocytes can show distinct, sometimes desynchronised, patterns of activity from neighbouring neurons (Volterra, Liaudet and Savtchouk, 2014; Bindocci *et al.*, 2017). In some experimental preparations, astrocyte detection of a signal precedes that of neurons at least at the level of $[Ca^{2+}]_i$ response (Rogers, Ritter and Hermann, 2016; Rogers *et al.*, 2018). Secondly, the blockade of D-serine release from astrocytes (a signalling molecule, not a metabolic factor) disrupts information processing and memory (Papouin, Dunphy, *et al.*, 2017). Taken together these observations suggest that astrocyte activity reflects more than just the metabolic demands of neighbouring neurons.

Neurons are understood to be a very heterogeneous population of cells showing an extraordinary range of diversity across the nervous system. Neurons are classified based on their morphology, gene expression, neurotransmitters, connectivity and electrophysiology (Luo, Callaway and Svoboda, 2008). A brain region such as the cortex, which obeys a very ordered circuit organisation has 10 major neuronal cell types, which can be further subdivided into classes (Harris and Shepherd, 2015). In contrast, there are widely considered to be two principal broad classes of astrocyte determined by their location alone; those in the white matter and those in the grey (Miller and Raff, 1984). Research is beginning to show that this is likely a massive underestimation of astrocyte diversity. It appears

that between brain regions (Chai *et al.*, 2017; Morel *et al.*, 2017), within brain regions (Lanjakornsiripan *et al.*, 2018; Miller *et al.*, 2019; Batiuk *et al.*, 2020; Bayraktar *et al.*, 2020) and even within individual circuits (Martín *et al.*, 2015), astrocytes are heterogeneous to a level not previously appreciated. This will surely be an area of growing interest and future research will hopefully investigate what makes NTS astrocytes different from their neighbours in other brain nuclei and each other.

6.4 | Conclusion

This study has addressed key questions in the field regarding NTS astrocytes and food intake by demonstrating that they respond to increases in food intake and that their chemogenetic activation reduces feeding by excitation of appetite supressing neuronal circuits. This suggests that in normal food intake, NTS astrocytes are recruited following a meal possibly, *via* vagal glutamate, circulating leptin, local GLP1 or some combination of these and other as yet unknown factors. This activation appears to reduce food intake by increasing the activity of NTS neurons which suppress appetite, either by direct excitation and/or modulation of vagal afferent input. Future work to better understand how real-time astrocyte activity relates to food intake will hopefully elucidate the details of this astrocyte activation, while detailed electrophysiological studies could better identify mechanisms of astrocyte-neuronal communication.

References

Accorsi-Mendonca, D. *et al.* (2015) ‘Enhanced firing in NTS induced by short-term sustained hypoxia is modulated by glia-neuron interaction’, *Journal of Neuroscience*, 35(17), pp. 6903–6917. doi: 10.1523/JNEUROSCI.4598-14.2015.

Accorsi-Mendonça, D. *et al.* (2013) ‘Glial cells modulate the synaptic transmission of NTS neurons sending projections to ventral medulla of Wistar rats’, *Physiological Reports*, 1(4), pp. 1–13. doi: 10.1002/phy2.80.

Accorsi-Mendonça, D., Bonagamba, L. G. H. and Machado, B. H. (2019) ‘Astrocytic modulation of glutamatergic synaptic transmission is reduced in NTS of rats submitted to short-term sustained hypoxia’, *Journal of Neurophysiology*, 121(5), pp. 1822–1830. doi: 10.1152/jn.00279.2018.

Accorsi-Mendonça, D. and Machado, B. H. (2013) ‘Synaptic transmission of baro- and chemoreceptors afferents in the NTS second order neurons’, *Autonomic Neuroscience: Basic and Clinical*, 175(1–2), pp. 3–8. doi: 10.1016/j.autneu.2012.12.002.

Adamantidis, A. *et al.* (2015) ‘Optogenetics: 10 years after ChR2 in neurons - views from the community’, *Nature Neuroscience*, 18(9), pp. 1202–1212. doi: 10.1038/nn.4091.

Adamsky, A. *et al.* (2018) ‘Astrocytic activation generates de novo neuronal potentiation and memory enhancement’, *Cell*, 174(1), pp. 59–71. doi: 10.1016/j.cell.2018.05.002.

Ahlma, R. S. *et al.* (1996) ‘Role of leptin in the neuroendocrine response to fasting’, *Nature*, 382(6588), pp. 250–252. doi: 10.1038/382250a0.

Aklan, I. *et al.* (2020) ‘NTS catecholamine neurons mediate hypoglycemic hunger via medial hypothalamic feeding pathways’, *Cell Metabolism*, 31, pp. 313–326. doi: 10.1016/j.cmet.2019.11.016.

Alhadeff, A. L. *et al.* (2017) ‘Excitatory hindbrain–forebrain communication is required for cisplatin-induced anorexia and weight loss’, *Journal of Neuroscience*, 37(2), pp. 362–370. doi: 10.1523/JNEUROSCI.2714-16.2017.

Alhadeff, A. L. *et al.* (2018) ‘A neural circuit for the suppression of pain by a competing need state’, *Cell*, 173(1), pp. 140–152. doi:

10.1016/j.cell.2018.02.057.

Alhadeff, A. L. *et al.* (2019a) 'Natural and drug rewards engage distinct pathways that converge on coordinated hypothalamic and reward circuits', *Neuron*. Elsevier Inc., 103(5), pp. 891–908. doi: 10.1016/j.neuron.2019.05.050.

Alhadeff, A. L. *et al.* (2019b) 'Natural and Drug Rewards Engage Distinct Pathways that Converge on Coordinated Hypothalamic and Reward Circuits', *Neuron*. Elsevier Inc., 103(5), pp. 891-908.e6. doi: 10.1016/j.neuron.2019.05.050.

Alhadeff, A. L., Rupprecht, L. E. and Hayes, M. R. (2012) 'GLP-1 neurons in the nucleus of the solitary tract project directly to the ventral tegmental area and nucleus accumbens to control for food intake', *Endocrinology*, 153(2), pp. 647–658. doi: 10.1210/en.2011-1443.

Alonso, E. *et al.* (2007) 'Yohimbine prevents morphine-induced changes of glial fibrillary acidic protein in brainstem and a2-adrenoceptor gene expression in hippocampus', *Neuroscience Letters*, 412(2), pp. 163–167. doi: 10.1016/j.neulet.2006.11.002.

Andermann, M. L. and Lowell, B. B. (2017) 'Toward a Wiring Diagram Understanding of Appetite Control', *Neuron*, 95(4), pp. 757–778. doi: 10.1016/j.neuron.2017.06.014.

Andresen, M. C. and Yang, M. (1990) 'Non-NMDA receptors mediate sensory afferent synaptic transmission in medial nucleus tractus solitarius', *American Journal of Physiology - Heart and Circulatory Physiology*, 259(4 28-4). doi: 10.1152/ajpheart.1990.259.4.h1307.

Aponte, Y., Atasoy, D. and Sternson, S. M. (2011) 'AGRP neurons are sufficient to orchestrate feeding behavior rapidly and without training.', *Nature Neuroscience*, 14(3), pp. 351–355. doi: 10.1038/nn.2739.

Appleyard, S. M. *et al.* (2005) 'Proopiomelanocortin neurons in nucleus tractus solitarius are activated by visceral afferents: Regulation by cholecystokinin and opioids', *Journal of Neuroscience*, 25(14), pp. 3578–3585. doi: 10.1523/JNEUROSCI.4177-04.2005.

Appleyard, S. M. *et al.* (2007) 'Visceral afferents directly activate catecholamine

neurons in the solitary tract nucleus', *Journal of Neuroscience*, 27(48), pp. 13292–13302. doi: 10.1523/JNEUROSCI.3502-07.2007.

Araneda, S. *et al.* (2008) 'VEGF overexpression in the astroglial cells of rat brainstem following ozone exposure', *NeuroToxicology*, 29(6), pp. 920–927. doi: 10.1016/j.neuro.2008.09.006.

Araque, A. *et al.* (1999) 'Tripartite synapses : glia , the unacknowledged partner', *Trends in Neurosciences*, 22(5), pp. 208–214.

Araque, A. *et al.* (2002) 'Synaptically released acetylcholine evokes Ca2+ elevations in astrocytes in hippocampal slices', *Journal of Neuroscience*, 22(7), pp. 2443–2450. doi: 10.1523/jneurosci.22-07-02443.2002.

Araque, A. *et al.* (2014) 'Gliotransmitters travel in time and space', *Neuron*, 81(4), pp. 728–739. doi: 10.1016/j.neuron.2014.02.007.

Ariyasu, H. *et al.* (2001) 'Stomach is a major source of circulating ghrelin, and feeding state determines plasma ghrelin-like immunoreactivity levels in humans', *Journal of Clinical Endocrinology and Metabolism*, 86(10), pp. 4753–4758. doi: 10.1210/jcem.86.10.7885.

Armbruster, B. N. *et al.* (2007) 'Evolving the lock to fit the key to create a family of G protein-coupled receptors potently activated by an inert ligand', *Proceedings of the National Academy of Sciences of the United States of America*, 104(12), pp. 5163–5168. doi: 10.1073/pnas.0700293104.

Atasoy, D. *et al.* (2008) 'A FLEX switch targets Channelrhodopsin-2 to multiple cell types for imaging and long-range circuit mapping.', *Journal of Neuroscience*, 28(28), pp. 7025–7030. doi: 10.1523/JNEUROSCI.1954-08.2008.

Atasoy, D. *et al.* (2012) 'Deconstruction of a neural circuit for hunger', *Nature*, 488, pp. 172–177. doi: 10.1038/nature11270.

Ayala, J. E. *et al.* (2010) 'Standard operating procedures for describing and performing metabolic tests of glucose homeostasis in mice', *DMM Disease Models and Mechanisms*, 3(9–10), pp. 525–534. doi: 10.1242/dmm.006239.

Bagnol, D. *et al.* (1999) 'Anatomy of an endogenous antagonist: relationship between Agouti-related protein and proopiomelanocortin in brain.', *Journal of*

Neuroscience, 19(18), pp. 1–7. doi: 10.1523/jneurosci.19-18-j0004.1999.

Bai, L. *et al.* (2019) 'Genetic identification of vagal afferents that control hunger', *Cell*, 179, pp. 1129–1143. doi: 10.1016/j.cell.2019.10.031.

Bailey, T. W. *et al.* (2008) 'Organization and properties of GABAergic neurons in solitary tract nucleus (NTS)', *Journal of Neurophysiology*, 99(4), pp. 1712–1722. doi: 10.1152/jn.00038.2008.

Bak, L. K., Schousboe, A. and Waagepetersen, H. S. (2006) 'The glutamate/GABA-glutamine cycle: Aspects of transport, neurotransmitter homeostasis and ammonia transfer', *Journal of Neurochemistry*, 98(3), pp. 641–653. doi: 10.1111/j.1471-4159.2006.03913.x.

Bak, L. K. and Walls, A. B. (2018) 'CrossTalk opposing view: lack of evidence supporting an astrocyte-to-neuron lactate shuttle coupling neuronal activity to glucose utilisation in the brain', *Journal of Physiology*, 596(3), pp. 351–353. doi: 10.1113/JP274945.

Balland, E. and Cowley, M. A. (2017) 'Short-term high-fat diet increases the presence of astrocytes in the hypothalamus of C57BL6 mice without altering leptin sensitivity', *Journal of Neuroendocrinology*, 29(10), pp. 1–7. doi: 10.1111/jne.12504.

Balthasar, N. *et al.* (2004) 'Leptin receptor signaling in POMC neurons is required for normal body weight homeostasis', *Neuron*, 42(6), pp. 983–991. doi: 10.1016/j.neuron.2004.06.004.

Balthasar, N. *et al.* (2005) 'Divergence of melanocortin pathways in the control of food intake and energy expenditure', *Cell*, 123(3), pp. 493–505. doi: 10.1016/j.cell.2005.08.035.

Bang, J., Kim, H. Y. and Lee, H. (2016) 'Optogenetic and chemogenetic approaches for studying astrocytes and gliotransmitters', *Experimental Neurobiology*, 25(5), pp. 205–221. doi: 10.5607/en.2016.25.5.205.

Barros, L. F. and Weber, B. (2018) 'CrossTalk proposal: an important astrocyte-to-neuron lactate shuttle couples neuronal activity to glucose utilisation in the brain', *Journal of Physiology*, 596(3), pp. 347–350. doi: 10.1113/JP274944.

Bartel, D. L. (2012) 'Glial responses after chorda tympani nerve injury', *Journal*

of Comparative Neurology, 520(12), pp. 2712–2729. doi: 10.1002/cne.23069.

Batiuk, M. Y. *et al.* (2020) 'Identification of region-specific astrocyte subtypes at single cell resolution', *Nature Communications*, 11, pp. 1–15. doi: 10.1038/s41467-019-14198-8.

Bayraktar, O. A. *et al.* (2020) 'Astrocyte layers in the mammalian cerebral cortex revealed by a single-cell in situ transcriptomic map', *Nature Neuroscience*. doi: 10.1038/s41593-020-0602-1.

Bazargani, N. and Attwell, D. (2016) 'Astrocyte calcium signaling: the third wave.', *Nature Neuroscience*, 19(2), pp. 182–9. doi: 10.1038/nn.4201.

Bazargani, N. and Attwell, D. (2017) 'Amines, astrocytes, and arousal', *Neuron*, 94(2), pp. 228–231. doi: 10.1016/j.neuron.2017.03.035.

Bélanger, M., Allaman, I. and Magistretti, P. J. (2011) 'Brain energy metabolism: Focus on Astrocyte-neuron metabolic cooperation', *Cell Metabolism*, 14(6), pp. 724–738. doi: 10.1016/j.cmet.2011.08.016.

van den Berg, C. J. and Garfinkel, D. (1971) 'A stimulation study of brain compartments. Metabolism of glutamate and related substances in mouse brain.', *The Biochemical Journal*, 123(2), pp. 211–218. doi: 10.1042/bj1230211.

Berkseth, K. E. *et al.* (2014) 'Hypothalamic gliosis associated with high-fat diet feeding is reversible in mice: A combined immunohistochemical and magnetic resonance imaging study', *Endocrinology*, 155(8), pp. 2858–2867. doi: 10.1210/en.2014-1121.

Berthoud, H. R. and Neuhuber, W. L. (2000) 'Functional and chemical anatomy of the afferent vagal system', *Autonomic Neuroscience: Basic and Clinical*, 85(1–3), pp. 1–17. doi: 10.1016/S1566-0702(00)00215-0.

Betley, J. N. *et al.* (2013) 'Parallel, redundant circuit organization for homeostatic control of feeding behavior', *Cell*, 155(6), pp. 1337–1350. doi: 10.1016/j.cell.2013.11.002.

Betley, J. N. *et al.* (2015) 'Neurons for hunger and thirst transmit a negative-valence teaching signal', *Nature*, 521(7551), pp. 180–185. doi: 10.1038/nature14416.

Beutler, L. R. *et al.* (2017) 'Dynamics of gut-brain communication underlying

hunger', *Neuron*, 96(2), pp. 461–475. doi: 10.1016/j.neuron.2017.09.043.

Bhandare, A., Huckstepp, R. and Dale, N. (2019) 'Analyzing the brainstem circuits for respiratory chemosensitivity in freely moving mice', *bioRxiv*. doi: 10.1017/CBO9781107415324.004.

Bindocci, E. *et al.* (2017) 'Three-dimensional Ca 2+ imaging advances understanding of astrocyte biology', *Science*, 356(6339). doi: 10.1126/science.aai8185.

Biondo, B. *et al.* (2004) 'Glial and neuronal alterations in the nucleus tractus solitarii of sudden infant death syndrome victims', *Acta Neuropathologica*, 108(4), pp. 309–318. doi: 10.1007/s00401-004-0895-2.

Blouet, C. *et al.* (2009) 'Mediobasal hypothalamic leucine sensing regulates food intake through activation of a hypothalamus-brainstem circuit', *Journal of Neuroscience*, 29(26), pp. 8302–8311. doi: 10.1523/JNEUROSCI.1668-09.2009.

Blouet, C. and Schwartz, G. J. (2012) 'Brainstem nutrient sensing in the nucleus of the solitary tract inhibits feeding', *Cell Metabolism*, 16(5), pp. 579–587. doi: 10.1016/j.cmet.2012.10.003.

Bonder, D. E. and McCarthy, K. D. (2014) 'Astrocytic Gq-GPCR-linked IP3R-dependent Ca2+ signaling does not mediate neurovascular coupling in mouse visual cortex in vivo', *Journal of Neuroscience*, 34(39), pp. 13139–13150. doi: 10.1523/JNEUROSCI.2591-14.2014.

Bouyakdan, K. *et al.* (2019) 'The gliotransmitter ACBP controls feeding and energy homeostasis via the melanocortin system', *Journal of Clinical Investigation*, 129(6), pp. 2417–2430. doi: 10.1172/JCI123454.

Boychuk, C. R. *et al.* (2015) 'Glucose sensing by GABAergic neurons in the mouse nucleus tractus solitarii', *Journal of Neurophysiology*, 114(2), pp. 999–1007. doi: 10.1152/jn.00310.2015.

Boychuk, C. R. *et al.* (2019) 'A hindbrain inhibitory microcircuit mediates vagally-coordinated glucose regulation', *Scientific Reports*, 9(1), p. 2722. doi: 10.1038/s41598-019-39490-x.

Boyden, E. S. *et al.* (2005) 'Millisecond-timescale, genetically targeted optical

control of neural activity.', *Nature Neuroscience*, 8(9), pp. 1263–8. doi: 10.1038/nn1525.

Boyden, E. S. (2011) 'A history of optogenetics: The development of tools for controlling brain circuits with light', *F1000 Biology Reports*, 3(1), pp. 1–12. doi: 10.3410/B3-11.

Briggs, D. I. *et al.* (2014) 'Evidence that diet-induced hyperleptinemia, but not hypothalamic gliosis, causes ghrelin resistance in NPY/AgRP neurons of male mice', *Endocrinology*, 155(7), pp. 2411–2422. doi: 10.1210/en.2013-1861.

Brobeck, J. R. (1946) 'Mechanism of the Development of Obesity in Animals with Hypothalamic Lesions', *Physiological Reviews*, 26(4), pp. 541–559.

Buckman, L. B. *et al.* (2013) 'Regional astrogliosis in the mouse hypothalamus in response to obesity', *Journal of Comparative Neurology*, 521(6), pp. 1322–1333. doi: 10.1002/cne.23233.

Buckman, L. B. *et al.* (2015) 'Evidence for a novel functional role of astrocytes in the acute homeostatic response to high-fat diet intake in mice', *Molecular Metabolism*, 4(1), pp. 58–63. doi: 10.1016/j.molmet.2014.10.001.

Bull, C. *et al.* (2014) 'Rat nucleus accumbens core astrocytes modulate reward and the motivation to self-administer ethanol after abstinence.', *Neuropsychopharmacology*, 39, pp. 2835–2845. doi: 10.1038/npp.2014.135.

Burnett, C. J. *et al.* (2016) 'Hunger-Driven Motivational State Competition', *Neuron*, 92, pp. 187–201. doi: 10.1016/j.neuron.2016.08.032.

Burnett, C. J. *et al.* (2019) 'Need-based prioritization of behavior', *eLife*, 8, pp. 1–26. doi: 10.7554/eLife.44527.

Buzsáki, G. and Mizuseki, K. (2014) 'The log-dynamic brain: How skewed distributions affect network operations', *Nature Reviews Neuroscience*, 15(4), pp. 264–278. doi: 10.1038/nrn3687.

Camandola, S. (2018) 'Astrocytes, emerging stars of energy homeostasis', *Cell Stress*, 2(10), pp. 246–252. doi: 10.15698/cst2018.10.157.

Campos, C. A. *et al.* (2016) 'Parabrachial CGRP neurons control meal termination', *Cell Metabolism*, 23(5), pp. 811–820. doi: 10.1016/j.cmet.2016.04.006.

Campos, C. A. *et al.* (2018) ‘Encoding of danger by parabrachial CGRP neurons’, *Nature*, 555(7698), pp. 617–622. doi: 10.1038/nature25511.

Card, J. P. *et al.* (2018) ‘GLP-1 neurons form a local synaptic circuit within the rodent nucleus of the solitary tract’, *Journal of Comparative Neurology*, pp. 2149–2164. doi: 10.1002/cne.24482.

Cardin, J. A. *et al.* (2009) ‘Driving fast-spiking cells induces gamma rhythm and controls sensory responses’, *Nature*, 459(7247), pp. 663–667. doi: 10.1038/nature08002.

Carter, M. E. *et al.* (2013) ‘Genetic identification of a neural circuit that suppresses appetite.’, *Nature*, 503, pp. 111–114. doi: 10.1038/nature12596.

Carter, M. E., Han, S. and Palmiter, R. D. (2015) ‘Parabrachial calcitonin gene-related peptide neurons mediate conditioned taste aversion’, *Journal of Neuroscience*, 35(11), pp. 4582–4586. doi: 10.1523/JNEUROSCI.3729-14.2015.

Cavanaugh, A. R., Schwartz, G. J. and Blouet, C. (2015) ‘High-fat feeding impairs nutrient sensing and gut brain integration in the caudomedial nucleus of the solitary tract in mice’, *PLoS ONE*, 10(3), pp. 1–12. doi: 10.1371/journal.pone.0118888.

Cerritelli, S. *et al.* (2016) ‘Activation of brainstem proopiomelanocortin neurons produces opioidergic analgesia, bradycardia and bradypnoea’, *PLoS ONE*, 11(4), pp. 1–26. doi: 10.1371/journal.pone.0153187.

Chai, H. *et al.* (2017) ‘Neural circuit-specialized astrocytes: Transcriptomic, proteomic, morphological, and functional evidence’, *Neuron*, 95(3), pp. 531–549. doi: 10.1016/j.neuron.2017.06.029.

Chambers, A. P., Sandoval, D. A. and Seeley, R. J. (2013) ‘Integration of satiety signals by the central nervous system’, *Current Biology*, 23(9), pp. 379–388. doi: 10.1016/j.cub.2013.03.020.

Chang, R. B. *et al.* (2015) ‘Vagal sensory neuron subtypes that differentially control breathing’, *Cell*, 161(3), pp. 622–633. doi: 10.1016/j.cell.2015.03.022.

Chen, N. *et al.* (2016) ‘Direct modulation of GFAP-expressing glia in the arcuate nucleus bi-directionally regulates feeding’, *eLife*, 5, pp. 1–21. doi:

10.7554/eLife.18716.

Chen, Y. *et al.* (2015) 'Sensory detection of food rapidly modulates arcuate feeding circuits', *Cell*, 160(5), pp. 829–841. doi: 10.1016/j.cell.2015.01.033.

Chen, Y. *et al.* (2016) 'Hunger neurons drive feeding through a sustained, positive reinforcement signal', *eLife*, 5, p. e18640. doi: 10.7554/eLife.18640.

Cheng, W. *et al.* (2020) 'Calcitonin receptor neurons in the mouse nucleus tractus solitarius control energy balance via the non-aversive suppression of feeding', *Cell Metabolism*. Elsevier Inc., 31(2), pp. 301–312. doi: 10.1016/j.cmet.2019.12.012.

Cheunsuang, O. and Morris, R. (2005) 'Astrocytes in the arcuate nucleus and median eminence that take up a fluorescent dye from the circulation express leptin receptors and neuropeptide Y Y1 receptors', *Glia*, 52(3), pp. 228–233. doi: 10.1002/glia.20239.

Chih, C. P., Lipton, P. and Roberts, E. L. (2001) 'Do active cerebral neurons really use lactate rather than glucose?', *Trends in Neurosciences*, 24(10), pp. 573–578. doi: 10.1016/S0166-2236(00)01920-2.

Chounlamountry, K. *et al.* (2015) 'Remodeling of glial coverage of glutamatergic synapses in the rat nucleus tractus solitarii after ozone inhalation', *Journal of Neurochemistry*, 134(5), pp. 857–864. doi: 10.1111/jnc.13193.

Chounlamountry, K. and Kessler, J. P. (2011) 'The ultrastructure of perisynaptic glia in the nucleus tractus solitarii of the adult rat: Comparison between single synapses and multisynaptic arrangements', *Glia*, 59(4), pp. 655–663. doi: 10.1002/glia.21135.

Coles, J. A. and Poulain, D. A. (1991) 'Extracellular K+ in the supraoptic nucleus of the rat during reflex bursting activity by oxytocin neurones.', *The Journal of Physiology*, 439(1), pp. 383–409. doi: 10.1113/jphysiol.1991.sp018672.

Cone, R. D. (2005) 'Anatomy and regulation of the central melanocortin system.', *Nature Neuroscience*, 8(5), pp. 571–578. doi: 10.1038/nn1455.

Cork, S. C. *et al.* (2015) 'Distribution and characterisation of Glucagon-like peptide-1 receptor expressing cells in the mouse brain', *Molecular Metabolism*,

4(10), pp. 718–731. doi: 10.1016/j.molmet.2015.07.008.

Cork, S. C. (2018) ‘The role of the vagus nerve in appetite control: Implications for the pathogenesis of obesity’, *Journal of Neuroendocrinology*, 30(11), pp. 1–10. doi: 10.1111/jne.12643.

Cornell-Bell, A. H. *et al.* (1990) ‘Glutamate induces calcium waves in cultured astrocytes: Long-range glial signaling’, *Science*, 247(24), pp. 2–5.

Covelo, A. and Araque, A. (2018) ‘Neuronal activity determines distinct gliotransmitter release from a single astrocyte’, *eLife*, 7, pp. 1–19. doi: 10.7554/eLife.32237.

Cowley, M. A. *et al.* (1999) ‘Integration of NPY, AgRP, and melanocortin signals in the hypothalamic paraventricular nucleus: Evidence of a cellular basis for the adipostat’, *Neuron*, 24(1), pp. 155–163. doi: 10.1016/S0896-6273(00)80829-6.

Cowley, M. A. *et al.* (2001) ‘Leptin activates anorexigenic POMC neurons through a neural network in the arcuate nucleus’, *Nature*, 411(6836), pp. 480–484. doi: 10.1038/35078085.

Cowley, M. A. *et al.* (2003) ‘The distribution and mechanism of action of ghrelin in the CNS demonstrates a novel hypothalamic circuit regulating energy homeostasis’, *Neuron*, 37(4), pp. 649–661. doi: 10.1016/S0896-6273(03)00063-1.

Cui, R. J., Roberts, B. L., Zhao, H., Andresen, M. C., *et al.* (2012) ‘Opioids inhibit visceral afferent activation of catecholamine neurons in the solitary tract nucleus’, *Neuroscience*, 222, pp. 181–190. doi: 10.1016/j.neuroscience.2012.07.010.

Cui, R. J., Roberts, B. L., Zhao, H., Zhu, M., *et al.* (2012) ‘Serotonin activates catecholamine neurons in the solitary tract nucleus by increasing spontaneous glutamate inputs’, *Journal of Neuroscience*, 32(46), pp. 16530–16538. doi: 10.1523/jneurosci.1372-12.2012.

Cui, R. J., Li, X. and Appleyard, S. M. (2011) ‘Ghrelin inhibits visceral afferent activation of catecholamine neurons in the solitary tract nucleus’, *Journal of Neuroscience*, 31(9), pp. 3484–3492. doi: 10.1523/jneurosci.3187-10.2011.

Cummings, D. E. *et al.* (2001) ‘A preprandila rise in plasma ghrelin levels

suggests a role in meal initiation in humans', *Diabetes*, 50, pp. 1714–1719. doi: 10.1016/s0002-9378(37)90859-7.

D'Agostino, G. *et al.* (2016) 'Appetite controlled by a cholecystokinin nucleus of the solitary tract to hypothalamus neurocircuit', *eLife*, 5, pp. 1–15. doi: 10.7554/eLife.12225.

D'Agostino, G. *et al.* (2018) 'Nucleus of the solitary tract serotonin 5-HT 2C receptors modulate food intake', *Cell Metabolism*, 28(4), pp. 619–630. doi: 10.1016/j.cmet.2018.07.017.

Dallaporta, M. *et al.* (2010) 'Glial cells of the nucleus tractus solitarius as partners of the dorsal hindbrain regulation of energy balance: A proposal for a working hypothesis', *Brain Research*, 1350, pp. 35–42. doi: 10.1016/j.brainres.2010.04.025.

Date, Y. *et al.* (2002) 'The role of the gastric afferent vagal nerve in Ghrelin-induced feeding and growth hormone secretion in rats', *Gastroenterology*, 123(4), pp. 1120–1128. doi: 10.1053/gast.2002.35954.

Deisseroth, K. (2015) 'Optogenetics: 10 years of microbial opsins in neuroscience', *Nature Neuroscience*, pp. 1213–1225. doi: 10.1038/nn.4091.

Denis, R. G. P. *et al.* (2015) 'Palatability can drive feeding independent of AgRP neurons', *Cell Metabolism*, 22(4), pp. 646–657. doi: 10.1016/j.cmet.2015.07.011.

Dickson, S. L. and Luckman, S. M. (1997) 'Induction of c-fos messenger ribonucleic acid in neuropeptide Y and growth hormone (GH)-releasing factor neurons in the rat arcuate nucleus following systemic injection of the GH secretagogue, GH-releasing peptide-6', *Endocrinology*, 138(2), pp. 771–777. doi: 10.1210/endo.138.2.4907.

Dietrich, M. O. *et al.* (2015) 'Hypothalamic Agrp neurons drive stereotypic behaviors beyond feeding', *Cell*, 160(6), pp. 1222–1232. doi: 10.1016/j.cell.2015.02.024.

Ding, F. *et al.* (2013) 'α1-Adrenergic receptors mediate coordinated Ca2+ signaling of cortical astrocytes in awake, behaving mice', *Cell Calcium*. Elsevier Ltd, 54(6), pp. 387–394. doi: 10.1016/j.ceca.2013.09.001.

Dorfman, M. D. *et al.* (2017) 'Sex differences in microglial CX3CR1 signalling determine obesity susceptibility in mice', *Nature Communications*, 8(May 2016). doi: 10.1038/ncomms14556.

Douglass, J. D. *et al.* (2017) 'Astrocyte IKKβ/NF-κB signaling is required for diet-induced obesity and hypothalamic inflammation', *Molecular Metabolism*, 6(4), pp. 366–373. doi: 10.1016/j.molmet.2017.01.010.

Doyle, M. W. *et al.* (2004) 'Strategies for cellular identification in nucleus tractus solitarius slices', *Journal of Neuroscience Methods*, 137(1), pp. 37–48. doi: 10.1016/j.jneumeth.2004.02.007.

Doyle, M. W. and Andresen, M. C. (2001) 'Reliability of monosynaptic sensory transmission in brain stem neurons in vitro', *Journal of Neurophysiology*, 85(5), pp. 2213–2223. doi: 10.1152/jn.2001.85.5.2213.

Duffy, S. and MacVicar, B. A. (1995) 'Adrenergic calcium signaling in astrocyte networks within the hippocampal slice', *Journal of Neuroscience*, 15(8), pp. 5535–5550. doi: 10.1523/jneurosci.15-08-05535.1995.

Durkee, C. A. *et al.* (2019) 'Gi/o protein-coupled receptors inhibit neurons but activate astrocytes and stimulate gliotransmission', *Glia*, 67(6), pp. 1076–1093. doi: 10.1002/GLIA.23589.

Ebel, D. L., Torkilsen, C. G. and Ostrowski, T. D. (2017) 'Blunted respiratory responses in the streptozotocin-induced Alzheimer's disease rat model', *Journal of Alzheimer's Disease*, 56(3), pp. 1197–1211. doi: 10.3233/JAD-160974.

El-Brolosy, M. A. and Stainier, D. Y. R. (2017) 'Genetic compensation: A phenomenon in search of mechanisms', *PLoS Genetics*, 13(7), pp. 1–17. doi: 10.1371/journal.pgen.1006780.

Ellacott, K. L. J. *et al.* (2010) 'Assessment of feeding behavior in laboratory mice', *Cell Metabolism*, 12(1), pp. 10–17. doi: 10.1016/j.cmet.2010.06.001.

Ellacott, K. L. J., Halatchev, I. G. and Cone, R. D. (2006) 'Characterization of leptin-responsive neurons in the caudal brainstem', *Endocrinology*, 147(7), pp. 3190–3195. doi: 10.1210/en.2005-0877.

Erecinska, M. and Silver, I. A. (1990) 'Metabolism and role of glutamate in mammalian brain', *Progress in Neurobiology*, 35, pp. 947–955.

Essner, R. A. *et al.* (2017) 'AgRP neurons can increase food intake during conditions of appetite suppression and inhibit anorexigenic parabrachial neurons', *Journal of Neuroscience*, 37(36), pp. 0798–17. doi: 10.1523/JNEUROSCI.0798-17.2017.

Fan, W. *et al.* (2004) 'Cholecystokinin-mediated suppression of feeding involves the brainstem melanocortin system', *Nature Neuroscience*, 7(4), pp. 335–336. doi: 10.1038/nn1214.

Fernandes-Junior, S. A. *et al.* (2018) 'Correlation between neuroanatomical and functional respiratory changes observed in an experimental model of Parkinson's disease', *Experimental Physiology*, 103(10), pp. 1377–1389. doi: 10.1113/EP086987.

Ferriera, T. A. *et al.* (2014) 'Neuronal morphometry directly from bitmap images', *Nature Methods*, 11(10), pp. 981–984. doi: 10.1038/nmeth.3102.

Fiacco, T. A. and McCarthy, K. D. (2018) 'Multiple lines of evidence indicate that gliotransmission does not occur under physiological conditions', *Journal of Neuroscience*, 38(1), pp. 3–13. doi: 10.1523/jneurosci.0016-17.2017.

Fonnum, F., Johnsen, A. and Hassel, B. (1997) 'Use of fluorocitrate and fluoroacetate in the study of brain metabolism', *Glia*, 21(1), pp. 106–113. doi: 10.1002/(SICI)1098-1136(199709)21:1<106::AID-GLIA12>3.0.CO;2-W.

Frederich, R. C. *et al.* (1995) 'Leptin levels reflect body lipid content in mice: Evidence for diet-induced resistance to leptin action', *Nature Medicine*, 1(12), pp. 1311–1314. doi: 10.1038/nm1295-1311.

Fuente-Martín, E. *et al.* (2012) 'Leptin regulates glucose and glutamate transporters in hypothalamic astrocytes', *Journal of Clinical Investigation*, 122(11), pp. 3900–3913. doi: 10.1038/srep23673.

Fuente-Martín, E. *et al.* (2016) 'Ghrelin regulates glucose and glutamate transporters in hypothalamic astrocytes', *Scientific reports*, 6. doi: 10.1038/srep23673.

Füzesi, T. *et al.* (2016) 'Hypothalamic CRH neurons orchestrate complex behaviours after stress', *Nature Communications*, 7(May), pp. 1–14. doi: 10.1038/ncomms11937.

García-Cáceres, C. *et al.* (2011) 'Differential acute and chronic effects of leptin on hypothalamic astrocyte morphology and synaptic protein levels', *Endocrinology*, 152(5), pp. 1809–1818. doi: 10.1210/en.2010-1252.

Garcia de Mateos-Verchere, J. *et al.* (2001) 'The octadecaneuropeptide [diazepam-binding inhibitor (33-50)] exerts potent anorexigenic effects in rodents', *European Journal of Pharmacology*, 414(2–3), pp. 225–231. doi: 10.1016/S0014-2999(01)00771-3.

Garfield, A. S. *et al.* (2012) 'Neurochemical characterization of body weight-regulating leptin receptor neurons in the nucleus of the solitary tract', *Endocrinology*, 153(10), pp. 4600–4607. doi: 10.1210/en.2012-1282.

Garfield, A. S. *et al.* (2015) 'A neural basis for melanocortin-4 receptor–regulated appetite', *Nature Neuroscience*, 18(6), pp. 863–871. doi: 10.1038/nn.4011.

Gaykema, R. P. *et al.* (2017) 'Activation of murine pre-proglucagon-producing neurons reduces food intake and body weight', *Journal of Clinical Investigation*, 127(3), pp. 1031–1045. doi: 10.1172/JCI81335.

Goldstein, N. *et al.* (2018) 'Hypothalamic neurons that regulate feeding can influence sleep/wake states based on homeostatic need', *Current Biology*, 28(23), pp. 3736-3747.e3. doi: 10.1016/j.cub.2018.09.055.

Gomez, J. L. *et al.* (2017) 'Chemogenetics revealed: DREADD occupancy and activation via converted clozapine', *Science*, 357(6350), pp. 503–507. doi: 10.1126/science.aan2475.

Gourine, A. *et al.* (2010) 'Astrocytes control breathing through pH-dependent release of ATP', *Science*, 329, pp. 571–576. doi: 10.1126/science.1229223.

Grill, H. J. *et al.* (2002) 'Evidence that the caudal brainstem is a target for the inhibitory effect of leptin on food intake', *Endocrinology*, 143(1), pp. 239–246. doi: 10.1210/endo.143.1.8589.

Grill, H. J. and Hayes, M. R. (2012) 'Hindbrain neurons as an essential hub in the neuroanatomically distributed control of energy balance', *Cell Metabolism*, 16(3), pp. 296–309. doi: 10.1016/j.cmet.2012.06.015.

Guillebaud, F. *et al.* (2017) 'Glial endozepines inhibit feeding-related autonomic

functions by acting at the brainstem level', *Frontiers in Neuroscience*, 11(May). doi: 10.3389/fnins.2017.00308.

Hajós, F. and Kálmán, M. (1989) 'Distribution of glial fibrillary acidic protein (GFAP)-immunoreactive astrocytes in the rat brain. II. Mesencephalon, rhombencephalon and spinal cord', *Experimental Brain Research*, 78, pp. 164–173.

Hall, K. D. *et al.* (2012) 'Energy balance and its components: Implications for body weight regulation', *American Journal of Clinical Nutrition*, 95(4), pp. 989–994. doi: 10.3945/ajcn.112.036350.

Hamilton, N. B. and Attwell, D. (2010) 'Do astrocytes really exocytose neurotransmitters?', *Nature Reviews Neuroscience*, 11(4), pp. 227–238. doi: 10.1038/nrn2803.

Han, W. *et al.* (2018) 'A neural circuit for gut-induced reward', *Cell*, 175(3), pp. 655–678. doi: 10.1016/j.cell.2018.08.049.

Hanna, L. *et al.* (2017) 'Geniculohypothalamic GABAergic projections gate suprachiasmatic nucleus responses to retinal input', *The Journal of Physiology*, 595(11), pp. 3621–3649. doi: 10.1113/JP273850.

Hanna, L. *et al.* (2020) 'Changes in neuronal activity across the mouse ventromedial nucleus of the hypothalamus in response to low glucose: evaluation using an extracellular multi-electrode array approach', *Journal of Neuroendocrinology*, 32(3). doi: 10.1111/jne.12824.

Hardy, R. N. *et al.* (2018) 'Aging affects isoproterenol-induced water drinking, astrocyte density, and central neuronal activation in female Brown Norway rats', *Physiology and Behavior*, 192(November 2017), pp. 90–97. doi: 10.1016/j.physbeh.2018.03.005.

Harris, K. D. and Shepherd, G. M. G. (2015) 'The neocortical circuit: Themes and variations', *Nature Neuroscience*, 18(2), pp. 170–181. doi: 10.1038/nn.3917.

Haskell-Luevano, C. *et al.* (1999) 'Characterization of the neuroanatomical distribution of agouti-related protein immunoreactivity in the rhesus monkey and the rat', *Endocrinology*, 140(3), pp. 1408–1415. doi: 10.1210/endo.140.3.6544.

Haskell-Luevano, C. and Monck, E. K. (2001) 'Agouti-related protein functions as an inverse agonist at a constitutively active brain melanocortin-4 receptor', *Regulatory Peptides*, 99(1), pp. 1–7. doi: 10.1016/S0167-0115(01)00234-8.

Hayes, M. R. *et al.* (2010) 'Endogenous leptin signaling in the caudal nucleus tractus solitarius and area postrema is required for energy balance regulation', *Cell Metabolism*, 11(1), pp. 77–83. doi: 10.1016/j.cmet.2009.10.009.

Hermann, G. E. *et al.* (2009) 'Proteinase-activated receptors in the nucleus of the solitary tract: Evidence for glial-neural interactions in autonomic control of the stomach', *Journal of Neuroscience*, 29(29), pp. 9292–9300. doi: 10.1523/JNEUROSCI.6063-08.2009.

Hermann, G. E. and Rogers, R. C. (2009) 'TNF activates astrocytes and catecholaminergic neurons in the solitary nucleus: Implications for autonomic control', *Brain Research*, 1273(Dmv), pp. 72–82. doi: 10.1016/j.brainres.2009.03.059.

Herrero-Mendez, A. *et al.* (2009) 'The bioenergetic and antioxidant status of neurons is controlled by continuous degradation of a key glycolytic enzyme by APC/C-Cdh1', *Nature Cell Biology*, 11(6), pp. 747–752. doi: 10.1038/ncb1881.

Hetherington, A. W. and Ranson, S. W. (1940) 'Hypothalamic lesions and adiposity in the rat', *The Anatomical Record*, 78(2), pp. 149–172. doi: 10.1111/j.1753-4887.1983.tb07169.x.

Hirrlinger, P. G. *et al.* (2006) 'Temporal control of gene recombination in astrocytes by transgenic expression of the tamoxifen-inducible DNA recombinase variant CreERT2', *Glia*, 54, pp. 11–20. doi: 10.1002/glia.

Hirschberg, S. *et al.* (2017) 'Functional dichotomy in spinal-vs prefrontal-projecting locus coeruleus modules splits descending noradrenergic analgesia from ascending aversion and anxiety in rats', *eLife*, 6(Lc), pp. 1–26. doi: 10.7554/eLife.29808.001.

Holt, M. K., Richards, J. E., *et al.* (2019) 'Preproglucagon neurons in the nucleus of the solitary tract are the main source of brain GLP-1, mediate stress-induced hypophagia, and limit unusually large intakes of food', *Diabetes*, 68(1), pp. 21–33. doi: 10.2337/db18-0729.

Holt, M. K., Pomeranz, L. E., *et al.* (2019) 'Synaptic inputs to the mouse dorsal vagal complex and its resident preproglucagon neurons', *Journal of Neuroscience*, 39(49), pp. 9767–9781. doi: 10.1523/JNEUROSCI.2145-19.2019.

Horvath, T. L. *et al.* (2010) 'Synaptic input organization of the melanocortin system predicts diet-induced hypothalamic reactive gliosis and obesity.', *Proceedings of the National Academy of Sciences of the United States of America*, 107(33), pp. 14875–80. doi: 10.1073/pnas.1004282107.

Hsu, J. Y. *et al.* (2017) 'Non-homeostatic body weight regulation through a brainstem-restricted receptor for GDF15', *Nature*, 550(7675), pp. 255–259. doi: 10.1038/nature24042.

Hsuchou, H. *et al.* (2009) 'Leptin receptor mRNA in rat brain astrocytes', *Peptides*, 30(12), pp. 2275–2280. doi: 10.1016/j.peptides.2009.08.023.

Huda, R., McCrimmon, D. R. and Martina, M. (2013) 'pH modulation of glial glutamate transporters regulates synaptic transmission in the nucleus of the solitary tract', *Journal of Neurophysiology*, 110(2), pp. 368–377. doi: 10.1152/jn.01074.2012.

Hung, C. Y. *et al.* (2006) 'Hindbrain administration of NMDA receptor antagonist AP-5 increases food intake in the rat', *American Journal of Physiology - Regulatory Integrative and Comparative Physiology*, 290(3), pp. 642–651. doi: 10.1152/ajpregu.00641.2005.

Huszar, D. *et al.* (1997) 'Targeted disruption of the melanocortin-4 receptor results in obesity in mice', *Cell*, 88(1), pp. 131–141. doi: 10.1016/S0092-8674(00)81865-6.

Jacquin, T. D. *et al.* (2000) 'Prenatal X-irradiation increases GFAP- and calbindin D28k-immunoreactivity in the medial subdivision of the nucleus of solitary tract in the rat', *Journal of the Autonomic Nervous System*, 80(1–2), pp. 8–13. doi: 10.1016/S0165-1838(99)00085-5.

Jennings, A. *et al.* (2017) 'Dopamine elevates and lowers astroglial Ca2+ through distinct pathways depending on local synaptic circuitry', *Glia*, 65(3), pp. 447–459. doi: 10.1002/glia.23103.

Johnstone, L. E., Fong, T. M. and Leng, G. (2006) 'Neuronal activation in the hypothalamus and brainstem during feeding in rats', *Cell Metabolism*, 4(4), pp. 313–321. doi: 10.1016/j.cmet.2006.08.003.

Kálmán, M. and Hajós, F. (1989) 'Distribution of glial fibrillary acidic protein (GFAP)-immunoreactive astrocytes in the rat brain - I. Forebrain', *Experimental Brain Research*, 78(1), pp. 147–163. doi: 10.1007/BF00230694.

Kanemaru, K. *et al.* (2014) 'In Vivo visualization of subtle, transient, and local activity of astrocytes using an ultrasensitive Ca2+ indicator', *Cell Reports*, 8(1), pp. 311–318. doi: 10.1016/j.celrep.2014.05.056.

Karp, N. A. *et al.* (2017) 'Prevalence of sexual dimorphism in mammalian phenotypic traits', *Nature Communications*, 8. doi: 10.1038/ncomms15475.

Kieffer, T. J., Mc Intosh, C. H. S. and Pederson, R. A. (1995) 'Degradation of glucose-dependent insulinotropic polypeptide and truncated glucagon-like peptide 1 in vitro and in vivo by dipeptidyl peptidase iv', *Endocrinology*. doi: 10.1210/endo.136.8.7628397.

Kim, J. G. *et al.* (2014) 'Leptin signaling in astrocytes regulates hypothalamic neuronal circuits and feeding.', *Nature Neuroscience*, 17(7), pp. 908–10. doi: 10.1038/nn.3725.

King, C. M. *et al.* (2020) 'Local resting Ca2+ controls the scale of astroglial Ca2+ signals', *Cell Reports*, 30(10), pp. 3466-3477.e4. doi: 10.1016/j.celrep.2020.02.043.

Kishi, T. and Elmquist, J. K. (2005) 'Body weight is regulated by the brain: A link between feeding and emotion', *Molecular Psychiatry*. doi: 10.1038/sj.mp.4001638.

Kojima, M. *et al.* (1999) 'Ghrelin is a growth-hormone-releasing acylated peptide from stomach', *Nature*, 402(6762), pp. 656–660. doi: 10.1038/45230.

Kranz, A. *et al.* (2010) 'An improved flp deleter mouse in C57Bl/6 based on flpo recombinase', *Genesis*, 48(8), pp. 512–520. doi: 10.1002/dvg.20641.

Krashes, M. J. *et al.* (2011) 'Rapid, reversible activation of AgRP neurons drdives feeding behavior in mice', *The Journal of Clinical Investigation*, 121(4), pp. 1424–28. doi: 10.1172/JCI46229DS1.

Krashes, M. J. *et al.* (2013) 'Rapid versus delayed stimulation of feeding by the endogenously released AgRP neuron mediators GABA, NPY, and AgRP', *Cell Metabolism*, 18(4), pp. 588–595. doi: 10.1016/j.cmet.2013.09.009.

Krashes, M. J. *et al.* (2014) 'An excitatory paraventricular nucleus to AgRP neuron circuit that drives hunger.', *Nature*, 507(7491), pp. 238–42. doi: 10.1038/nature12956.

Krashes, M. J., Lowell, B. B. and Garfield, A. S. (2016) 'Melanocortin-4 receptor-regulated energy homeostasis', *Nature Neuroscience*, 19(2), pp. 206–219. doi: 10.1038/nn.4202.

Kreisler, A. D., Davis, E. A. and Rinaman, L. (2014) 'Differential activation of chemically identified neurons in the caudal nucleus of the solitary tract in non-entrained rats after intake of satiating vs. non-satiating meals', *Physiology and Behavior*, 136, pp. 47–54. doi: 10.1016/j.physbeh.2014.01.015.

Kupari, J. *et al.* (2019) 'An atlas of vagal sensory neurons and their molecular specialization', *Cell Reports*, 27(8), pp. 2508–2523. doi: 10.1016/j.celrep.2019.04.096.

De La Zerda, D. J. *et al.* (2018) 'Ibuprofen does not reverse ventilatory acclimatization to chronic hypoxia', *Respiratory Physiology and Neurobiology*, 256(April 2017), pp. 29–35. doi: 10.1016/j.resp.2017.07.009.

Lalo, U. *et al.* (2006) 'NMDA receptors mediate neuron-to-glia signaling in mouse cortical astrocytes', *Journal of Neuroscience*, 26(10), pp. 2673–2683. doi: 10.1523/JNEUROSCI.4689-05.2006.

Lamy, C. M. *et al.* (2014) 'Hypoglycemia-activated GLUT2 neurons of the nucleus tractus solitarius stimulate vagal activity and glucagon secretion', *Cell Metabolism*, 19(3), pp. 527–538. doi: 10.1016/j.cmet.2014.02.003.

Lanjakornsiripan, D. *et al.* (2018) 'Layer-specific morphological and molecular differences in neocortical astrocytes and their dependence on neuronal layers', *Nature Communications*, 9(1), p. 1623. doi: 10.1038/s41467-018-03940-3.

Lazic, S. E., Clarke-Williams, C. J. and Munafò, M. R. (2018) 'What exactly is "N" in cell culture and animal experiments?', *PLOS Biology*, 16(4).

Lehre, K. P. *et al.* (1995) 'Differential expression of two glial glutamate

transporters in the rat brain: Quantitative and immunocytochemical observations', *Journal of Neuroscience*, 15(3), pp. 1835–1853.

Li, C. *et al.* (2019) 'Defined paraventricular hypothalamic populations exhibit differential responses to food contingent on caloric state', *Cell Metabolism*, 29(3), pp. 681–694. doi: 10.1016/j.cmet.2018.10.016.

Li, D. *et al.* (2020) 'Neurochemical regulation of the expression and function of glial fibrillary acidic protein in astrocytes', *Glia*, 68(5), pp. 878–897. doi: 10.1002/glia.23734.

Li, M. M. *et al.* (2019) 'The paraventricular hypothalamus regulates satiety and prevents obesity via two genetically distinct circuits', *Neuron*, 102(3), pp. 653–667. doi: 10.1016/j.neuron.2019.02.028.

Li, X.-Y. *et al.* (2019) 'AGRP neurons project to the medial preoptic area and modulate maternal nest-building', *Journal of Neuroscience*, 39(3), pp. 456–471. doi: 10.1523/JNEUROSCI.0958-18.2018.

Liddelow, S. A. *et al.* (2017) 'Neurotoxic reactive astrocytes are induced by activated microglia', *Nature*, 541(7638), pp. 481–487. doi: 10.1038/nature21029.

Lin, L.-H. *et al.* (2013) 'Astrocytes in the rat nucleus tractus solitarii are critical for cardiovascular reflex control', *Journal of Neuroscience*, 33(47), pp. 18608–18617. doi: 10.1523/JNEUROSCI.3257-13.2013.

Liu, H. *et al.* (2003) 'Transgenic mice expressing green fluorescent protein under the control of the melanocortin-4 receptor promoter', *Journal of Neuroscience*, 23(18), pp. 7143–7154. doi: 10.1523/jneurosci.23-18-07143.2003.

Llewellyn-Smith, I. J. *et al.* (2011) 'Preproglucagon neurons project widely to autonomic control areas in the mouse brain', *Neuroscience*, 180, pp. 111–121. doi: 10.1016/j.neuroscience.2011.02.023.

Longoni, R. *et al.* (2011) 'The MEK inhibitor SL327 blocks acquisition but not expression of lithium-induced conditioned place aversion: A behavioral and immunohistochemical study', *Psychopharmacology*, 216(1), pp. 63–73. doi: 10.1007/s00213-011-2192-9.

Luo, L., Callaway, E. M. and Svoboda, K. (2008) 'Genetic dissection of neural circuits', *Neuron*, 57(5), pp. 634–660. doi: 10.1016/j.neuron.2008.01.002.

Luo, L., Callaway, E. M. and Svoboda, K. (2018) 'Genetic dissection of neural circuits: A decade of progress', *Neuron*, 98(2), pp. 256–281. doi: 10.1016/j.neuron.2018.03.040.

Luquet, S. *et al.* (2005) 'NPY/AgRP neurons are essentials for feeding in adult mice but can be ablated in neonates', *Science*, 310(5748), pp. 683–685. doi: 10.1126/science.1115524.

Machaalani, R. *et al.* (2019) 'Effects of prenatal cigarette smoke exposure on BDNF, PACAP, microglia and gliosis expression in the young male mouse brainstem', *NeuroToxicology*, 74(February), pp. 40–46. doi: 10.1016/j.neuro.2019.05.009.

Machado, B. H. (2001) 'Neurotransmission of the cardiovascular reflexes in the nucleus tractus solitarii of awake rats', *Annals of the New York Academy of Sciences*, 940, pp. 179–196. doi: 10.1111/j.1749-6632.2001.tb03676.x.

MacVicar, B. A. *et al.* (1989) 'GABA-activated Cl- channels in astrocytes of hippocampal slices', *Journal of Neuroscience*, 9(10), pp. 3577–3583. doi: 10.1523/jneurosci.09-10-03577.1989.

Makhmutova, M. *et al.* (2019) 'Pancreatic islets communicate with the brain via vagal sensory neurons', *bioRxiv*. doi: 10.1101/780395.

Malmberg, A. B. and Bannon, A. W. (2001) 'Models of nociception: Hot-plate, tail-flick, and formalin tests in rodents', *Current Protocols in Neuroscience*, pp. 1–15. doi: 10.1002/0471142301.ns0809s06.

Mandelblat-Cerf, Y. *et al.* (2015) 'Arcuate hypothalamic AgRP and putative pomc neurons show opposite changes in spiking across multiple timescales', *eLife*, 4(JULY 2015), pp. 1–25. doi: 10.7554/eLife.07122.

Maniscalco, J. W. and Rinaman, L. (2018) 'Vagal Interoceptive Modulation of Motivated Behavior', *Physiology*, 33(2), pp. 151–167. doi: 10.1152/physiol.00036.2017.

Marina, N. *et al.* (2017) 'Brain metabolic sensing and metabolic signaling at the level of an astrocyte', *Glia*, 66(6), pp. 1185–1199. doi: 10.1002/glia.23283.

Martin-Fernandez, M. *et al.* (2017) 'Synapse-specific astrocyte gating of amygdala-related behavior', *Nature Neuroscience*, 20(11), pp. 1540–1548. doi: 10.1038/nn.4649.

Martín, R. *et al.* (2015) 'Circuit-specific signaling in astrocyte-neuron networks in basal ganglia pathways.', *Science*, 349(6249), pp. 730–4. doi: 10.1126/science.aaa7945.

Martinez-Hernandez, A., Bell, K. P. and Norenberg, M. D. (1977) 'Glutamine synthetase: Glial localization in brain', *Science*, 195(4284), pp. 1356–1358. doi: 10.1126/science.14400.

Marty, N. *et al.* (2005) 'Regulation of glucagon secretion by glucose transporter type 2 (glut2) and astrocyte- dependent glucose sensors', *J Clin Invest.*, 115(12), pp. 3545–3554. doi: 10.1172/JCI26309.branches.

Maslow, A. H. (1943) 'A theory of human motivation', *Psychological Review*, 50(4), pp. 370–396. doi: 10.1037/h0054346.

Mastitskaya, S. *et al.* (2019) 'Astrocytes modulate baroreceptor reflex sensitivity at the level of the nucleus of the solitary tract', *bioRxiv*. doi: http://dx.doi.org/10.1101/725770.

Matott, M. P. *et al.* (2016) 'Excitatory amino acid transporters tonically restrain nTS synaptic and neuronal activity to modulate cardiorespiratory function', *Journal of Neurophysiology*, 115(3), pp. 1691–1702. doi: 10.1152/jn.01054.2015.

Matott, M. P., Kline, D. D. and Hasser, E. M. (2017) 'Glial EAAT2 regulation of extracellular nTS glutamate critically controls neuronal activity and cardiorespiratory reflexes', *The Journal of Physiology*, 595(17), pp. 6045–6063. doi: 10.1113/JP274620.

Matsushita, N. *et al.* (2002) 'Dynamics of tyrosine hydroxylase promoter activity during midbrain dopaminergic neuron development', *Journal of Neurochemistry*, 82(2), pp. 295–304. doi: 10.1046/j.1471-4159.2002.00972.x.

McDougal, D. H. *et al.* (2013) 'Astrocytes in the hindbrain detect glucoprivation and regulate gastric motility', *Autonomic Neuroscience: Basic and Clinical*, 175(1–2), pp. 61–69. doi: 10.1016/j.autneu.2012.12.006.

McDougal, D. H., Hermann, G. E. and Rogers, R. C. (2011) ‘Vagal afferent stimulation activates astrocytes in the nucleus of the solitary tract via AMPA receptors: Evidence of an atypical neural-glial interaction in the brainstem’, *Journal of Neuroscience*, 31(39), pp. 14037–14045. doi: 10.1523/JNEUROSCI.2855-11.2011.

McDougal, D. H., Hermann, G. E. and Rogers, R. C. (2013) ‘Astrocytes in the nucleus of the solitary tract are activated by low glucose or glucoprivation: evidence for glial involvement in glucose homeostasis.’, *Frontiers in neuroscience*, 7(December), p. 249. doi: 10.3389/fnins.2013.00249.

Melo, M. R. *et al.* (2019) ‘Importance of the commissural nucleus of the solitary tract in renovascular hypertension’, *Hypertension Research*, 42(5), pp. 587–597. doi: 10.1038/s41440-018-0190-6.

Le Merrer, J. *et al.* (2011) ‘Deletion of the δ opioid receptor gene impairs place conditioning but preserves morphine reinforcement’, *Biological Psychiatry*, 69(7), pp. 700–703. doi: 10.1016/j.biopsych.2010.10.021.

Michaud, J. L. *et al.* (1998) ‘Development of neuroendocrine lineages requires the bHLH-PAS transcription factor SIM1’, *Genes and Development*, 12(20), pp. 3264–3275. doi: 10.1101/gad.12.20.3264.

Michaud, J. L. *et al.* (2001) ‘Sim1 haploinsufficiency causes hyperphagia , obesity and reduction of the paraventricular nucleus of the hypothalamus’, *Human Molecular Genetics*, 10(14), pp. 1465–1474.

Miller, R. H. and Raff, M. C. (1984) ‘Fibrous and protoplasmic astrocytes are biochemically and developmentally distinct’, *Journal of Neuroscience*, 4(2), pp. 585–592. doi: 10.1523/jneurosci.04-02-00585.1984.

Miller, S. J. *et al.* (2019) ‘Molecularly defined cortical astroglia subpopulation modulates neurons via secretion of Norrin’, *Nature Neuroscience*, 22(5), pp. 741–752. doi: 10.1038/s41593-019-0366-7.

Min, S. *et al.* (2019) ‘Arterial baroreceptors sense blood pressure through decorated aortic claws’, *Cell Reports*, 29(8), pp. 2192–2201. doi: 10.1016/j.celrep.2019.10.040.

Molofsky, A. V. and Deneen, B. (2015) ‘Astrocyte development: A guide for the

perplexed', *Glia*, 63(8), pp. 1320–1329. doi: 10.1002/glia.22836.

Moran, T. H. (2000) 'Cholecystokinin and satiety: Current perspectives', *Nutrition*, 16(10), pp. 858–865. doi: 10.1016/S0899-9007(00)00419-6.

Morel, L. *et al.* (2017) 'Molecular and functional properties of regional astrocytes in the adult brain', *Journal of Neuroscience*. doi: 10.1523/JNEUROSCI.3956-16.2017.

Mothet, J. P. *et al.* (2005) 'Glutamate receptor activation triggers a calcium-dependent and SNARE protein-dependent release of the gliotransmitter D-serine', *Proceedings of the National Academy of Sciences of the United States of America*, 102(15), pp. 5606–5611. doi: 10.1073/pnas.0408483102.

Mountjoy, K. G. *et al.* (1994) 'Localization of the melanocortin-4 receptor (MC4-R) in neuroendocrine and autonomic control circuits in the brain', *Molecular Endocrinology*, 8(10), pp. 1298–1308. doi: 10.1210/me.8.10.1298.

Mullier, A. *et al.* (2010) 'Differential distribution of tight junction proteins suggests a role for tanycytes in blood-hypothalamus barrier regulation in the adult mouse brain', *Journal of Comparative Neurology*, 518(7), pp. 943–962. doi: 10.1002/cne.22273.

Nagase, M. *et al.* (2014) 'On-site energy supply at synapses through monocarboxylate transporters maintains excitatory synaptic transmission', *Journal of Neuroscience*, 34(7), pp. 2605–2617. doi: 10.1523/jneurosci.4687-12.2014.

Nakazato, M. *et al.* (2001) 'A role for ghrelin in the central regulation of feeding', *Nature*, 409(6817), pp. 194–198. doi: 10.1038/35051587.

Naskar, K. and Stern, J. E. (2014) 'A functional coupling between extrasynaptic NMDA receptors and A-type K+ channels under astrocyte control regulates hypothalamic neurosecretory neuronal activity', *Journal of Physiology*, 592(13), pp. 2813–2827. doi: 10.1113/jphysiol.2014.270793.

Nedergaard, M. (1994) 'Direct signaling from astrocytes to neurons in cultures of mammalian brain cells', *Science*, 263, pp. 1768–1771.

Nedergaard, M., Ransom, B. and Goldman, S. A. (2003) 'New roles for astrocytes: Redefining the functional architecture of the brain', *Trends in*

Neurosciences, 26(10), pp. 523–530. doi: 10.1016/j.tins.2003.08.008.

Nichols, N. R. *et al.* (1993) 'Gfap messenger-RNA increases with age in rat and human brain', *Neurobiology of Aging*, 14(5), pp. 421–429. doi: Doi 10.1016/0197-4580(93)90100-P.

Nizar, K. *et al.* (2013) 'In vivo stimulus-induced vasodilation occurs without IP3 receptor activation and may precede astrocytic calcium increase', *Journal of Neuroscience*, 33(19), pp. 8411–8422. doi: 10.1523/JNEUROSCI.3285-12.2013.

Nuzzaci, D. *et al.* (2020) 'Postprandial hyperglycemia stimulates neuroglial plasticity in hypothalamic POMC neurons after a balanced meal', *Cell Reports*, 30, pp. 3067–3078. doi: 10.1016/j.celrep.2020.02.029.

Oberheim, N. A. *et al.* (2006) 'Astrocytic complexity distinguishes the human brain', *Trends in Neurosciences*, 29(10), pp. 547–553. doi: 10.1016/j.tins.2006.08.004.

Ogata, K. and Kosaka, T. (2002) 'Structural and quantitative analysis of astrocytes in the mouse hippocampus', *Neuroscience*, 113(1), pp. 221–233. doi: 10.1016/S0306-4522(02)00041-6.

Oliet, S. H. R. and Bonfardin, V. D. J. (2010) 'Morphological plasticity of the rat supraoptic nucleus - cellular consequences', *European Journal of Neuroscience*, 32(12), pp. 1989–1994. doi: 10.1111/j.1460-9568.2010.07514.x.

Oliet, S. H. R., Piet, R. and Poulain, D. A. (2001) 'Control of glutamate clearance and synaptic efficacy by glial coverage of neurons', *Science*, 292(5518), pp. 923–926. doi: 10.1126/science.1059162.

Padilla, S. L. *et al.* (2016) 'Agouti-related peptide neural circuits mediate adaptive behaviors in the starved state', *Nature Neuroscience*, 19(5), pp. 734–741. doi: 10.1038/nn.4274.

Page, S. J., Zhu, M. and Appleyard, S. M. (2018) 'Effects of acute and chronic nicotine on catecholamine neurons of the nucleus of the solitary tract', *American Journal of Physiology-Regulatory, Integrative and Comparative Physiology*, 316(1), pp. R38–R49. doi: 10.1152/ajpregu.00344.2017.

Palmiter, R. D. (2018) 'The parabrachial nucleus: CGRP neurons function as a

general alarm', *Trends in Neurosciences*, 41(5), pp. 280–293. doi: 10.1016/j.tins.2018.03.007.

Pan, W. *et al.* (2008) 'Astrocyte leptin receptor (ObR) and leptin transport in adult-onset obese mice', *Endocrinology*, 149(6), pp. 2798–2806. doi: 10.1210/en.2007-1673.

Panatier, A. *et al.* (2006) 'Glia-Derived d-Serine Controls NMDA Receptor Activity and Synaptic Memory', *Cell*, 125(4), pp. 775–784. doi: 10.1016/j.cell.2006.02.051.

Panatier, A. *et al.* (2011) 'Astrocytes are endogenous regulators of basal transmission at central synapses', *Cell*, 146(5), pp. 785–798. doi: 10.1016/j.cell.2011.07.022.

Papouin, T., Henneberger, C., *et al.* (2017) 'Astroglial versus neuronal D-serine: Fact checking', *Trends in Neurosciences*, 40(9), pp. 517–520. doi: 10.1016/j.tins.2017.05.007.

Papouin, T., Dunphy, J. M., *et al.* (2017) 'Septal cholinergic neuromodulation tunes the astrocyte-dependent gating of hippocampal NMDA receptors to wakefulness', *Neuron*, 94(4), pp. 840–854. doi: 10.1016/j.neuron.2017.04.021.

Parpura, V. *et al.* (1994) 'Glutamate-mediated astrocyte-neuron signalling', *Nature*, 369, pp. 744–747.

Patel, S. *et al.* (2019) 'GDF15 provides an endocrine signal of nutritional stress in mice and humans', *Cell Metabolism*, 29(3), pp. 707–718. doi: 10.1016/j.cmet.2018.12.016.

Paxinos, G and Franklin, K. B. J. (2001) *Mouse Brain in Stereotaxic Coordinates*. Second Edi. San Diego: Academic Press. doi: 10.1016/S0306-4530(03)00088-X.

Pellerin, L. *et al.* (1998) 'Evidence supporting the existence of an activity-dependent astrocyte-neuron lactate shuttle', *Developmental Neuroscience*, 20(4–5), pp. 291–299. doi: 10.1159/000017324.

Pellerin, L. and Magistretti, P. J. (2012) 'Sweet sixteen for ANLS', *Journal of Cerebral Blood Flow and Metabolism*, 32(7), pp. 1152–1166. doi: 10.1038/jcbfm.2011.149.

Peters, J. H. *et al.* (2010) ‘Primary afferent activation of thermosensitive TRPV1 triggers asynchronous glutamate release at central neurons’, *Neuron*, 65(5), pp. 657–669. doi: 10.1016/j.neuron.2010.02.017.

Petravicz, J., Boyt, K. M. and McCarthy, K. D. (2014) ‘Astrocyte IP3R2-dependent Ca2+ signaling is not a major modulator of neuronal pathways governing behavior’, *Frontiers in Behavioral Neuroscience*, 8(November), pp. 1–13. doi: 10.3389/fnbeh.2014.00384.

Petravicz, J., Fiacco, T. A. and McCarthy, K. D. (2008) ‘Loss of IP3 receptor-dependent Ca2+ increases in hippocampal astrocytes does not affect baseline CA1 pyramidal neuron synaptic activity’, *Journal of Neuroscience*, 28(19), pp. 4967–4973. doi: 10.1523/JNEUROSCI.5572-07.2008.

Piet, R. *et al.* (2004) ‘Physiological contribution of the astrocytic environment of neurons to intersynaptic crosstalk.’, *Proceedings of the National Academy of Sciences of the United States of America*, 101(7), pp. 2151–2155. doi: 10.1073/pnas.0308408100.

Porter, J. T. and McCarthy, K. D. (1996) ‘Hippocampal astrocytes in situ respond to glutamate released from synaptic terminals’, *Journal of Neuroscience*, 16(16), pp. 5073–5081.

Powell, F. L. and Fu, Z. (2008) ‘HIF-1 and ventilatory acclimatization to chronic hypoxia’, *Respiratory Physiology and Neurobiology*, 164(1–2), pp. 282–287. doi: 10.1037/a0032811.Child.

Raffan, E. *et al.* (2016) ‘A Deletion in the Canine POMC Gene Is Associated with Weight and Appetite in Obesity-Prone Labrador Retriever Dogs’, *Cell Metabolism*, 23(5), pp. 893–900. doi: 10.1016/j.cmet.2016.04.012.

Reeves, A., Shigetomi, E. and Khakh, B. S. (2011) ‘Bulk loading of calcium indicator dyes to study astrocyte physiology: Key limitations and improvements using morphological maps’, *Journal of Neuroscience*, 31(25), pp. 9353–9358. doi: 10.1523/jneurosci.0127-11.2011.

Reiner, D. J. *et al.* (2016) ‘Astrocytes regulate GLP-1 receptor-mediated effects on energy balance’, *Journal of Neuroscience*, 36(12), pp. 3531–3540. doi: 10.1523/JNEUROSCI.3579-15.2016.

Rinaman, L. (2010) ‘Ascending projections from the caudal visceral nucleus of the solitary tract to brain regions involved in food intake and energy expenditure’, *Brain Research*, 1350, pp. 18–34. doi: 10.1016/j.brainres.2010.03.059.

Ritter, S. *et al.* (2011) ‘Minireview: The value of looking backward: The essential role of the hindbrain in counterregulatory responses to glucose deficit’, *Endocrinology*, 152(11), pp. 4019–4032. doi: 10.1210/en.2010-1458.

Roberts, B. L. *et al.* (2017) ‘High glucose increases action potential firing of catecholamine neurons in the nucleus of the solitary tract by increasing spontaneous glutamate inputs’, *Am J Physiol regul Integr Comp Physiol*. doi: 10.1152/ajpregu.00413.2016.

Robertson, S. D. *et al.* (2013) ‘Developmental origins of central norepinephrine neuron diversity.’, *Nature neuroscience*, 16(8), pp. 1016–23. doi: 10.1038/nn.3458.

Robin, L. M. *et al.* (2018) ‘Astroglial CB 1 receptors determine synaptic D-serine availability to enable recognition memory’, *Neuron*, 98(5), pp. 935–944. doi: 10.1016/j.neuron.2018.04.034.

Rogers, R. C. *et al.* (2018) ‘Response of catecholaminergic neurons in the mouse hindbrain to glucoprivic stimuli is astrocyte dependent’, *American Journal of Physiology-Regulatory, Integrative and Comparative Physiology*, 315(1), pp. R153–R164. doi: 10.1152/ajpregu.00368.2017.

Rogers, R. C. *et al.* (2019) ‘Evidence that hindbrain astrocytes in the rat detect low glucose with a glucose transporter 2-phospholipase C-calcium release mechanism’, *American Journal of Physiology-Regulatory, Integrative and Comparative Physiology*, 318, pp. 38–48. doi: 10.1152/ajpregu.00133.2019.

Rogers, R. C., Ritter, S. and Hermann, G. E. (2016) ‘Hindbrain cytoglucopenia-induced increases in systemic blood glucose levels by 2-deoxyglucose depend on intact astrocytes and adenosine release’, *American Journal of Physiology - Regulatory Integrative and Comparative Physiology*, 310(11), pp. R1102–R1108. doi: 10.1152/ajpregu.00493.2015.

Roman, C. W., Derkach, V. A. and Palmiter, R. D. (2016) ‘Genetically and functionally defined NTS to PBN brain circuits mediating anorexia’, *Nature*

Communications, 7(May), p. 11905. doi: 10.1038/ncomms11905.

Roman, C. W., Sloat, S. R. and Palmiter, R. D. (2017) 'A tale of two circuits: CCKNTSneuron stimulation controls appetite and induces opposing motivational states by projections to distinct brain regions', *Neuroscience*, 358, pp. 316–324. doi: 10.1016/j.neuroscience.2017.06.049.

Rossi, M. A. and Stuber, G. D. (2018) 'Overlapping brain circuits for homeostatic and hedonic feeding', *Cell Metabolism*, 27(1), pp. 42–56. doi: 10.1016/j.cmet.2017.09.021.

Roth, B. L. (2016) 'DREADDs for neuroscientists', *Neuron*, 89(4), pp. 683–694. doi: 10.1016/j.neuron.2016.01.040.

Rui, L. (2013) 'Brain regulation of energy balance and body weight', *Reviews in Endocrine and Metabolic Disorders*. doi: 10.1007/s11154-013-9261-9.

Saab, A. S. *et al.* (2016) 'Oligodendroglial NMDA receptors regulate glucose import and axonal energy metabolism', *Neuron*, 91(1), pp. 119–132. doi: 10.1016/j.neuron.2016.05.016.

Sanjakdar, S. S. *et al.* (2015) 'Differential roles of α6β2∗ and α4β2∗ neuronal nicotinic receptors in nicotine- and cocaine-conditioned reward in mice', *Neuropsychopharmacology*, 40(2), pp. 350–360. doi: 10.1038/npp.2014.177.

Savtchouk, I. and Volterra, A. (2018) 'Gliotransmission: Beyond black-and-white', *Journal of Neuroscience*, 38(1), pp. 14–25. doi: 10.1523/jneurosci.0017-17.2017.

Schindelin, J. *et al.* (2012) 'Fiji: An open-source platform for biological-image analysis', *Nature Methods*, 9(7), pp. 676–682. doi: 10.1038/nmeth.2019.

Schipke, C. G., Heuser, I. and Peters, O. (2011) 'Antidepressants act on glial cells: SSRIs and serotonin elicit astrocyte calcium signaling in the mouse prefrontal cortex', *Journal of Psychiatric Research*, 45(2), pp. 242–248. doi: 10.1016/j.jpsychires.2010.06.005.

Schwarz, Y. *et al.* (2017) 'Astrocytes control synaptic strength by two distinct v-SNARE-dependent release pathways', *Nature Neuroscience*, 20(11). doi: 10.1038/nn.4647.

Scofield, M. D. *et al.* (2015) 'Gq-DREADD selectively initiates glial glutamate release and inhibits cue-induced cocaine seeking', *Biological Psychiatry*, 78(7), pp. 441–451. doi: 10.1016/j.biopsych.2015.02.016.

Scofield, M. D. *et al.* (2016) 'Cocaine self-administration and extinction leads to reduced glial fibrillary acidic protein expression and morphometric features of astrocytes in the nucleus accumbens core', *Biological Psychiatry*, 80(3), pp. 207–215. doi: 10.1016/j.biopsych.2015.12.022.

Scott, M. M. *et al.* (2011) 'Leptin receptor expression in hindbrain Glp-1 neurons regulates food intake and energy balance in mice', *Journal of Clinical Investigation*, 121(6), pp. 2413–2421. doi: 10.1172/JCI43703.

Shah, B. P. *et al.* (2014) 'MC4R-expressing glutamatergic neurons in the paraventricular hypothalamus regulate feeding and are synaptically connected to the parabrachial nucleus.', *Proceedings of the National Academy of Sciences of the United States of America*, 111(36), pp. 13193–8. doi: 10.1073/pnas.1407843111.

SheikhBahaei, S. *et al.* (2018) 'Morphometric analysis of astrocytes in brainstem respiratory regions', *Journal of Comparative Neurology*, 526(13), pp. 2032–2047. doi: 10.1002/cne.24472.

Shi, X. *et al.* (2017) 'Acute activation of GLP-1-expressing neurons promotes glucose homeostasis and insulin sensitivity', *Molecular Metabolism*, 6(11), pp. 1350–1359. doi: 10.1016/j.molmet.2017.08.009.

Shigetomi, E. *et al.* (2013) 'Imaging calcium microdomains within entire astrocyte territories and endfeet with GCaMPs expressed using adeno-associated viruses', *The Journal of General Physiology*, 141(5), pp. 633–647. doi: 10.1085/jgp.201210949.

Sholl, D. a. (1953) 'Dendritic organization in the neurons of the visual and motor cortices of the cat', *Journal of Anatomy*, 87(4), pp. 387–406.

Sofroniew, M. V. (2015) 'Astrogliosis', *Cold Spring Harbor Perspectives in Biology*, 7(2), pp. 1–17.

Sohal, V. S. *et al.* (2009) 'Parvalbumin neurons and gamma rhythms enhance cortical circuit performance', *Nature*, 459(7247), pp. 698–702. doi:

10.1038/nature07991.

Srinivasan, R. *et al.* (2015) ‘Ca2+ signaling in astrocytes from Ip3r2 -/- mice in brain slices and during startle responses in vivo’, *Nature Neuroscience*, 18(5), pp. 708–717. doi: 10.1038/nn.4001.

Stein, L. M. *et al.* (2020) ‘Dorsal vagal complex and hypothalamic glia differentially respond to leptin and energy balance dysregulation’, *Translational Psychiatry*, 10(1), p. 90. doi: 10.1038/s41398-020-0767-0.

Sternson, S. M. (2013) ‘Hypothalamic survival circuits: Blueprints for purposive behaviors’, *Neuron*. Elsevier Inc., 77(5), pp. 810–824. doi: 10.1016/j.neuron.2013.02.018.

Sternson, S. M. and Roth, B. L. (2014) ‘Chemogenetic tools to interrogate brain functions’, *Annual Review of Neuroscience*, 37, pp. 387–407. doi: 10.1146/annurev-neuro-071013-014048.

Stokes, J. A. *et al.* (2017) ‘Minocycline blocks glial cell activation and ventilatory acclimatization to hypoxia’, *Journal of Neurophysiology*, 117(4), pp. 1625–1635. doi: 10.1152/jn.00525.2016.

Su, Z., Alhadeff, A. L. and Betley, J. N. (2017) ‘Nutritive, post-ingestive signals are the primary regulators of AgRP neuron activity’, *Cell Reports*, 21(10), pp. 2724–2736. doi: 10.1016/j.celrep.2017.11.036.

Swerdlow, N. R. *et al.* (1983) ‘Cholecystokinin produces conditioned place-aversions, not place-preferences, in food-deprived rats: Evidence against involvement in satiety’, *Life Sciences*, 32, pp. 2087–2093.

Tadmouri, A., Champagnat, J. and Morin-Surun, M. P. (2014) ‘Activation of microglia and astrocytes in the nucleus tractus solitarius during ventilatory acclimatization to 10% hypoxia in unanesthetized mice’, *Journal of Neuroscience Research*, 92(5), pp. 627–633. doi: 10.1002/jnr.23336.

Takahashi, K. A. and Cone, R. D. (2005) ‘Fasting induces a large, leptin-dependent increase in the intrinsic action potential frequency of orexigenic arcuate nucleus neuropeptide Y/Agouti-related protein neurons’, *Endocrinology*, 146(3), pp. 1043–1047. doi: 10.1210/en.2004-1397.

Talman, W. T., Dragon, D. N. and Lin, L. H. (2017) ‘Reduced responses to

glutamate receptor agonists follow loss of astrocytes and astroglial glutamate markers in the nucleus tractus solitarii', *Physiological Reports*, 5(5), pp. 1–11. doi: 10.14814/phy2.13158.

Thaler, J. *et al.* (2012) 'Obesity is associated with hypothalamic injury in rodents and humans', *Journal of Clinical Investigation*, 122(1), p. 153. doi: 10.1172/JCI59660.adjacent.

Thek, K. R. *et al.* (2019) 'Extensive inhibitory gating of viscerosensory signals by a sparse network of somatostatin neurons', *Journal of Neuroscience*, 39(41), pp. 8038–8050. doi: 10.1523/JNEUROSCI.3036-18.2019.

Theodosis, D. T. *et al.* (2004) 'Neuronal, glial and synaptic remodeling in the adult hypothalamus: Functional consequences and role of cell surface and extracellular matrix adhesion molecules', *Neurochemistry International*, 45(4), pp. 491–501. doi: 10.1016/j.neuint.2003.11.003.

Tian, L. *et al.* (2009) 'Imaging neural activity in worms, flies and mice with improved GCaMP calcium indicators', *Nature Methods*, 6(12), pp. 875–881. doi: 10.1038/nmeth.1398.

Treece, B. R. *et al.* (1998) 'Delay in meal termination follows blockade of N-methyl-D-aspartate receptors in the dorsal hindbrain', *Brain Research*, 810(1–2), pp. 34–40. doi: 10.1016/S0006-8993(98)00867-1.

Tsai, C. Y. *et al.* (2017) 'Nitrosative stress-induced disruption of baroreflex neural circuits in a rat model of hepatic encephalopathy: A DTI study', *Scientific Reports*, 7(January 2016), pp. 1–12. doi: 10.1038/srep40111.

Turton, M. D. *et al.* (1996) 'A role for glucagon-like peptide-1 in the central regulation of feeding', *Nature*. doi: 10.1038/379069a0.

Vaarmann, A., Gandhi, S. and Abramov, A. Y. (2010) 'Dopamine induces Ca2+ signaling in astrocytes through reactive oxygen species generated by monoamine oxidase', *Journal of Biological Chemistry*, 285(32), pp. 25018–25023. doi: 10.1074/jbc.M110.111450.

Vaisse, C. *et al.* (1998) 'A frameshift mutation in human MC4R is associated with a dominant form of obesity [2]', *Nature Genetics*, 20(2), pp. 113–114. doi: 10.1038/2407.

Valassi, E., Scacchi, M. and Cavagnini, F. (2008) ‘Neuroendocrine control of food intake’, *Nutrition, Metabolism and Cardiovascular Diseases*, 18(2), pp. 158–168. doi: 10.1016/j.numecd.2007.06.004.

Vance, K. M., Rogers, R. C. and Hermann, G. E. (2015) ‘PAR1-activated astrocytes in the nucleus of the solitary tract stimulate adjacent neurons via NMDA receptors’, *Journal of Neuroscience*, 35(2), pp. 776–785. doi: 10.1523/JNEUROSCI.3105-14.2015.

Verkhratsky, A. and Nedergaard, M. (2016) ‘The homeostatic astroglia emerges from evolutionary specialization of neural cells’, *Philosophical Transactions of the Royal Society B: Biological Sciences*, 371(1700). doi: 10.1098/rstb.2015.0428.

Volterra, A., Liaudet, N. and Savtchouk, I. (2014) ‘Astrocyte Ca(2+) signalling: an unexpected complexity.’, *Nature Reviews Neuroscience*, 15(5), pp. 327–35. doi: 10.1038/nrn3725.

Wang, C. and Xu, Y. (2019) ‘Mechanisms for sex differences in energy homeostasis’, *Journal of Molecular Endocrinology*, 62(2), pp. R129–R143. doi: 10.1530/JME-18-0165.

Wang, D. *et al.* (2015) ‘Whole-brain mapping of the direct inputs and axonal projections of POMC and AgRP neurons’, *Frontiers in Neuroanatomy*, 9(March), p. 40. doi: 10.3389/fnana.2015.00040.

Wang, X. *et al.* (2006) ‘Astrocytic Ca2+ signaling evoked by sensory stimulation in vivo’, *Nature Neuroscience*, 9(6), pp. 816–823. doi: 10.1038/nn1703.

Wang, Y. *et al.* (2015) ‘Role of astrocytes in leptin signaling’, *Journal of Molecular Neuroscience*, 56(4), pp. 829–839. doi: 10.1007/s12031-015-0518-5.

West, D. B. *et al.* (1987) ‘Lithium chloride, cholecystokinin and meal patterns: Evidence that cholecystokinin suppresses meal size in rats without causing malaise’, *Appetite*, 8(3), pp. 221–227. doi: 10.1016/0195-6663(87)90021-3.

Williams, E. K. K. *et al.* (2016) ‘Sensory neurons that detect stretch and nutrients in the digestive system’, *Cell*, 166(1), pp. 209–221. doi: 10.1016/j.cell.2016.05.011.

Wolosker, H., Balu, D. T. and Coyle, J. T. (2016) ‘The rise and fall of the D-

serine-mediated gliotransmission hypothesis', *Trends in Neurosciences*, 39(11), pp. 712–721. doi: 10.1080/0163660X.2014.1002150.

Wolosker, H., Balu, D. T. and Coyle, J. T. (2017) 'Astroglial versus neuronal D-serine: Check your controls!', *Trends in Neurosciences*, 40(9), pp. 520–522. doi: 10.1016/j.tins.2017.06.010.

Wu, Q. *et al.* (2014) 'The temporal pattern of cfos activation in hypothalamic, cortical, and brainstem nuclei in response to fasting and refeeding in male mice', *Endocrinology*, 155(3), pp. 840–853. doi: 10.1210/en.2013-1831.

Wu, Q., Boyle, M. P. and Palmiter, R. D. (2009) 'Loss of GABAergic signaling by AgRP neurons to the parabrachial nucleus leads to starvation', *Cell*, 137(7), pp. 1225–1234. doi: 10.1016/j.cell.2009.04.022.

Wu, Q., Howell, M. P. and Palmiter, R. D. (2008) 'Ablation of neurons expressing agouti-related protein activates fos and gliosis in postsynaptic target regions', *Neuroscience*, 28(37), pp. 9218–9226. doi: 10.1523/JNEUROSCI.2449-08.2008.

Wu, S. wen, Fenwick, A. J. and Peters, J. H. (2014) 'Channeling satiation: A primer on the role of TRP channels in the control of glutamate release from vagal afferent neurons', *Physiology and Behavior*, 136, pp. 179–184. doi: 10.1016/j.physbeh.2014.09.003.

Wyss, M. T. *et al.* (2011) 'Labeled acetate as a marker of astrocytic metabolism', *Journal of Cerebral Blood Flow and Metabolism*, 31(8), pp. 1668–1674. doi: 10.1038/jcbfm.2011.84.

Xanthos, D. N. and Sandkühler, J. (2014) 'Neurogenic neuroinflammation: inflammatory CNS reactions in response to neuronal activity.', *Nature Reviews Neuroscience*, 15(1), pp. 43–53. doi: 10.1038/nrn3617.

Yamamoto, K. *et al.* (2010) 'Distinct target cell-dependent forms of short-term plasticity of the central visceral afferent synapses of the rat', *BMC Neuroscience*. BioMed Central Ltd, 11(1), p. 134. doi: 10.1186/1471-2202-11-134.

Yamamoto, K. and Mifflin, S. (2018) 'Inhibition of glial glutamate transporter GLT1 in the nucleus of the solitary tract attenuates baroreflex control of

sympathetic nerve activity and heart rate', *Physiological Reports*, 6(18), pp. 1–9. doi: 10.14814/phy2.13877.

Yamamoto, M. *et al.* (2003) 'Reversible suppression of glutamatergic neurotransmission of cerebellar granule cells in vivo by genetically manipulated expression of tetanus neurotoxin light chain', *Journal of Neuroscience*, 23(17), pp. 6759–6767. doi: 10.1523/jneurosci.23-17-06759.2003.

Yang, L., Qi, Y. and Yang, Y. (2015) 'Astrocytes control food intake by inhibiting AGRP neuron activity via adenosine A1 receptors', *Cell Reports*, 11(5), pp. 798–807. doi: 10.1016/j.celrep.2015.04.002.

Yeo, G. S. H. *et al.* (1998) 'A frameshift mutation in MC4R associated with dominantly inherited human obesity [1]', *Nature Genetics*, 20(2), pp. 111–112. doi: 10.1038/2404.

Yue, J. T. Y. *et al.* (2016) 'Inhibition of glycine transporter-1 in the dorsal vagal complex improves metabolic homeostasis in diabetes and obesity', *Nature Communications*, 7, pp. 1–11. doi: 10.1038/ncomms13501.

Yulyaningsih, E. *et al.* (2017) 'Acute lesioning and rapid repair of hypothalamic neurons outside the blood-brain barrier', *Cell Reports*, 19(11), pp. 2257–2271. doi: 10.1016/j.celrep.2017.05.060.

Yun, S. P. *et al.* (2018) 'Block of A1 astrocyte conversion by microglia is neuroprotective in models of Parkinson ' s disease', *Nature Medicine*, 24(7), pp. 931–938. doi: 10.1038/s41591-018-0051-5.

Zhan, C. *et al.* (2013) 'Acute and long-term suppression of feeding behavior by POMC neurons in the brainstem and hypothalamus, respectively.', *Journal of Neuroscience*, 33(8), pp. 3624–3632. doi: 10.1523/JNEUROSCI.2742-12.2013.

Zhang, J. *et al.* (2019) 'Sour sensing from the tongue to the brain', *Cell*, 179(2), pp. 392–402. doi: 10.1016/j.cell.2019.08.031.

Zhang, L. L. and Ashwell, K. W. S. (2001) 'Development of the cyto- and chemoarchitectural organization of the rat nucleus of the solitary tract', *Anatomy and Embryology*, 203(4), pp. 265–282. doi: 10.1007/s004290000151.

Zhang, T. *et al.* (2019) 'Glutamatergic neurons in the medial prefrontal cortex mediate the formation and retrieval of cocaine-associated memories in mice',

Addiction Biology, (July 2018), pp. 1–11. doi: 10.1111/adb.12723.

Zhang, X. *et al.* (2008) 'Hypothalamic IKKβ/NF-κB and ER stress link overnutrition to energy imbalance and obesity', *Cell*, 135(1), pp. 61–73. doi: 10.1016/j.cell.2008.07.043.

Zhang, Y. *et al.* (2017) 'Astrocytic process plasticity and IKKβ/NF-κB in central control of blood glucose, blood pressure, and body weight', *Cell Metabolism*, 25(5), pp. 1091–1102. doi: 10.1016/j.cmet.2017.04.002.

Zhang Y *et al.* (1994) 'Positional cloning of the mouse obese gene and its human homologue.', *Nature*, 372, pp. 425–432.

Zhao, H. *et al.* (2015) 'Frequency-dependent facilitation of synaptic throughput via postsynaptic NMDA receptors in the nucleus of the solitary tract', *The Journal of Physiology*, 593(1), pp. 111–125. doi: 10.1113/jphysiol.2013.258103.

Zimmers, T. A. *et al.* (2005) 'Growth differentiation factor-15/macrophage inhibitory cytokine-1 induction after kidney and lung injury', *Shock*, 23(6), pp. 543–548. doi: 10.1097/01.shk.0000163393.55350.70.

Zonta, M. *et al.* (2003) 'Neuron-to-astrocyte signaling is central to the dynamic control of brain microcirculation', *Nature Neuroscience*, 6(1), pp. 43–50. doi: 10.1038/nn980.